Pattern Formation in NO+H$_2$ Reaction on a Potassium Promoted Rh(110) Surface

Von
Dipl. Phys. Hong Liu
geboren am 09. Okt. 1978, in Wan Xian, China

July 2008

Referent: Prof. Dr. R. Imbihl

Koreferent: Prof. Dr. H. Pfnür

Tag der Promotion: 16. Juli 2008

Raffiniert ist der Herr Gott, aber boshaft ist er nicht.

A. Eistein

To **Apple**

Kurzzusammenfassung

Das System $NO+H_2/Rh(110)$ ist wohlbekannt für seine Fähigkeit, eine Vielzahl chemischer Wellenmuster zu erzeugen. Der Einfluss koadsorbierten Kaliums auf die Musterbildung wurde an diesem System mit Hilfe von Photoelektronenemissionsmikroskopie (PEEM), eines LEEM-Mikroskops (LEEM = low energy electron microscopy), Röntgenphotoelektronenspektroskopie (XPS) und der Beugung niederenergetischer Elektronen (LEED) untersucht.

Ausgehend von einer homogenen, mit Kalium bedeckten Oberfläche wurden unter Reaktionsbedingungen folgende chemische Wellenmuster gefunden: einfache Reaktionsfronten und Pulse sowie stationäre Turing-ähnliche Konzentrationsmuster. In den stationären Mustern findet eine Phasentrennung in eine K+O-Koadsorbatphase und in stickstoffreiche Phasen statt („reaktive Phasentrennung"). Im anregbaren Bereich der Reaktion bleibt der grundlegende Anregungsmechanismus des unpromotierten Systems intakt, aber man findet, dass die Pulse jetzt Kalium transportieren. Mit spektroskopischen LEEM (SPLEEM) und Mikro-LEED wurden die Konzentrationsprofile der Pulse und die darin vorkommenden geordneten Adsorbatphasen bestimmt. Unterstützt von realistischen, mathematischen Simulationen wurde gezeigt, dass der Kalium-Transport im wesentlichen auf die repulsiven Wechselwirkungen zwischen Kaliuöm und Stickstoff zurückzuführen sind. Die starke attraktive Wechselwirkung zwischen Sauerstoff und Kalium hingegen ist vermutlich für die Ausbildung der stationären Muster verantwortlich und für die Phasentrennung in N und K+O. Der Existenzbereich der Muster wurde in Form eines Bifurkationsdiagrammes für verschiedene Kaliumbedeckungen im Bereich von $\theta_K = 0.025$ bis $\theta_K = 0.12$ bestimmt. Verglichen zum unpromotierten System sind die Bereichsgrenzen mit Kalium zu höheren P_{H2} verschoben.

Schlüsselwörter: heterogene Katalyse, Musterbildung, chemische Wellen, Rh, Alkalimetall, Reaktions-Diffusions-System, Massentransport, Phasentrennung, LEED, LEEM, XPS.

Abstract

The NO $+H_2$ reaction on Rh(110) surface is well known for its ability to form various spatiotemporal concentration patterns.   The influence of coadsorbed alkali metals (AM), like Potassium, is studied in this system by PEEM (Photoemission electron microscopy), LEEM (Low energy electron microscopy), XPS (X-ray photoemission spectroscopy) and LEED (Low energy electron diffraction).

Starting with an initially homogeneous potassium distribution in the NO+H_2/K/Rh(110) system, chemical wave patterns involving simple reaction fronts and pulses and stationary Turing-like patterns have been observed.   The stationary patterns involve a phase separation into K+O coadsorbate phase and nitrogen covered surface ("reactive phase separation").   In the excitable regime the basic excitation cycle of the unpromoted system remains intact but the pulses are now transporting potassium.   With SPLEEM (Spectroscopic LEEM) and μLEED the concentration profiles of pulses were taken and the distribution of ordered adsorbate phases was determined.   As supported by simulations with a realistic mathematical model the K mass transport is essentially due to repulsive interaction between coadsorbed nitrogen and potassium.   The strong attraction between oxygen and potassium is presumably responsible for the stationary patterns and for the phase separation into N and K+O.   The existence diagram for the patterns has been mapped out for varying K coverages from $\theta_K = 0.025$ML up to $\theta_K = 0.12$ML.   Compared to the unpromoted patterns the boundaries are shifted towards higher P_{H2} in the presence of coadsorbed K.

Keywords: heterogeneous catalysis, pattern formation, chemical waves, Rh, alkali metal, reaction-diffusion system, mass transport, phase separation, LEED, LEEM, PEEM, XPS.

Content

I. Introduction

The central motivation of this thesis is toward the self-organization in a heterogeneous catalytic system: the catalytic reduction of NO with H_2 on a potassium promoted Rh(110) surface.

Self-organization, according to the definition of H. Haken, is a phenomenon when a system acquires a spatial, temporal or functional structure without specific interference from the outside. By "specific" it means the structure or functioning is not impressed onto the system, but that the system is acted upon from the outside in a nonspecific fashion [1]. For example, the "Bénard cells" - hexagonal cells formed in a thin layer of fluid when it is heated from below in an entirely uniform fashion, is in fig.1.1.
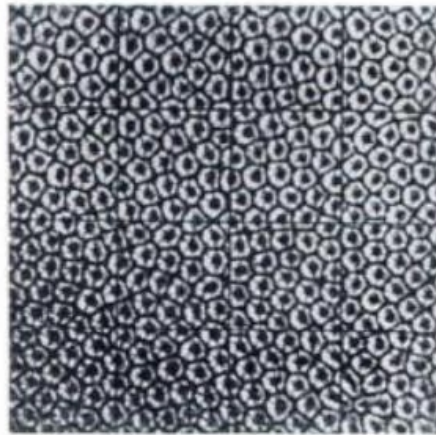
Fig.1.1 Original photograph of Bénard cells in a layer of spermaceti 0.810mm deep. Visualization was with graphite powder. After Bénard [2, 3]

There are different types of self-organization in physics, chemistry, biochemistry, etc., and among them, the self-organization of systems far from thermal equilibrium attracts most attention of the scientists, because under these conditions, interesting new phenomena appear, for example, the laser which emits a coherent light wave, the Belousov-Zhabotinsky reaction (BZ reaction) which produces rate oscillation of products and spatio-temporal patterns in the solution [4, 5], or biochemical patterns formed by cells of ameoba, or CO oxidation on a Pt surface. The latter system also has rate oscillations in CO_2 formation and exhibits spatial-temporal patterns on the surface.

Although these systems are related to different fields of science, many of them can have similar behavior.   On example is the pattern formed by one kind of amoeba called "Dictyostelium discoideum", due to pulses of cAMP (Cyclic adenosine monophosphate, a molecule which is important for information transferring in cells) traveling across the field in the form of circular or spiral waves, and the "spider web" pattern which is obtained in the NO+H_2/K/Rh(110) reaction, as shown in fig.1.2
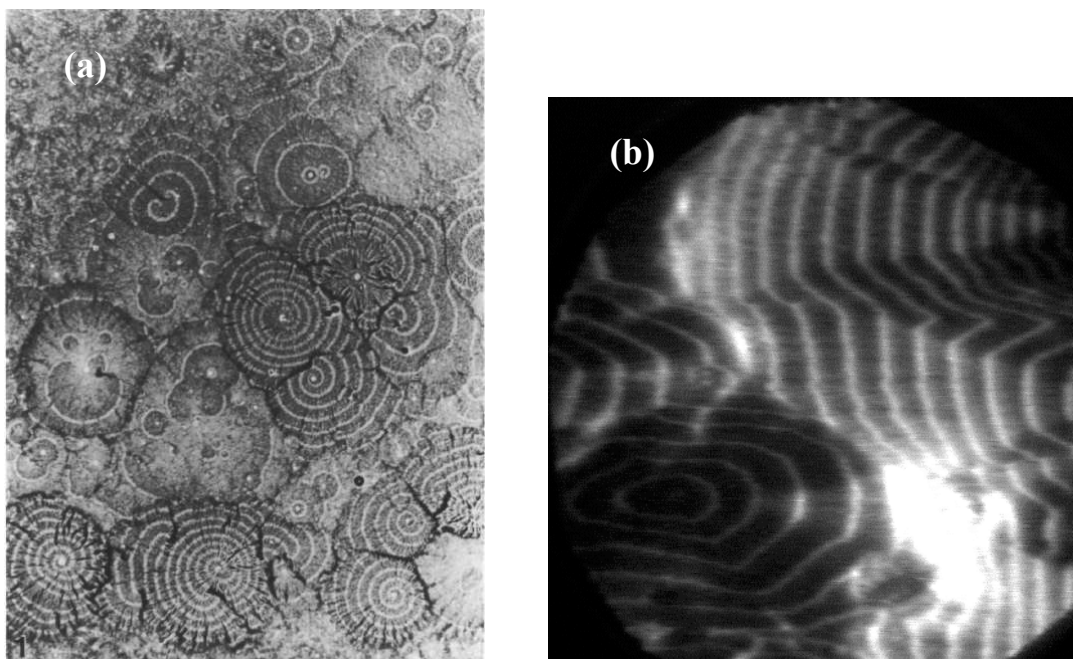
Fig.1.2 Pattern formation in different system, (a) Target and spiral patterns in Dictyostelium discoideum [from Newell, 1983, courtesy of P. C. Newell, 6], (b) PEEM image of NO+H_2/K/Rh(110) reaction, as shown in fig.6.15 in chapter VI.

In fig.1.2 (a) and (b), both patterns are both formed on the surface, and both of them might be related to a spatial-temporal pattern called chemical waves which is related to distribution of chemical species.

But despite of the similarity, the pattern in fig.1.2(a) actually belongs to self-organization in a higher level, which is formed by interactions between biological cells (amoeba) and molecules (cAMP) on the surface, while the pattern in fig.1.2(b) is actually self-organization on a more basic level, which is formed in an inorganic chemical reaction.   The reactants are simply adsorbed gas molecules (NO, H_2) and alkali metal atoms (K) on a solid surface (rhodium).   Thus the system belongs to the class of heterogeneous catalytic reactions.

Heterogeneous catalysis is very important in industry, since many important catalytic

processes happen on the surface of a solid catalyst, like the Haber-Bosch process for ammonia synthesis on Fe surface [7], Fischer-Tropsch process for hydrocarbon productions on Fe or Co surface [8, 9], CO oxidation on a Pt surface [10] and NO reduction with H_2 on Rh surfaces [11, 10]. Especially for the CO oxidation on Pt and NO reduction on Rh, the fundamental research in ultrahigh vacuum (UHV) is helpful for understanding the basic mechanisms of those important heterogeneous catalyzed reactions. During these reactions, rate oscillation and various spatio-temporal patterns can be observed. A large amount of work was done for CO oxidation on Pt surfaces, and for the $NO+H_2$ reaction on Rh surfaces. In previous research the clean and the adsorbate covered Rh(110), (111), (100) surface were studied

Potassium is a well known electronic promoter in many important catalytic reactions because it can significantly modify the local electronic properties of the surface. Previously, experiments and theoretical works on H_2+O_2/ K / Rh(110) system demonstrated that alkali metals not only modify the surface electronic properties but also participate in the spatiotemporal dynamics of a surface reaction [12, 13]. Since the unpromoted $NO+H_2$/Rh(110) system has already complicated spatio-temporal dynamics [14], pattern formation in the presence of a coadsorbed promoter represents a considerable challenge both for classifying the phenomenology and for understanding the mechanism. The aim of this thesis is to explore the new phenomena in this system and to use modern spectro-
-microscopic techniques to understand the underlying mechanisms.

II. General Theoretical Methods

2.1 Self-organization and reaction

In the theory of thermodynamics, there are generally three kinds of thermodynamic systems: Open system, with energy and particle exchange; closed system, with only energy exchange but without particle exchange; and isolated system, with no energy and no particle exchange.

The self-organization is a process in which the ordering within a system is increased without being guided by an outside source. A general entropy balance of such a system in environment is shown below in fig.2.1:

$$\Delta S_{total} = \Delta S_{local} + \Delta S_{env} \geq 0$$
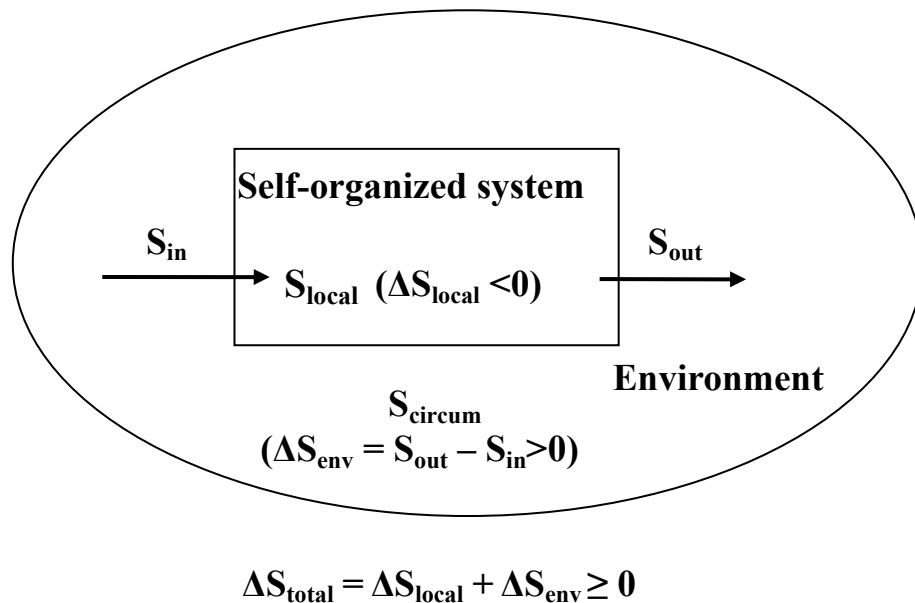
Fig.2.1 Entropy description of self-organized system

In fig.2.1, the ΔS_{local} is the entropy change of the local system, and ΔS_{env} is the entropy change of its environment. The whole system (the self organized system and its circumstance) can be together considered as an isolated system. Then we see the total entropy S_{total} still satisfies the second law, that $S_{total} \geq 0$. As shown in fig.2.1, $S_{out} - S_{in} > 0$, which means the entropy flow from this local system to the environment is positive, so the self-organized system is kind of dissipative system.

The focus of our work is on a special class of systems called reaction-diffusion (RD) system.

The heterogeneous catalyzed reactions belong to this class which exhibits complicate behavior of spatio-temporal organizations.

The general description of such a system can be written by this way:

$$\frac{\partial c_i}{\partial t} = f_i(\lambda, \vec{c}) + D_i \frac{\partial^2 c_i}{\partial x^2} , \qquad\qquad (2.1)$$

c_i - the concentration of a certain species

f_i - the function depending on reaction kinetics

λ - experimental parameter depending on temperature, pressure…etc

$\vec{c}$ - vector (c_1, c_2, …c_N) which denotes concentration of all species, N is the total number of species

D_i - the diffusion factor for certain reaction specie

From equation (2.1) we can see that this system is a combination of a normal chemical reaction system and a normal diffusion system.   For a self-organized system like the BZ reaction, the form of $f_i(\lambda, \vec{c})$ is nonlinear.

2.2 Activator-inhibitor models for chemical waves.

As mentioned in 3.3, the concept of reaction-diffusion (RD) system is used to describe heterogeneous reactions on the surface.

Despite of the complexity, a large number of dynamic behaviors of such systems can be described by models called activator- inhibitor model, in which only two species antagonistic operate, called "activator" and "inhibitor".   The model consists of two equations:

$$\frac{\partial u}{\partial t} = f(u,v) ,$$
$$\frac{\partial v}{\partial t} = g(u,v) ,$$

u and v are activator and inhibitor, respectively. One famous activator-inhibitor model is the Fitzhugh-Nagumo (FHN) model with 2 ordinary differential equations (ODE's) [15]:

$$\frac{du}{dt} = \frac{1}{\varepsilon}(u - \frac{u^3}{3} - v) = f(u,v) ,$$

$$\frac{dv}{dt} = u + b - av = g(u,v)$$

To describe a RD system, one has to combine the ODE's which describe the reaction term and diffusion term describing mobile species. Applying the FHN model, we get:

$$\frac{du}{dt} = f(u,v) + D_u \nabla^2 u$$

$$\frac{dv}{dt} = g(u,v) + D_v \nabla^2 v$$

2.3 Types of Media: Bistable, excitable and oscillatory

Details of the solution will not be discussed here, but generally, different types of the solutions correspond to various types of media: bistable, excitable, or oscillatory. Different media can support variant types of chemical wave patterns. For example, in a bistable media, after a initial perturbation, a reaction front can be formed. In an excitable media, a perturbation can generate a pulse and the media will return to the initial state after the pulse passes by. In an oscillatory media, the system oscillates autonomously with its own characteristic frequency. Finally, if the inhibitor diffuses much faster than the activator, a stationary pattern may result, which is known as Turing pattern.

III. Experimental Background

3.1. Experimental methods

3.1.1 Photoemission Electron Microscopy (PEEM)

The PEEM is a spatial resolving analytical method.   It gives the information of the local work function on the surface of a metal or a semiconductor.   By applying an outer light source (ultraviolet, X-ray, etc.) to the surface, the emitted electrons from the surface are collected and imaged by an optical system using electrostatic lenses.   The image amplified by a channelplate is finally visualized by a fluorescence screen, as shown in fig.3.1.
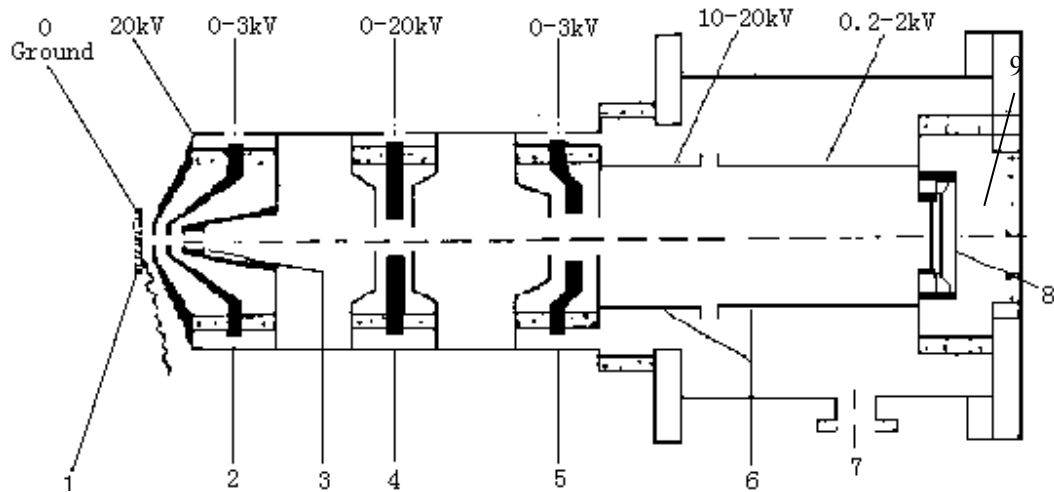
Fig.3.1 Schematic of a normal PEEM: 1. sample; 2. Objective lens; 3. Fixed aperture; 4. Intermediate lens; 5. Projective lens; 6. Decelerating tube lens; 7. To differential pump; 8. Channelplate; 9. Fluorescence screen. [16]

According to Fowler, the PEEM intensity I has a relationship with the local work function:

$I(\Delta\phi) \propto (h\nu - \phi - \Delta\phi)^2$ [17, 18], hν is the photon energy of the light source, Φ is the work function of the unpromoted Rh(110) surface, and ΔΦ is the work function change.   The area with lower work function in the PEEM image has relatively higher PEEM intensity.
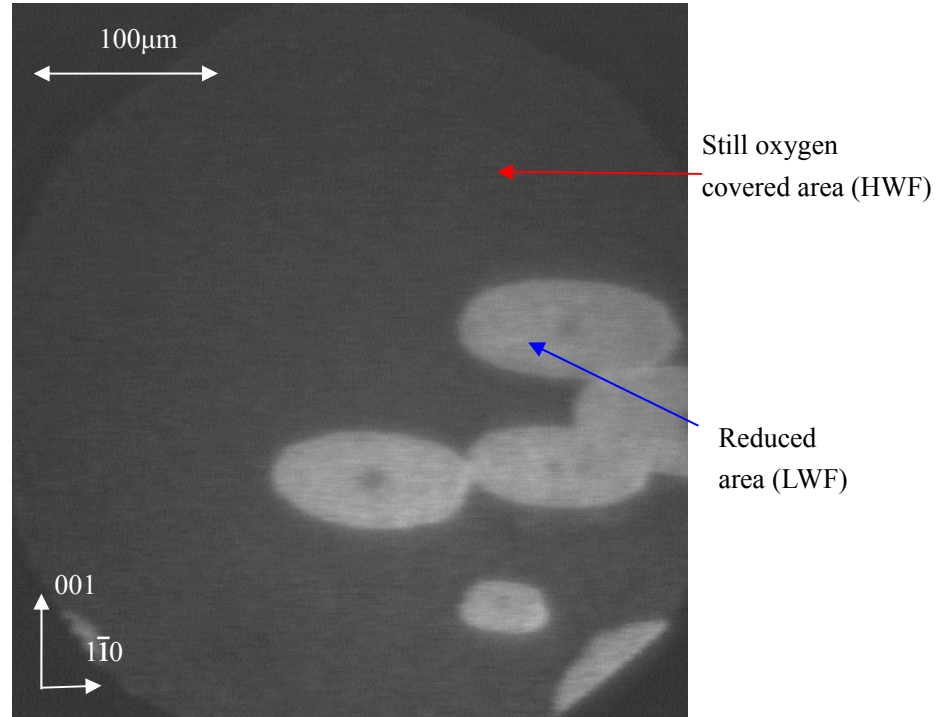
Fig.3.2 Reduction fronts, in $NO+H_2$/ Rh (110) reaction,

P_{NO} =1.54x10^{-6} mbar, P_{H2} = 1.85x10^{-5} mbar, T=550K

Fig.3.2 is a typical PEEM image.   The bright area has a relatively low work function (LWF), and the dark area has a relatively high work function (HWF).   In the $H_2 + O_2$ / Rh(110) reaction and $NO+H_2$ /Rh(110) reaction, the reduced area has a relatively lower work function than the area which is still covered by oxygen.   So the reduced area has relatively higher PEEM intensity.

3.1.2 X-Ray Photoelectron Spectroscopy (XPS)

For an atom of a certain element, there are different binding energies for electrons at different orbits.   When applying a monochromized X-ray beam with certain photon energy to the sample, electrons will be emitted from the atoms.   The electrons which escape from the solid without extra energy loss will give rise to discrete energy peaks whose energies obey:

$$E_k = h\nu - E_B^F - \Phi$$

E_k is the kinetic energy of emitted electrons, and $h\nu$ is the photon energy of the X-rays. For metal and semiconductor, E_B^F is the electron binding energy relative to Fermi level, Φ is the

work function difference between the sample and the detector.
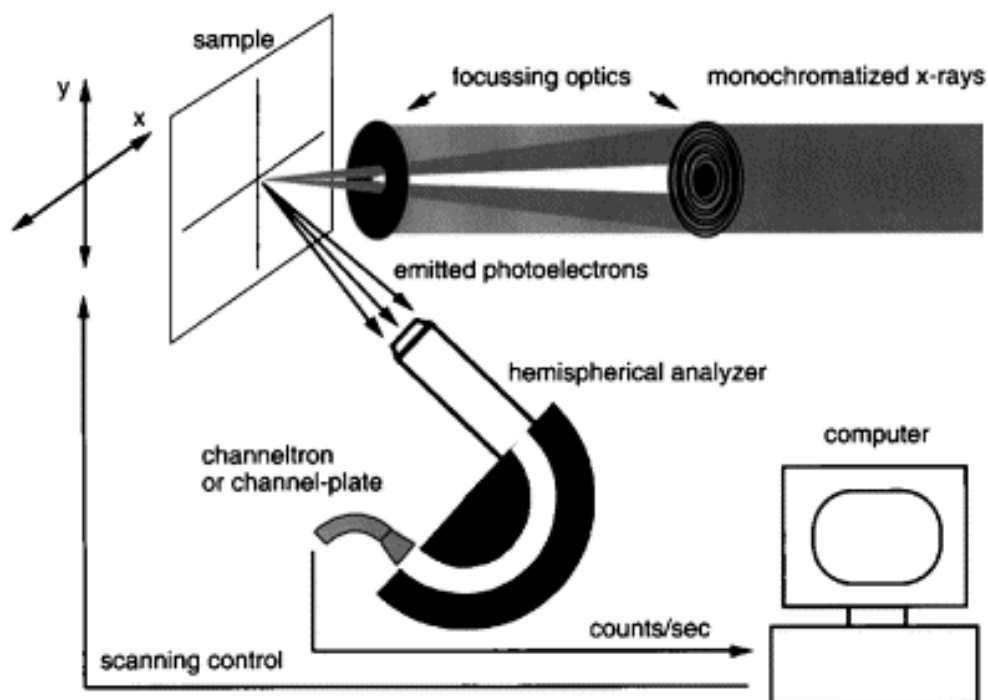
Fig.3.3 A principal diagram of XPS, in the variant of scanning photoelectron microscopy (SPEM) [19]

A principal diagram of XPS setup is shown in fig.3.3.　The XPS is a surface sensitive detection method, since only elastic emitted electrons emitted from the surface or near surface region will be detected as signal.　Thus it becomes a very helpful tool for surface analysis.

3.1.3 Auger Electron Spectroscopy (AES)

Auger electron spectroscopy (AES) is a method for determining the elemental composition of the outermost few atomic layers of materials.

Like XPS, AES is also kind of electron spectroscopy, which means, it analyzes the electrons from the sample which carry information of the emitting element.　In AES, a sample is probed by electron beam instead of X-ray.　The electron energy is typically from 3 to 10keV, resulting in the ejection of core level electrons from atoms to a depth up to about 1nm.

Electrons in atoms have different orbits (K, L, M, etc.). After the high energy electron is incident into the atoms, and it collides with one inner shell level electron, the energy removes the K electron so that the atom is ionized and K level has a hole.　Then one

electron in the L orbit will fall down to K level, and the released energy can cause another electron in the L orbit to be emitted out, with an energy which depends on the orbit structure. Different element has different orbit structure, so for a certain element, there is a certain energy distribution of the emitted electron. By measuring the energy of emitted electrons, the target element can be identified.

Furthermore, the AES can also be applied to quantitative analysis. The general equation of Auger current I_i from atom species i (consider the KLM transition) can be written as [20]:

$$I_i = I_p \sigma_i \gamma_i (1 + \gamma_i) T \frac{1}{4\pi} \iiint n_i(z) \exp \frac{-z}{\lambda_i \cos \theta} \sin \theta d\theta d\varphi dz$$

I_i is the intensity of the beam of the primary electrons of energy E_p ;

σ_i is the ionization cross-section of the core level K by electrons of energy E_p;

$(1+r_i)$ is the backscattering factor which accounts for the effects of backscattering of primary electrons;

$n_i(z)$ is the number of atoms i as a function of depth z;

$\exp(-z/(\lambda_i \cos\theta))$ describes the probability of non-loss escape of Auger electrons from depth z;

T characterizes the transmission of the energy analyzer;

From the above we can see, if the coverage of a certain species is in submonolayer range (for K under T>473K on Rh(110), θ_K <0.22ML), then the integration over z is simply proportional to the atom density n_i in the first layer, i.e., the Auger intensity of this species, for example, K, is approximately linearly proportional to its coverage.

3.1.4 Low Energy Electron Diffraction (LEED)

The low energy electron diffraction (LEED) is a commonly applied method of surface science providing structural information of the sample. The structural information is conventionally gained from analysis of elastically scattered electrons.

The general principle is described as following [20]:

Suppose an electron with wave vector $\vec{k}_0$ (with which a momentum $\hbar\vec{k}$) is injected to a single crystal surface, the scattered wave vector is $\vec{k}$, so the change of the wave vector is

$$\vec{k} - \vec{k}_0 = \vec{k}_G$$

Since only elastic scattered electrons formed the diffraction pattern, we have $\left|\vec{k}\right| = \left|\vec{k}_0\right|$.

Under the law of conservation of momentum, the momentum change must satisfy:

$$\vec{k}_G = \vec{G}_{hkl},$$

$\vec{G}_{hkl}$ is the reciprocal lattice vector, which only depends on the property of the crystal.

For LEED, with the typical low electron energy (30-200eV), the wavelength of electrons is about 1-2Å which satisfies the atomic diffraction condition, at the order of or less than atom distances, and the mean free path of electrons at this energy is very short, just at an order of a few atomic layers.

So LEED provides mostly information of the 2D surface structure of the crystal, and one can rewrite the condition into $\vec{k}_{G//} = \vec{G}_{hk}$, as shown by the so called "Ewald construction" in fig.3.3
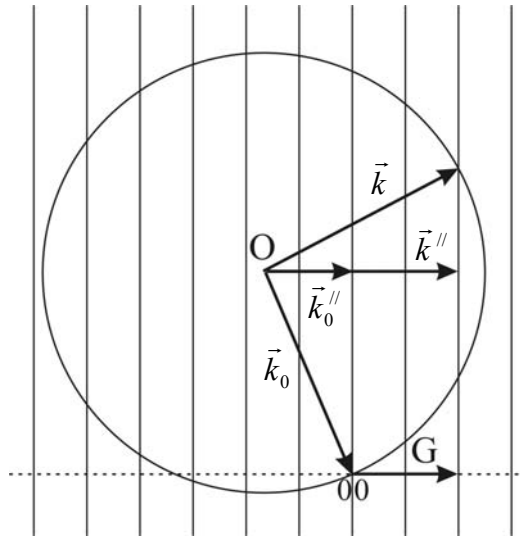
Fig.3.3 Ewald construction for diffraction on a 2D surface lattice

Dashed line marks the direction parallel to the surface. In contrast to the 3D reciprocal lattice points, here each of the reciprocal lattice rods is attributed to a 2D reciprocal lattice point of the surface.
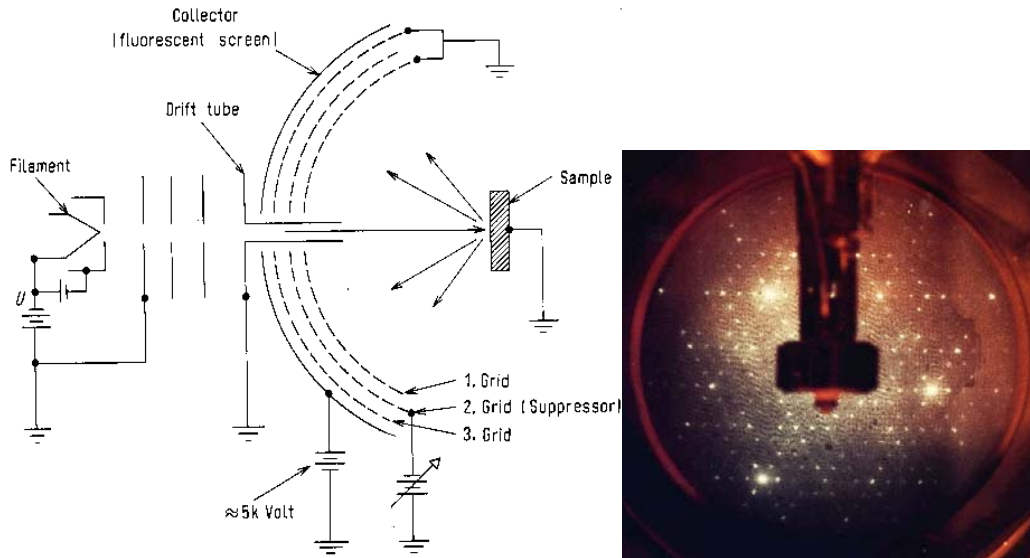
Fig.3.4 Schematic diagram of a standard four-grid LEED setup and LEED pattern of a Si(111)7x7 surface

The experimental schematic of a standard LEED device is shown as in fig.3.4. With analysis on the profile of LEED pattern with different k, one can get more information of the surface, for example, the vertical and horizontal roughness of the surface, the angle of facets, orientation of steps, etc.

3.1.5 Low Energy Electron Microscopy (LEEM) and Mirror Electron Microscopy (MEM)
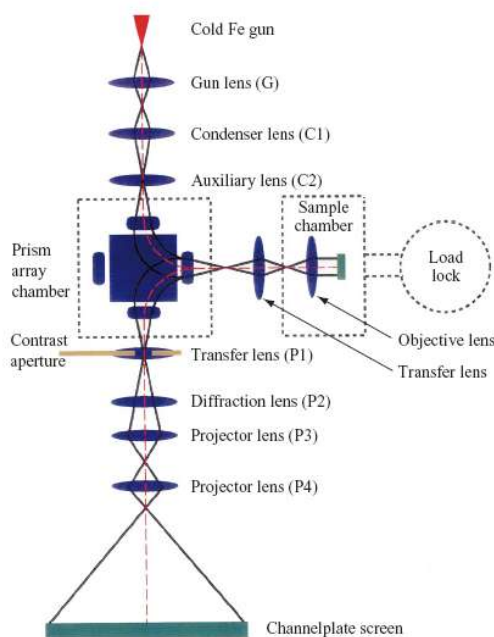
Fig.3.5. Experimental setup for low-energy electron microscopy (after Tromp [21])

Like LEED, LEEM uses diffracted electrons from the surface, but the difference is an imaging optical system is added in front of the LEED diffraction plane. What we get is a direct surface imaging which is related to structural information. A typical structure of a normal LEEM is as shown in fig.3.5.

To get a good contrast, the imaging of LEEM can be normally divided into bright field imaging and dark field imaging by selecting different diffracted beams at the diffraction plane. If the beam at (0,0) point is chosen to image, the resulting image is called bright field image, and if the beam at other point is chosen, the image is called dark field image.

In a bright field image, the contrast depends on local differences in the low energy electron reflectivity due to differences in crystal orientation, surface reconstruct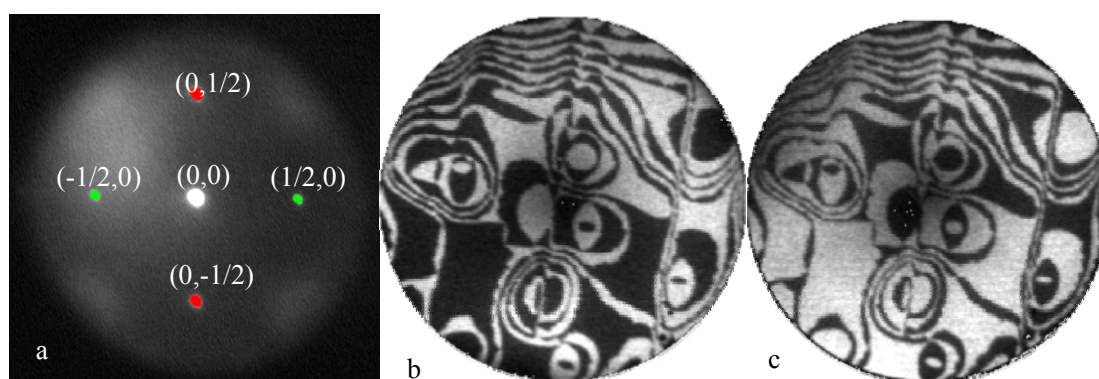ion, adsorbate coverage, etc. The dark field image can show the distribution of different structure on the surface, for example, the 1x2 and 2x1, as shown in fig.3.6.

Fig.3.6 (a) LEED image of clean Si(100)2x1 surface; (b) Dark-field LEEM image of the surface, taken from (1/2, 0) or (-1/2,0) spot in (a); (c) Dark-field LEEM image taken from (0,1/2) or (0,-1/2) spot in (a)[22]

A LEEM image can be acquired very quickly(<1ms), so it is a suitable tool to probe dynamic process on the surface, especially for those related to local structural change, like the film growth, adsorbate induced reconstruction, etc.

MEM (Mirror electron microscopy) is another method of electro microscopy but can use the same device of LEEM. The electron energy is reduced to zero in the limit, before they hit the sample surface. All height variations on the sample surface, such as surface structures,

adsorbates, etc., will change the local properties of the retarding field and therefore take influence on the reflected electron beam. The intensity of the reflected beam can be related to local work function change, the place with higher work function will normally have higher MEM intensity, in contrast to PEEM [23].

3.1.6 Kelvin Probe

Kelvin probe is a typical instrument for work function measurement.   The configuration is shown in fig.3.10 (a), the sample is connected into the circuit so that the surface of the sample and the surface of the head of the sample form a vibrating capacitor, whose capacity is influenced by the changing of surface work function.
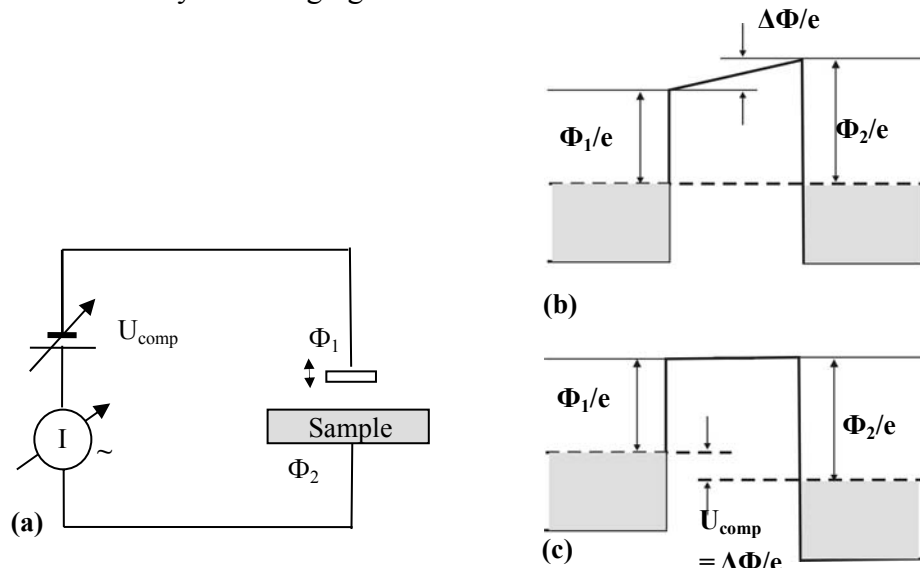
Fig.3.7. Principle of Kelvin probe vibrating capacitor method for relative measurements of work function.
 (a) Schematic of the circuit including a capacitor of variable capacitance formed by the vibrating probe electrode and the sample surface, variable voltage source and AC ammeter. AC current generated by vibration is compensated by adjusting U_{comp}; (b) Variation of potential between the probe and the surface when U_{comp} =0; (c) Variation of potential between the probe and the surface when U_{comp} = -$\Delta\Phi$/e [20]

The Kelvin probe is generally working with so called vibrating capacitor method, as shown in fig.3.7.   The probe and the sample surface form a capacitor whose capacitance can be changed (by distance or work function on the sample).   In the circuit shown in fig.3.7(a), two electrodes are connected to them together with an ammeter and a variable voltage source.   The voltage between the sample and the probe is :

$$U = \Delta\phi / e + U_{comp},$$

$\Delta\Phi/e = (\Phi_2 - \Phi_1)/e$ is the contact potential and U_{comp} is the voltage of the variable voltage source. So the capacitor carries a charge:

$$Q = CU = C(\Delta\phi / e + U_{comp})$$

If the probe is vibrating at a certain frequency (vibrating is generated by a piezo ceramic fixed together which is connected to a signal generator), the capacitance is changing periodically, giving an AC current in the circuit:

$$I = \frac{dQ}{dt} = \frac{dC}{dt}(\Delta\phi / e + U_{comp})$$

By adjusting the U_{comp}, the AC current can be reset to 0, U_{comp} must satisfy $U_{comp} = -\Delta\phi / e$

So by measuring the compensation voltage, we can get the work function of the sample surface related to the probe.

3.1.7 Quadrapole Mass Spectrometry (QMS)
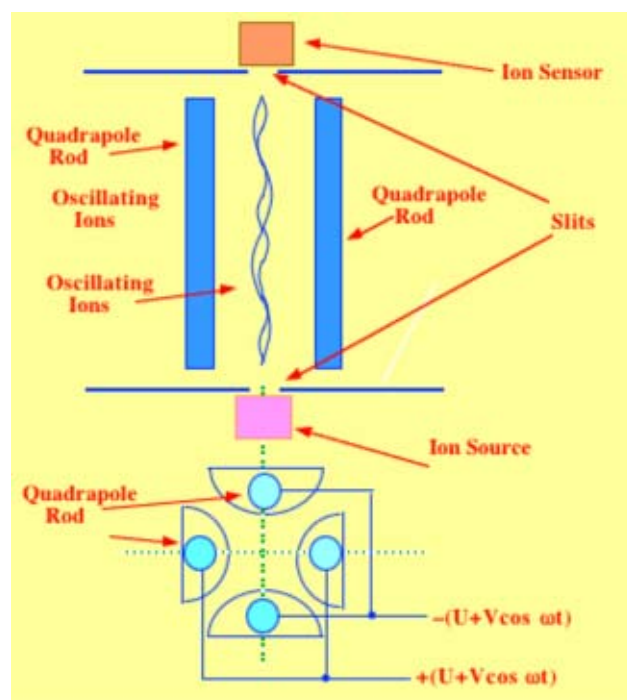
Fig.3.8. Principle schematic of a QMS (after Scott [24])

Mass spectrometry is a normal detection method in analyzing molecules. In surface science,

17

the quadrapole mass spectrometer is more often used for analyzing gas in vacuum or products from surface reactions.

As shown in fig.3.8, the main part of QMS consists of an ion source, a quadrapole mass analyzer and a detector.   Firstly the molecules will be ionized by an ion source and can possible split into charged fragments with a certain mass-charge ratio distribution depending only on the sort of molecule.   It forms a quadrapole electric field which can be adjusted from outside.   When a charged particle was introduced into the field, only the one with a certain mass-charge ratio will pass through and be detected by the analyzer, the others will be deflected.   By this way for a certain molecule, its mass-charge spectrum will be identified.

3.2. Experimental setup

3.2.1 Experimental Setup 1(PEEM, Hannover)

(a) Top view

(b) Side view

Fig.3.9. Schematic of experimental setups, (a) Top view; (b) Side view: **(1)** PEEM. **(2)** UV Lamp. **(3)** LEED. **(4)** AES. **(5)** Ion Gun. **(6)** Window. **(7)** Sample. **(8)** Main Chamber. **(9)** K Dispenser. **(10)**QMS. **(11)** Kelvin Probe
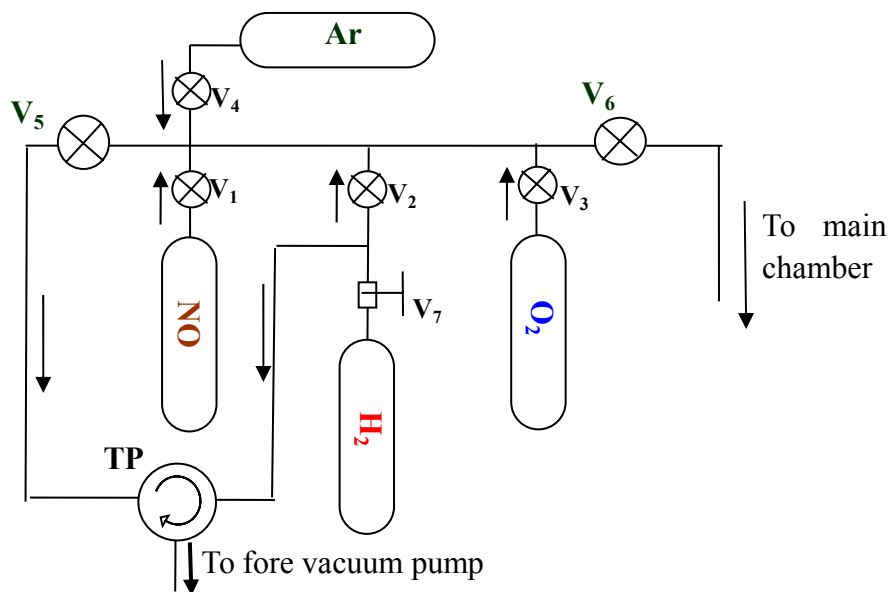
Fig.3.10 Schematic of the Gasline, $V_1 - V_4$: leak valves; V_5 , V_6: main valve; V_7 : Programmable Flow Controller; **P**: Turbo Pump

The experiment of chapter IV was carried out in the PEEM setup in university of Hannover,

which generally described by fig.3.9 and fig.3.10.   It was equipped with AES, LEED, QMS and PEEM using a D_2 discharge ultraviolet lamp.   The setup basically works under a background pressure of 10^{-10} mbar and can do experiments at pressure range up to 10^{-4} mbar (At this pressure we need to be aware of possible discharge which damages the channel plate of PEEM).

3.2.2 Experimental Setup (LEEM/XPEEM, Trieste)

3.2.2.1. Overview
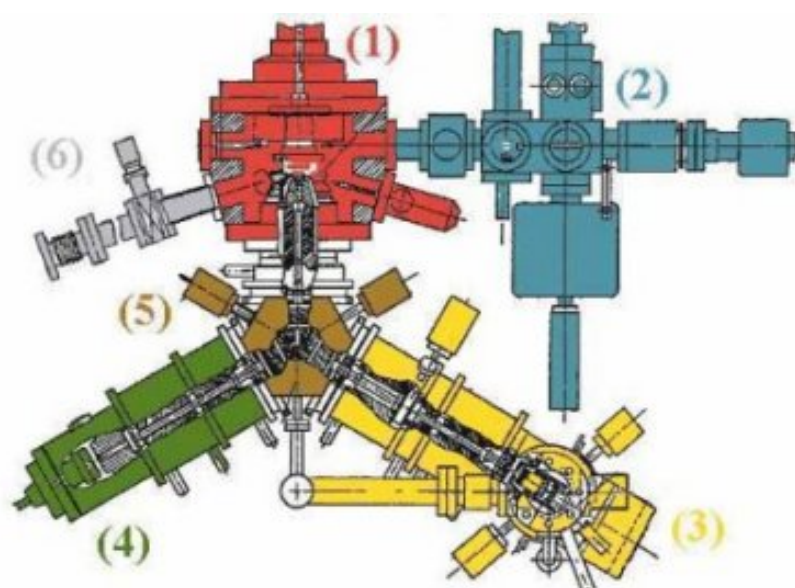
Fig.3.11 Schematic of LEEM/XPEEM setups (1)Main Chamber; (2)Sample Preparation Chamber; (3) Image Column; (4) Electron Gun; (5) Beam Separator; (6) Connection to The Beam Line.[25]

Chemical and structural analysis of the experiment was done in the nanospectroscopy lab in Elettra, Trieste, which was equipped with a LEEM/XPEEM device using synchrotron light as the light source.   On this device, one can make local analysis of the sample using different modes as XPEEM, µXPS, LEEM/MEM, and µLEED.   The setup works generally under a pressure up to 1×10^{-6}, above that pressure, the setup will possibly be damaged.

3.2.2.2 Operation modes
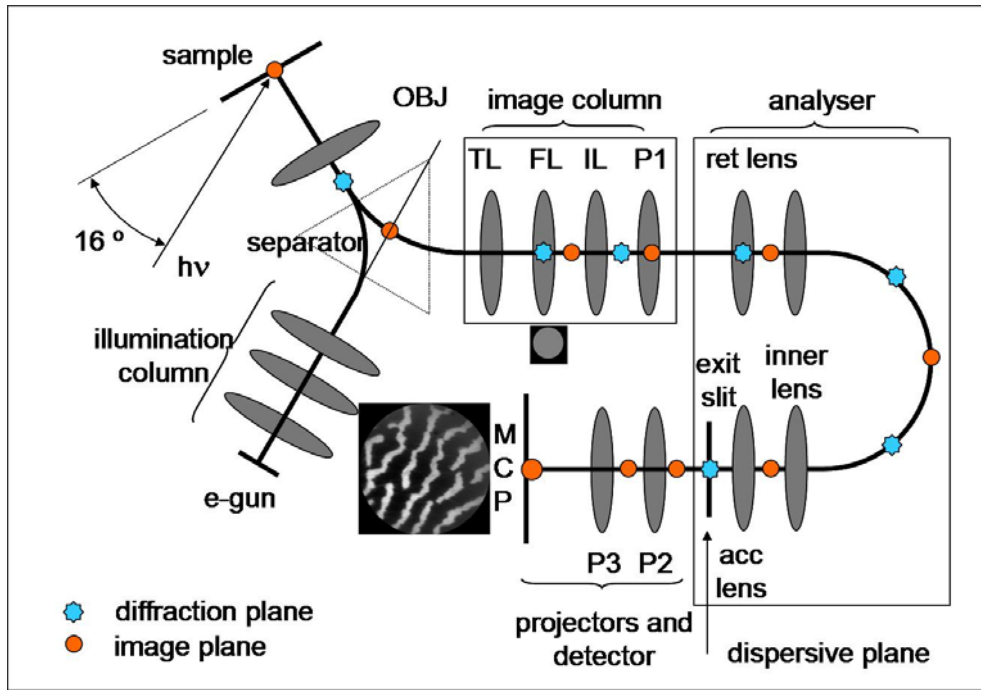
-XPEEM and LEEM Imaging mode

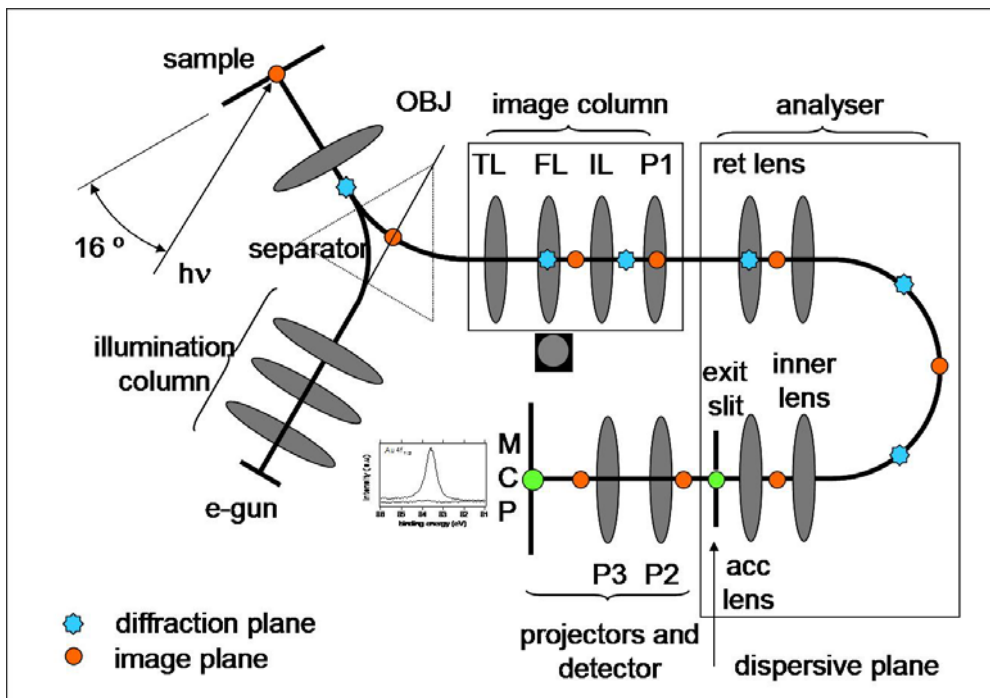**Fig.3.12** XPEEM and LEEM Imaging mode

-Micro XPS mode

Fig.3.13 Micro XPS mode

-Micro LEED mode
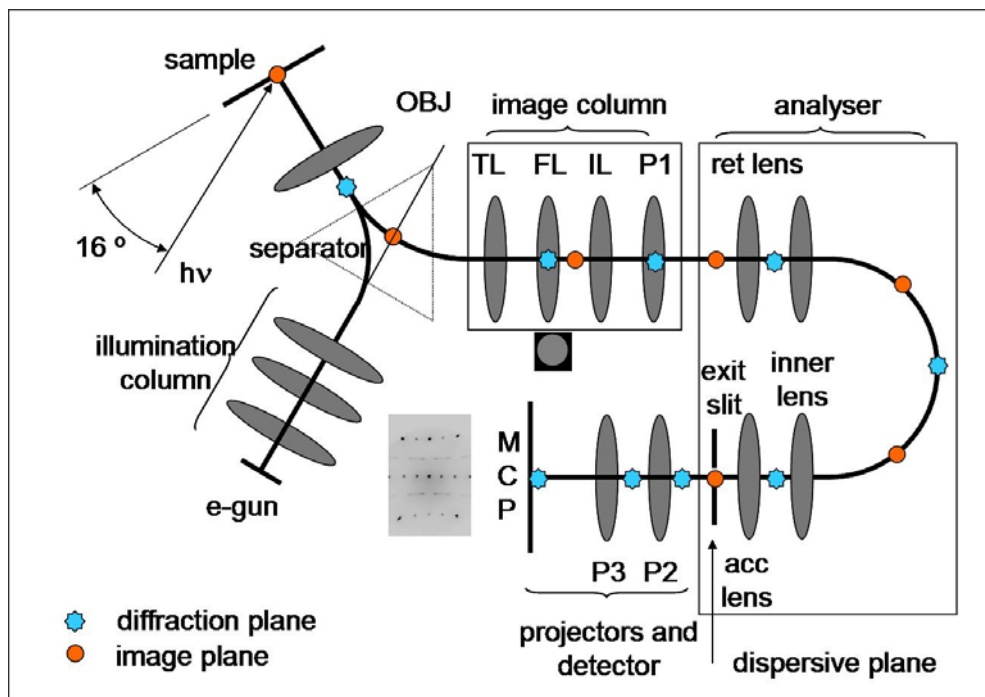
Fig.3.14 Micro LEED mode

3.3 Preparation for experiments

3.3.1 Sample treatment

The sample is treated by using a four-step cleaning cycle repeatedly (normally about 30-40 times for fresh sample):

1. Sputtering by Ar^+ ion flux (1keV acceleration) for about 45minutes, under about 800K

2. Annealing to about 1400K by electron bombardment heating for about 2 minutes.

3. Oxygen treatment under about 1000K for about 15minutes, $P_{O_2} = 2x10^{-6}$ mbar.

4. Annealing to about 1400K by electron bombardment heating for about 2 minutes.

3.3.2 K evaporation:

The K was evaporated from a SAES dispenser and deposited to the sample when the sample is heated (at about 500K) so that the distribution is homogeneous.

Before each evaporation the K dispenser was warmed up with current of 4 A for 10 minutes, so that the gases from its surface desorb and 6A for 10 seconds so that the evaporation curve

is more flat.

3.3.3 Calibrating gas pressure

In the experiments we mostly uses ion gauge to display the gas pressure. Unfortunately the normal ion gauges have different efficiency for different gases, for example, introducing 1×10^{-6} mbar H_2 or 1×10^{-6} mbar O_2 will have different displayed values. This is due to that different emission current coming from variant ionization effect of the gauge on different kinds of gases.

In order to get the true pressure, we have to calibrate the ion gauge using a viscosity gauge, which can give the true pressure of a certain kind of gas. The general procedure is to introduce a certain kind of gas with different pressure, and compare the values from the ion gauge and the viscosity gauge. From this way we can get a relationship of true pressure and the pressure displayed by the ion gauge. For different gases, the relationship is different, as shown in fig.3.15 and fig.3.16.
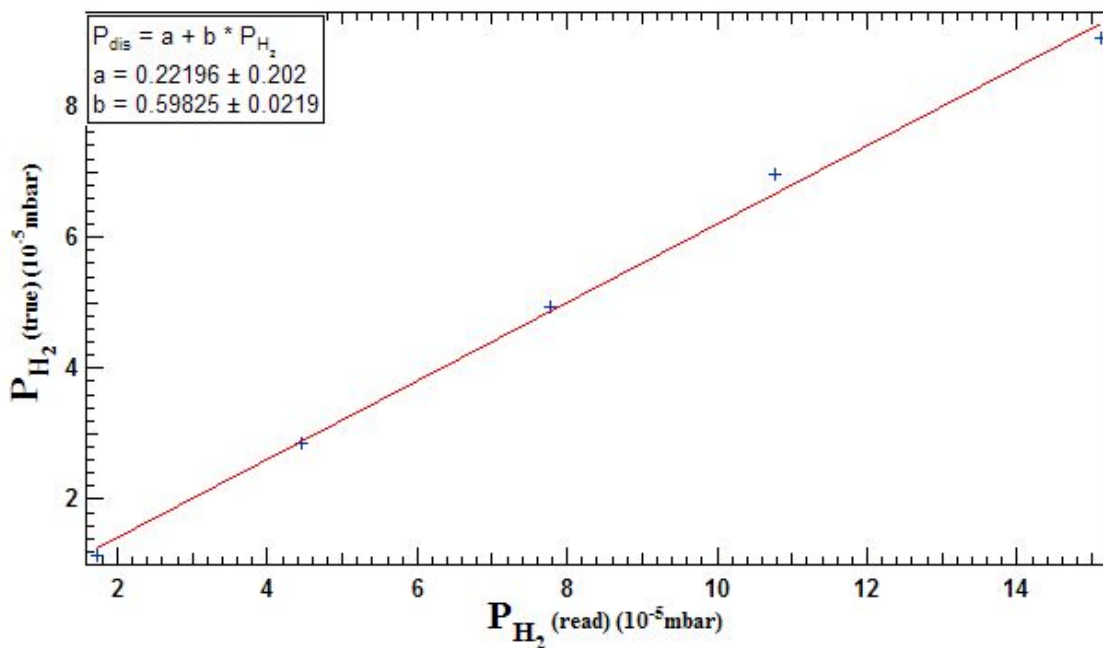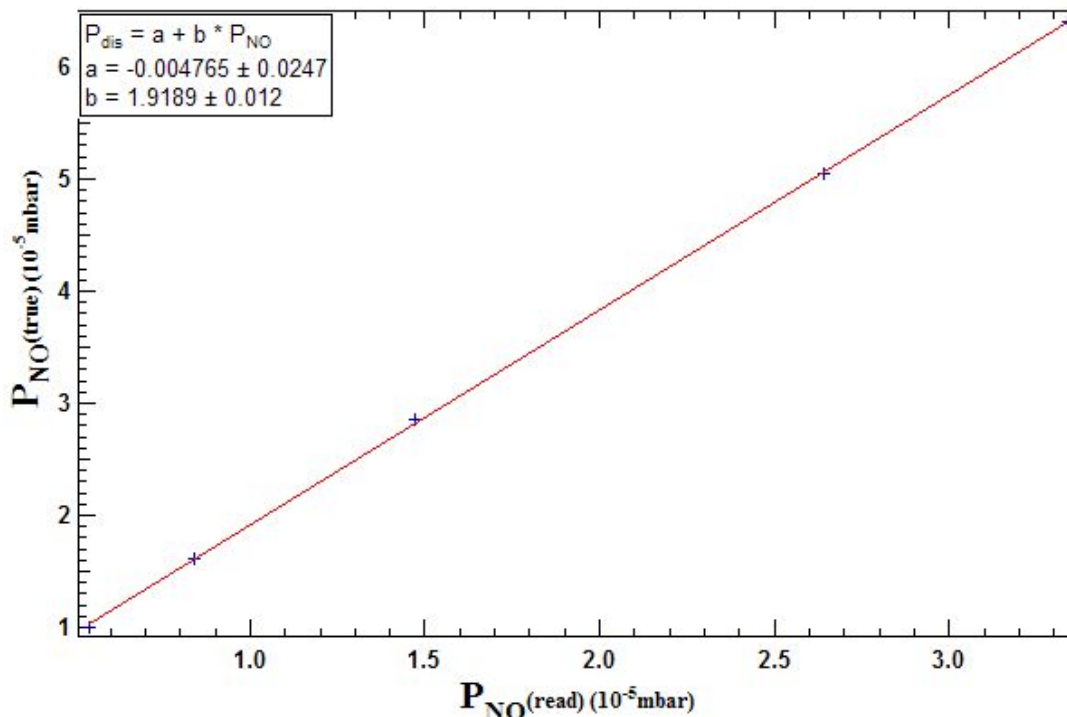

Fig.3.15 H_2 pressure calibration, using a viscosity gauge.

23

Fig.3.16 NO pressure calibration

As from the previous measurement, the calibration factors between real and displayed pressure are

$b_{H2} = P_{H2}$ (displayed)/P_{H2}(real) = 0.598±0.022,

$b_{NO} = P_{NO}$(displayed)/P_{NO}(real) = 1.919±0.012

These factors are only for the chamber for PEEM in Hannover. All the pressures in the LEEM/XPEEM in Trieste (including the chemical and structural analysis) are uncalibrated value.

3.3.4 Standard procedure of reaction:

The gases were introduced to the reaction chamber through the gasline. The pressure was controlled by leak valves between the gas bottles and the gasline. The NO was kept constant during reaction. H_2 pressure was controlled by a flow controller by combination with a differential pump.

Before each reaction experiment, NO was kept constant. For the first time of experiment, the sample was annealed to about 473K so that the distribution of potassium is really homogeneous (in PEEM image it can be seen that the image intensity is homogeneous).

Then the H_2 pressure was increased step by step for each reaction. For one experiment, the H_2 pressure was maintained constant for 10min. During that the development of patterns was observed. The final pattern was marked in the bifurcation diagram. At the end of each experiment, first H_2 was turned off and then sample is annealed to 700 K until the distribution of the K became homogeneous.

IV. Basics of the NO+H_2 /K/Rh(110) System

4.1 Structures on Rh(110) surface
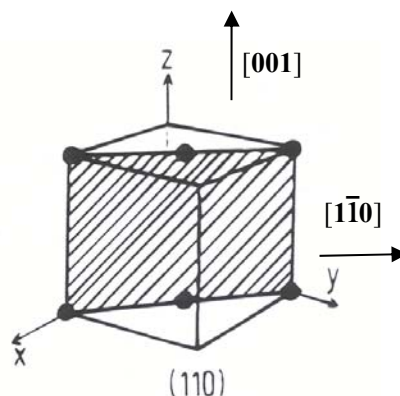
Fig.4.1. Rh(110) plane (shadow part) in the fcc Rh crystal, black dots are Rh atoms

Rhodium works as an important catalyst in heterogeneous catalytic processes like NO reduction with H_2.   The Rh crystal has a regular face centered cubic (fcc) structure, and its (110) plane, as shown in fig.2.1, has a rectangular structure.
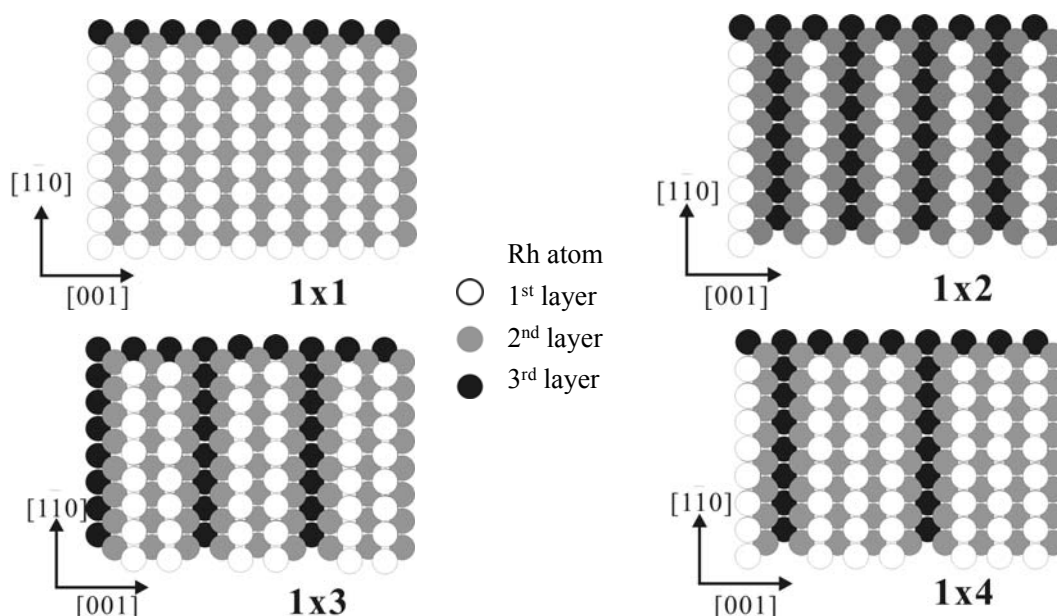
Fig.4.2: Missing-row reconstruction of Rh(110) surface (without adsorbates)

Depending on the adsorbate and its coverage, the Rh(110) surface can have different reconstructions, for example, many adsorbates, like oxygen, potassium, and K+O induce reconstructions of the 1x2, 1x3 or 1x4 "missing-row" type reconstructions, as shown in fig.4.2.   Other type of reconstruction like 2x1 induced by nitrogen is not shown here.

Structure with O
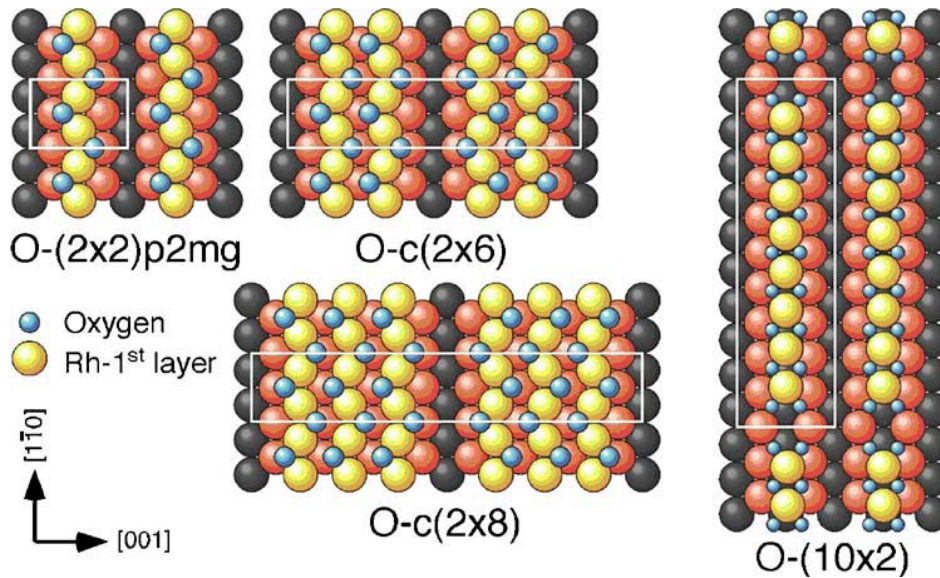
Fig.4.3. Hard-sphere models of (2x2) p2mg, c(2x6), c(2x8) oxygen adsorbate structure(with oxygen Coverage of 0.5ML, 0.66ML, and 0.75ML), together with a metastable 10x2 structure [26].

In the experimental condition of our experiments, when O is adsorbed on Rh(110), it will induce different surface reconstruction depending on oxygen coverage, respectively, as shown in fig.4.3.

(a) p(2x2) p2mg   (b) c(2x6)   (c)c(2x8)
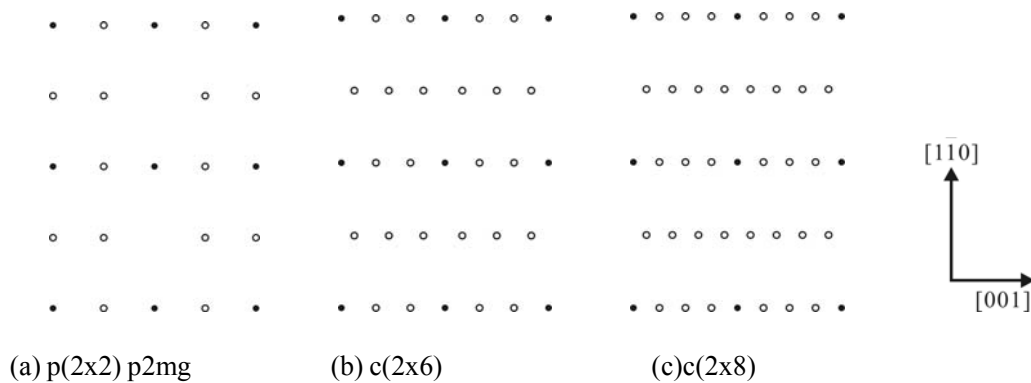
Fig.4.4 LEED pattern of Rh(110) with different O coverage, (a) p(2x2)p2mg(0.5ML); (b)c(2x6)(0.66ML); (c)c(2x8)(0.75ML), the black points are original 1x1 points.

When adsorbing O to Rh(110) surface at different coverage, the corresponding LEED pattern will change in an order p(2x2) p2mg→c(2x6) →c(2x8).   Furthermore, during K and O coadsorption, the metastable 10x2 structure can be a stable structure, as also shown in fig.4.9.

Structures with N

In the experimental condition of our experiments, when N is adsorbed on Rh(110), it will induce a 3x1 or 2x1 structure, related to nitrogen coverage of 0.33ML and 0.5ML, respectively, as shown in fig.4.5
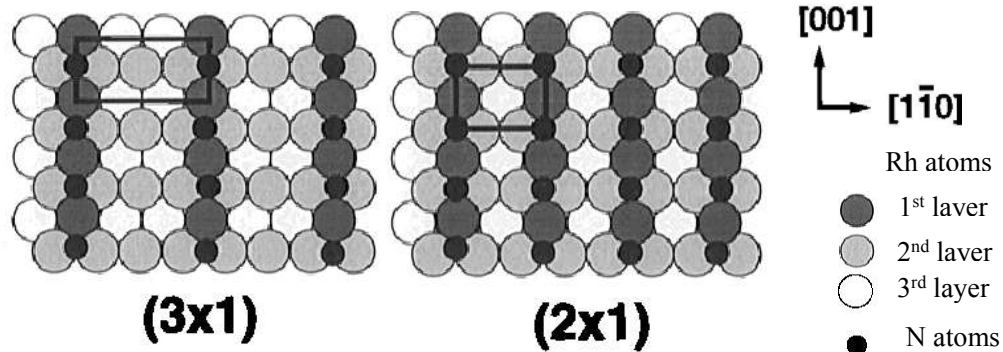
Fig.4.5 Hard-sphere models of 3x1 and 2x1 nitrogen induced reconstruction on Rh(110) (with nitrogen coverage of 0.33ML and 0.5ML), together with a metastable 10x2 structure (modified from[27])

(a) 3x1   (b) 2x1
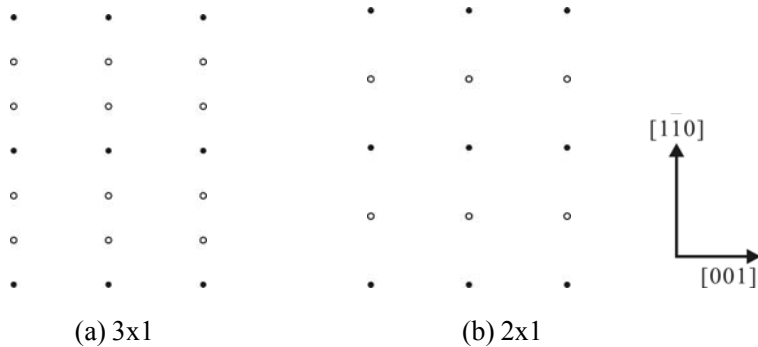
Fig.4.6 LEED pattern of Rh(110) with different N coverage, (a)3x1(0.33ML); (b)2x1(0.5ML) the black points are original 1x1 points.

Typical LEED pattern related to N adsorption is 2x1 and 3x1 corresponding coverage of 0.33ML and 0.5ML, as shown in fig.4.6.

Adsorbate structure with K

Generally, when K is added to the Rh(110) surface, the Rh surface reconstructs with (1xn) (n=2, 3, 4) missing row structure.   It is found that K will be adsorb onto the troughs.   With increasing K coverage, the following reconstructions can be found: 1x4, 1x3, 1x2, 1x3, 1x4, with corresponding LEED patterns shown in fig.4.7.
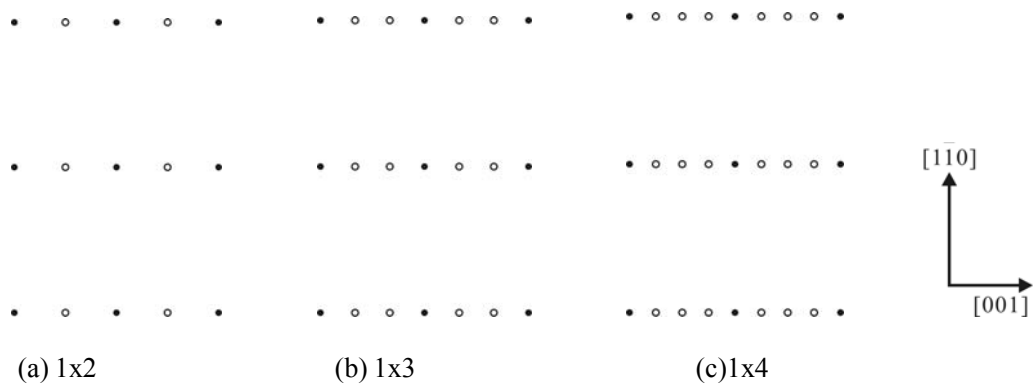
(a) 1x2 (b) 1x3 (c)1x4

Fig.4.7 LEED pattern of Rh(110) with different K coverage, (a) 1x2; (b) 1x3; (c)1x4, the black points are

original 1x1 points.

When K is deposited onto the Rh(110) surface at about 473K, the LEED pattern of the surface changes in the order of 1x4→1x3→1x2→1x3→1x4→1x1.   The phase diagram is shown in fig.4.8 ([26])
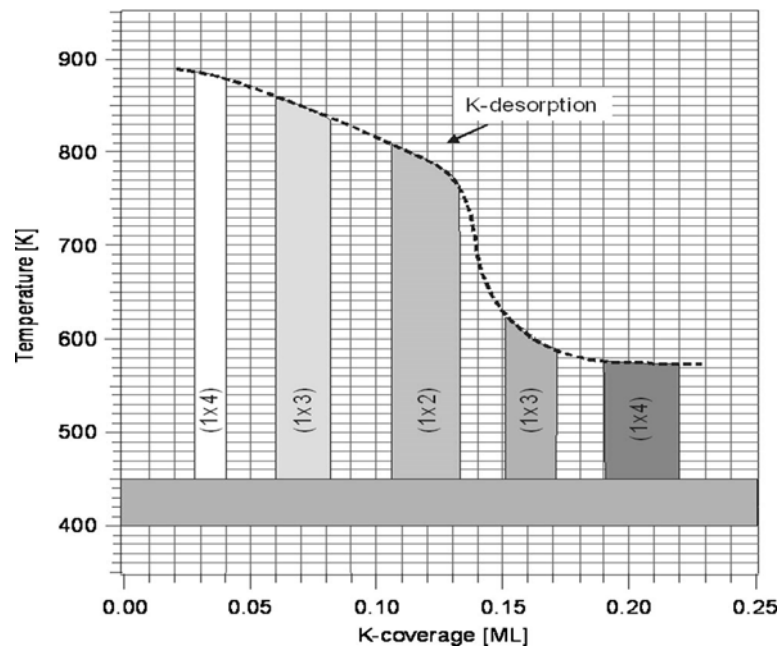
Fig.4.8. LEED phase diagram for Rh(110) at different θ_K ([26])

Structures related to K+O coadsorption

When K and O are coadsorbed on the Rh(110) surface, except 1x4, 1x2 at low oxygen coverage, p(2x2) p2mg and c(2x2n) (n=2,3,4) can be found at higher oxygen coverage.   In addition, 2nx2 (n = 4, 5, 6) structure can also occur.   Fig.4.9(a) shows a typical 2nx2-type LEED structure.
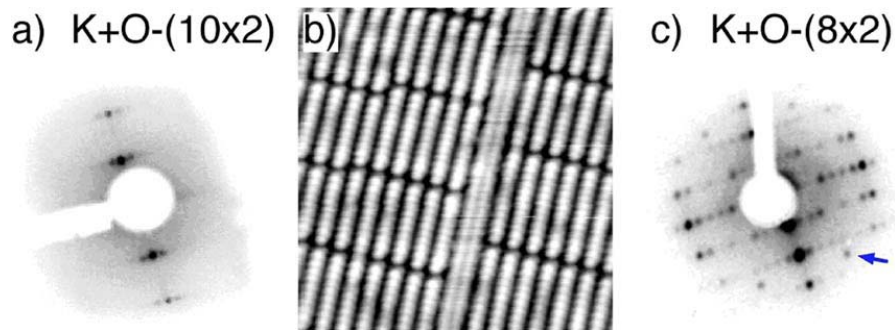
Fig.4.9 (a) LEED pattern of a nonperfect K+O−(10x2) structure with θ_K=0.12 ML saturated with oxygen at 520 K, E_{kin}=56 eV. (b) STM image (120x120 Å^2) of a nonperfect K+O−(10x2) structure. $\theta_K \geq$0.14 ML saturated with oxygen at 520 K. (c) LEED pattern of a well-ordered K+O−(8x2) structure, obtained after the following cycles: oxidation (23 L O$_2$ at 300 K+46 L O$_2$ at 570 K)- reduction (23 L H$_2$ at 660 K)- oxidation (110 L O$_2$ at 660 K). The arrow indicates a LEED spot corresponding to a coexisting c(2x4)surface oxide phase. θ_K =0.16 ML and E_{kin}=80 eV.[26]

Moreover, at very high potassium(>0.12ML) coverage and high oxygen dose (~10^1L), a 2nx2+c(2x4) with missing points structure will appear, which is due to oxide formation.

The phase diagram of LEED patterns of K+O coadsorption is shown in fig.4.10.
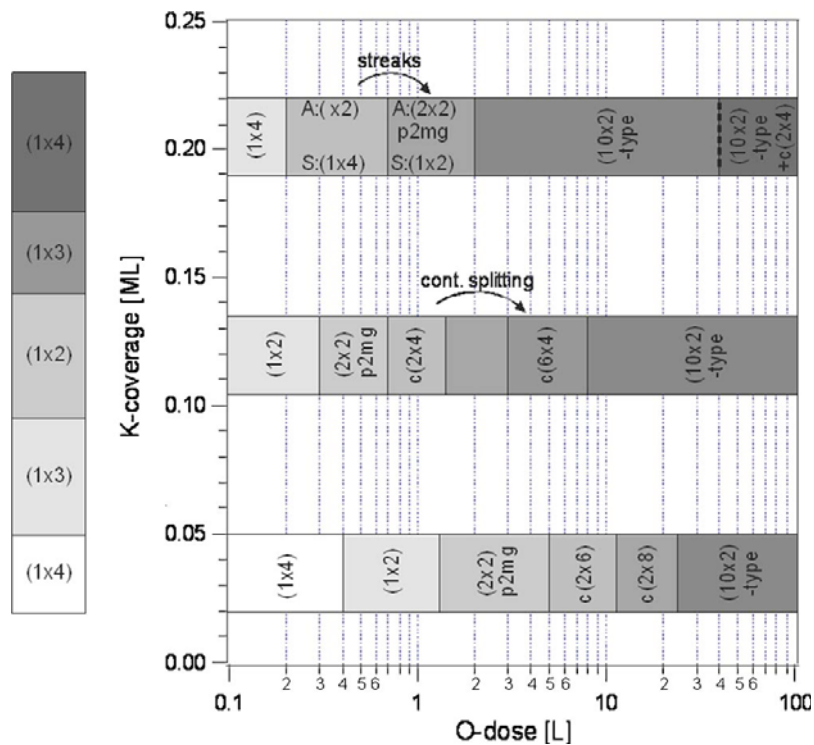

Fig.4.10 LEED patterns observed with increasing oxygen dose by exposing Rh(110) with three different K coverages to O$_2$ (450K<T<570K). In the top panel spots related to the adsorbate (A) and the substrate reconstruction (S) are indicated. The S spots were more intense, and the A spots were weaker and often streaky due to the poorer order of the species [26]

Furthermore, during the K+O coadsorption, according to previous research, a 2nx2 (n =4,5,6) structure and more complicated structures like c(6x4) can appear at different K and

O coverage and temperatures [26], the detailed will not be described here.

4.2 Alkali metals on metal surface

When alkali metal is deposited onto a metal surface, for example, onto copper, due to the lower electronic affinity of the alkali metal, there is a negative charge transfer from the adsorbed alkali metal atoms to the local metal atoms.   Therefore dipoles are formed on the surface, depending on the sign the work function of the metal surface can be decreased or increased.   The typical work function change by alkali metal on a metal surface is shown in fig.4.11, as the Na coverage increases, the work function of Cu reaches a minimum and then slightly increases again until the surface is saturated.   Then the work function begins to approach the work function of bulk alkali metal.
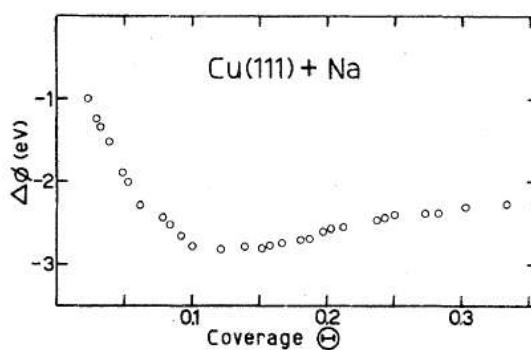
Fig.4.11 Work function change of Cu(111) substrate versus Na coverage, the monolayer is close packed at about θ_{Na} =0.5ML [28]

Alikali metal in catalysis

Alkali metals play an important role as so called electronic promoters in heterogeneous catalysis, for example in chemical industry, the famous ammonia synthesis by the Haber-Bosch process, hydrocarbon production by the Fischer-Tropsch process. It can significantly increase the production rate by several orders of magnitude.   In NO reduction, alkali metal atoms can reduce the activation energy for NO dissociation and stabilize the adsorption of an electronic negative reactant like NO, so that K can be a very effective electronic promoter in the NO+H_2 /K/Rh(110) reaction as well [29].
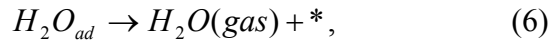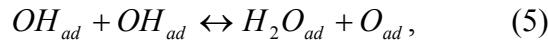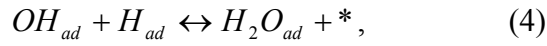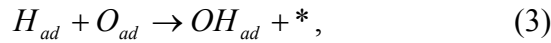
4.3. H_2+ O_2 / Rh(110) system (unpromoted)

Previous experimental results

The unpromoted H_2+O_2 / Rh(110) system under experimental conditions (T:500-650K, p: $\sim 10^{-8}$-10^{-6} mbar) is bistable, according to previous experiments, reaction fronts can be found [30].

Mechanism

The reaction mechanism of a H_2+O_2 reaction on the unpromoted Rh(110) surface is shown as below [31]:

$$H_2 + 2^* \leftrightarrow 2H_{ad}, \qquad (1)$$

$$O_2 + 2^* \leftrightarrow 2O_{ad}, \qquad (2)$$

$$H_{ad} + O_{ad} \rightarrow OH_{ad} + ^*, \qquad (3)$$

$$OH_{ad} + H_{ad} \leftrightarrow H_2O_{ad} + ^*, \qquad (4)$$

$$OH_{ad} + OH_{ad} \leftrightarrow H_2O_{ad} + O_{ad}, \qquad (5)$$

$$H_2O_{ad} \rightarrow H_2O(gas) + ^*, \qquad (6)$$
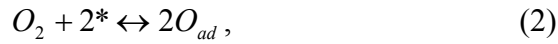
(* denotes a vacant adsorption site)

Under our experimental condition (T>500K) the water desorption (6) can be considered as an irreversible process.

$$\frac{\partial \theta_H}{\partial t} = \tilde{k}_1 p_{H_2}(1-\theta_H-\beta\theta_O)^2 - \gamma_1 k_1 p_{H_2}(1-\theta_H)^2 - k_2\theta_H{}^2 - 2k_3\theta_H\theta_O + D_H\frac{\partial^2\theta_H}{\partial x^2} \qquad (4.1)$$

$$\frac{\partial \theta_O}{\partial t} = k_4 p_{O_2}(1-\theta_H-\theta_O)^2 - k_5\theta_O{}^2 - k_3\theta_H\theta_O + D_O\frac{\partial^2\theta_O}{\partial x^2} \qquad (4.2)$$

θ_H and θ_O are the coverages of H and O on the substrate. The rate constant of adsorption of H_2 and O_2 are denoted by k_1 and k_4, and the rate constant of their desorption is denoted by k_2 and k_5. The k_3 is the rate constant of OH formation in step (3). γ denotes the influence of defects on H_2 adsorption, and β denotes the inhibition effect of O on H_2 adsorption. D_H and D_O are the diffusion constants factor of H and O atoms on the surface.

Formation of reduction fronts
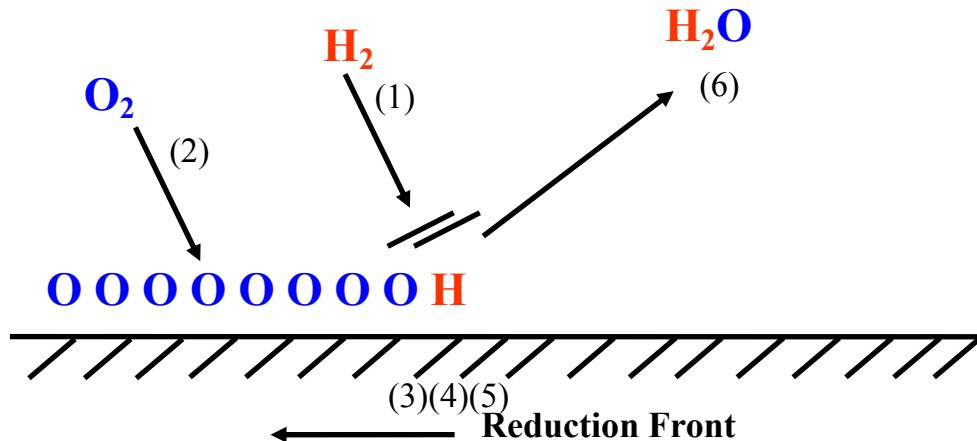
Fig.4.12 Formation of reduction fronts in unpromoted $H_2 + O_2$ /Rh(110) reaction

Starting from an oxygen covered surface, first all adsorption sites are occupied by O atoms, except near some defects. When H_2 pressure reaches a certain value, H_2 will adsorb dissociatively near those defects. Then the H atoms react with neighboring O atoms. The product H_2O desorbs under our experimental conditions (T>500K) and leave a bare surface. On the vacant sites H_2 can adsorb again. Thus reduction fronts are formed, as shown in fig.4.12.

4.4. $H_2 + O_2$ / Rh(110) system promoted by potassium

Previous experimental results

After depositing K onto the Rh(110) surface, if starting from a oxygen covered surface, the reduction fronts can still exist if the reaction, then due to the mass transport of K irregular Stationary pattern can result, if starting from a reduced surface with constant H_2 pressure, more regular Turing-like stationary pattern can be formed [13, 32]. In both cases, the process is not reversible, so it is not really bistable anymore.

Modeling

For the H_2+O_2 / K/Rh(110) system, here comes the second part: the diffusion of K, (under our experimental condition, the K desorption is ignorable), and considering the two processes: the reaction and the diffusion of K, finally a mathematical model can be

constructed.

The equation of (4.1) is changed into

$$\frac{\partial \theta_H}{\partial t} = \widetilde{k}_1 p_{H_2}(1-\theta_H-\beta\theta_O)^2 - \gamma_1 k_1 p_{H_2}(1-\theta_H)^2 - k_2\theta_H{}^2 - 2k_3\theta_H\theta_O + D_H\frac{\partial^2\theta_H}{\partial x^2} \qquad (4.3)$$

Equation (4.2) is unchanged.   And K diffusion is described by:

$$\frac{\partial \theta_K}{\partial t} = \nabla(D_K\nabla\theta_K) - \nabla[\frac{D_K\widetilde{\theta}_K(1-\widetilde{\theta}_K)}{RT}E_b\nabla\theta_O] \qquad (4.4)$$

k_1 in equation (4.1) replaced by

$$\widetilde{k}_1 = k_1\exp(-\delta\theta_K) , \text{ and } \quad \widetilde{\theta}_K = \frac{\theta_K}{\theta_K^{max}} , \quad \theta_K^{max} = 0.22$$

With a initially homogeneously K covered Rh surface, reaction fronts start from oxygen covered surface.   Reduction fronts as in the unpromoted system will still be formed, but due to the chemical affinity between K and O, there will be a redistribution of K.   Finally an irregular stationary pattern results [12].   The front motion is irreversible, which means for this situation, the system is no longer bistable.   In later experiments in NO+H$_2$/K/Rh(110) system, for $\theta_K \geq 0.05$ML, similar phenomena again appeared.   For convenience of description, we still name the region in the bifurcation diagram "bistable".

4.5 NO+H$_2$/ Rh(110) system (unpromoted)

Previous experimental results

In the unpromoted NO+H$_2$/Rh(110) system, under a constant NO pressure (1.6x10^{-6} mbar) pattern formation in the temperature range of 500-650K was investigated, and different patterns like wave fragments, spiral waves and target waves (rectangular or elliptic) , reduction fronts (rectangular or elliptic) were found, depending on different H$_2$ pressure[11, 14].   A complete bifurcation diagram in temperature range of 500-650 was built from previous experiments, as shown in fig. 6.1 [33]

Mechanism of the reaction

In our experimental condition on rhodium (110) surface (Temperature: 500-600K, Pressure: 10^{-6} to 10^{-4} mbar, the reaction can be described by the sequence below, beside the sequence

(1)-(6) described in 4.3, there are additional processes as below:

$$NO + * \rightarrow NO_{ad} \, , (7)$$

$$NO_{ad} + * \rightarrow N_{ad} + O_{ad} \, , (8)$$

$$2N_{ad} \rightarrow N_2 + 2* \, , (9)$$
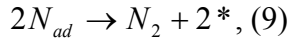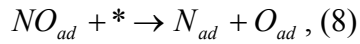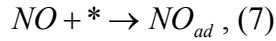
In the experimental conditions here (Temperature: 500-600K, Pressure: 10^{-9} mbar to 10^{-4} mbar), the NH_x species can be neglected, so the process for them will not be shown.

Excitation mechanism

The unpromoted $NO+H_2/Rh(110)$ system can be bistable when H_2 pressure is high (depending on the temperature and NO pressure, can be seen in bifurcation diagram as shown in fig.6.1 in Chapter VI [33]).

However, at lower H_2 pressure, this system can be excitable, where spiral waves and target patterns can be found.   The excitation mechanism is as below [34]:

1. First, NO molecules adsorb onto the surface dissociatively and nitrogen soon desorbs under our experimental condition (T>500K), so all the adsorption sites of the surface were covered by oxygen except near some defects.   When the H_2 pressure reaches a certain value, H_2 will adsorb dissociatively near those defects.   Then the H atoms react with neighboring O atoms.   The product H_2O desorbs under our experimental conditions (T>500K) and leave a bare surface.

2. On the bare surface thus created both NO and H_2 can adsorb but since oxygen is removed by hydrogen, nitrogen accumulates leading to the (3x1)/(2x1)-N phases.   On On the vacant site after the water desorption, NO can also be adsorbed, formed a N+O coadsorption structure,

3. On the nitrogen covered surface NO can still adsorb disscociatively while the sticking coefficient of hydrogen is strongly reduced.   A mixed c(2x4)-2O,N overlayer is formed

4. The strong repulsion between adsorbed oxygen and nitrogen destabilizes the nitrogen, so the nitrogen desorbs.   The c(2x4)-2O,N layer is converted into c(2x6)-O layer, with only oxygen left.

The whole process is schematically shown in fig.4.13.   In the excitable state, this process repeatedly takes place.   Thus pulses are formed.
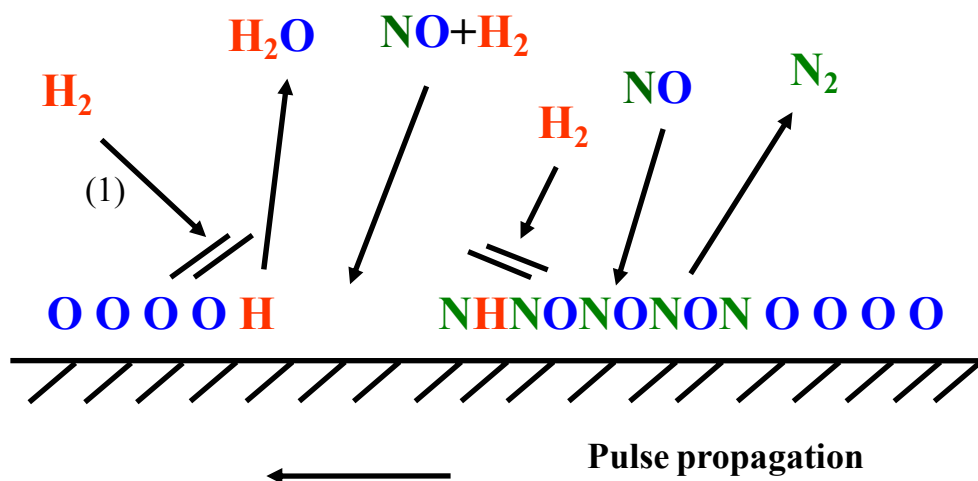
Fig.4.13. Excitation mechanism of the unpromoted NO+H$_2$ /Rh(110) reaction.

4.6 The NO+H$_2$/ Rh(110) system promoted by potassium

Previously, some experiments in the NO+H$_2$/K/Rh(110) system were conducted and some results were found, for example, the "zebra-like" pattern [35]. But a systematic investigation in a wide temperature range (from 500K-600K) and different potassium coverage is needed, which is described in the following part of this thesis.

V. Surface Characterization

5.1. Estimation of K coverage by combination of LEED and AES

During the reaction experiments, it is desirable to know the K coverage before and after the reaction, and to determine whether the K distribution is homogeneous. From the introduction of AES in chapter III, we can see that under our experimental conditions (θ_K <0.22ML), the Auger signal from K is approximately linear proportional to coverage of K. The Auger signal of Rh is monotonously depending on K coverage, therefore the signal ratio of K to Rh is monotonously depending on the K coverage (which can be estimated from LEED pattern after K was deposited on the clean sample).

It was also found that the Rh intensity doesn't change much (<1%) after the K deposited Rh surface was saturated by NO. So in the experiments of pattern formation, this method can also be applied after the reaction, when the surface is covered by NO and K together.

To accomplish this, first an Auger spectrum of a clean Rh(110) surface was taken, then K was deposited onto the sample at about 473 K at a certain amount (determined from LEED patterns), then the AES spectrum was taken again and compared with the Auger spectrum of the clean surface, because in the Auger spectra, the largest peak of K is at ~250eV, and the largest peaks of Rh are at ~250eV and 300eV, so the ratio of K and Rh intensity can be approximately obtained from:

$$\alpha = \frac{I'(250eV)}{I'(300eV)} - \frac{I(250eV)}{I(300eV)},$$

I (250eV), I (300eV): peak to peak intensity of Auger signal at 250eV and 300eV on clean Rh surface, contributed from rhodium

I′(250eV): peak to peak intensity of Auger signal at 250eV Rh surface after potassium is deposited, contributed from rhodium and potassium.

I′(300eV): peak to peak intensity of Auger signal at 250eV on clean Rh surface, contributed from rhodium
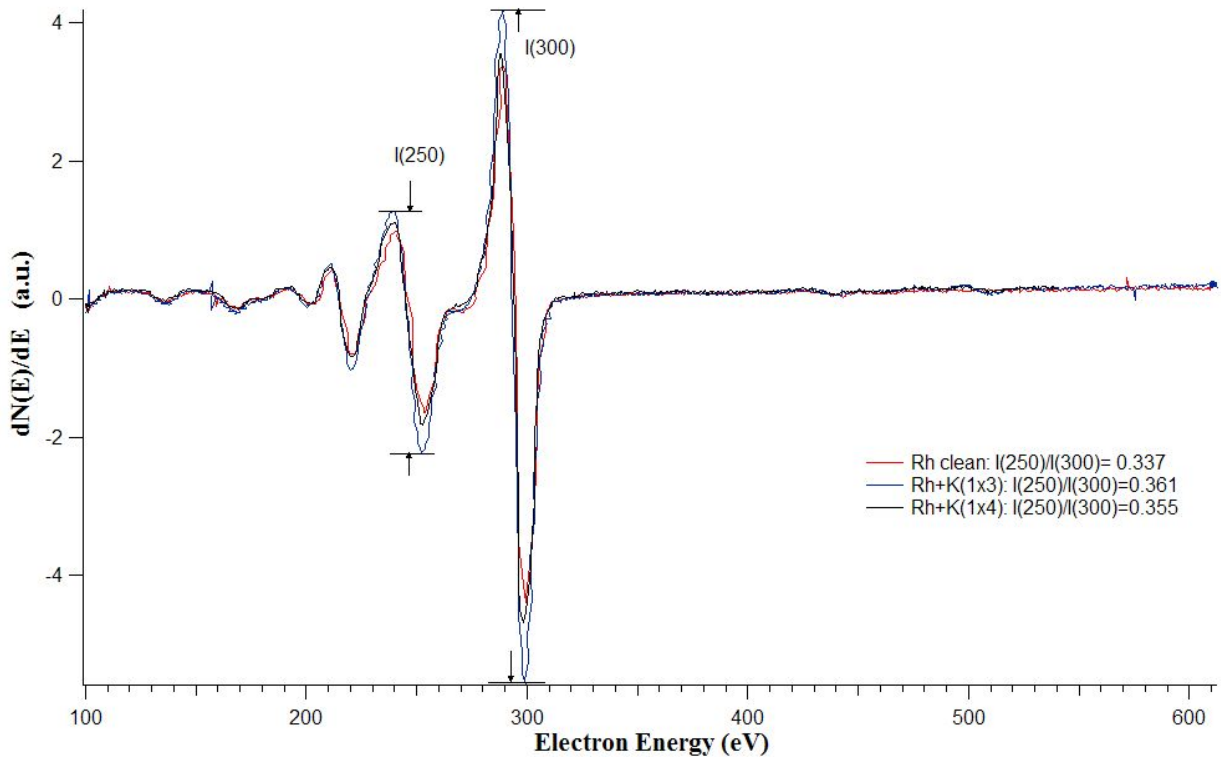
Fig.5.1. Auger spectra of Rh(110) at different K coverage (clean surface, $\theta_K \sim 0.025ML$ for LEED (1x4), and $\theta_K \sim 0.067ML$ for LEED (1x3)). Deposition condition for K is: I=6.00A, T=473K)

For an example, Auger spectra of Rh(110) surface for different K coverage is shown in fig.5.1. From the ratio at different conditions, the corresponding value of α is determined. For more precise quantitative measurement, we have to apply XPS.

5.2. Work function change during K+O coadsorption

It has been theoretically discussed about the work function (WF) change by oxygen coadsorbed with K ([36]).   In our experiments we applied the Kelvin probe for the WF measurements.

First of all, the work function change of sample without potassium deposited was measured during O_2 adsorption, in order to check them with the literature values [36].

Then the sample was cleaned.   Afterwards K was deposited at a certain coverage onto the surface, the WF was measured on the rhodium surface with only K covered, then O_2 was introduced again, and the work function change during the O_2 adsorption.   The coverage of K was determined by corresponding LEED pattern.   In this way, the work function change during O_2 adsorption at different K coverages was measured.
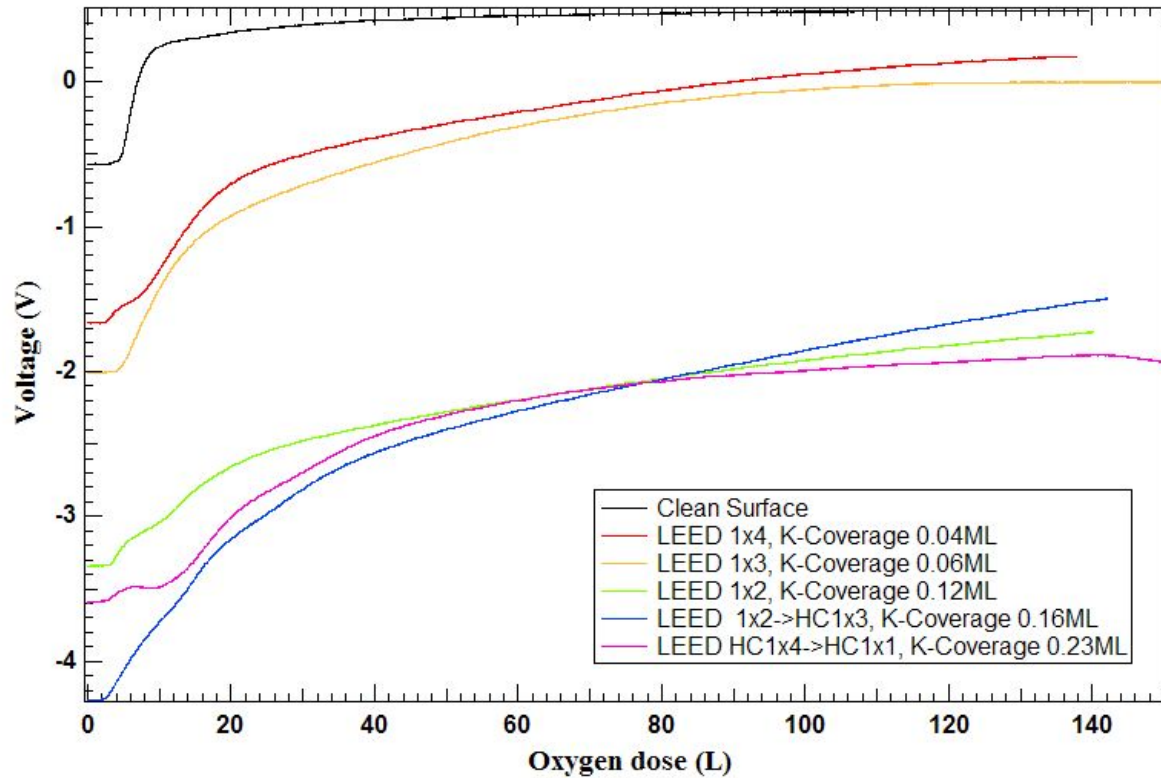
Fig.5.2 Work function change with K deposited on Rh(110) surface during oxygen adsorption,

$P_{O2} = 1 \times 10^{-7}$ mbar, $T = 510$K

From fig.5.2, it can be seen that for different K coverage, the work function change when the surface is saturated during O_2 adsorption is changing.   At zero K coverage, the saturation work function change is fairly coincident with the theoretical prediction, which is about 1eV [36].   With increasing K coverage, the saturation work function change during O_2 adsorption was slowly increasing.   At $\theta_K \sim 0.16$ML, the change of   the work function (when the surface is saturated by O) reaches a maximum value of about 2.8eV, which is significantly larger than the theoretical prediction of ~ 1.77eV [36].   Additionally, as shown in fig.5.3, at $\theta_K \sim 0.16$ML, the surface without O_2 adsorption has lowest work function of -4.3eV.

Connecting the initial points of those curves, the work function change of clean surface depending on different K coverages can also be built, as shown in fig.5.3.
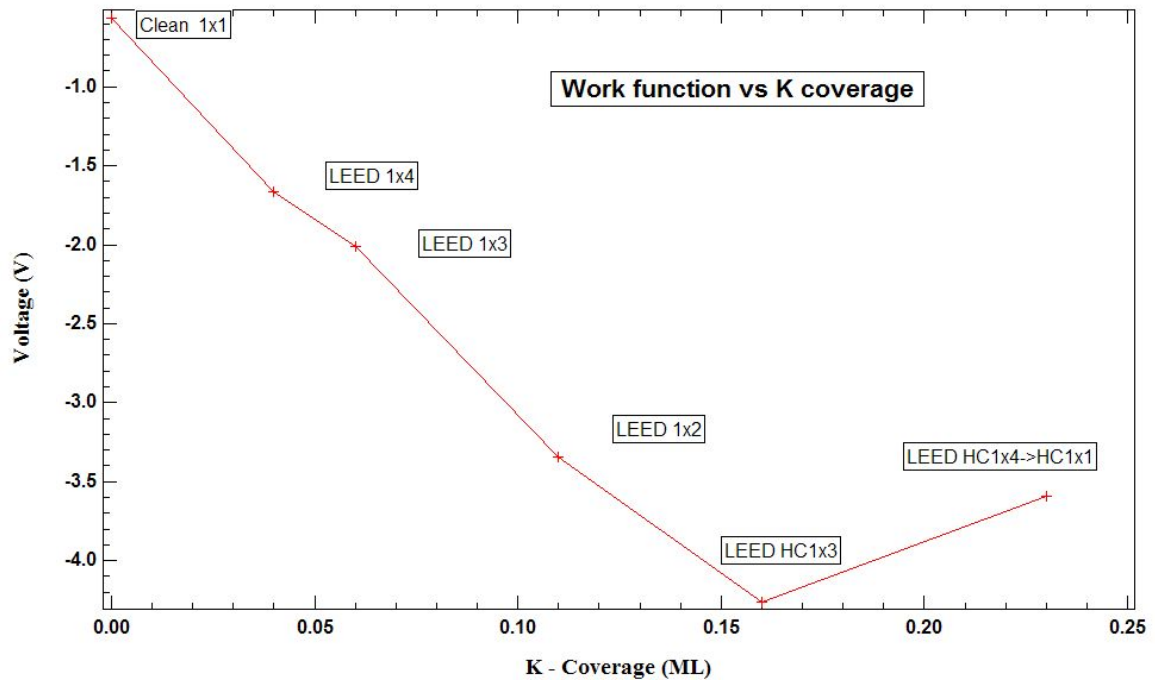
Fig.5.3 work function change for different K coverage on clean Rh(110) surface, T = 510K

Furthermore, from fig.5.2 it can be seen after O_2 was introduced for 1800s, the work function of the surface became quite flat (except the curve for $\theta_K\sim0.16ML$), which indicates that O_2 led to saturation. The saturation value of work function as a function of the potassium coverage is shown in fig.5.4. This will be useful in our later discussion for coverage estimation using PEEM.
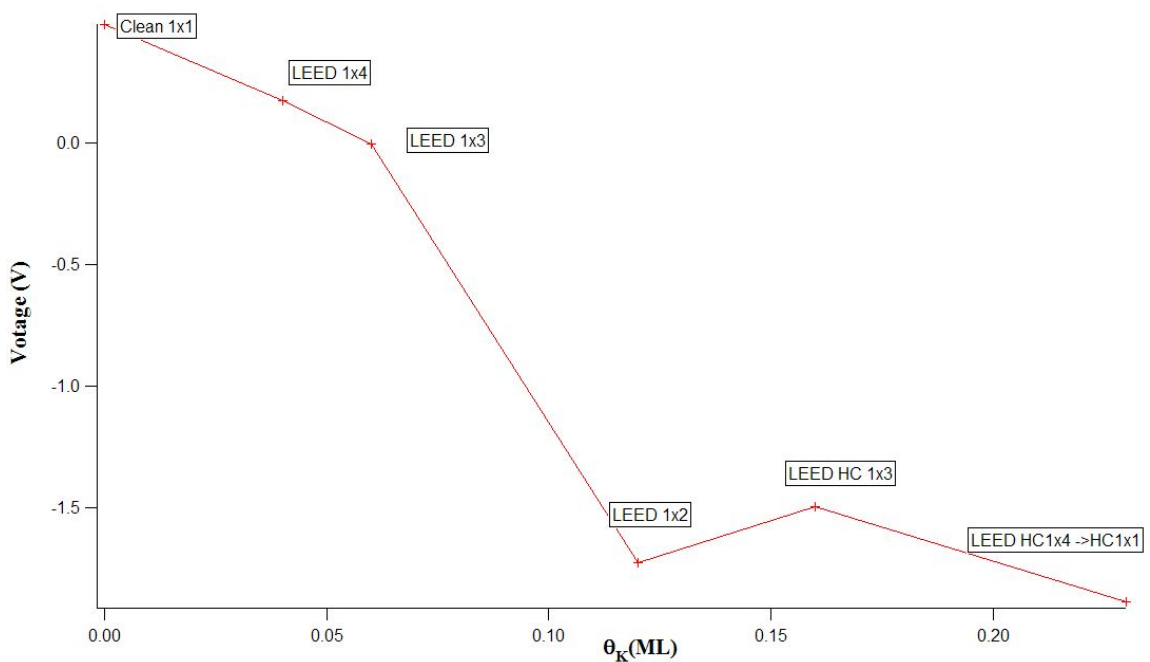
Fig.5.4 Work function vs θ_K , when O_2 adsorption was saturated roughly at t = 1800s (corresponding oxygen dose was 135L), $P_{O_2} = 1 \times 10^{-7}$ mbar, T = 510K),

5.3. Calibration of coverage by XPS

To calibrate the coverage of N, O and K coverage locally, we first took reference spectrums of each element. Depending on different coverage of the adsorbate alone, there are different corresponding LEED patterns. For nitrogen, the corresponding coverage of the (2x1)-N structure is 0.5ML. For oxygen, the corresponding coverage for pattern c(2x8) is 0.75ML. For potassium, the corresponding coverage is 0.08ML for LEED pattern (1x3), and 0.12ML for LEED pattern (1x2). The ratio of the XPS signal from different elements versus the XPS signal from Rh was calculated and taken as reference. In later experiments, the ratios of N, O and K versus Rh were compared with the reference ratio. In this way, the absolute coverage was obtained.

To control the K amount which is deposited, K is deposited on a clean surface at constant evaporation current, and XPS series of K and Rh were taken. Comparing the ratio of K and Rh with the reference value, we get the coverage versus time curve of the K evaporator. One can assume that during a short time period the characteristics of the evaporator don't change very much. So in the later experiments, the K amount which is deposited can be controlled by choosing the appropriate deposition time.

The calibration of coverage was done generally by comparison of LEED phase diagram of K, N, O and XPS peak intensity under different coverage.

For optimized signal, N1s, O1s, K2p and Rh3d were chosen as characterization reference, and photon energy of 459eV is chosen to measure N1s, K2p and Rh3d signal, photon energy of 635eV was chosen to measure O1s signal.

5.3.1 Calibration of K coverage

Reference XPS spectra were taken for certain adlayer structure of Rh(110)/K as shown by LEED. For example, when depositing K onto the sample, a 1x2 LEED pattern is obtained corresponding to a K coverage of 0.12ML. Then the peak intensity of K and Rh substrate is measured and their ratio is calculated.

This was repeated for different K deposition times, and the XPS spectra of K and Rh were

alternatively taken (with a time delay of 2 seconds between each another), and their ratio of intensity is calculated. Comparing these ratio of K/Rh3d with the one from reference spectra (suppose it is 0.12 ML, corresponding to a 1x2 LEED pattern), and picking out the ratio which is the same with the reference, its corresponding absolute intensity of K peak is X. Suppose the absolute intensity of K peak of another point is I. Then the corresponding coverage of K of this point is calculated from "(I/X) x 0.12" (ML). Finally a curve of K coverage versus the ratio of XPS signal of K and Rh is obtained. With this curve one can easily obtain K coverage from XPS measurement of K and Rh signal.

(1) Reference spectra

LEED(sharp 1x2), corresponding coverage 0.12ML
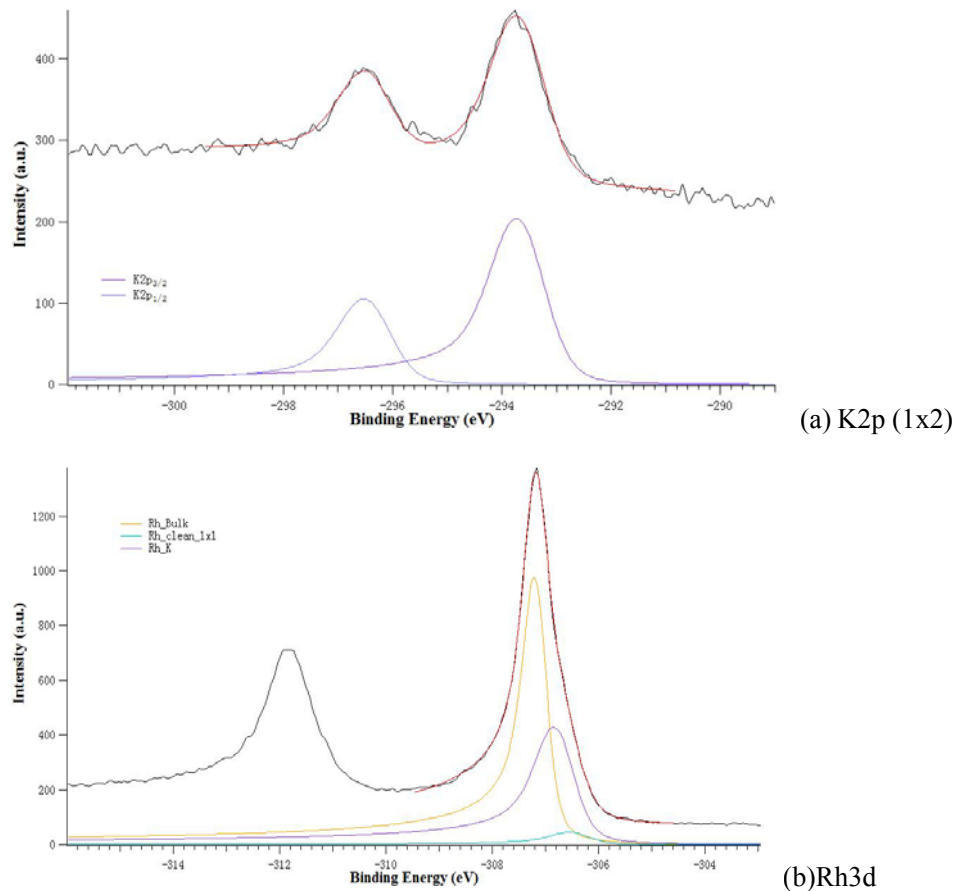
(a) K2p (1x2)

(b)Rh3d

Fig.5.5. XPS reference spectrum for coverage calibration: (a) K2p (1x2, sharp), (b) Rh3d

K2p absolute intensity(162eV, 2sx32)	573.392
Rh3d absolute intensity (148eV, 0.5sx32)	1997.61
Ratio of two intensities (K2p/Rh3d)	0.28704
Ratio of two intensities (K2p/Rh3d), same exposure time	0.071760

(2) Calibration
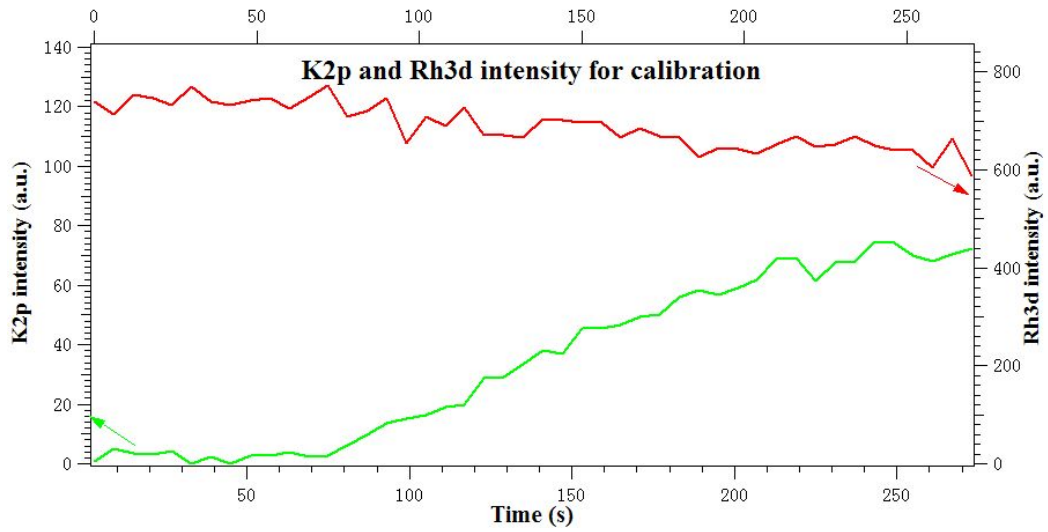
Fig.5.6. K2p and Rh3d intensity (fitted) during deposition

The XPS signal of K2p and Rh3d were taken alternatively (with a time delay of 2s), as shown in fig.5.6.
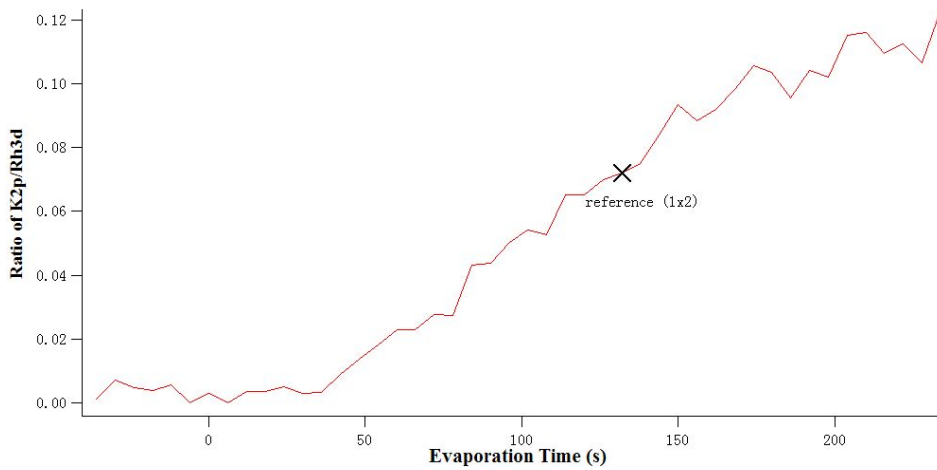
Fig.5.7 Ratio of K2p and Rh3d intensity versus time

As shown in fig.5.7, the ratio of K2p and Rh3d intensity is calculated and shown versus time.

The point which matches the 1x2 reference spectrum is marked by black cross, with an absolute intensity of 49.2177.

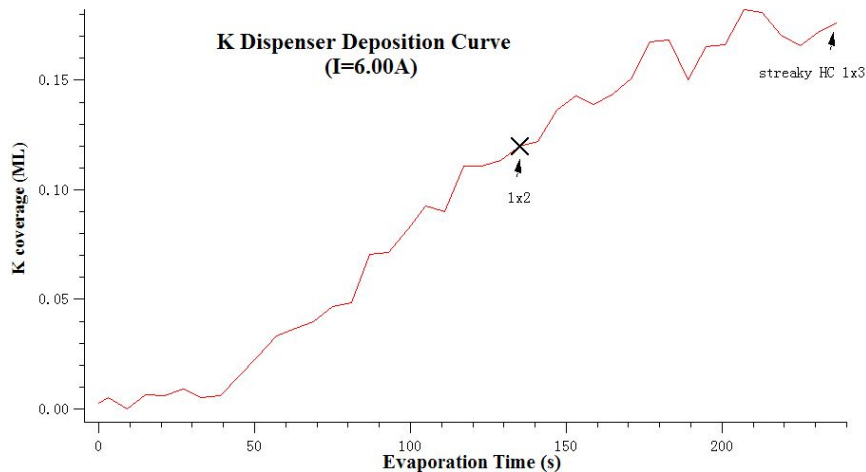**Fig.5.8.** Calculated K coverage versus time, the second arrow marks the LEED pattern in the end

From result of fig.5.8, the coverage for all points is calculated by (absolute intensity) * 0.12/49.2177, so we get the K coverage curve versus evaporation time as shown in fig.5.8. This can be also used as characteristic curve of the K dispenser, for estimating deposited K amount per time.
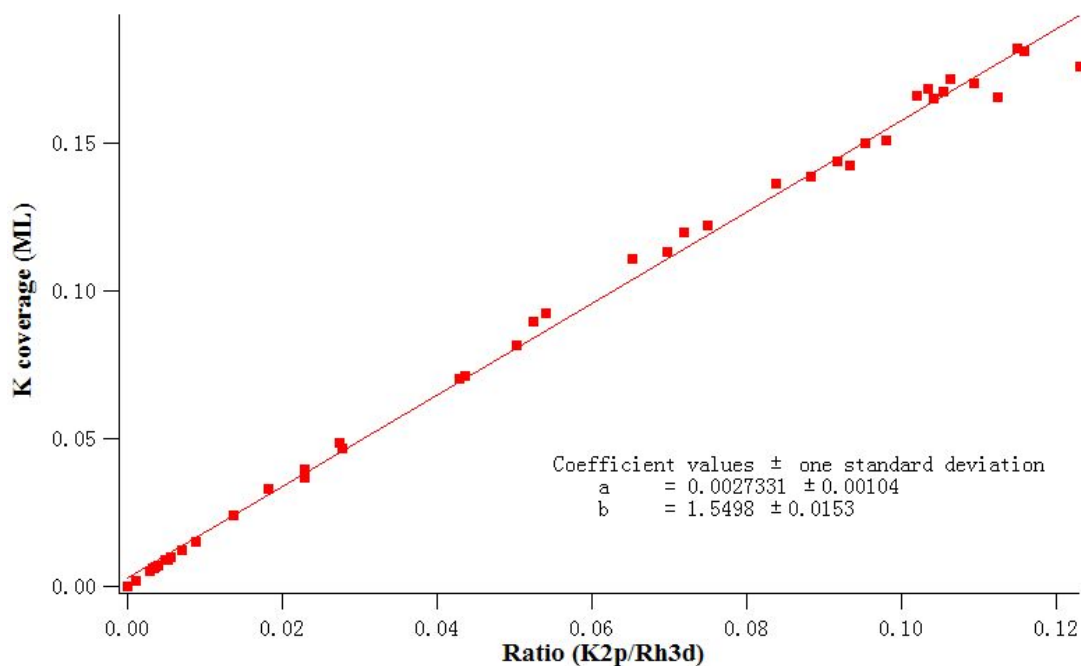
Fig.5.9 Calculated K coverage versus ratio of K2p and Rh3d intensity

From fig.5.9 we get a equation to calculate K coverage from the ratio of K2p and Rh3d XPS intensities, in the form of $y = a + bx$, where y is the K coverage, and x is the ratio of K2p and Rh3d XPS signal. The error is about 1%, which is reasonably well for our other experiments.

5.3.2 Calibration of N coverage

For the calibration of nitrogen coverage, similar process like in the measurement for K coverage may not work, since it is hard to make nitrogen titration in our experiments. So here we calibrate the nitrogen coverage in a different way. We measure the N1s and corresponding Rh3d signal intensity alternatively during a reaction, follow the N1s/Rh3d ratio changing with time, pick out the N1s/Rh3d ratio which matches the (2x1)-N reference measurement, and record the absolute intensity of N1s at that point as reference. Thus we can get finally the coverage of all the other points.

(1) Reference spectra

N(2x1), corresponding coverage of 0.5ML
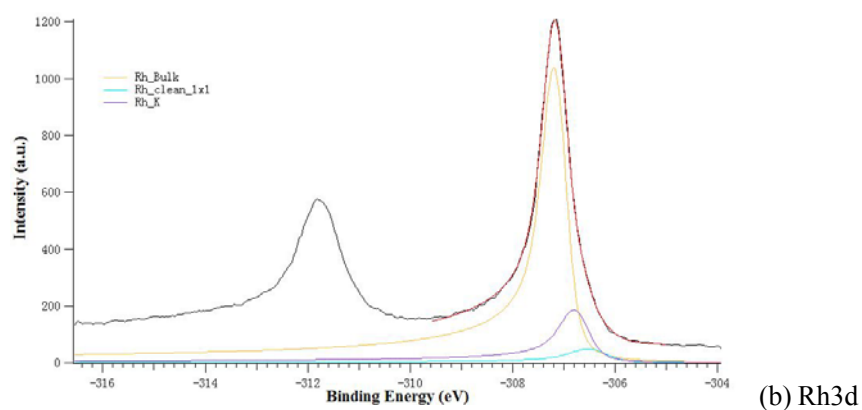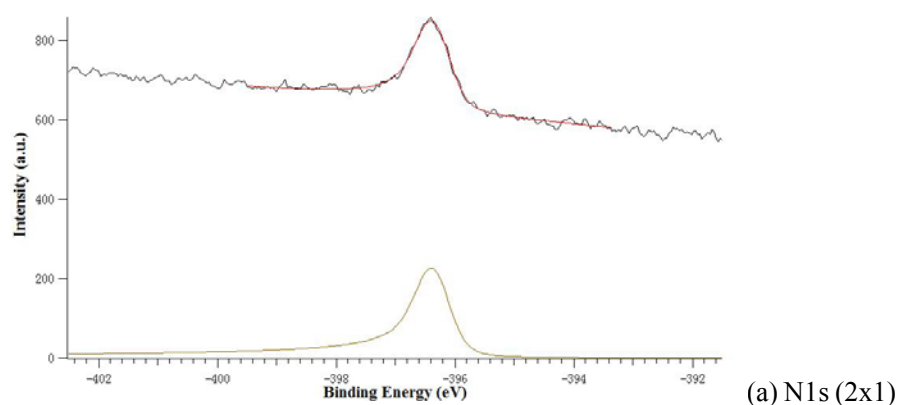
(a) N1s (2x1)

(b) Rh3d

Fig.5.10. XPS reference spectrum for coverage calibration, (a) N1s (2x1) (V_{MCP} =1300V); (b) Rh3d

N1s absolute intensity(162eV, 2sx32)	50.0638
Rh3d absolute intensity (148eV, 0.5sx32)	395.836
Ratio of two intensities I(N1s)/I(Rh3d)	0.12647611637

(2) Calibration
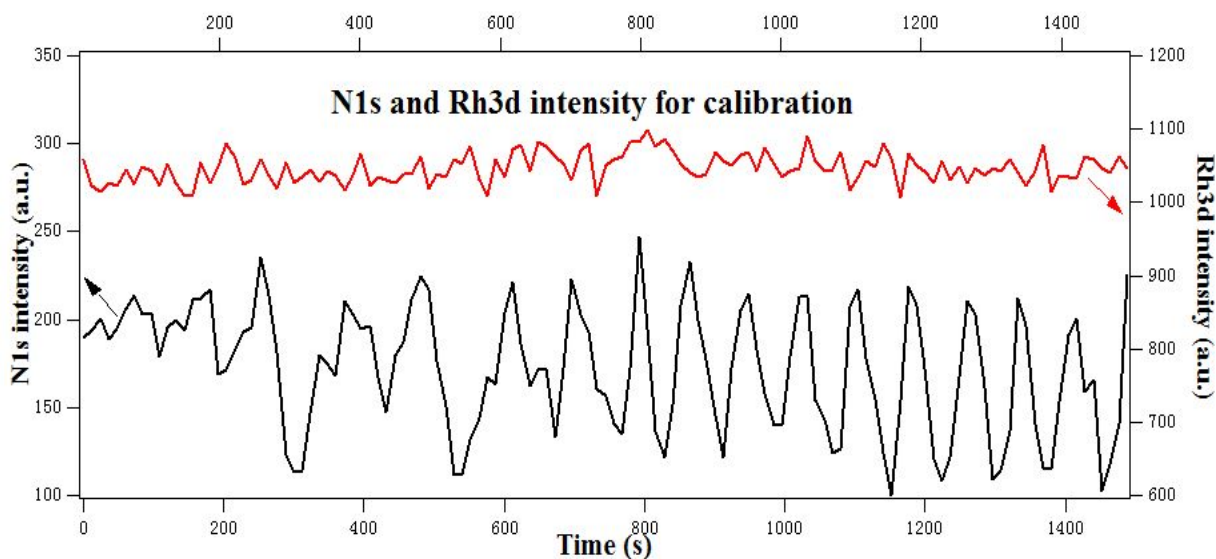
Fig.5.11. Absolute XPS intensity of N1s and Rh3d taken alternatively (with a time delay of 2s between each other) during reaction on the unpromoted Rh(110) surface.   The peaks of XPS signal of N1s and Rh3d are fitted by IGOR separately

In order to demonstrate this method, we follow the reactions of NO and H_2 on the unpromoted Rh(110) surface and the N1s and Rh3d signals were taken alternatively, as shown in fig.5.11.
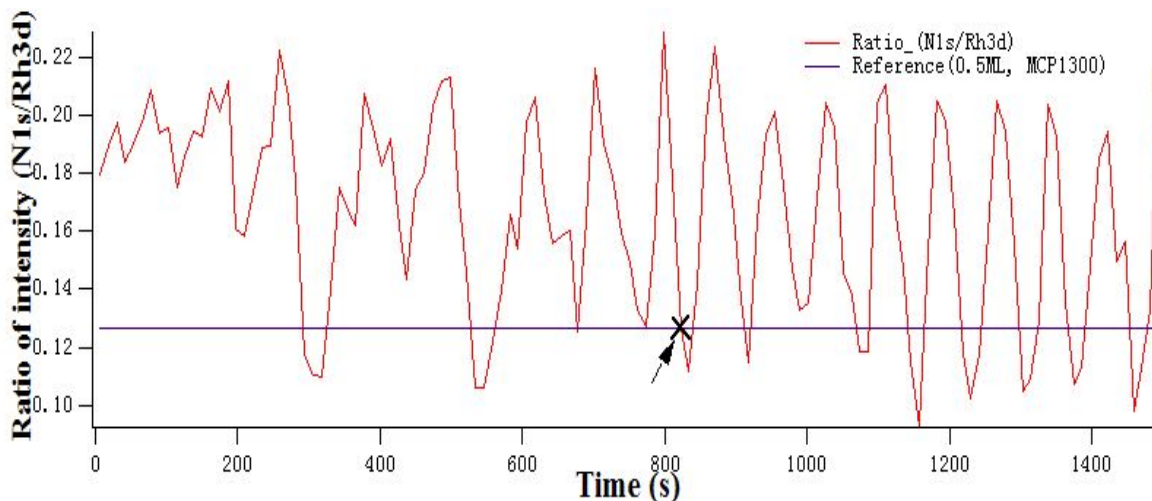
Fig.5.12. Ratio of N1s and Rh3d intensity versus time, point taken as reference to calculate marked by black cross

The point at time 816s, marked by black cross in fig.5.12, has a similar intensity ratio of N1s and Rh3d as the (2x1)-N reference value : ~0.12651.   This point is taken as reference for a coverage of 0.5ML.
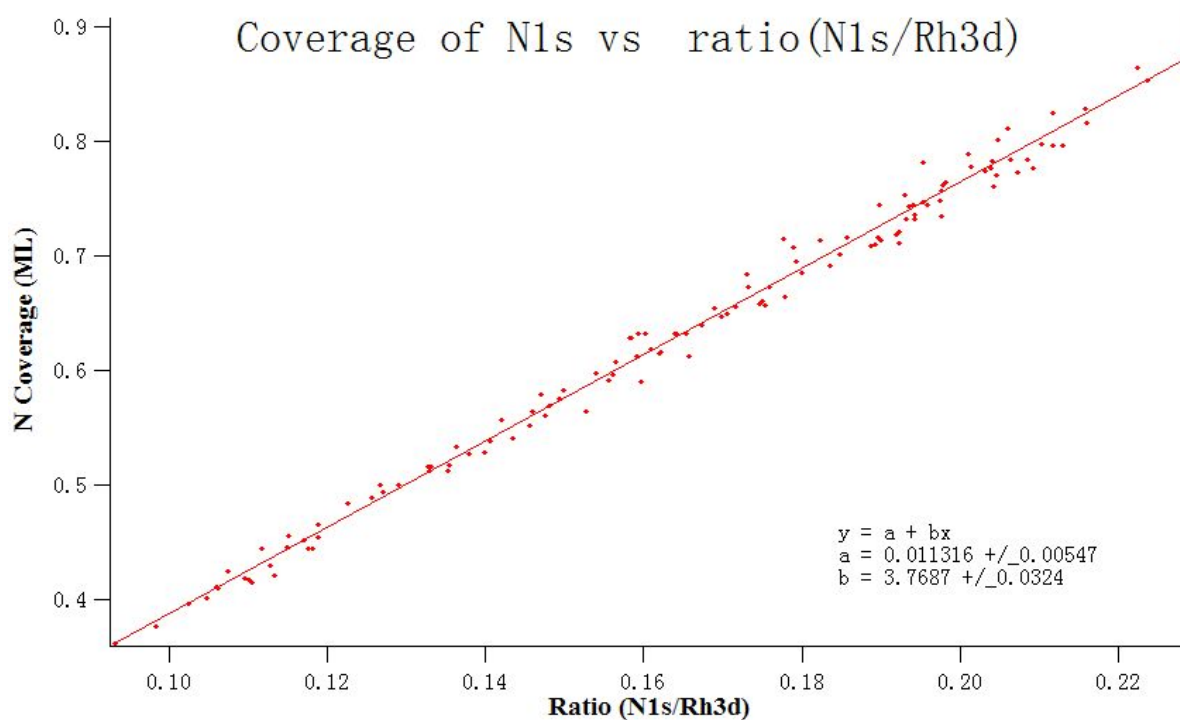
Fig.5.13. Relationship of Nitrogen coverage and ratio of N1s and Rh3d intensities

From the calculation, we get the variation of N coverage and of the ratio of N1s/Rh3d peak intensities (Here we use line fitting).   As shown in fig.5.13, the relationship of nitrogen coverage vs ratio of N1s/Rh3d intensities is quite linear.   The error of the line fitting is about 2%.   The equation can be used for later calculation of N1s coverage, especially for those spectrums where the N1s and Rh3d were taken alternatively.

5.3.3 Calibration of O coverage

(1) Reference spectra

O(c(2x8), corresponding coverage 0.75ML
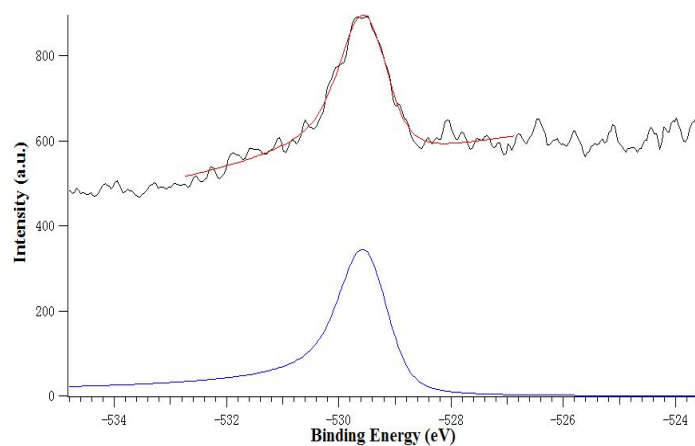
(a) O1s (c(2x8), 0.75ML)
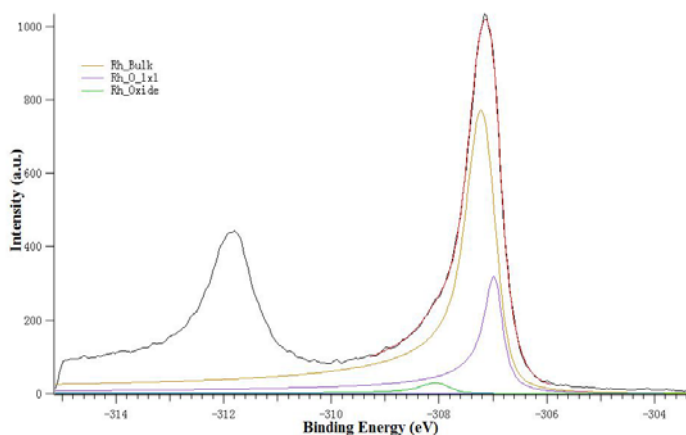
(b) Rh3d (hv=635eV)
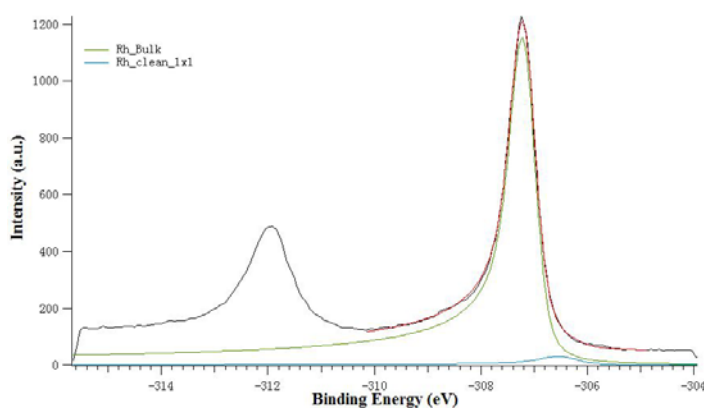
(c) Rh3d (hv=459eV)

Fig.5.14. XPS reference spectrum for coverage calibration: (a) O1s c(2x8) ; (b) Rh3d. (hv=635eV)

K2p absolute intensity(105eV, 5sx8)	603.723
Rh3d absolute intensity (323eV, 2.5sx8)	1511.96
Ratio of two intensities I(O1s)/I(Rh3d)	0.39930
Ratio of two intensities I(O1s)/I(Rh3d), same exposure time	0.19965

(2) Calibration

Like the calibration of nitrogen coverage, the calibration of oxygen coverage was also conducted during an reaction in the unpromoted NO+H_2 /Rh(110) system.   The method is the same with the one in nitrogen coverage measurement.
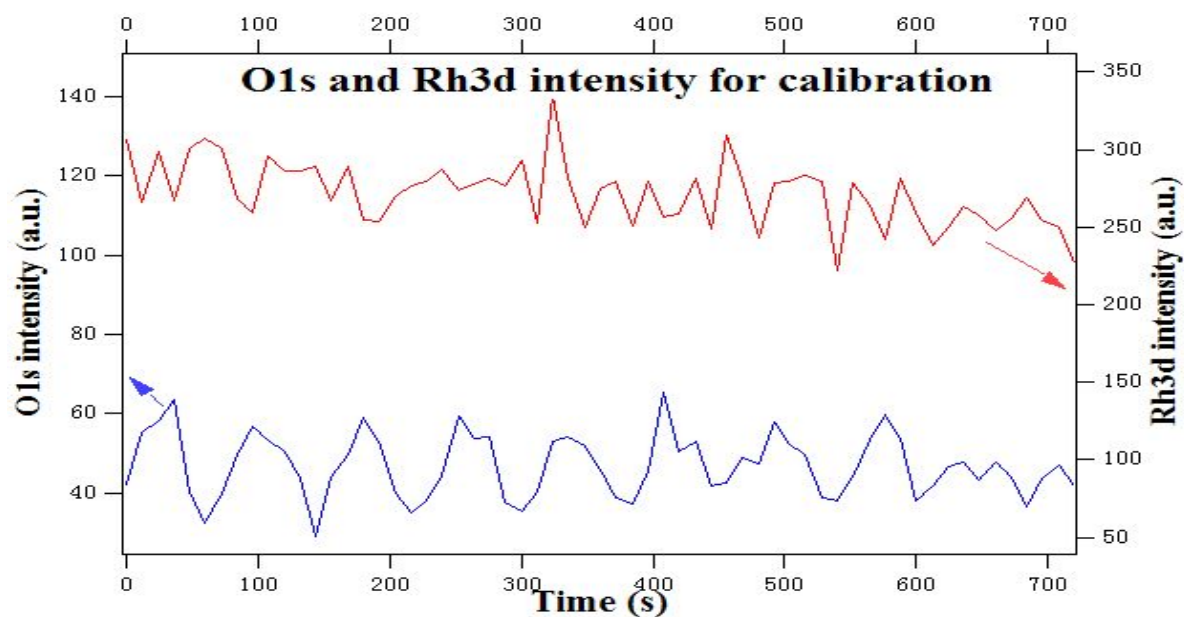
Fig.5.15. Absolute XPS intensity of O1s and Rh3d (fitted) taken alternatively (with a time delay of 2s between each other) during reaction on the unpromoted Rh(110) surface.   The peaks of XPS signal of O1s and Rh3d are fitted by IGOR separately
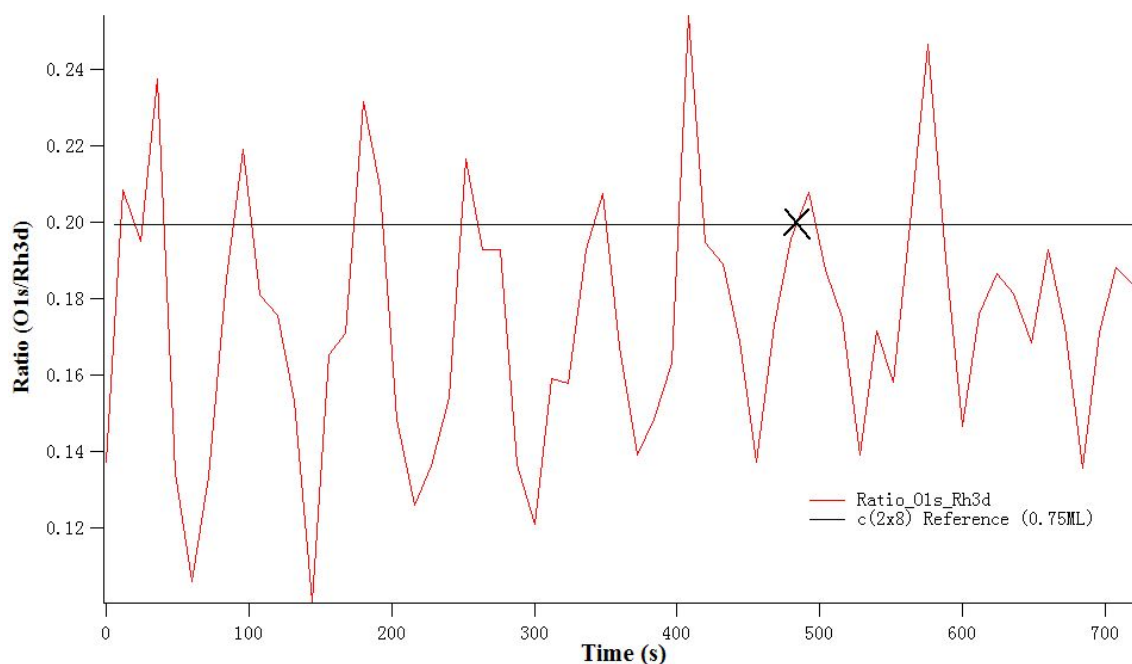
Fig.5.16. Ratio of O1s and Rh3d intensity versus time, point taken as reference to calculate marked by black cross

In this experiment, as shown in fig.5.16, point at about 480s (marked by black cross) has similar ratio of O1s/Rh3d intensity as the c(2x8) reference.   This point is taken as reference for a coverage of 0.75ML.   Afterwards, we can get the relationship of O coverage and O1s/Rh3d ratio,as shown in fig.5.17:
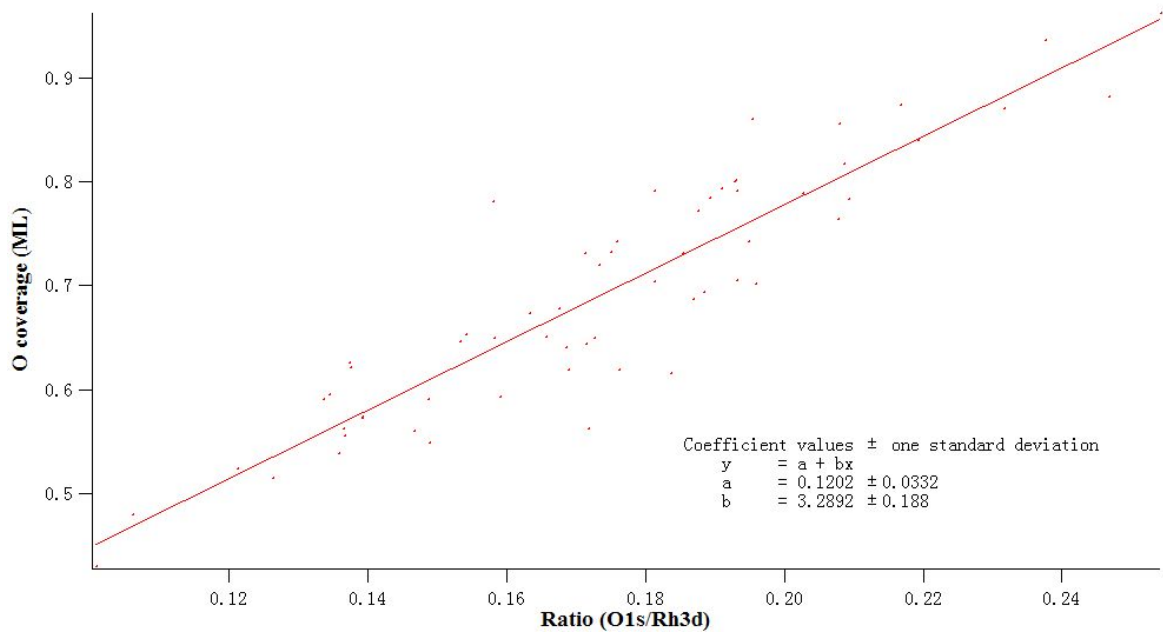
Fig.5.17. Relationship of oxygen coverage and ratio of O1s and Rh3d intensities.　Here linear fitting was

conducted.

The error of the curves which shows coverage vs ratio of O1s/Rh3d intensity is relatively

higher (~10%).　This is possibly due to high coverage of oxygen.

VI. Pattern formation of NO+H$_2$/K/Rh(110) system at various θ_K

As described in Chapter III, O$_2$+H$_2$/K/Rh(110) and NO+H$_2$/Rh(110 system have been investigated and shown interesting phenomena such as stationary pattern and phase separation in O$_2$+H$_2$/K/Rh(110) system [32] and various kinds of different patterns such as wave fragments, spiral waves (elliptic, rectangular), target patterns (elliptic, rectangular), reduction fronts, etc. in the NO+H$_2$ /Rh(110) system, at different temperature and H$_2$ partial pressure when NO pressure is fixed. Furthermore, a "zebra pattern" has been discovered on a K deposited Rh(110) surface with a Pt pad as ignition center during the NO+H$_2$ reaction [35]. In our experiment, the main task is to systematically investigate the behavior of the NO+H$_2$ /K/Rh(110) reaction and to study the influence of K coverage on patterns.

In previous experiments, the standard procedure of experiment was as following: When the sample is set to a certain temperature, first NO is introduced and kept fixed, then H$_2$ pressure is increased very rapidly to 10^{-5} mbar until the surface is totally reduced, then the pressure is decreased as fast as possible (normally in a few seconds) to the desired value. In our experiments, with coadsorbed K the old procedure is hard to realize, since as shown by PEEM the Rh(110) surface with K did not become homogeneous (which indicates the K distribution is not homogeneous) after reducing the surface with H$_2$. The surface was still not homogeneous even after raising the temperature to 700K (already the desorption temperature for K for θ_K>0.15ML). If instead, the surface was covered by NO and annealed to 700K, the PEEM intensity of the surface became homogenous very quickly. So in order to make the initial condition of every experiment identical, the standard experimental steps were modified in this way:

The standard procedure

1. K is deposited onto the Rh(110) surface at about 473 K, the K coverage is checked by LEED and AES.
2. Temperature is set to the desired value by a programmed temperature controller
3. NO pressure is fixed (at 1.54x10^{-6} mbar) until the PEEM image of the surface is

homogeneous, then the H_2 pressure is slowly increased directly to the desired value, after a waiting period of 10 minutes we observe the patterns on the surface.

4. After each experiment, the H_2 is turned off and the surface is annealed to about 700K (below the K desorption temperature when θ_K <0.15ML according to fig.4.8), so that the PEEM image of the surface becomes homogeneous again. Then another experiment is carried out.

6.1 Patterns at different K coverage

6.1.1 Patterns on Rh(110) surface without coadsorbed potassium

(1) General

For a systematic comparison with the patterns with K, the experiment of the system NO+H_2/Rh(110) were repeated in the new standard procedure.
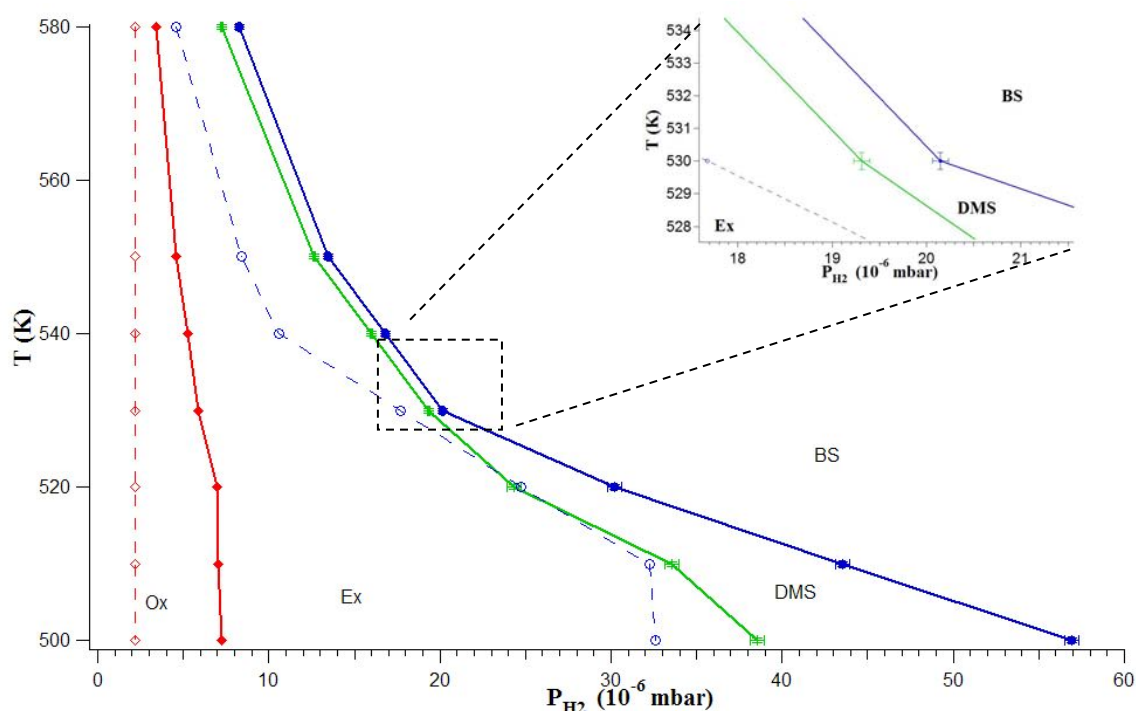
Fig.6.1. Bifurcation diagram of NO+H_2 /Rh(110) system, (dashed lines are the result   from A.Schaak

using another standard experimental procedure [37]) . P_{NO} =1.54x10^{-6} mbar

Ox = Oxygen covered surface,   Ex = Excitable,   DMS = Double metastable,   BS = Bistable.

The result is as shown in fig.6.1 together with the result by A.Schaak et al. [33, 37], which are denoted by dashed lines.   The values of the data points are reproducible.

The significant difference between the experiments with the new standard procedure and the old procedure on the unpromoted Rh(110) surface is the shift toward high H_2 partial pressure for both boundaries. The boundary condition (red) the resting to the excitable state shifts by at least 2×10^{-6} mbar compared to the old result. When temperature is decreased to 500K, the difference is 5×10^{-6} mbar. For second boundary the excitable state to the bistable state, the shift is also larger than 2×10^{-6} mbar.

(2) Excitable state

Wave fragments

In a pressure range of about 5×10^{-7} mbar from the border between resting state and excitable state, wave fragments traveling in the [001]-direction are obtained, which is similar to previous research on clean Rh(110) sample.

Spiral waves and target patterns

The pressure range where traveling wave fragments are obtained is always very narrow (just around 5×10^{-7} mbar) in experimental conditions of T = 500K-580K. Upon further increasing the H_2 partial pressure, target pattern or spiral waves can appear, depending on temperature and H_2 pressure. The target patterns are rectangular or elliptical.

(3) Double metastable state

In our experiments, in the region "DMS", firstly a reduction front was formed, then the center became dark again, in the center another reduction front is formed but differently shaped. This agrees with what has been observed before [38].

(4) Bistability regime

When the H_2 pressure is further increased, as shown in fig.6.1, the system reaches the bistable regime, i.e., after the reaction is ignited, reduction fronts develop and cover the whole surface. Unless the H_2 pressure is decreased again, the surface remains reduced. This is consistent with previous result, too [38].

6.1.2 Low K coverage (~0.025ML).

(1) General

When the K coverage is low (~0.025ML, as determined by LEED which shows a very weak 1x4 structure), displayed in fig.6.2, the bifurcation diagram is generally similar to that of the unpromoted surface, but the H_2 partial pressure where ignition occurs is significantly decreased for T<550K.   At lower temperature, the effect becomes more significant.   The area "DMS" in NO+H_2/Rh(110) system in the bifurcation diagram in fig.6.1 is replaced by "CP" which means "complicated pattern".   In this regime, one finds for example, a "hybrid pattern" which looks like composited spiral/target patterns, broad pulses, and turbulence-like pattern.   Sometimes in a small range, a intensity oscillation of the whole surface are observed.   At higher K coverage ($\geq$ 0.05ML), Turing-like stationary patterns can be found.
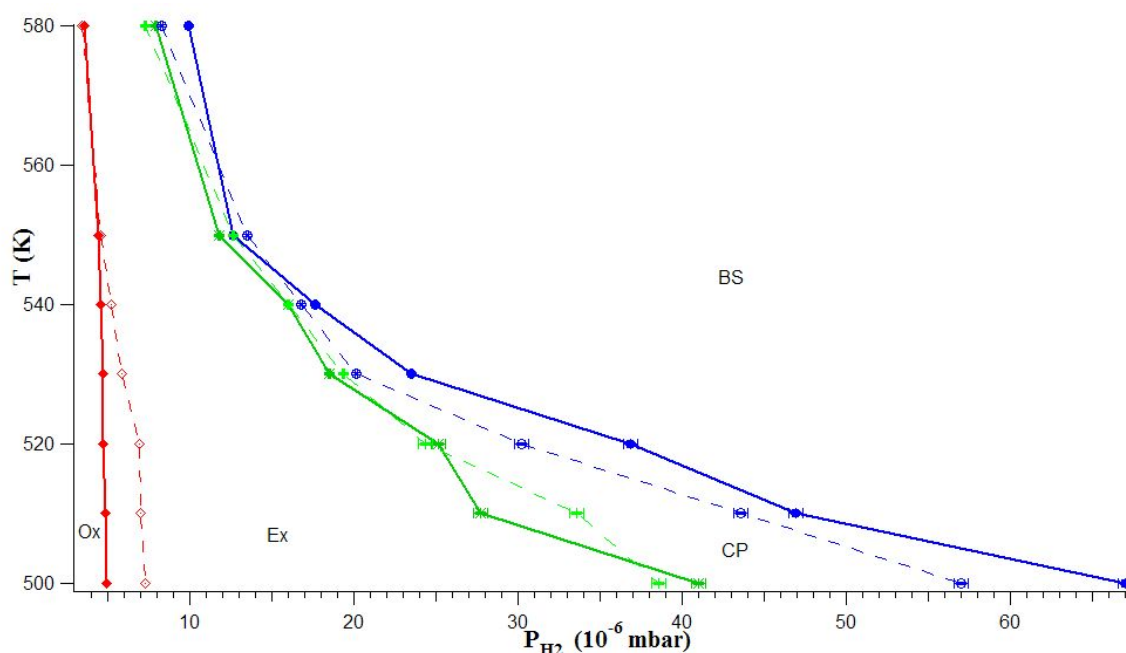
Fig.6.2 Bifurcation diagram of NO+H_2 reaction on slightly promoted Rh(110) surface (Dashed lines are the bifurcation diagram on clean Rh(110) surface.). θ_K ~0.025ML, P_{NO} =1.54x10^{-6} mbar
Ox = Oxygen covered surface;   Ex = Excitable; CP = "Complicated pattern", BS-Bistable

(2) Excitable state

Traveling Wave fragments

At a K coverage of 0.025ML, the pressure range where wave fragments can exist becomes narrower (~3-4x10^{-7} mbar) compared to those on the unpromoted Rh(110) surface.   Due to

its small size, it has not been included in the bifurcation diagram in fig.6.2.
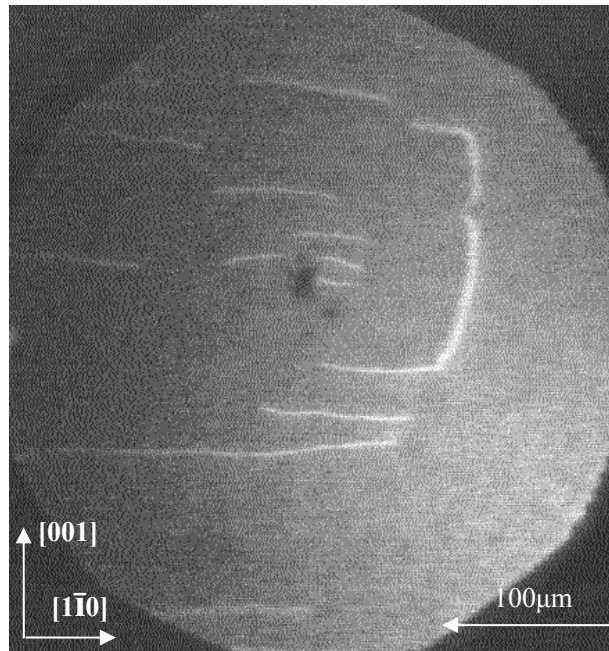
Fig.6.3. Wave fragments in NO+H$_2$/K/Rh(110) system, propagating in [001] and [1$\bar{1}$0] direction,

θ_K~0.025ML, P$_{NO}$ =1.54x10^{-6} mbar, P$_{H2}$ =3.43x10^{-6} mbar, T=580K

At low K coverage (~0.025ML), the wave fragments propagating in the [001]-direction and

in the [1$\bar{1}$0]-direction can coexist, as shown in fig.6.3.   If the H$_2$ is slightly increased (1x10^{-7} mbar), the pattern will simply change to target pattern.

Solitary waves

At low K coverage (θ_K~0.025ML), for T<520K, near the boundary between oxygen covered surface and excitable state, a single solitary wave instead of wave fragments will develop, i.e. after this solitary wave have passed by, the surface seems to be in the stable oxygen covered state again.   Fig.6.4. displays an example of this kind of wave.
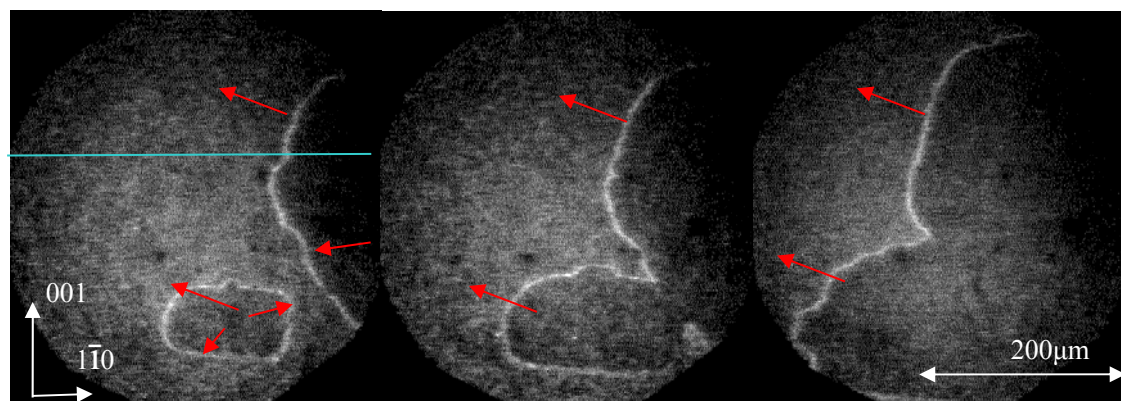
(a) t = 138s   (b) t = 258s   (c) t = 318s

Fig.6.4. Solitary wave, in NO+H_2 reaction at low K coverage on Rh(110) surface,
the blue line indicated in (a) was for the profile scanning in fig.6.5
$P_{NO} = 1.54 \times 10^{-6}$ mbar, $P_{H2} = 5.43 \times 10^{-6}$ mbar, T = 500K

As shown in fig.6.4(a), this solitary wave initially started just as normal target pattern,   but instead of periodically sending out waves as in a target pattern, the triggering center fires only one time.   It can be also seen from fig.6.4 that there was a little difference of the brightness at two sides of the solitary wave.   A PEEM profile measurement is shown in fig.6.5.

Discussion
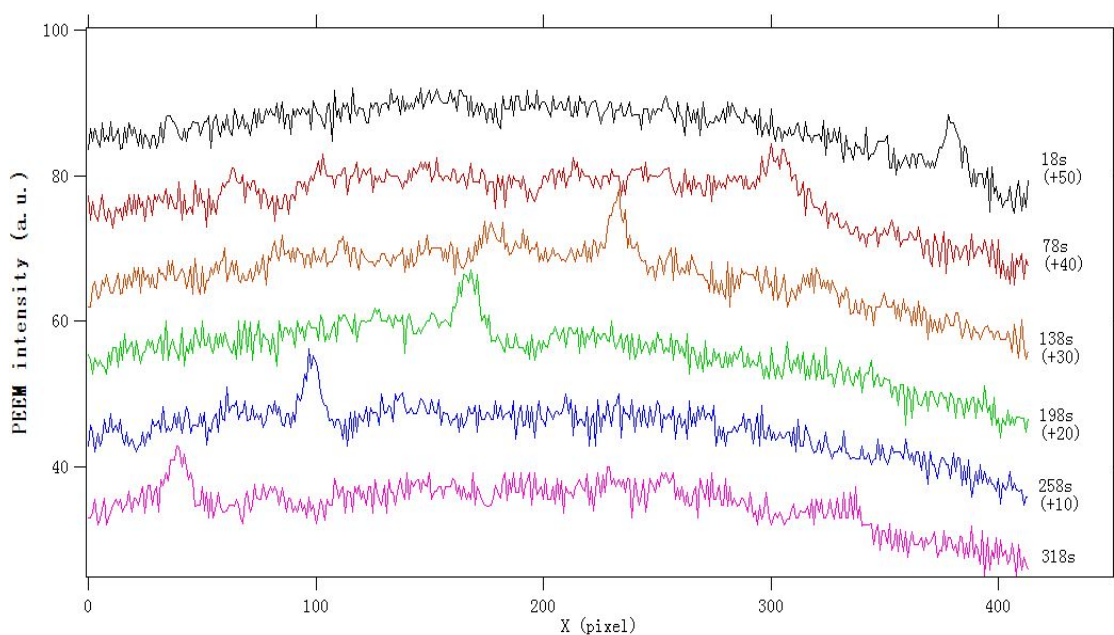
(a) Waterfall profile of the solitary wave

(b) Line Profile

As we can see from fig.6.5 (a), a little difference between the intensity of two sides of the solitary wave can be seen (especially at 198s and 258s), but compared to the peak intensity of the solitary wave their intensity is small that can be compared to the noise of the background.   And we can also see that the background is originally not homogeneous, but with a certain curvature (due to the alignment of PEEM).   If we put them together with no intensity offset as shown in fig.6.5(b), we can see the background intensity for all frames almost remain the same.   This indicates the fact that after the solitary wave have passed by, the surface returned to an oxygen covered state.

The second fact is that this pattern appears only at a narrow H_2 pressure range (~0.2×10^{-6} mbar) at low H_2 pressure (~$P_{H2} = 5.43 \times 10^{-6}$ mbar, near the boundary from oxygen covered surface to excitable state).   At $500K \leq T \leq 510K$, a further increase of the H_2 pressure causes the solitary wave to split into wave fragments. For $510K < T < 600K$, a further increase of the H_2 pressure to about 5.6×10^{-6} triggers another wave, and under this condition, more waves will be triggered with a very long distance (>300µm) between each other.

These two facts indicate that this solitary wave seems to be a new kind of pattern and might have different origin from the reduction fronts in the "bistable regime".

Spiral waves and target waves

(a) t = 414s   (b) t = 421s
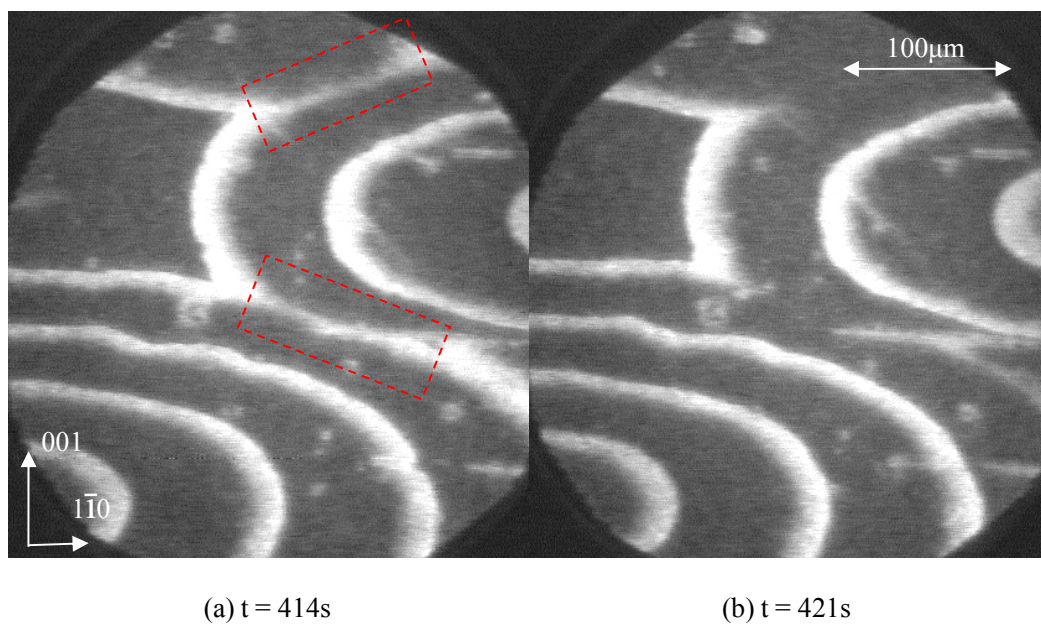
Fig.6.6. PEEM image: Target pattern, in $NO+H_2$ reaction with low K coverage on Rh(110) surface, (the

collision areas are marked by red dashed rectangle), θ_K ~0.025ML, P_{NO} = 1.54x10^{-6} mbar, P_{H2} = 1.18x10^{-5}

mbar, T = 550K,

In most part of the excitable region indicated in fig.6.2, target patterns appear.   At θ_K ~0.025ML, as shown in fig.6.6, when two pulses collide together, first there was some intensity left in the collision area, then this intensity disappeared.   If waiting long enough, like 30 minutes, the brightness the collision area would slightly increase.

(3) "Complicated patterns"

"Hybrid pattern"

(a) $\Delta t = 0s$ (b) $\Delta t = 5s$ (c) $\Delta t = 10s$

(d) $\Delta t = 15s$ (e) $\Delta t = 20s$
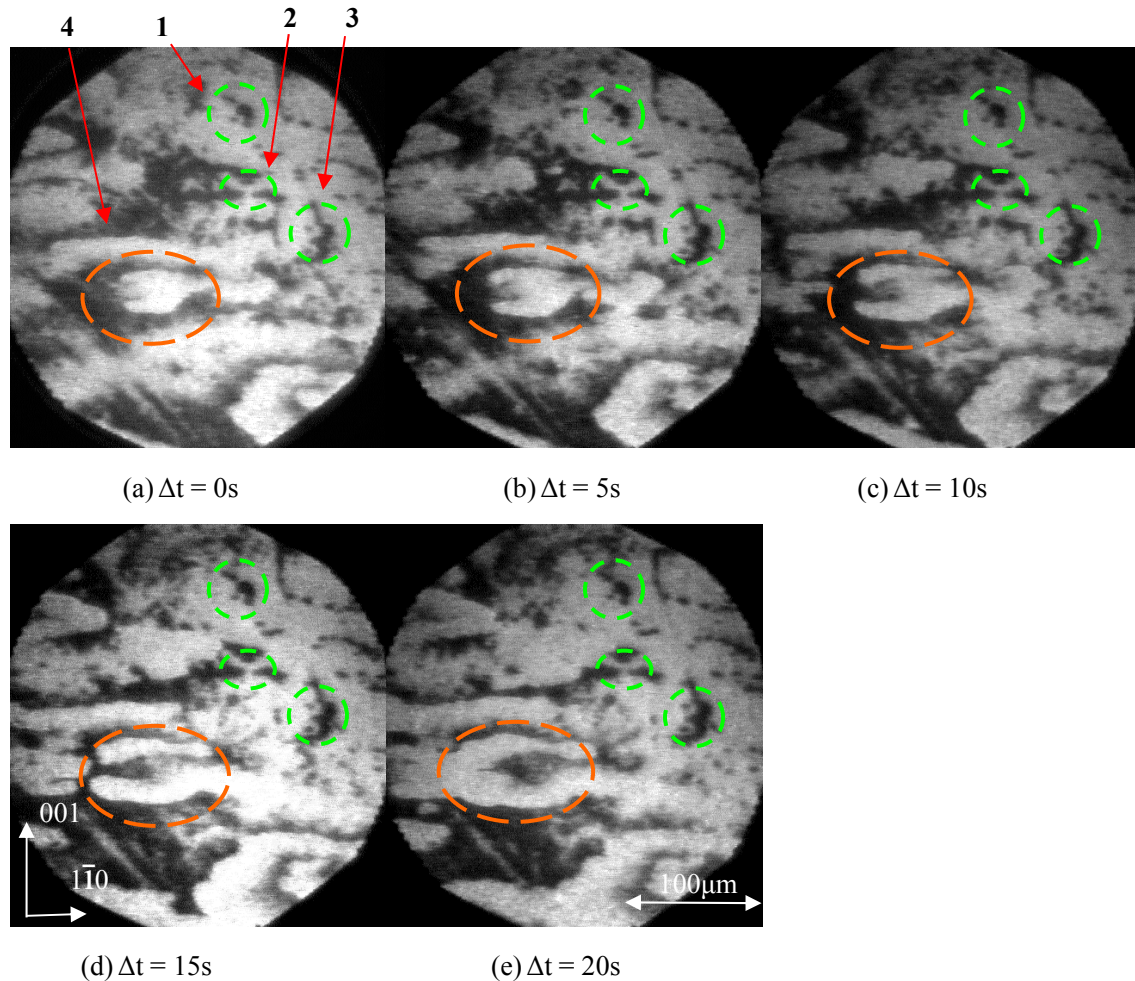
Fig.6.7. PEEM image of "Hybrid pattern" (consists of moving part as shown in orange ellipse (4), and stable part indicated by green dashed circles and ellipses (1,2,3)), in the NO+H$_2$ K/Rh(110) system, θ_K ~0.025ML, P_{NO} = 1.54x10^{-6} mbar, P_{H2} = 8.11x10^{-6} mbar, T = 580K

The "hybrid pattern" looked as shown in fig.6.7.   The whole pattern appeared chaotic at the

first glance, but if one takes a closer look, one sees that this pattern actually consists of different parts:

1. Very broad moving spiral or target patterns, for example, a pair of spiral waves as marked by the orange dashed ellipse (area 4) in fig.6.7

2. Almost stationary parts shown in green dashed circles and ellipses (area 1, 2, and 3) in fig.6.7 which did not move within time duration of the experiment

3. Turbulence like waves.   Except the almost stationary parts, spiral and target patterns mentioned in 1 and 2, the other area in the field of view is filled with turbulence-like waves.

Oscillations

t = 5s   t=10s   t=14s   t=19s

t=24s   t=29s   t=34s   t=39s
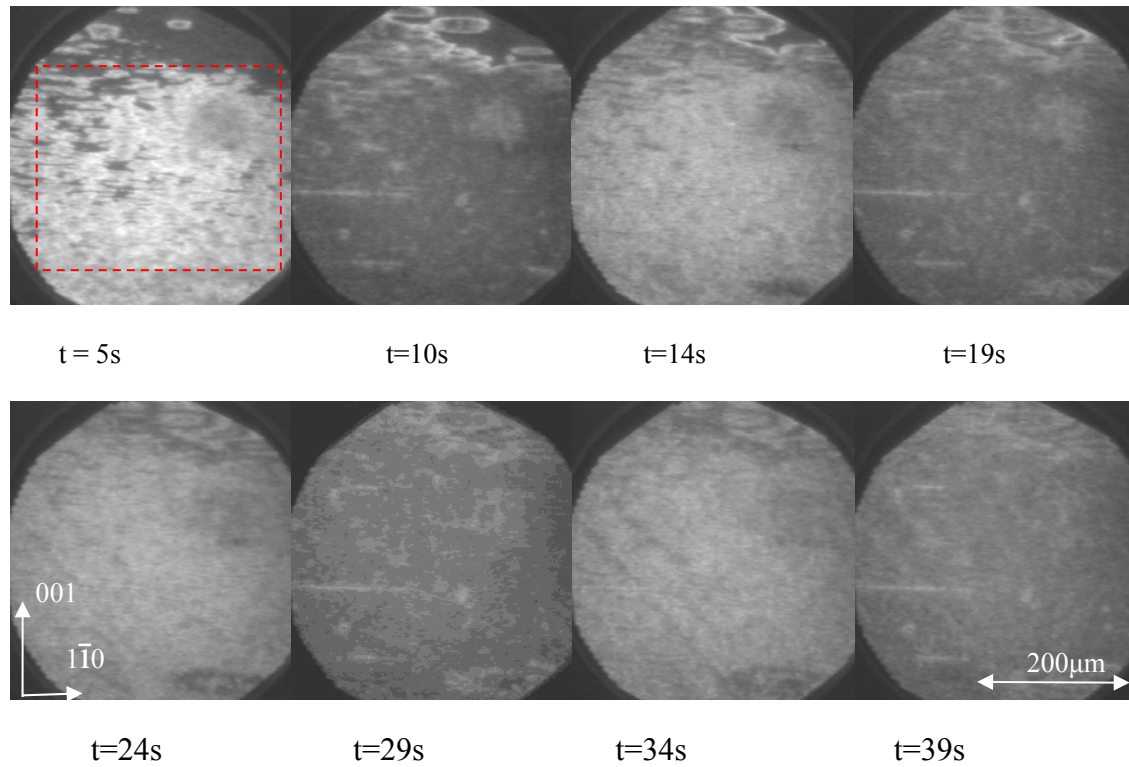
Fig.6.8 PEEM intensity oscillation in NO+H_2 reaction on Rh(110) surface, θ_K ~0.025ML

P_{NO} = 1.54x10^{-6} mbar, P_{H2} = 1.51x10^{-5} mbar, T = 550K

At a K coverage ~0.025ML, in the "complicate patterns" regime, under certain condition, intensity oscillations can be seen over the whole surface, as shown in fig.6.8.   In this case, wave fronts can not be found.
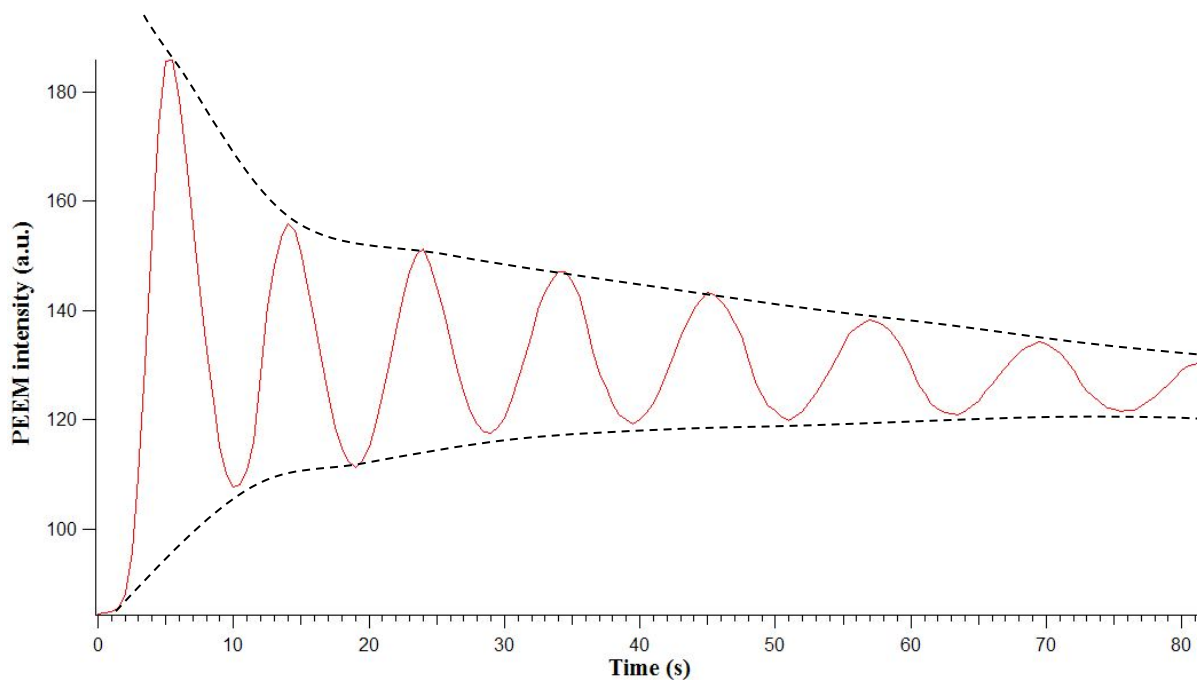
Fig.6.9. PEEM intensity oscillations of a large area (area marked by red rectangular in fig.6.8 (a)), The

decaying intensity oscillations exhibits a stable period of ~10s

As shown in fig.6.9, the PEEM intensity has a very regular oscillation period of 10s, (except the initial oscillation, which was a bit faster, with a period of 9s), and decreasing maximum intensity. One can suspect that the intensity oscillations are associated with rate oscillations, for example, the H_2O production.

(4) Bistable regime
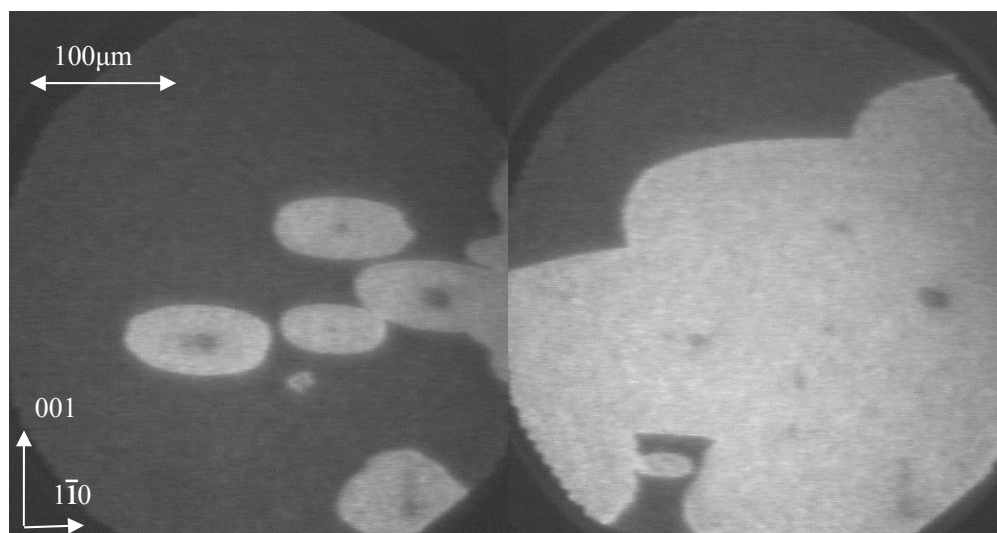
Fig.6.10. PEEM image of reduction fronts, in $NO+H_2$ /K/Rh(110) system, θ_K ~0.025ML,

$P_{NO} = 1.54 \times 10^{-6}$ mbar, $P_{H2} = 1.51 \times 10^{-5}$ mbar, T = 550K

At higher H_2 pressure, when the system reaches the bistable regime, the reduction fronts

look pretty similar to those on the unpromoted Rh(110) surface, as shown in fig.6.10.   The surface is finally homogeneously reduced.

6.1.3 Intermediate K coverage (~0.05ML)

(1) General
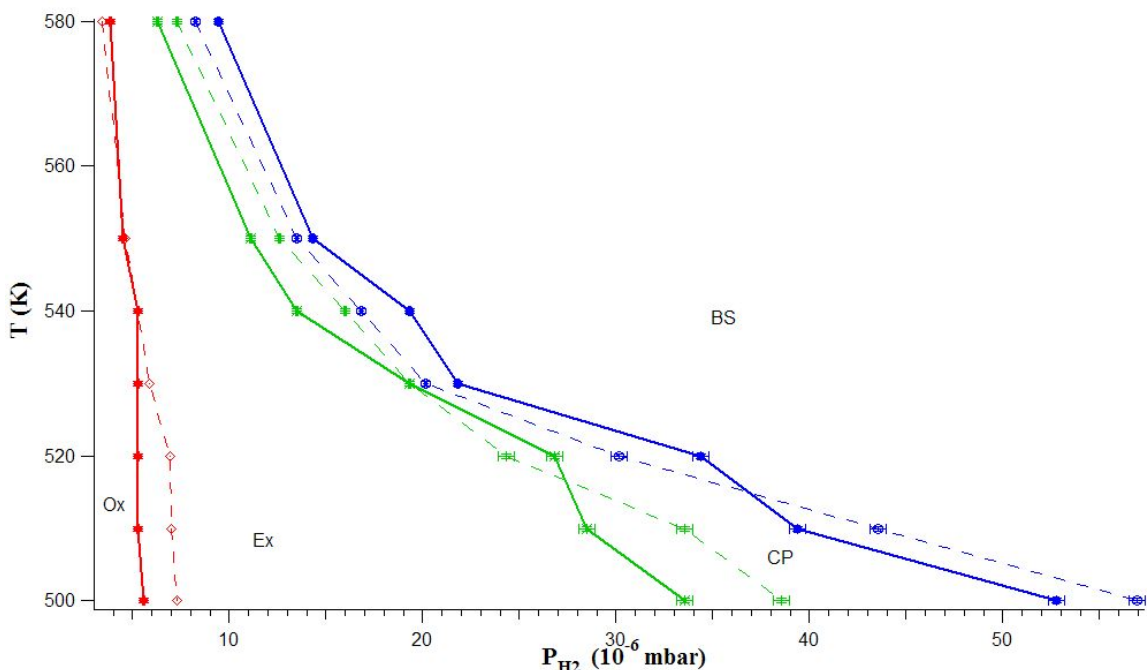
Fig.6.11. Bifurcation diagram of NO+H_2 reaction on Rh (110) surface with intermediate K coverage (Dashed lines are the bifurcation diagram on unpromoted Rh(110) surface), θ_K ~0.05ML, P_{NO} =1.54x10^{-6} mbar, Ox = Oxygen covered surface,   Ex = Excitable,   CP = "Complicated patterns", BS = Bistable

When the K coverage is higher (0.05ML, with a 1x4 LEED pattern), the boundaries of the bifurcation diagram exhibit a significant change compared to fig.6.7 which is at θ_K ~0.025ML, as shown in fig.6.11.

The boundary between the oxygen covered surface and the excitable state is slightly shifted to higher H_2 pressure side, which means the reaction needs higher H_2 pressure to ignite. The boundary between the bistable and "complicated patterns" regime is shifted to lower H_2 pressure side, which means to reach the bistable regime, a lower H_2 pressure is needed.

(2) Excitable state

Traveling Wave fragments
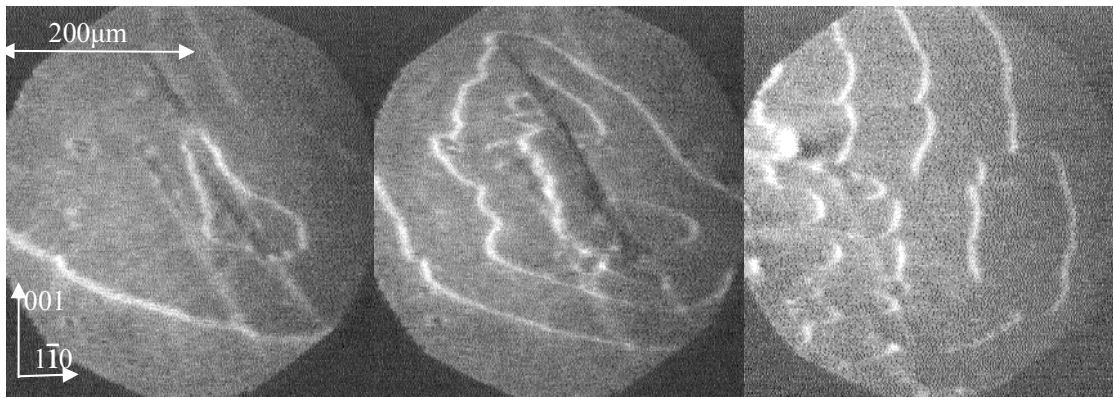
(a) t = 190s　　　　　　　(b) t = 300s　　　　　　　(c) t = 1250s

Fig.6.12 Development of wave fragments in NO+H$_2$/K/Rh(110) system with θ_K ~0.05ML,

P_{NO} = 1.54x10^{-6} mbar, P_{H2} = 5.94x10^{-6} mbar, T = 510K

At θ_K ~0.05ML, wave fragments traveling in the [001]-direction like on the unpromoted Rh(110) surface don't exist anymore. Instead, at the border from rest state to excitable state, only fragments traveling in [1$\bar{1}$0]]-direction are seen. To obtain this pattern, the H$_2$ partial pressure is slowly increased until it is a bit higher than the pressure for a solitary wave. Several waves (strongly modified near defects, as shown in fig.6.12.) develop, and split into fragments (with some curvature, as shown in fig.6.12b).

Differently from the fragments in the [001]-direction seen on the unpromoted Rh(110) surface, the fragments in [1$\bar{1}$0]-direction are not straight, most of them have a certain curvature, as shown in fig.6.12.(c). Different also from the later experiments at higher K coverage (see below), the accumulation of K through transport with the waves is not significant.

Solitary waves
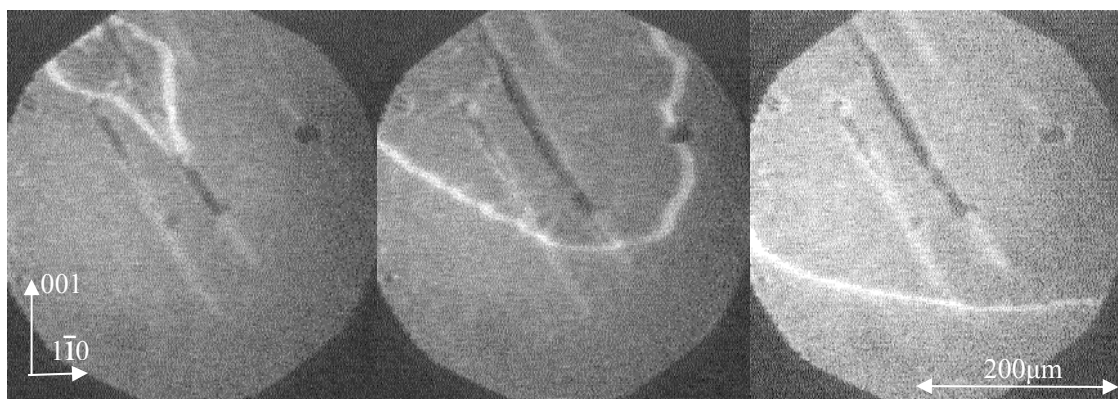
(a) t = 80s　　　　　　　(b) t =260s　　　　　　　(c) t = 440s

At a K coverage of 0.05ML, at T<520K, the solitary waves which were already observed at lower K coverage (~0.025ML) were again found, as shown in fig.6.13. They appeared near the boundary from the oxygen covered state to the excitable state in the bifurcation diagram of fig.6.11. This solitary wave often initiated near scratches, as shown in fig.6.13 (a). Its curvature is initially strongly affected by the scratc. The H$_2$ pressure range to get such solitary wave is very narrow, around ~3x10^7 mbar. Above that pressure, the solitary wave will split into wave fragments traveling in the [1$\bar{1}$0]-direction.

<u>Spiral waves and target waves</u>

(a) t = 80s   (b) t = 170s
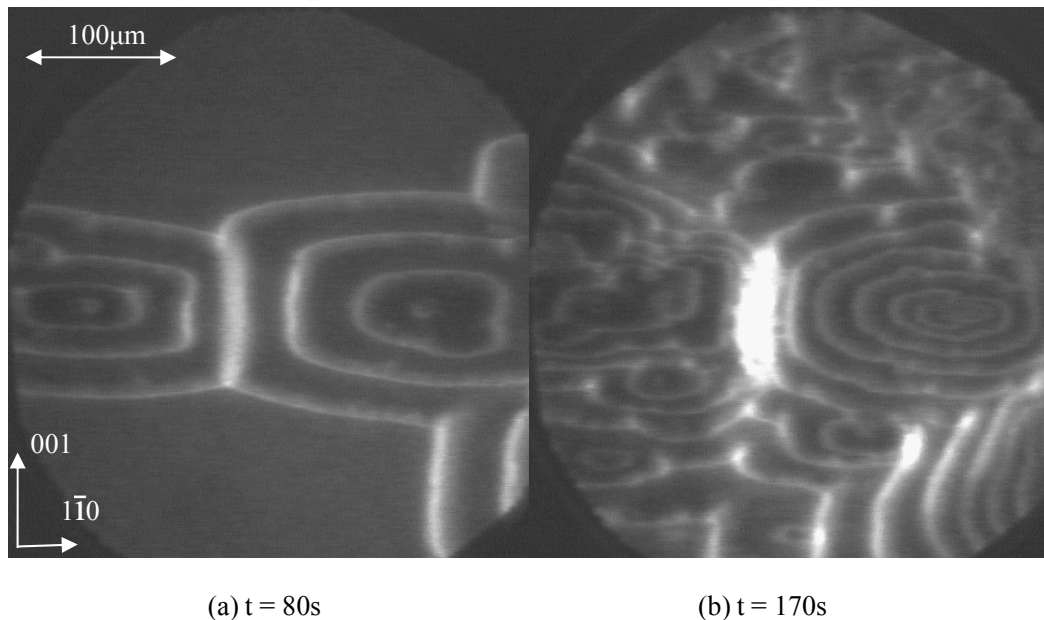
Fig.6.14. PEEM image of colliding target patterns, in NO+H$_2$/K/Rh(110) system , θ_K ~0.05ML,

P$_{NO}$ =1.54x10^{-6} mbar, P$_{H2}$ =5.936x10^{-6} mbar, T = 580K

When the H$_2$ partial pressure was further increased into the excitable region indicated in the bifurcation diagram in fig.6.11, the spiral waves and target waves developed. Different from lower potassium coverage (θ_K ~0.025ML) and the unpromoted Rh(110) surface, as shown in fig.6.14(a), after two pulses collided, the PEEM intensity of collision area remained bright, and the brightness increased as more pulses collided in the same area, as shown in fig.6.14(b). The bright region would also expand over time. After turning off H$_2$, the collision area still remained brighter than the surrounding area. This indicates a K

mass transport during wave propagation, which will be a subject of a separate chapter.

(a) t = 540s   (b) t = 740s   (c) t = 940s
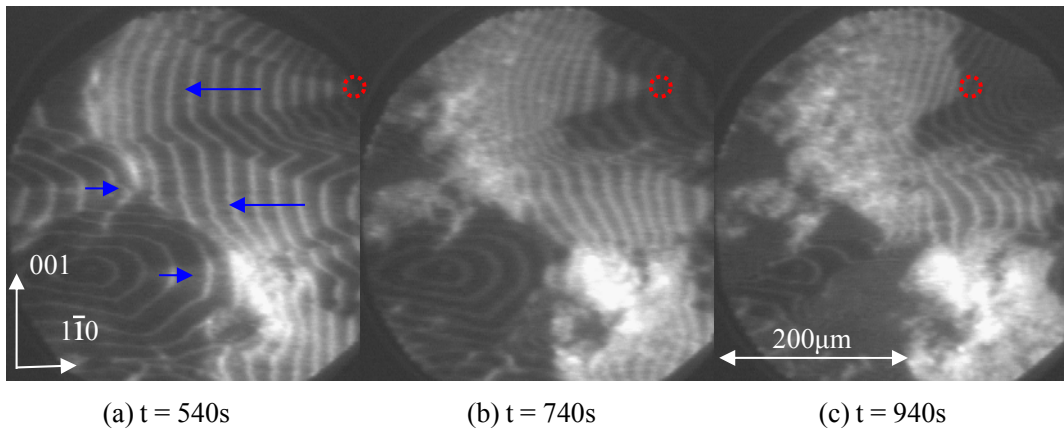
Fig.6.15 PEEM image of "Cone structures" among colliding target patterns, in NO+H_2/K/Rh(110)

system, θ_K ~0.05ML surface, P_{NO} = 1.54x10^{-6} mbar, P_{H2} = 8.44x10^{-6} mbar, T = 540K

As shown in fig.6.15, in the upper part of the images some kind of cone shaped structure (in the position of the blue arrow, which also marked the direction of the waves) was formed a few minutes (~5min) after ignition. It can also be seen that the position of the tip (marked by red dashed circle) of the cone first originated at the center of a target pattern and is slowly (about 0.01µm/s) moving during the reaction.

(3) Complicated patterns

"Hybrid pattern"

The "hybrid pattern" at θ_K ~0.05ML, compared to the one at θ_K ~0.025ML, it is more disordered, as shown in fig.6.16.

t = 20s   t=40s   t=170s
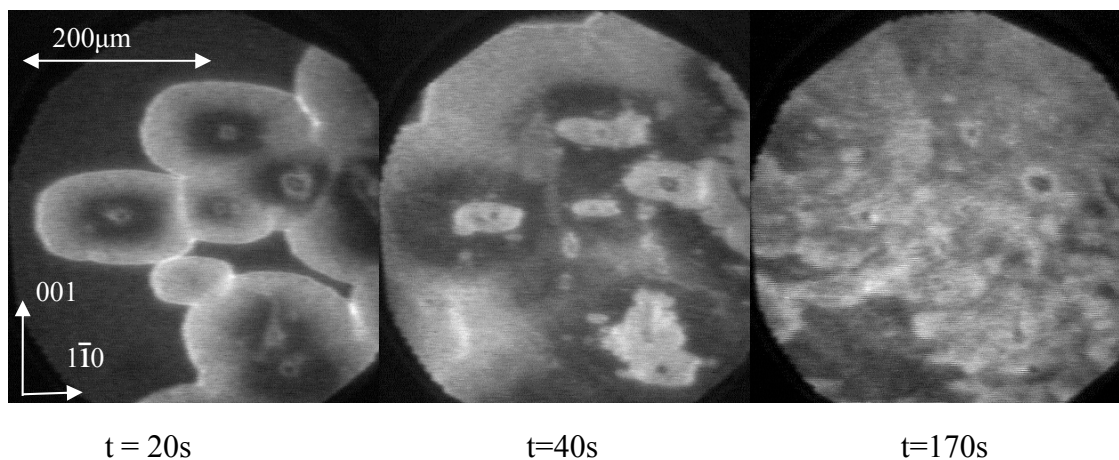
Fig.6.16 PEEM image: Development of "hybrid pattern", in NO+H_2 /K/Rh(110) system,

θ_K ~0.05ML, P_{NO} = 1.54x10^{-6} mbar, P_{H2} = 2.01x10^{-5} mbar, T = 530K

As shown in fig.6.16, at the beginning, fronts which look like the double metastable fronts in the unpromoted NO+H$_2$/Rh(110) system can also be seen from the beginning, but later they turned into the "hybrid pattern" described in 6.1.2.   When the reaction is run longer, as shown in fig.6.17, at 600s, it can be seen that the pattern can be actually regarded as a mixture of target patterns in the bottom part，and turbulence-like waves in the top part. The "hybrid pattern", appeared at the left side of the "complicated patterns" regime in the bifurcation diagram.   When the H$_2$ partial pressure is further increased, a stationary pattern may appear.
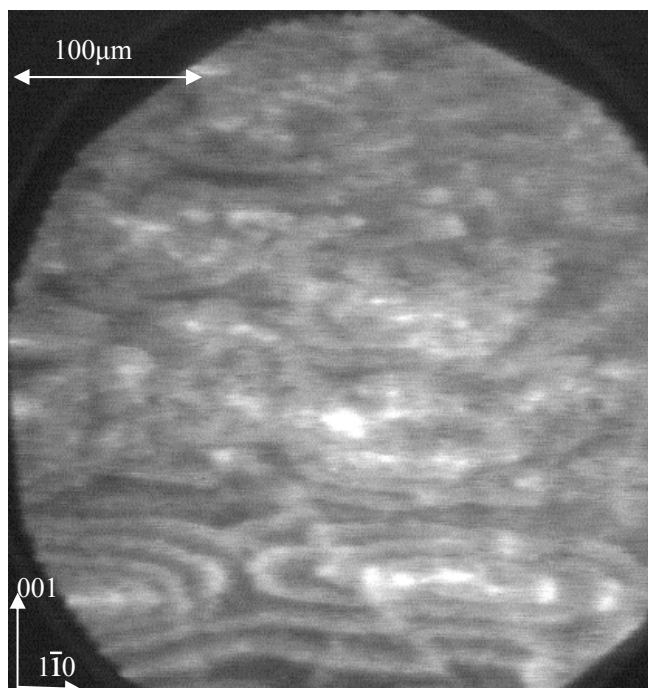
Fig.6.17 PEEM image of "hybrid pattern" after a long reaction time (t= 600s,), in NO+H$_2$ /K/Rh(110) system, θ_K ~0.05ML, P$_{NO}$ = 1.54x10^{-6} mbar, P$_{H2}$ = 2.01x10^{-5} mbar, T = 530K

Turing-like Stationary pattern

As mentioned above, significantly different from the unpromoted system, with a K coverage of ~ 0.05ML, stationary patterns can appear, as shown in fig.6.18.   The stationary patterns are formed in the right side of the "complicated patterns" regime of the bifurcation diagram in fig.6.11,
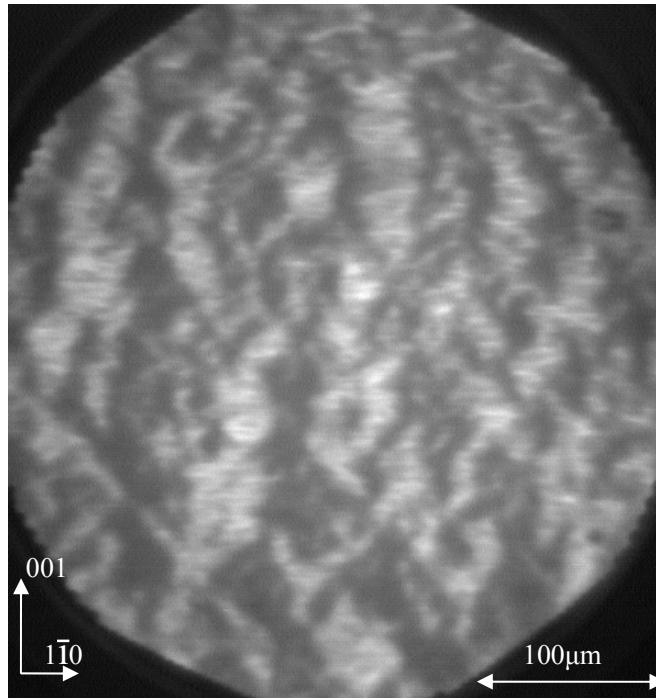
Fig.6.18 PEEM image of a "Turing-like" stationary pattern, in NO+H$_2$ /K/Rh(110) system, θ_K ~0.05ML

P$_{NO}$ = 1.54x10^{-6} mbar, P$_{H2}$ = 2.85x10^{-5} mbar, T = 510K

The stationary patterns in most case consist of bent stripes, all more or less oriented along the [001]-direction, as shown in fig.6.18.   Taking a closer look into those stripes, one finds some detailed structures which looked like small short "stick shaped" islands, with a width in the order of ~10^{0}µm along the [001]-direction and ~10^{1}µm along the [1$\bar{1}$0]-direction. This pattern looks similar to Turing pattern.   Because in the related NO+H$_2$/K/Rh(110) system, it was shown that the stationary patterns seen there do not originate from the different diffusion rate of inhibitor and activator, but are caused by attractive interactions and therefore were formed as "reactive phase separation", we call the patterns here also "Turing-like" stationary patterns.   A more detailed description will be in 5.1.4.

(4) Bistable regime

(a) t = 8.5s　　　　　　　　　　　　　(b) t = 13.5s

(c) t = 26s　　　　　　　　　　　　　(d) t = 51s
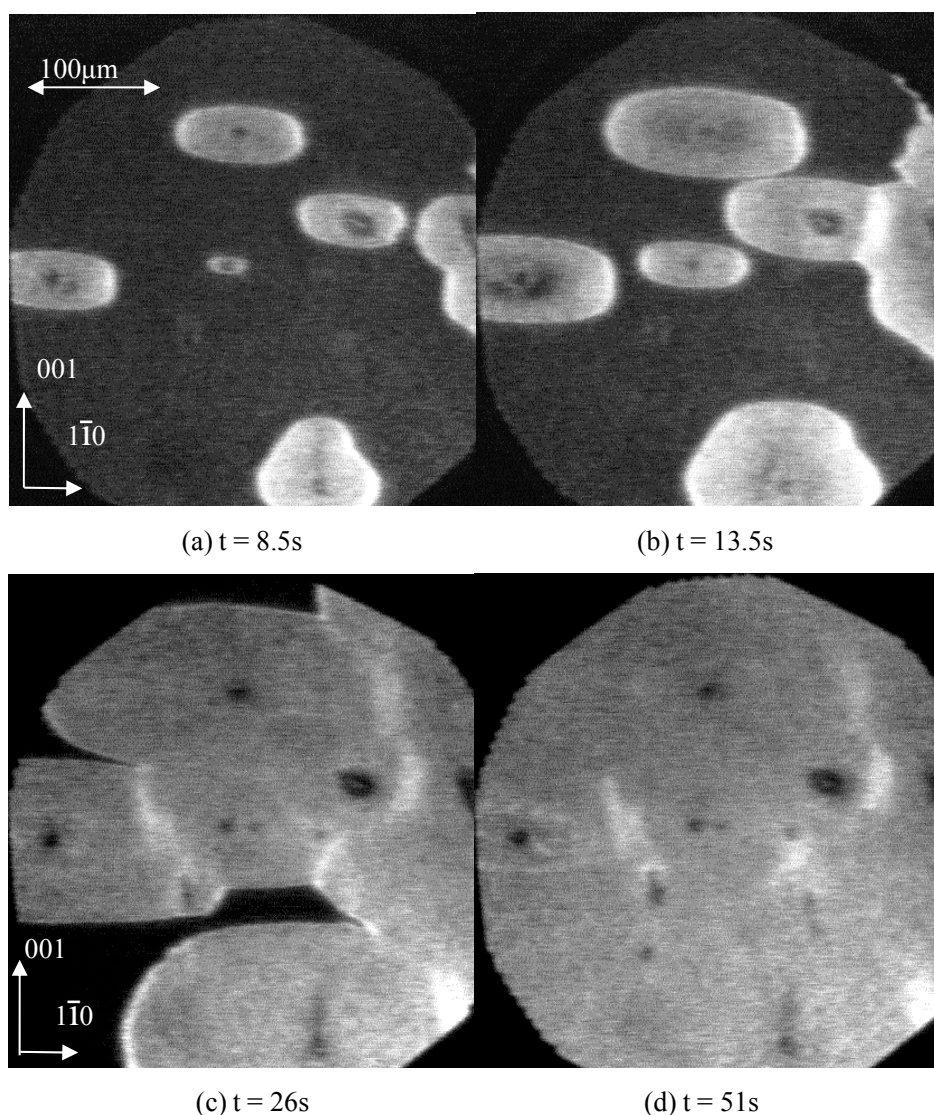
Fig.6.19. PEEM image of reduction fronts (a) (b)(c), finally resulted as a stationary pattern in collision

area (d), in NO+H_2/K/Rh(110) system, θ_K ~0.05ML, P_{NO} =1.54x10^{-6} mbar, P_{H2} = 1.51x10^{-5} mbar,

T=550K

At higher H_2 partial pressure as shown in the bifurcation diagram fig.6.11, we reach bistable

regime.　In this regime, reduction fronts developed, as shown in fig.6.19.　Significantly

different from the unpromoted Rh(110) system or Rh(110) surface with low K coverage

(<0.025ML), the collision area of the reduction fronts exhibits a relatively higher intensity,

compared to the surrounding area. Even after the surface was totally reduced, the intensity

of the surface is still not homogeneous.　The difference remained even after annealing the

surface to 700K (below the K desorption temperature).　This means that the system is not

reversible as in a real bistable system.　But for convenience of description, we still call this

state "bistable".　In fact, what finally formed was a stationary pattern similar to the one

discovered in the $H_2+O_2/K/Rh(110)$ system.   Only when H_2 was turned off and the sample was annealed to 700K, the surface became homogeneous again.

6.1.4 High K coverage (~0.067ML)

(1) General
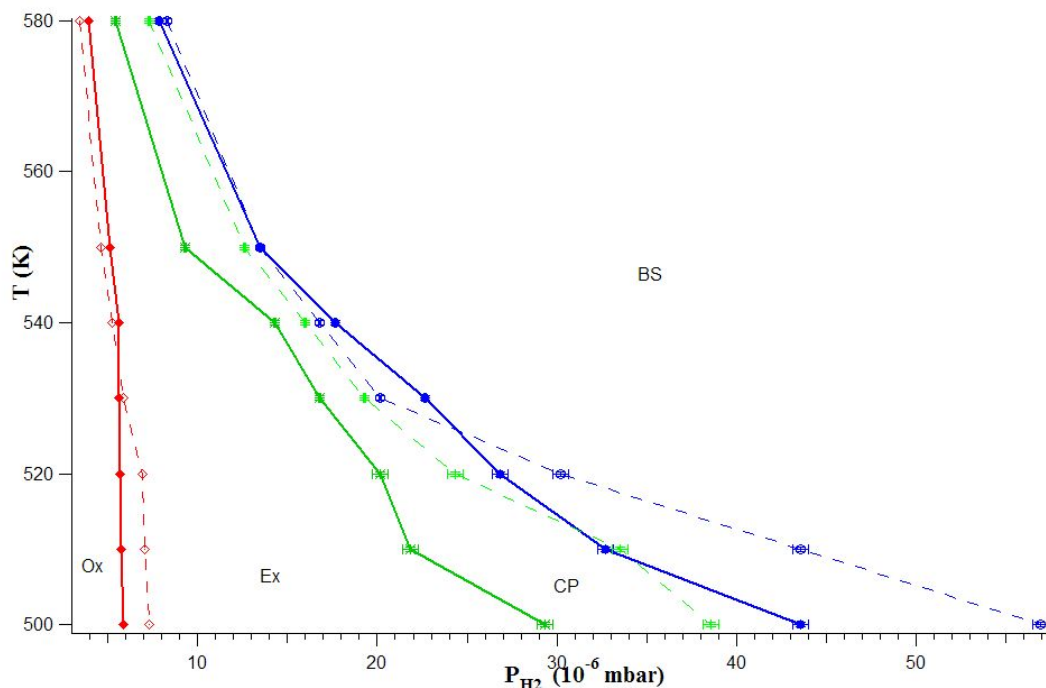
Fig.6.20. Bifurcation diagram of NO+H_2/K/Rh(110) system, (Dashed lines are the bifurcation diagram of the unpromoted Rh(110) surface), θ_K ~0.067ML, P_{NO} =1.54x10^{-6} mbar

Ox = oxygen covered surface, Ex = Excitable, CP = "Complicated patterns", BS = Bistable

The bifurcation diagram at θ_K ~ 0.067ML is shown in fig.6.20.   The K coverage of ~0.067ML was deduced from the observation that at this coverage the 1x3 LEED pattern just began to change into 1x2 structure.   Compared to the bifurcation diagram for θ_K ~ 0.05ML in fig.6.11, the boundary from the oxygen covered state (resting state) to the excitable state is further shifted to higher H_2 partial pressure.   The boundary from the "complicated patterns" regime to the bistable state regime is further shifted to lower H_2 partial pressure.

(2) Excitable state

Wave fragments

At such a high potassium coverage (~0.067ML), wave fragments traveling in the [001]-direction are no longer visible.   Instead, near the boundary from the resting state to the excitable state, fragments propagating in [1$\bar{1}$0]-direction appear.   Similar to θ_K ~0.05ML, in the beginning first target patterns appear. At t~295s the target patterns begin to break into wave fragments.   This breaking starts near the center of the target pattern, and finally spreads into the whole surface, as shown in fig.6.21

(a) t =285s	(b) t = 295s	(c) t =395s

(d) t = 455s	(e) t = 725s	(f) t = 910s
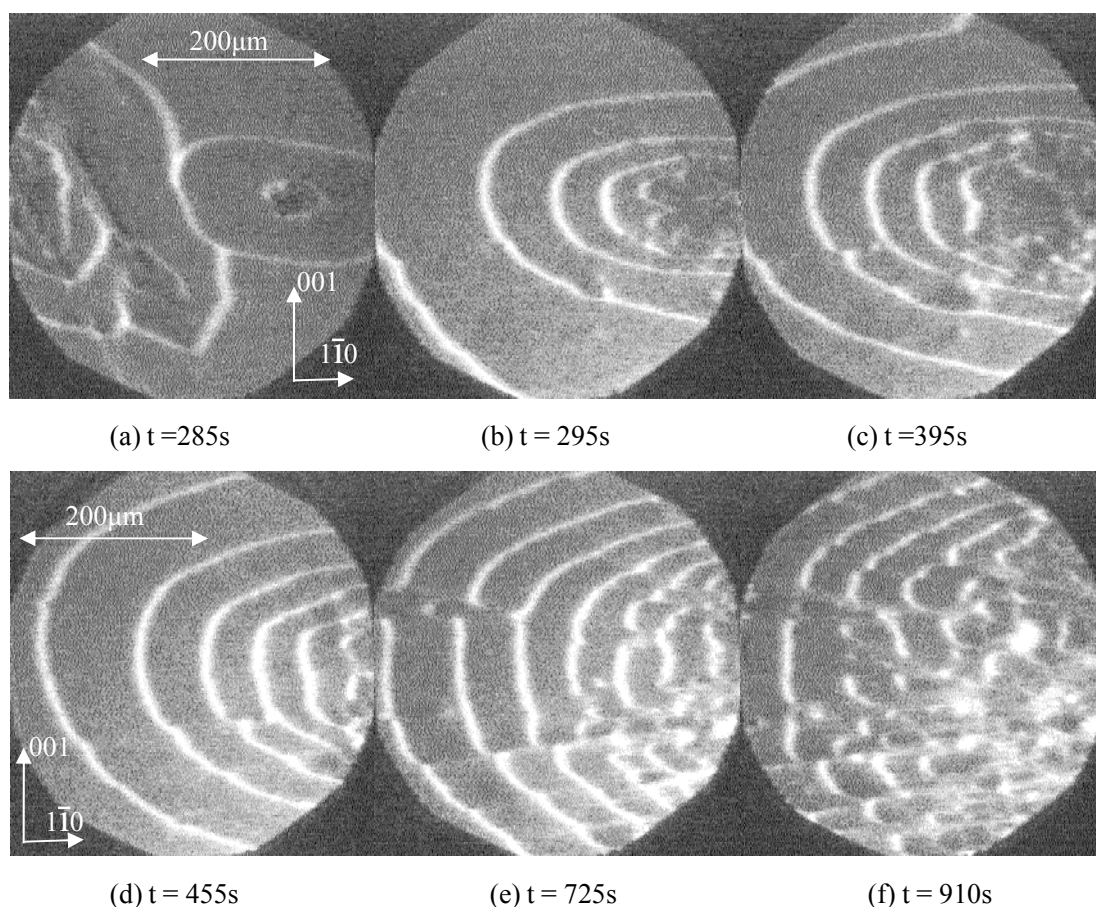
Fig.6.21. PEEM images showing at low H_2 partial pressure and high θ_K (~0.067ML), now target patterns broke into fragments, in NO+H_2 /K/Rh(110) system, P_{NO} =1.54x10^{-6} mbar, P_{H2} = 5.94x10^{-6} mbar, T = 520K.

From fig.6.21 we can also see that the development is very slow.   Compared to the case at θ_K ~0.05ML, the waves were more disordered.   Movement is only limited in the [1$\bar{1}$0]-direction.   "Cloud like" structures appear, which were not seen at θ_K ~0.05ML.

As the same experiment went on longer, as shown in fig.6.22, the whole surface was

covered by wave fragments moving in the [1$\bar{1}$0]-direction and "clouds" in between.   After

shutting down the H$_2$ gas and annealing the surface, the K distribution became

homogeneous again.   This experiment can then be repeated with the same result.
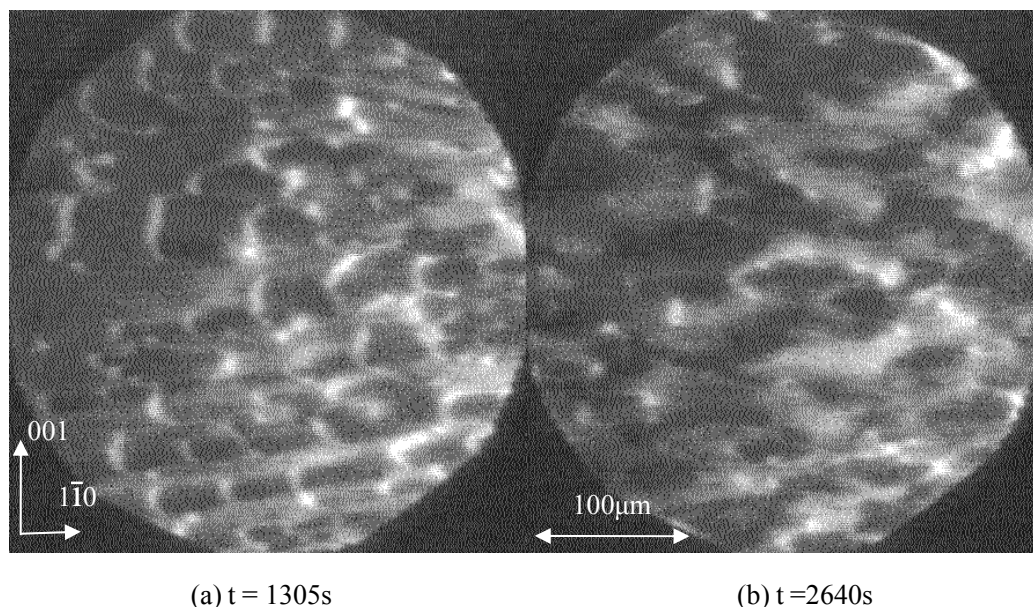
(a) t = 1305s   (b) t =2640s

Fig.6.22. PEEM images of wave fragments moving only in the [1$\bar{1}$0]-direction, in the NO+H$_2$/K/Rh(110)

system, θ_K ~0.067ML, same experiment as in fig.6.21, with longer times, (a) t = 1305s; (b) t

=2640s , P_{NO} =1.54x10^{-6} mbar, P_{H2} = 5.94x10^{-6} mbar,   T = 520K.

Spiral waves and target patterns

At θ_K ~0.067ML, in the excitable region, target patterns and spiral waves still exist, but

spiral waves are seldom seen at this coverage.   Two significant new phenomena are found

in this region.

Increased brightness in the collision area

At higher H$_2$ pressure, as indicated in the bifurcation diagram of fig.5.20, spiral waves and

target patterns can still develop.   Similar to the situation at θ_K ~0.05ML shown in fig.6.14

and fig.6.15, in the collision area of pulses, the intensity became brighter and broader as

time increases.   As will be shown later this effect is due to the K redistribution by the pulse

propagation.   Different from the H$_2$ +O$_2$ /K/Rh(110) system, this phenomena will not

finally result in a stationary pattern.   The bright area will slowly expand and change its

shape.   Inside the bright collision region, turbulence-like fragments still exists, which look

similar to the chemical turbulence discovered in NO+NH$_3$ reaction on Pt(100) surface [39]

"Spider web" patterns

In the excitable regime, under certain conditions, structures that looked like a spider web appeared, as shown in fig.6.23.   Therefore we call this pattern "spider web" pattern.
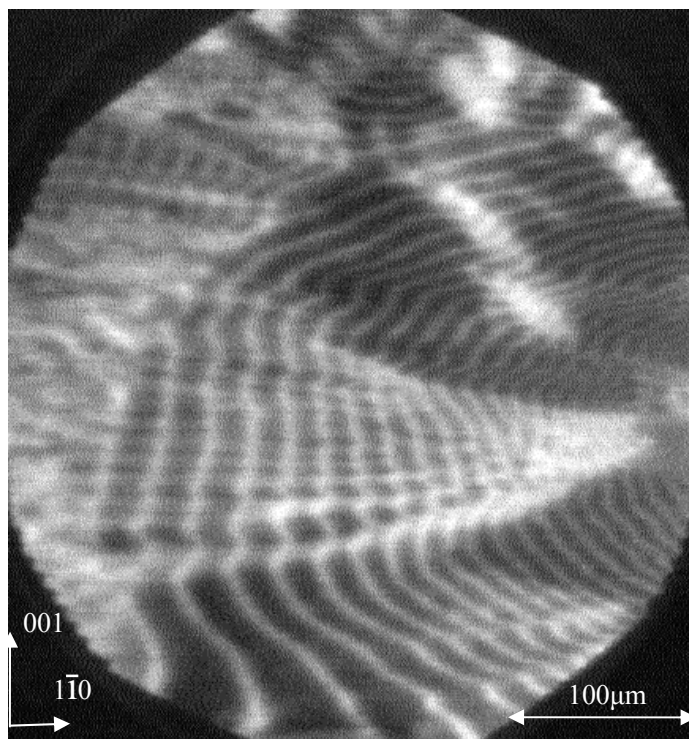
Fig.6.23. PEEM image: "Spider Web" structure in target pattern, in NO+H$_2$/K/Rh(110) system,

θ_K ~0.067ML, P$_{NO}$ =1.54x10^{-6} mbar, P$_{H2}$ =1.18x10^{-5} mbar, T = 530K

As shown in fig.6.23, this pattern looks very much like the "cone structure" shown in fig.6.15.   Clearly inside the cone, "stripe-like" structures connecting the pulses exist. Like the situation at θ_K~0.05ML, the tip of the cone also originally started near the center of the target pattern and then slowly moved in the [1$\bar{1}$0]-direction as time went on.

This kind of structure can be found all over the single crystal surface, as shown in fig.6.24, by another example.   One can also see that after a long reaction time, the number of the tips of the cones might be larger than the number of the target patterns, because some target patterns disappeared due to collisions with faster oscillations.
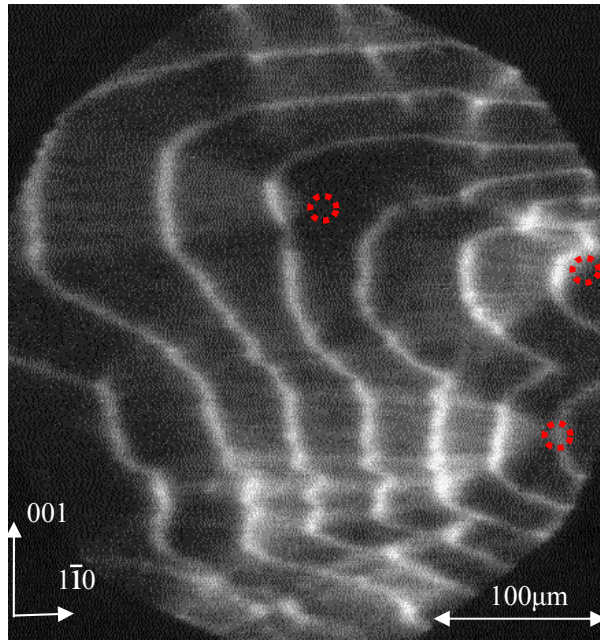
Fig.6.24. "Spider Web" structure in target patterns, at another position of the surface during the

same experiment in fig.6.23.   The tips of the cones are marked by red dashed circles,

P_{NO} =1.54x10^{-6} mbar, P_{H2} = 1.18x10^{-5} mbar.   T = 530K

(3) "Complicated patterns"

"Hybrid pattern"

(a) t = 45s   (b) t = 73s
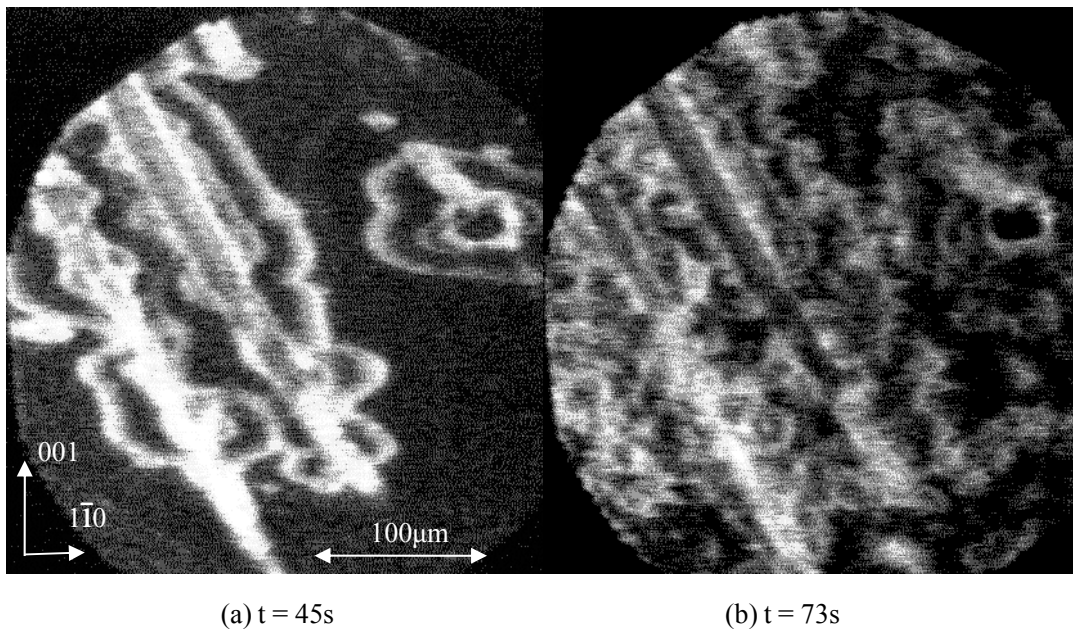
Fig.6.25 PEEM image of "hybrid pattern", in NO +H$_2$ /K/Rh(110) system, θ_K ~0.067ML,

P_{NO} =1.54x10^{-6} mbar, P_{H2} =2.18x10^{-5} mbar, T = 510K

The hybrid pattern at θ_K~0.067ML is similar to the pattern at 0.05ML, as shown in fig.6.25.

The time t = 0 was given by ignition of the patterns.   Fig.6.25 (a) shows broad pulses, and just after 28 s the whole surface became filled by "hybrid pattern" (fig.6.25(b)).   This pattern is more disordered than the ones at lower θ_K , as described in 6.1.2 and 6.1.3.

Stationary pattern

t =28s   t=43s   t=97s

t=111s   t=154.5s
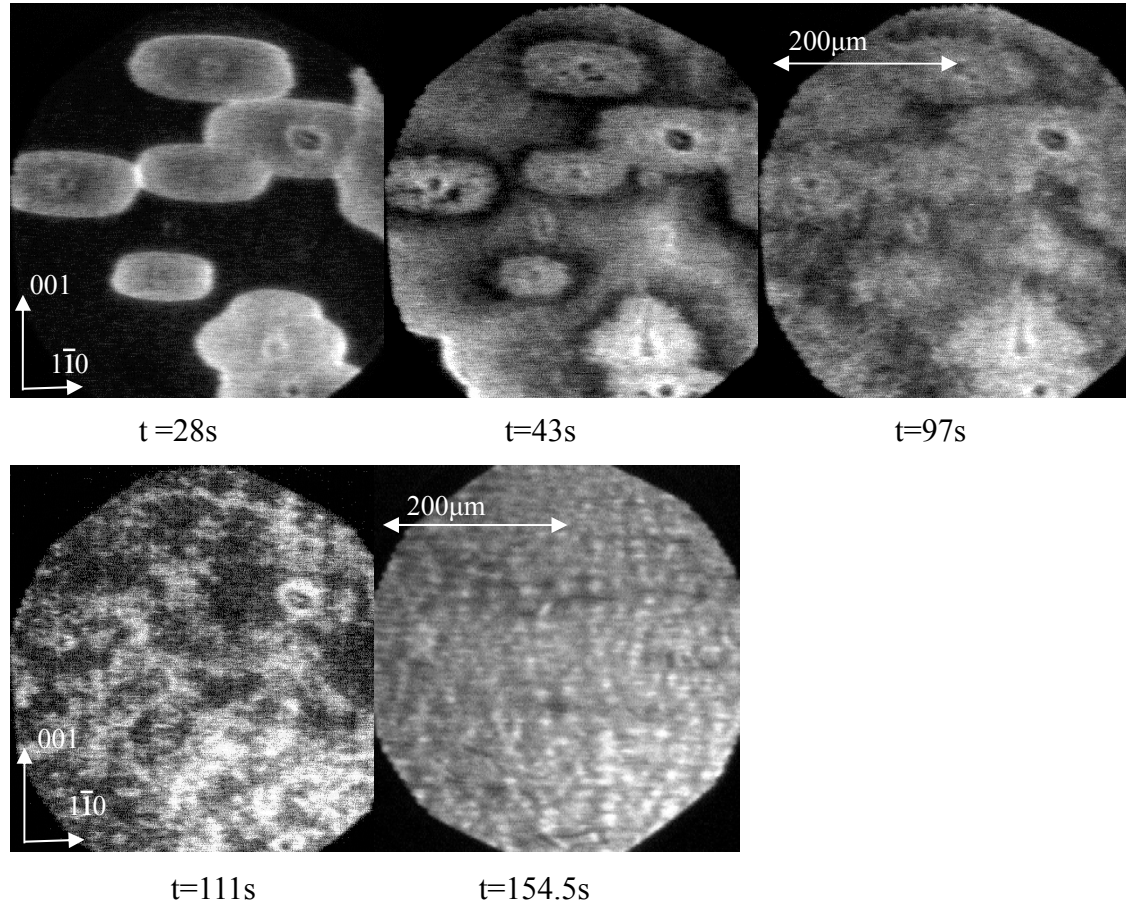
Fig.6.26. PEEM images: Development of the "Turing-like" stationary patterns, in the

NO+H_2/K/Rh(110) system, θ_K ~0.067ML, P_{NO} =1.54x10^{-6} mbar, P_{H2} = 2.52x10^{-5} mbar, T = 510K

At ignition, a few reduction fronts developed, which looked very much like the double metastable fronts of the unpromoted system.   Most of the surface seemed to be in a reduced state (from 43 seconds to 97 seconds).   After about 97 seconds, as shown in fig.6.26, the intensity rapidly changed, and stationary bright dots began to appear on a dark background. Finally a very stable stationary pattern developed.   This pattern is very stable and even after a long period it still remained unchanged.   Fig.6.27 was taken from another position on the sample.   Here the pattern looks more regular and some fine structure can be seen.
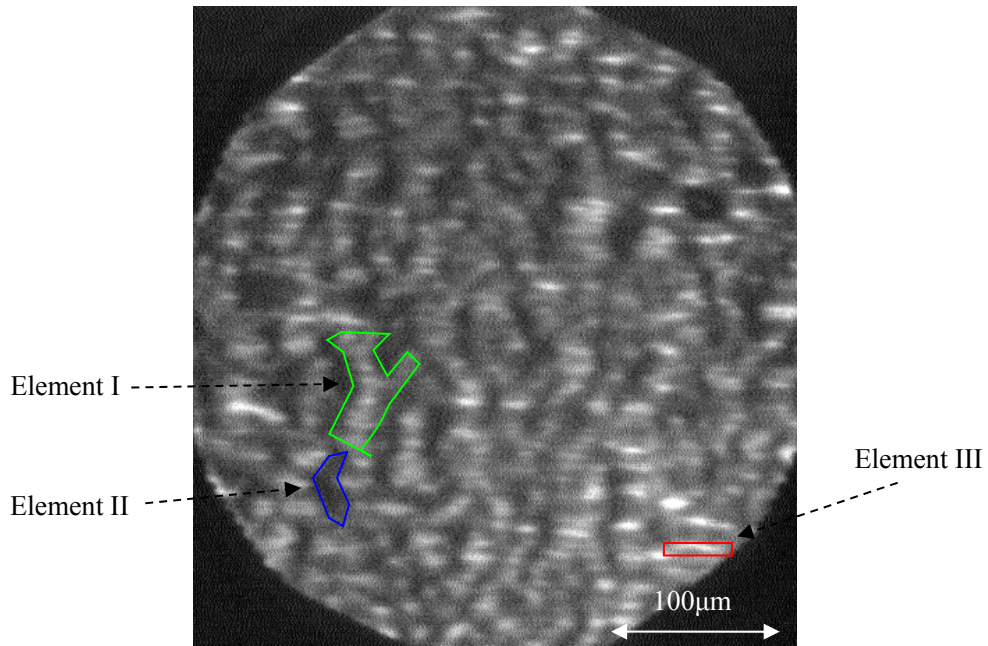
Fig.6.27 PEEM image of the "Turing like" stationary pattern, with three different elements (I, II, and III), The image was taken at another position on the sample during the same experiment as in fig.6.26, in NO+H$_2$/K/Rh(110) system, θ_K ~0.067ML, P$_{NO}$ =1.54x10^{-6} mbar, P$_{H2}$ = 2.52x10^{-5} mbar, T = 510K

As shown in fig.6.27, one can perhaps identify generally three kinds of elements: Gray bands with branches (element I), the dark area between the bands (element II), and the brightest small islands (element III). The shape of these small islands is anisotropic. They are longer (~10^1 µm) in the [1$\bar{1}$0]-direction and shorter (~10^{0}µm) in the [001]-direction. In the H$_2$ +O$_2$/K/Rh(110) system, stationary patterns were formed when two opposite directing reduction fronts collide.[12] It appear in the bistable region.

(4) Bistable regime
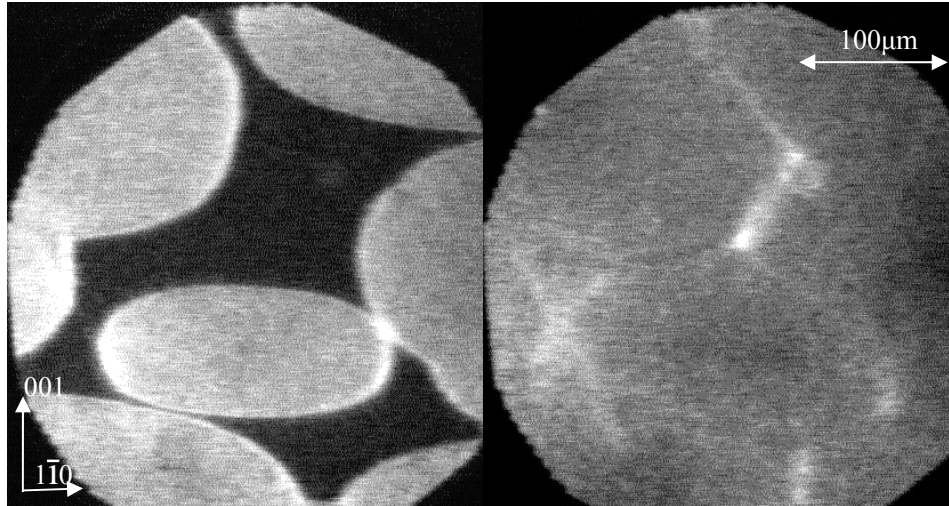
(a) t =33.25s   (b) t = 44s

Fig.6.28. PEEM image: Reduction fronts (a) collided with high intensity in collision area (b), in

NO+H$_2$/K/Rh(110) system, θ_K ~0.067ML, P_{NO} =1.54x10^{-6} mbar, P_{H2} = 2.35x10^{-5} mbar, T = 530K

At θ_K~0.067ML, similar to θ_K ~0.5ML, the collision area of reduction fronts exhibited an enhanced intensity, as shown in fig.6.28.   In this case, the bright areas are not the final pattern.   When the experiment progresses, we will see more interesting phenomenon shown as below:
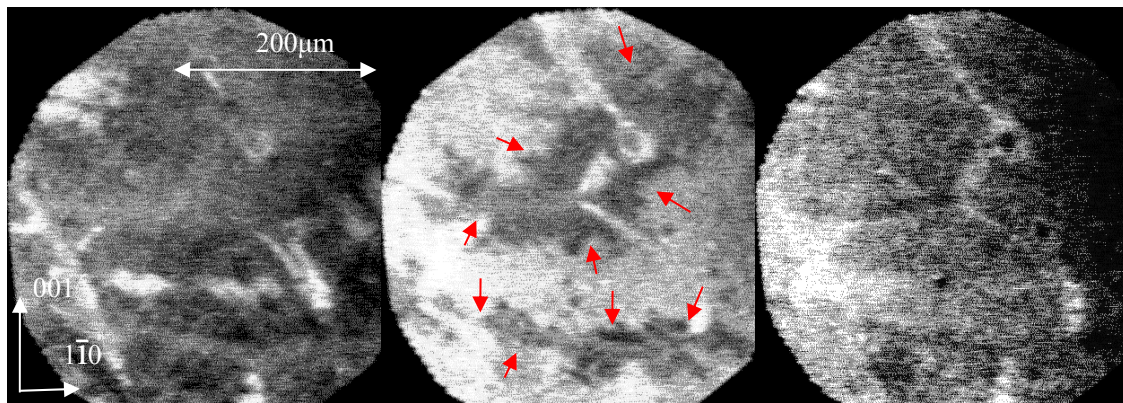
(a) t = 64s   (b) t = 72s   (c) t = 81.5s

Fig.6.29. Second reduction fronts from the same experiment in fig.6.28, in NO+H$_2$ /K/Rh(110) system,

θ_K ~0.067ML, P_{NO} =1.54x10^{-6} mbar, P_{H2} = 2.35x10^{-5} mbar.   T = 530K

As shown in fig.6.29, in the same experiment, after the reduction fronts shown in fig.6.28 completely had disappeared, the surface darkened as shown in fig.6.29 (a).   Then second "fronts" developed as shown in fig.6.29(b).   These "fronts" had a very irregular shape. After they covered the whole surface, the surface finally became stationary.   The resulting

pattern was just like the stationary pattern due to collision of reduction fronts in the bistable regime, which was described in 6.1.3.　When P_{H2} is further increased, this phenomenon disappeared.

6.1.5 Very high K coverage (~0.12ML)

(1) General
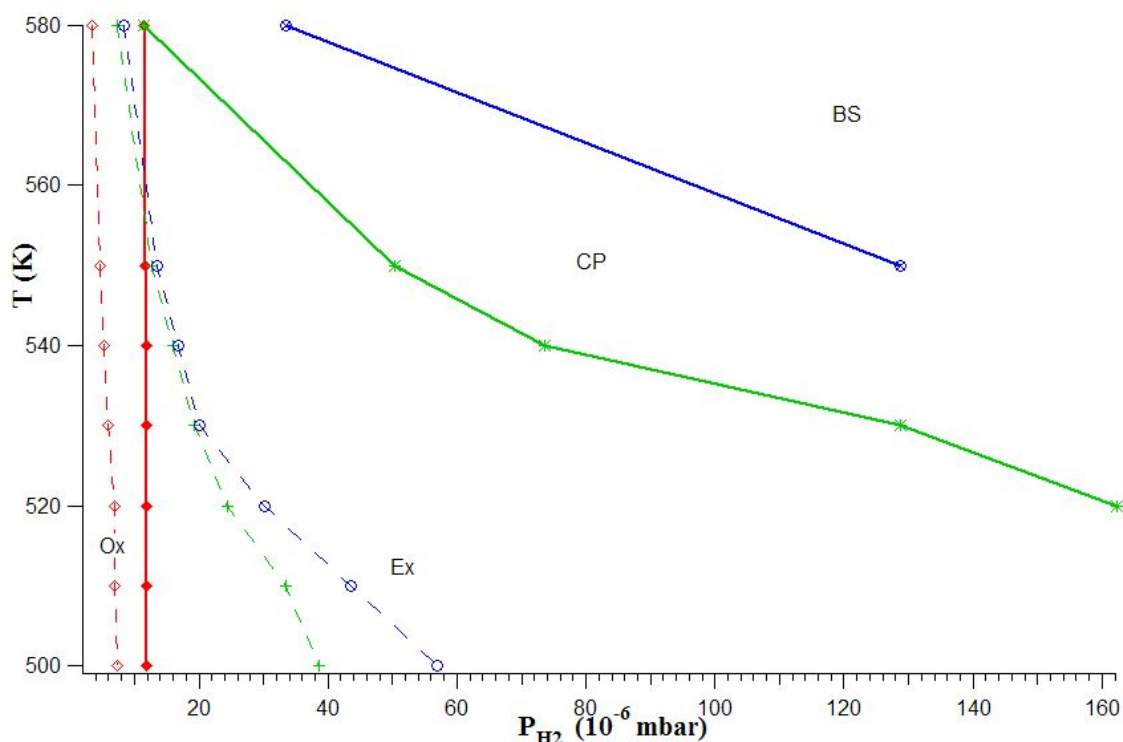
Fig.6.30. Bifurcation diagram of NO+H$_2$/K/Rh (110) system (Dashed lines are the bifurcation diagram of the unpromoted Rh(110) surface).　θ_K ~0.12ML , P_{NO} =1.54x10^{-6} mbar.

Ox = Oxygen covered surface; Ex = Excitable; CP = "Complicated patterns"; BS = Bistable.

At very high K coverage (~0.12ML, corresponding to a 1x2 LEED pattern), the bifurcation diagram is shown in fig.6.30.　The low P_{H2} border between the oxygen covered state and the excitable regime is shifted to high H$_2$ pressure, but meanwhile the border between the excitable and the bistable regime is drastically shifted to the high P_{H2} side.　The latter shift is different from the previous behavior observed at lower K coverage.

(2) Excitable state

Wave fragments

At very high K coverage (~0.12ML), wave fragments were not found, either because they just cannot be formed, or the H_2 partial pressure range became so narrow, that it cannot be experimentally controlled yet.

Target patterns and spiral waves

At very high K coverage (~0.12ML) and at temperature higher than or equal to 580K, an increasing H_2 partial pressure causes the system directly to go from the oxygen covered state to the "complicated patterns" regime.
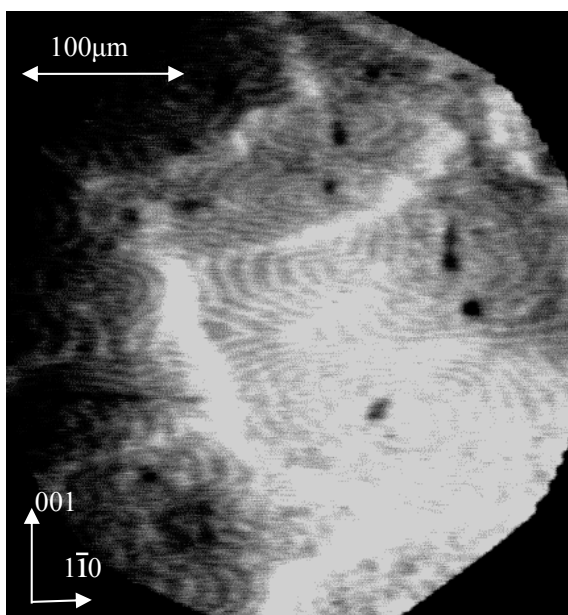
Fig.6.31 PEEM image. Target patterns, with high intensity of background, in NO+H_2/K/Rh(110) system , θ_K ~0.12ML, P_{NO} =1.54x10^{-6} mbar, P_{H2} = 4.52x10^{-5} mbar.   T = 510K

At this high K coverage like 0.12ML, the target patterns became very condensed, which means a very short wavelength, as can be seen in fig.6.31.   One can also note that in the center of the image, the whole pattern has a strong bright inhomogeneous background (not due to the alignment of PEEM).   This bright background might be related to   an inhomogeneous K distribution caused by possible mass transport of the potassium.

Wave trains（Zebra Pattern）

(a) $\Delta t=0s$ (b) $\Delta t=2.5s$

(c) $\Delta t=5s$ (d) $\Delta t=7.5s$
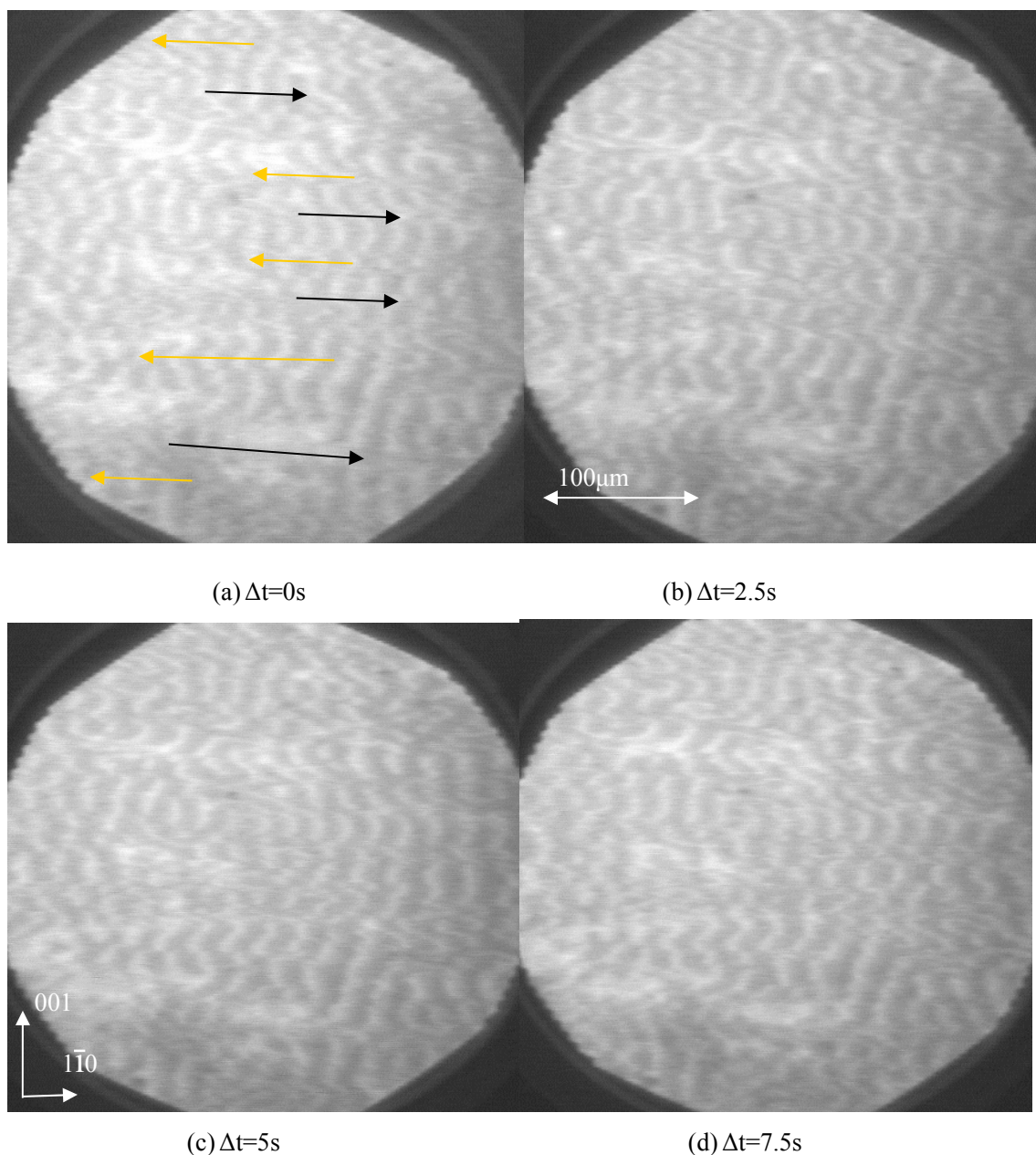
Fig.6.32. PEEM image of opposite traveling wave trains, in NO+H$_2$/K/ Rh (110) system, θ_K ~0.12ML,

P_{NO} =1.54x10^{-6} mbar, P_{H2} = 4.52x10^{-5} mbar.   T = 510K

When temperature is at 540K, and the pressure of H$_2$ is between 3.67x10^{-5} to 5.0x10^{-5} mbar, after ignition, first target patterns appeared. Soon after, they broke into opposite traveling wave trains, as shown in fig.6.32. The different direction of movement is marked by black and yellow arrows. This type of pattern has been reported by before [35], but with a Pt metal pad on the Rh(110) surface and at much lower K coverage (θ_K ~ 0.08ML). Now at θ_K ~ 0.12ML, in a temperature range from 500 to 510K, in a small pressure range near the boundary from the "excitable state" to the "complicated patterns" regime this pattern can be

reproduced.

(3) "Complicated patterns"

"Hybrid pattern"

At θ_K ~0.12ML, most "hybrid patterns" started from reduction fronts similar to those in the bistable regime, as shown in fig.6.33(a).   As demonstrated in fig.6.33(b), at t = 226s, some irregular dark regions began to grow at the positions of the original excitation center.   After about 7min, as shown in fig.6.33(c), they developed into a "hybrid pattern", consisting of a combination of irregular stationary islands and very chaotically moving waves in between.

(a) t= 15s   (b)t=226s   (c)t=416s
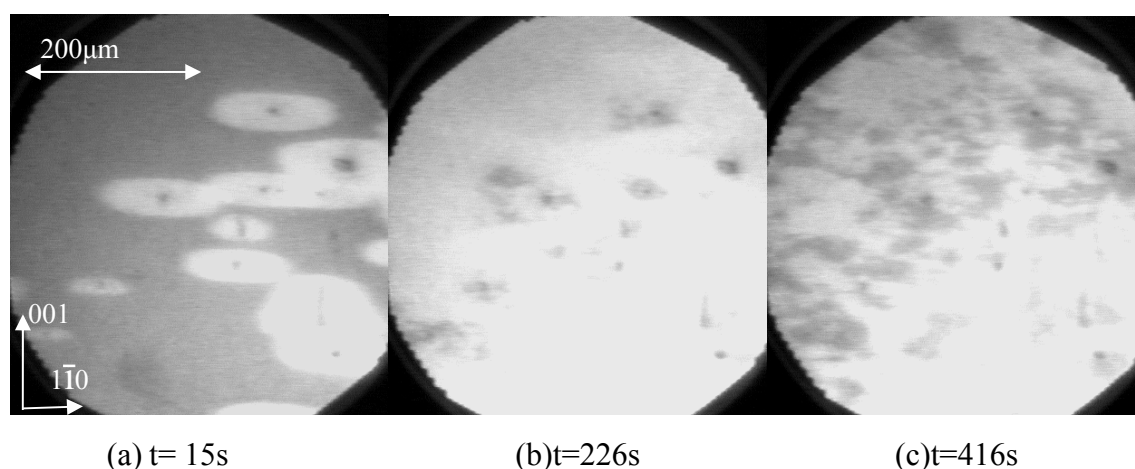
Fig.6.33 PEEM image of "hybridized pattern", in NO+H$_2$/K/Rh(110) system , θ_K ~0.12ML,

P_{NO} =1.54x10^{-6} mbar, P_{H2} = 6.20x10^{-5} mbar.   T = 550K

Stationary pattern

At θ_K ~0.12ML, the "Turing-like" stationary patterns found at θ_K ~0.05ML and θ_K ~0.067ML were not found.

(4) Bistable state

At θ_K ~0.12ML and T = 580K, after ignition of the reaction, the system directly went from resting state into complicate state, as shown in fig.6.30.   Only for T<580K, the excitable regime shows spiral waves and target patterns.

As shown in the bifurcation diagram in fig.6.30, the boundary of H$_2$ partial pressure from the "complicated patterns" regime to the bistable state dramatically shifts to high P_{H2} with decreasing temperature.   At 550K, this boundary became already so high that it reaches the

10^{-4} mbar range, which is out of the experimentally accessible range. One general conclusion is that: as the K coverage increases beyond 0.067ML, the H_2 pressure required to reach the bistable regime increases drastically with the K coverage. It is shown in fig.6.34 how reduction fronts look like under such high K coverage. At such high K coverage, the border between the reduction fronts and the remaining area became hard to identify.

(a) t =16.5s   (b) t = 74s
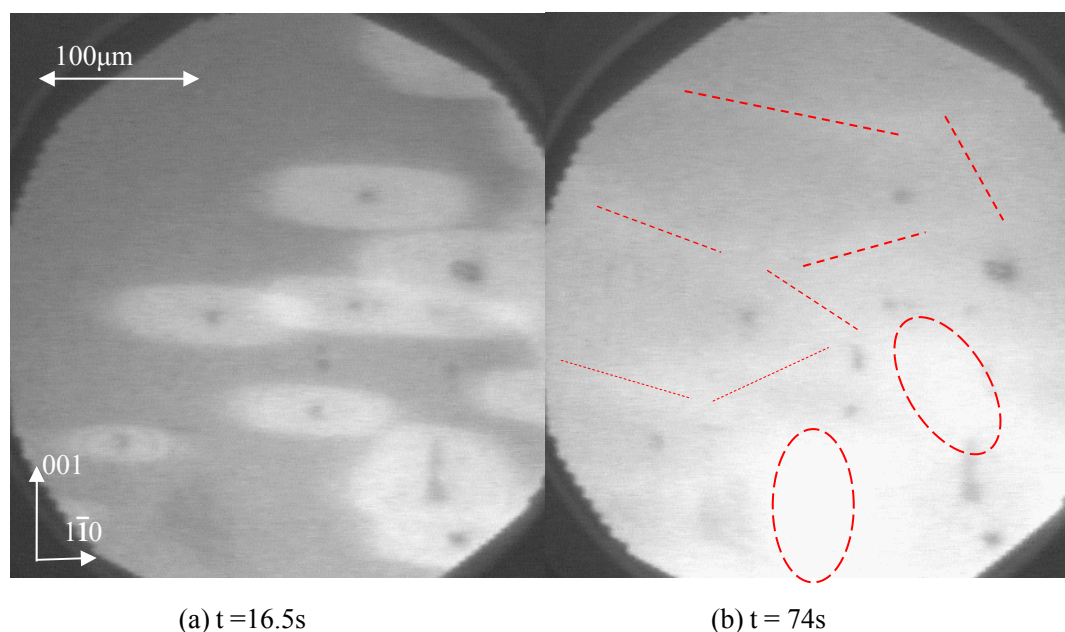
Fig.6.34 PEEM image of reduction fronts, in NO+H_2/K/Rh(110) system, collision areas are indicated by red dashed lines and eclipses, θ_K (~0.12ML), P_{NO} =1.54x10^{-6} mbar, P_{H2} = 4.52x10^{-5} mbar, T = 580K

As shown in the figure, the collision area became still very bright (marked by red dashed lines and circles). After the whole surface became reduced at 74s, the colliding areas were extremely bright at the bottom of the image where many fronts collided together, these areas are marked by red dashed circles.

6.1.6 Trial for higher K coverage (~0.15ML)

One attempt was made to study pattern formation at even higher θ_K ~0.15ML where LEED displays a high coverage 1x3 pattern. But at this high coverage, the border between reaction fronts or pulses and the remaining surface area turned out to be nearly impossible to identify. At T~580K, the K coverage cannot be maintained due to beginning of K desorption, according to the phase diagram in fig.4.8 in chapter IV. At T<550K, the initial K coverage is not homogeneous, which no longer allows defined experiments. So under

our experimental conditions at T=500K-580K, the investigation at high coverage had to end here

6.2 Pattern formation under higher temperature (T≥600K)

Generally, the bifurcation diagram so far was studied within the temperature range from 500K to 580K. Theoretically, above 580K on the unpromoted Rh(110) surface a monostable state is left. It is interesting to know what happens at T≥600K in the presence of coadsorbed K.
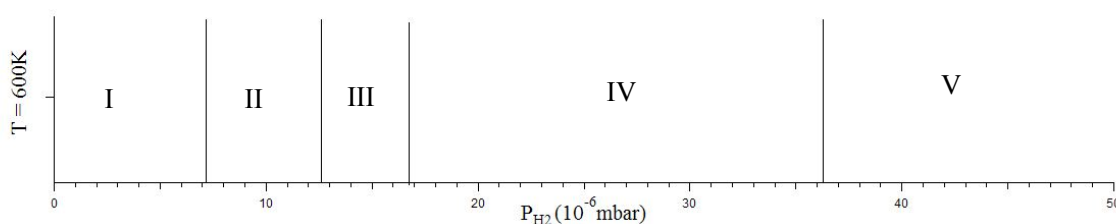
Fig.6.35 Bifurcation diagram of patterns in $NO+H_2$ /K/Rh(110) system, θ_K ~0.12ML, T=600K,

I = Oxygen covered, II = "Fingering", III = Fronts with fingering, IV = Bistable, V = Monostable

The bifurcation diagram obtained at 600K with K at ~0.12 ML is shown in. fig.6.35, we got interesting results. The meaning of the region II and region III will be explained in following text.

6.2.1 Area II
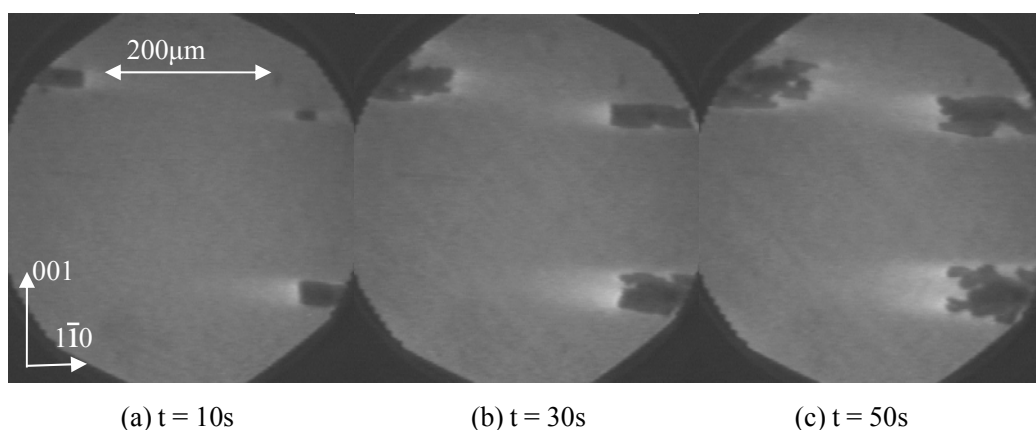
(a) t = 10s   (b) t = 30s   (c) t = 50s
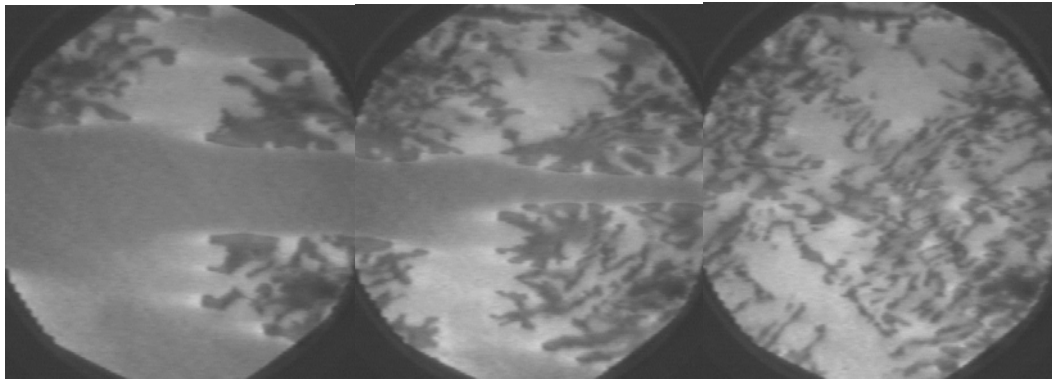
(d) t = 100s   (e) t = 170s   (f) t = 260s

Fig.6.36 "Fingering" structure, in $NO+H_2/K/Rh(110)$ system, θ_K ~0.12, T=600K

P_{NO} = 1.54x10^{-6} mbar, P_{H2} = 1.18x10^{-5} mbar

At area II, "fingering" like structure developed, as shown in fig.6.36. First, rectangular reduction fronts developed (fig.6.36(a)), but with a dark intensity in the fronts and diffuse bright part before the fronts. Soon at t=30s, some instabilities evolved in the fronts (fig.6.36(b)). The fronts then became more and more irregular (fig.6.36(c)). At t=100s, fingering-like structure developed (fig.6.36(d)). When the fronts collide, the collision area still exhibits an enhanced brightness (fig.6.36(e)). Finally the fingering-like structure invaded also the collision area and covered the whole surface (fig.6.36(f)).
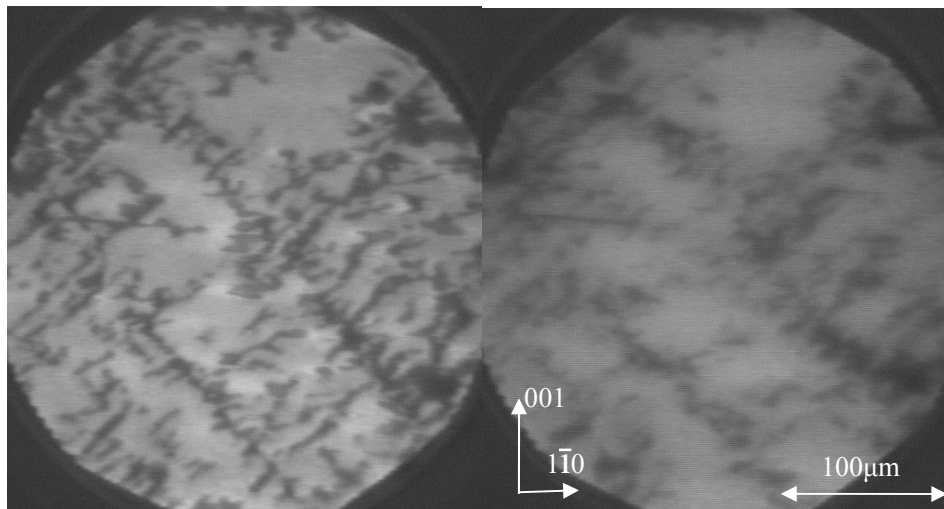
(a) t = 1450s   (b) t = 1800s

Fig.6.37 PEEM image of "fingering" structure in $NO+H_2/K/Rh(110)$ system, θ_K ~0.12, T=600K, (a) P_{NO} = 1.54x10^{-6} mbar, P_{NO} = 1.18x10^{-5} mbar , after long time (1450s); (b) H_2 off.

Even after a long reaction time (1450s), this structure still existed, as shown in fig.6.37 (a),

but those dark fingering structures were not stationary and slowly changing their shape.

Discussion

As shown in fig.6.37 (b), when H_2 was turned off, the contrast remained. If we don't consider possible unknown lowering effect of work function by reconstruction, this means the high brightness between the black fingering structures are possibly due to K accumulation, and the dark fingering structures are actually reduced area.   This seems to be more or less consistent with the result of chemical analysis of stationary pattern in chapter VIII.   There it was pointed out that the K is present in O enriched areas but is diminished in reduced area.   Therefore the oxygen covered areas in pattern formation can lower their work function through K coadsorption.

The real "viscous fingering" originates from invasion of a less viscous fluid in a more viscous fluid.   The instabilities of the interface are induced by competition between viscous and capillary force [40].   Naturally, one may speculate that the fingering observed here might come from the large difference at high temperature (600K), between the high mobility of the species like H_{ad}, K_{ad}, etc. on the reduced area (the fingers) and the low mobility of those species in the oxygen covered area between the fingers.

To get a definite answer, a local chemical and a local structural analysis like XPS and LEED are needed.

6.2.2 Area IV

(a) t = 5s   (b) t = 20s   (c) t = 60s
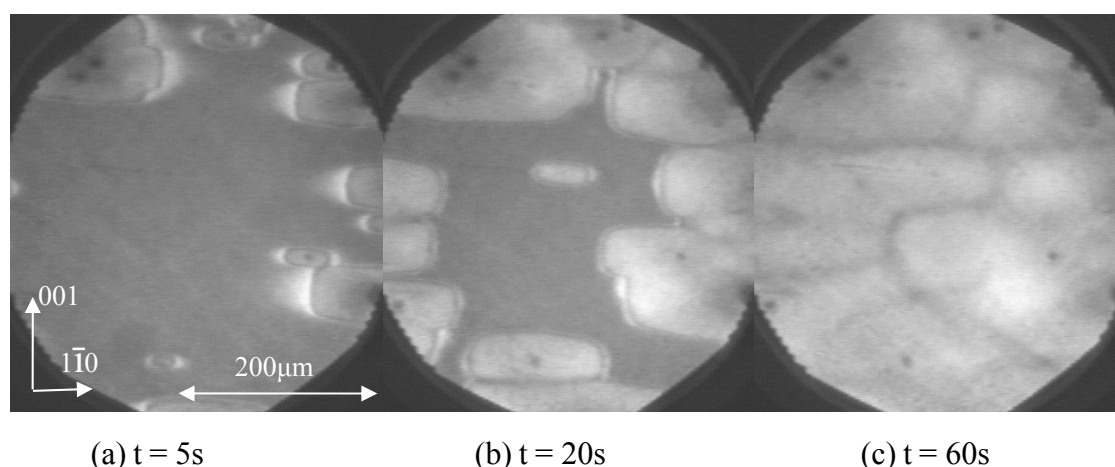
Fig.6.38 PEEM image of colliding reduction fronts, in NO+H_2/K/Rh(110) system, θ_K ~0.12ML,

T = 600K, P_{NO} = 1.54x10^{-6} mbar, P_{H2} = 2.85x10^{-5} mbar

At area IV, reduction fronts appear.   However, the collision area of the fronts remained dark, as shown in fig.6.38.   Another significant phenomenon is the broad edge in front of every reduction front.   This edge looked stronger and wider in the $[1\bar{1}0]$-direction.
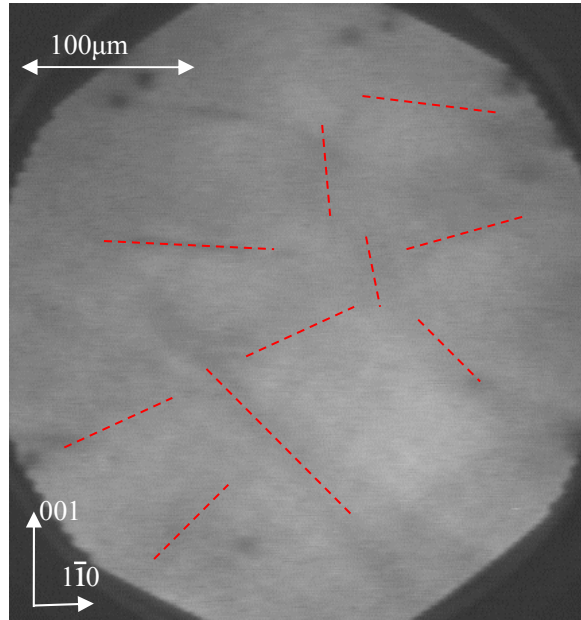
Fig.6.39. PEEM image of the same experiment in fig.6.38, 30s after H_2 was turned off.   The former collision areas in fig.6.38 (c) are indicated by red dashed lines

When H_2 was turned off, as shown in fig.6.39, the collision area remained darker than the surrounding area.   If we consider only the lowering of work function by K coadsorption, this fact indicates that the K distribution in the collision area is reduced, and K is mostly enriched at the area near the collision area.

6.2.3 Area III
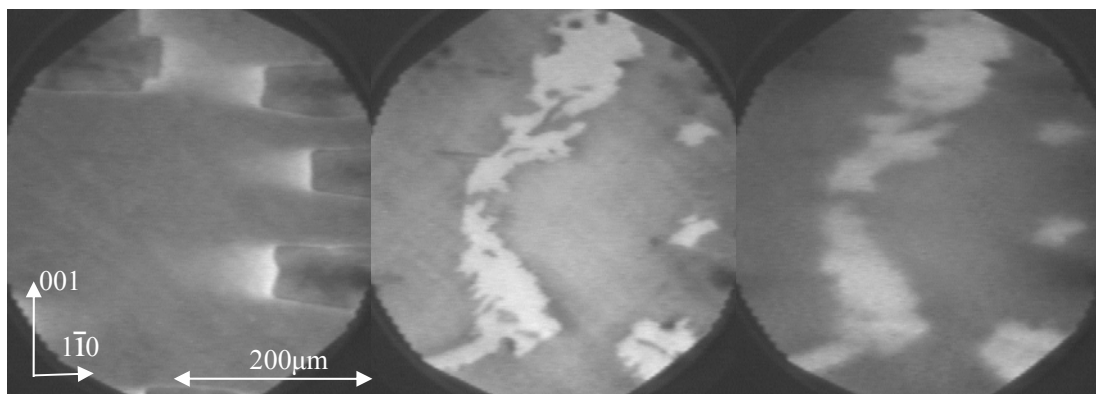
(a) t = 50s   (b) t = 410s   (c) t = 420s (H_2 off)

Fig.6.40. PEEM image of reduction fronts with coexisting "fingering" structure in area III in the

bifurcation diagram of fig.6.35, in NO+H$_2$/K/Rh (110) system, θ_K ~0.12ML, P_{NO} =1.54x10^{-6}

mbar, P_{H2} = 1.51x10^{-5} mbar, T = 600K

At area III, between area II and IV, an intermediate state exists. Reduction fronts exist, but in the collision area, some "fingering-like" structure appeared, as shown in fig.6.40. It should also be noticed that the bright collision area is elongated in the [1$\bar{1}$0]-direction but the collision area in the [001]-direction is dark.

6.3 General discussion

6.3.1 Shift of the boundaries with θ_K

a. From resting state and excitable state
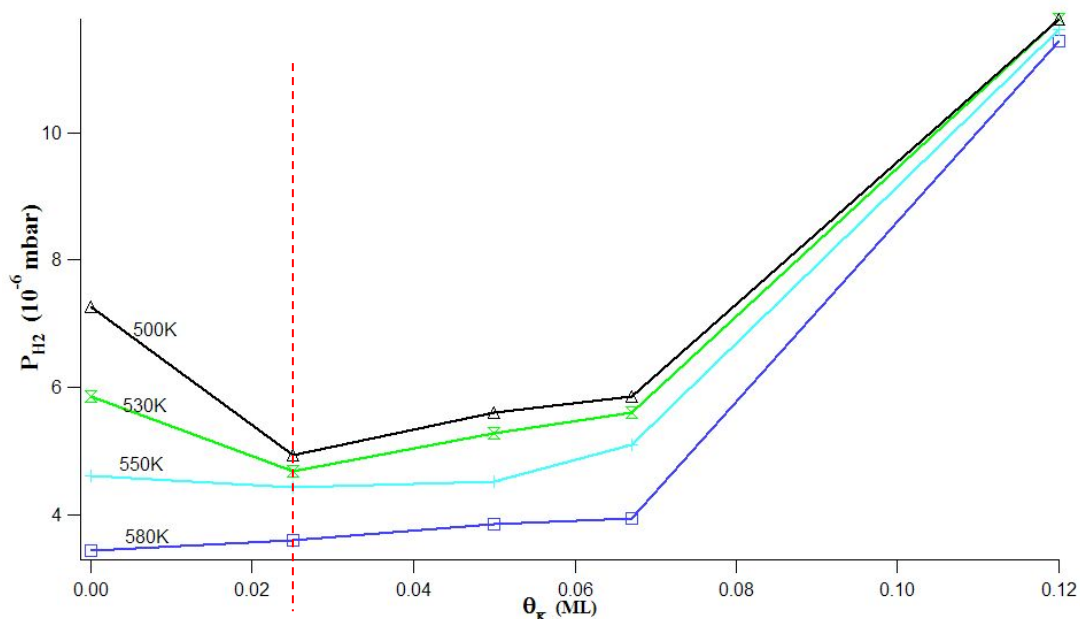
Fig.6.41. The boundaries from the oxygen covered state to the excitable state. The data are from fig.6.1, fig.6.2, fig.6.11, fig.6.20, and fig. 6.30.

The shift of the boundary is related to the ignition of the reaction, as shown in fig.6.41.

1) For θ_K <0.025ML, as the K coverage increases, the H$_2$ partial pressure for ignition decreases with increasing θ_K. At lower temperature, this effect is more significant. For the same coverage, the ignition pressure of H$_2$ is lower at higher temperature. This behavior means that the K actually "enhances" the ignition of the reaction.

2) For $\theta_K > 0.025ML$, the ignition pressure of H_2 increases with increasing K coverage. This tendency became especially significant at $\theta_K > 0.067ML$. As the K coverage increases, for fixed H_2 pressure, the temperature required to ignite the reaction is higher. This behavior means, the K existence actually is now "inhibiting" the ignition of the reaction.

b. The boundary between the "complicated patterns" and the bistable regime
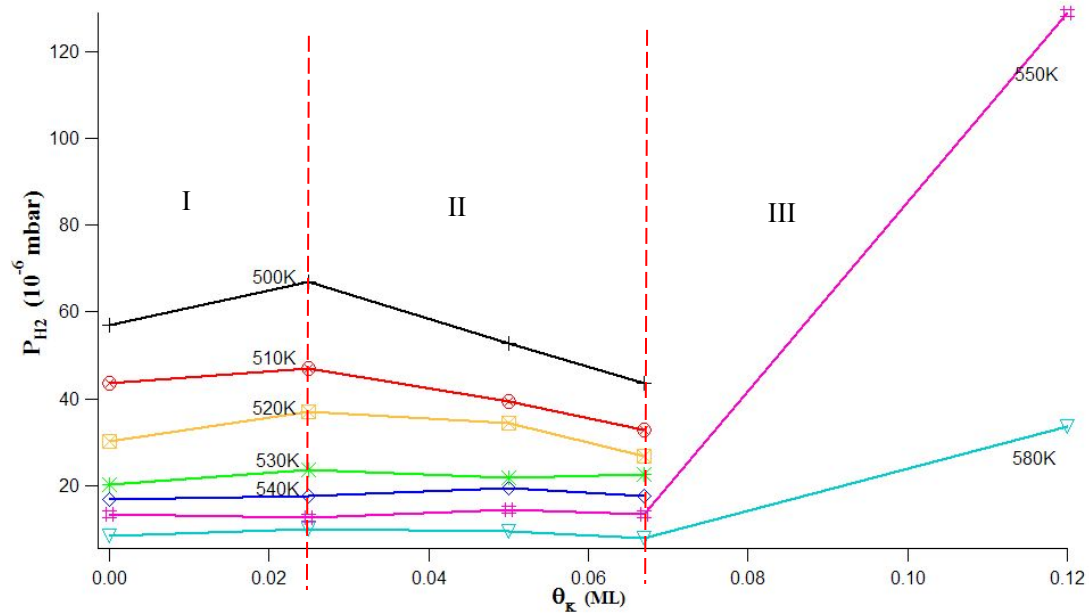
Fig.6.42. The boundaries from the "complicated patterns" to the bistable regime. Data are from bifurcation diagrams in fig.6.1, fig.6.2, fig.6.11, fig.6.20, and fig.6.30.

The change of the boundary from the "complicated pattern" regime to the bistable state regime with K coverage is shown in fig.6.42. Generally, for fixed K coverage, when increasing the temperature, the required H_2 partial pressure is significantly decreased. The graph can be further divided into three regions: below 0.025ML (area I), from 0.025ML to about 0.067ML (area II) and above 0.067ML (area III).

1) In area I, at 530-580K, the line is quite flat, which means for fixed temperature or H_2 pressure, as θ_K increases, the changing of boundary condition is quite small. At 500-530K, the slope is positive.

2) In area II, for fixed temperature, at 530-580K, the curves are quite flat, at 500-520K, the slope is negative, which means as θ_K increases, it is easier to enter the bistable regime.

3) In area III, the changes drastically with θ_K. For T<550K, the boundary to the bistable regime becomes so high in P_{H2} that experiments were no longer performed (high pressure

gas may cause a discharge in PEEM chamber which uses high voltage up to 10kV).   So only data for 580K and 550K were recorded.

c. From excitable state to complex state(for clean Rh surface it is double metastable state)
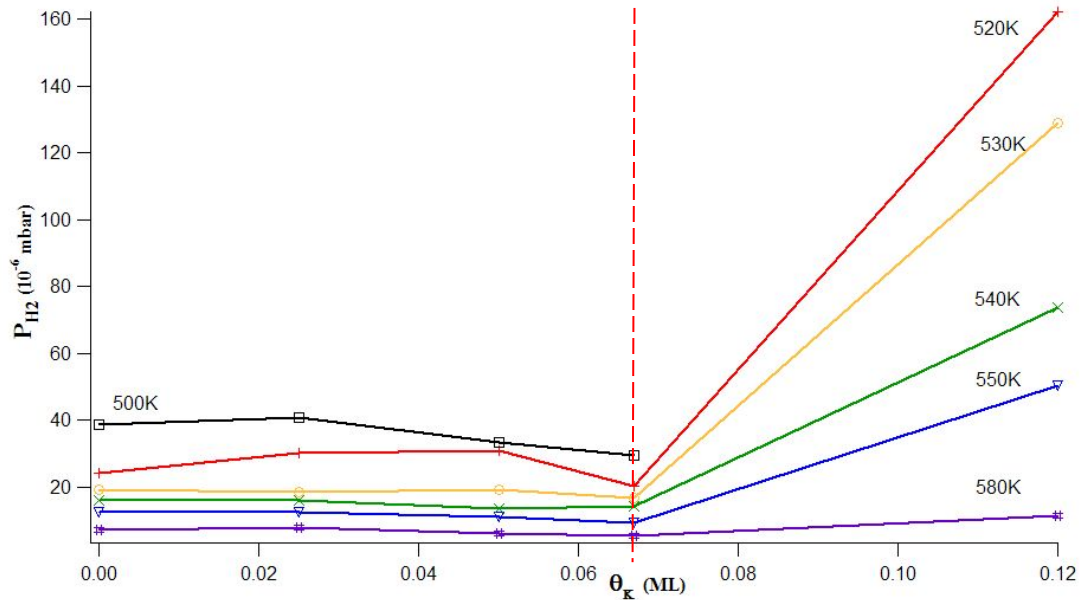
Fig.6.43. Boundary condition of H_2 pressure, when system changes from the excitable state to the "complicated pattern" regime. Taken from bifurcation diagrams in fig.6.1, fig.6.2, fig.6.11, fig.6.20, and fig.6.30

The boundaries from the excitable state to the "double metastable state" for $\theta_K = 0$ and "complicated patterns" regime for $\theta_K > 0$ from all bifurcation diagrams are shown in fig.6.43.

Generally, the for fixed K coverage, when the temperature increases, the required H_2 partial pressure for ignition is significantly decreased. The graph can be divided into 2 areas: θ_K below and above 0.067ML:

1) In area I, the curve is quite flat compared to area II, which means the influence of θ_K on the boundary is small..

2) In area II, again there was a drastic change.   The slope became positive, and increases with decreasing temperature.   This means for increasing θ_K, at a fixed temperature, the required H_2 pressure for the system to reach the "complicated patterns" regime became higher.

6.3.2 The anisotropy change of wave fragments.

General Phenomena

1. On the unpromoted Rh(110) surface, only wave fragments travels along the [001]-direction are seen.

2. As the K coverage increases, the propagation of wave fragments begins to change. At low potassium coverage, wave fragments can propagate in both the [001]- and [1$\bar{1}$0]-direction, as shown in fig.6.3.

3. When the potassium coverage reaches 0.067ML, only wave fragments traveling in the [1$\bar{1}$0]-direction can be found, and at this coverage, the patterns look very turbulent, as shown in fig.6.22.

From wave fragments to target pattern, on the unpromoted Rh(110) surface

One interesting point is how the traveling wave fragments change to target pattern or spiral waves, or vice versa. This point might be helpful to explain the anisotropy change of the wave fragments with rising K coverage. As shown in fig.6.44, after a target pattern was created, the H_2 pressure was carefully lowered, so that the target pattern slowly changed to wave fragments.

(a) t =130s   (b) t =140s   (c) t =150s
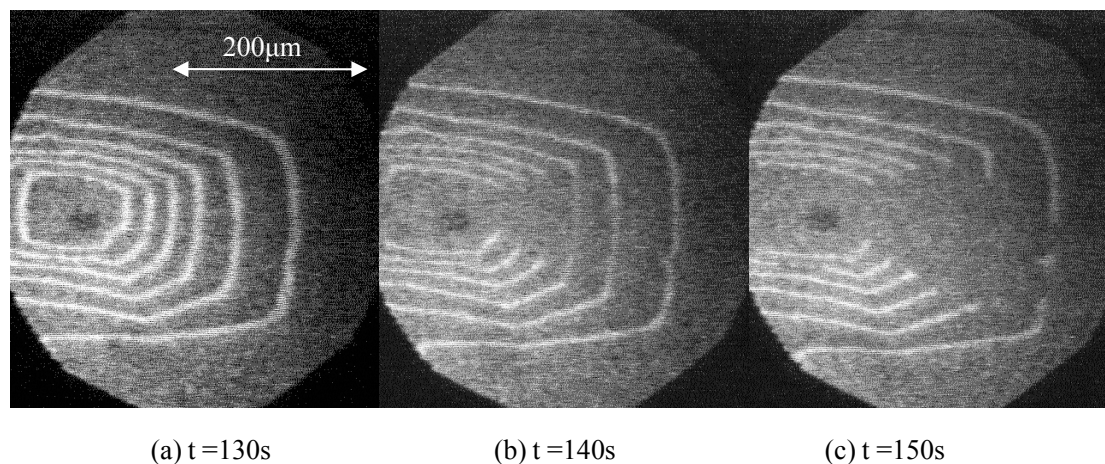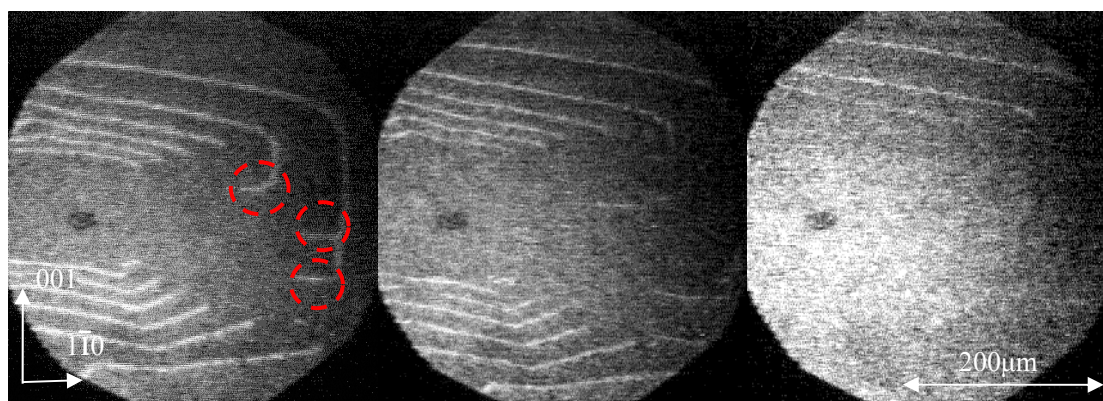
(d) t = 210s   (e) t = 270s   (f) t = 290s

Fig.6.44. From target pattern to wave fragments, NO+H_2 reaction on clean Rh(110) surface, P_{NO} = 1.54×10^{-6} mbar, P_{H2} =5.1×10^{-6} mbar (t<130s), P_{H2} =4.7×10^{-6} mbar (t>130s)

After a target pattern is generate as shown in fig.6.44(a), at 130s, the pressure of H_2 was decreased from 5.1×10^{-6} mbar to 4.7×10^{-6} mbar. 10 minutes later, as shown in fig.6.44 (b), the target pattern began to break, while the pulses already far from the center remained. At 150s, these pulses also began to break. At 210s, spirals developed at the edge of the early pulses (pointed by slash red circles in fig.6.44 (d)). At 270s, the spirals also began to break in the [1$\bar{1}$0]-direction. Finally as shown in fig.6.44 (f), at 290s, the whole pattern broke into wave fragments traveling in the [001]-direction.

The whole process shows when the target pattern breaks into wave fragments, the breaking first takes place in the [1$\bar{1}$0]-direction. A possible influence of K induced reconstruction or K coadsorption on the diffusion rate of the surface may be enrolled to the anisotropy change.

6.3.3 Formation of "Turing-like" stationary pattern

Previously, stationary patterns were found in the H_2+O_2/K/Rh(110) system, while in the unpromoted NO+H_2/Rh(110) system, no stationary pattern exists.

In the NO+H_2 /K/Rh(110) system, two types of stationary patterns were found: (i) stationary patterns caused by collision of two reduction fronts in "bistable" regime, (ii) a "Turing-like" stationary patterns in the "complicated patterns" regime. The images can be seen in fig.6.18 and fig.6.27 and a description is found in 6.1.3 and 6.1.4.

In the second type of stationary pattern, the brightest small islands (element III) exhibits an

anisotropic shape.   The brightness of element I and element III might be due to K enrichment, because after turning off H_2, the PEEM intensity of element I and III remained higher than the brightness of element II.

Since the element II exhibits the highest work function, it was first speculated that this surface is oxygen covered.   In later experiments with chemical analysis it was shown result that on the contrary, that the dark area with a higher work function is actually reduced surface which is N covered, whereas the bright area belongs to oxygen covered area enriched with K.

6.3.4 Influence of K on Wave propagation

(a) $\Delta t = 0s$ (b) $\Delta t = 210s$ (c) $\Delta t = 500s$

(d) $\Delta t = 700s$ (e) $\Delta t = 800s$
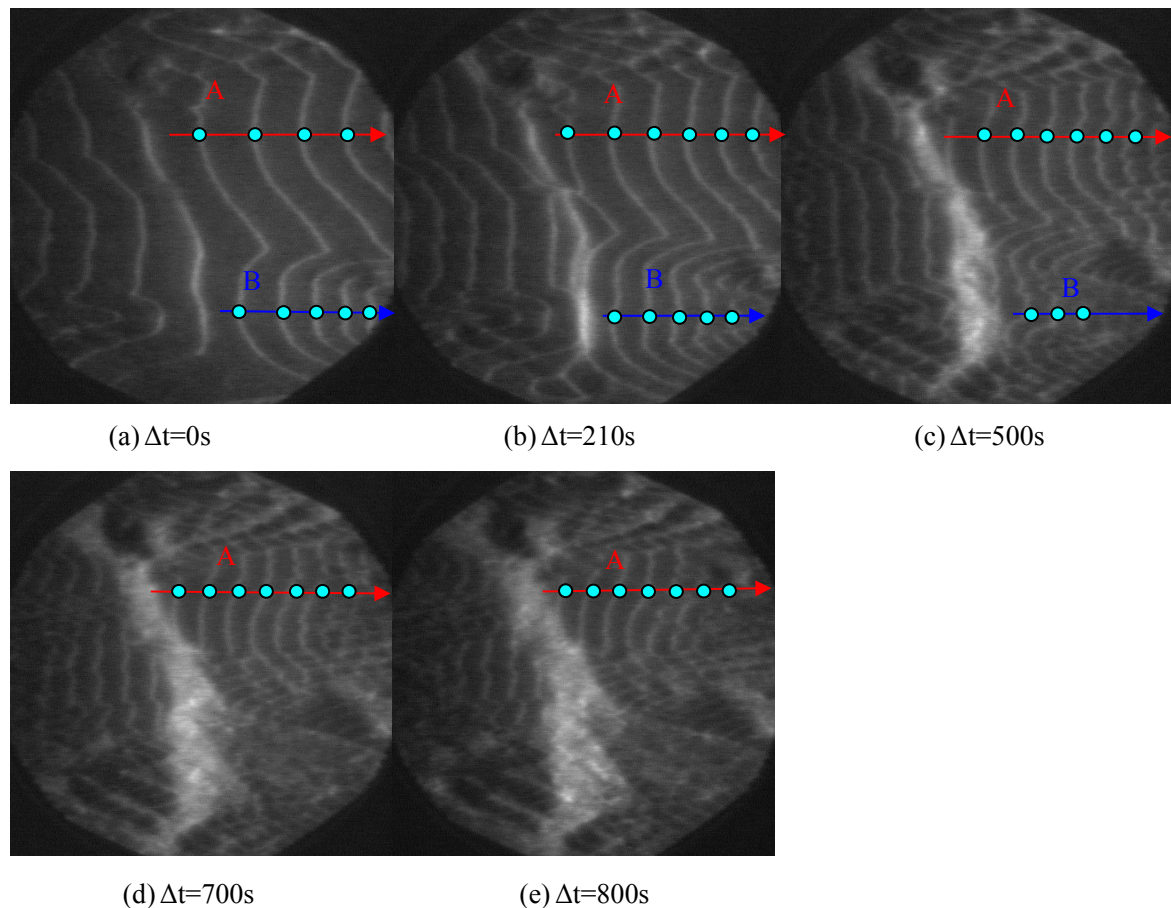
Fig.6.45. PEEM image of colliding target pattern in $NO+H_2$ /K/Rh(110) system, θ_K =0.067ML, P_{NO} =1.54x10^{-6} mbar, P_{H2} = 1.8x10^{-5} mbar, T=510K, Light blue points are taken for velocity measurement, along two different lines, A (red on the top) and B (blue at the bottom),   (a)Δt=0s;   (b)Δt=210s; (c)Δt=500s;   (d)Δt=700s;   (e)Δt=800s,

Shown in fig.6.45 is an area where two regular target patterns collide, wave speed was measured along two different lines, A and B (shown in fig.6.45. as red line and blue line), the

wave speed distribution of the two positions are shown in fig.6.46. and fig.6.47.

After 500s, as the bright area in collision area became continuously broadened, the left side of line B went inside that area.　The bottom part of the pattern there became turbulent.
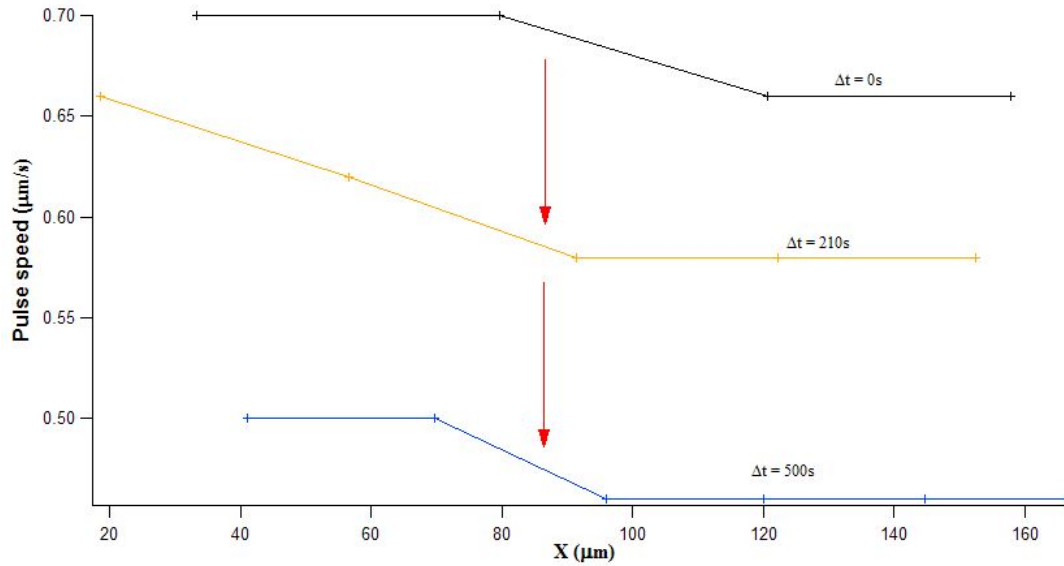
Fig.6.46 Wave velocity measured along line A in fig.6.45, t=0-500s
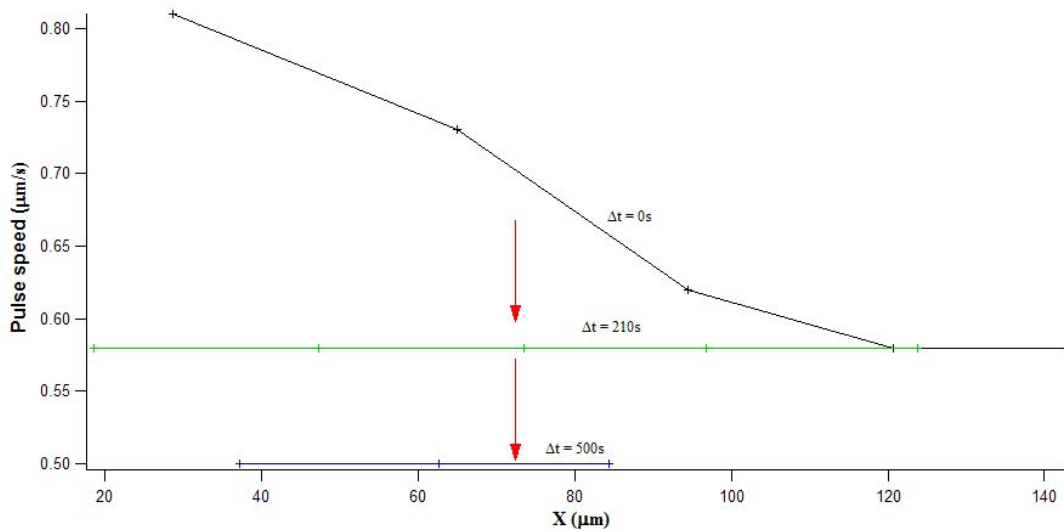
Fig.6.47 Wave velocity measured along line B in fig.6.45, t = 0-500s

From 0 to 500s, the wave velocity of waves measured in two different lines is shown in fig.6.46 and fig.6.47.　For both positions, the waves after the initial waves slowed down. In the position near the collision area (x=20μm), the wave velocity continuously slowed down during the reaction to a minimum value of 0.50μm/s.　Particularly, before the area in position B turned totally turbulent (from 210s), the wave velocity of pulses along the line B became the same, with a minimum value of 0.50μm/s.
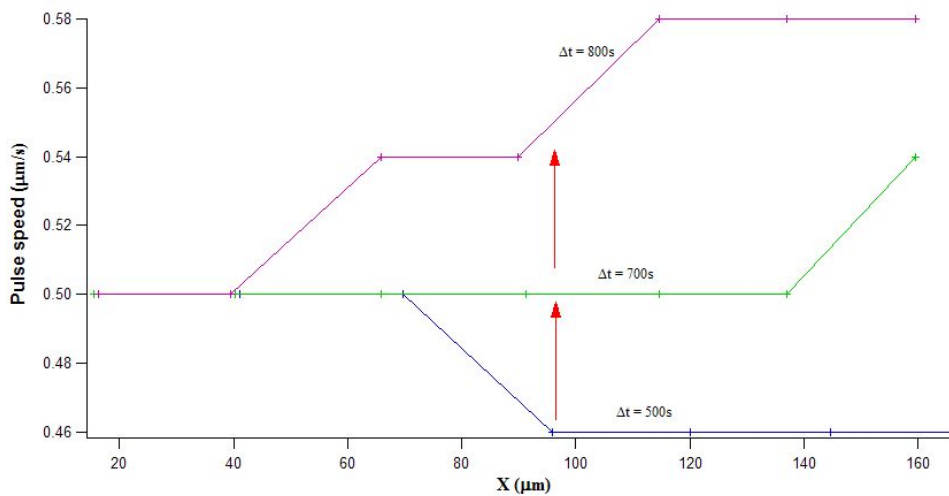
Fig.6.48 Pulse velocity distribution measured along line A in fig.6.45, t =500-800s

After 500s, at position A, the pulses survived till the end of experiment. In the area near the collision center (x=20μm), the pulse velocity can still be measured.   The velocity remained unchanged at the minimum value 0.50μm/s till the end of experiment.   In the area far from the collision area (x>80μm), after reaching minimum value of 0.46μm/s at 500s, the wave velocity of pulses began to increase.

From the velocity measurement, and measurement of the pulse wavelength, we can get a dispersion relation of the top and the bottom of the area as shown below in fig.6.49

Dispersion relation
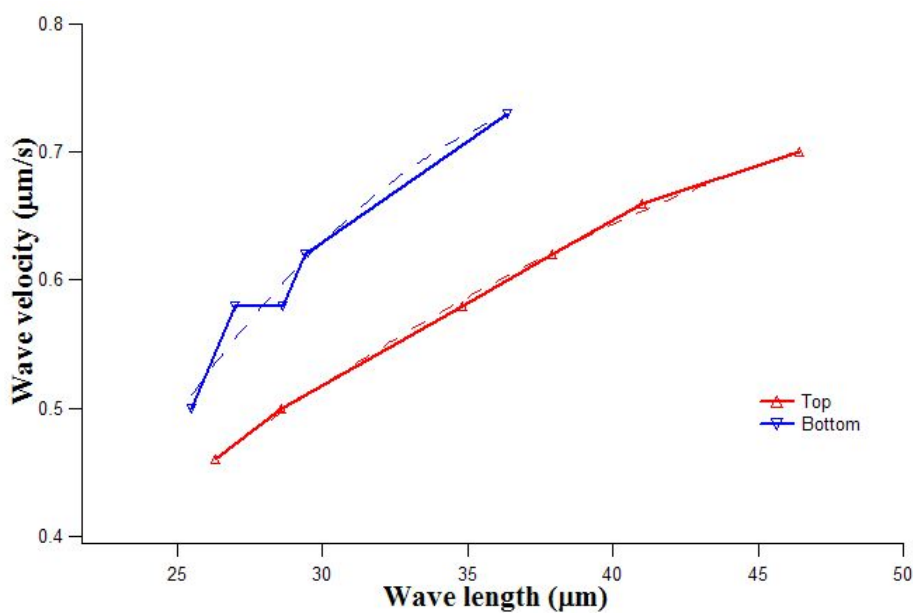
Fig.6.49 Dispersion relationship along the [1$\bar{1}$0]-direction in NO+H$_2$ /K/Rh(110) system for the pattern shown in fig.6.45.   θ$_K$ =0.067ML, T=510K, Data were measured at two position A(top) and B(bottom)

As shown in fig.6.49, if qualitatively compared to the NO+H_2 /Rh(110) system (shown in fig.6.50) [41], for the same wavelength, the wave velocity of the reaction in the NO+H_2/K/Rh(110) is significantly lower.   Actually, when the K coverage is higher, for example, 0.12ML, the wave velocity is even lower.   This means that K has an "inhibition effect" on the wave propagation.

One also notices that a difference between the two dispersion curves in fig.6.49 exists.   As we can see in fig.6.45, the bright area with turbulences in the collision zone grows faster at the bottom than that at the top.   If the formation of that kind of area is due to the mass transport of K, then area surrounding the collision area should be depleted of potassium by the mass transport.   So the possible reason for the higher wave velocity of the area near B in fig.6.49 might be due to a faster depletion of K in the area near B.   The disappearance of pulses in line B after 500s is because the fast increase of the K enriched area.
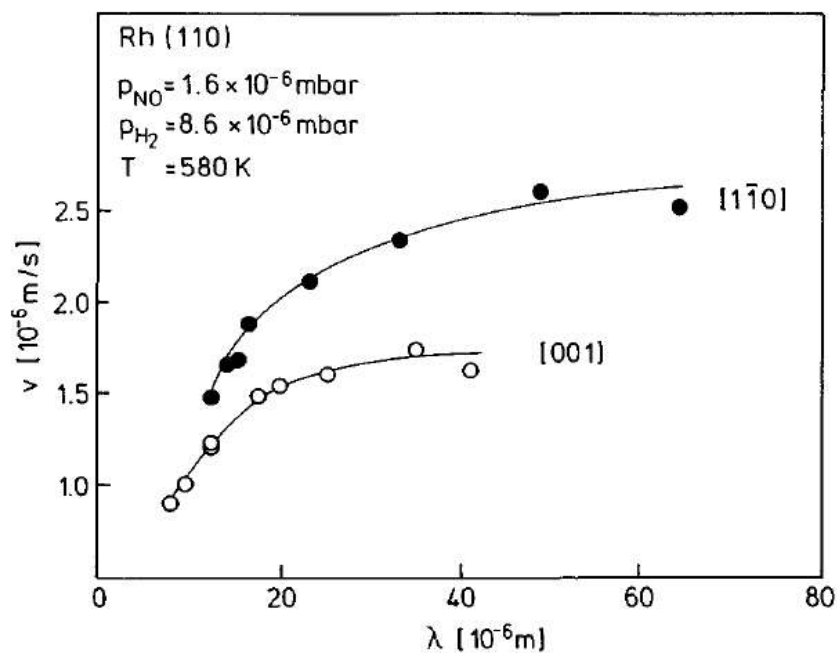
Fig.6.50 Dispersion relation for pulse propagation along the two main crystallographic directions of clean Rh(110) surface in NO+H_2 reactions [41]

6.3.5 Influence of K on wave propagation.

1. The turbulent structure in the collision area of pulses.

As shown in fig.6.45, at the area where two pulses collide together, the regular pulses break

into fragments, which look like the wave fragments observed under lower H_2 partial pressure at the same K coverage, or the wave fragments occur under the same H_2 pressure but at higher K coverage. These analogies together with the increasing PEEM intensity (corresponding to decreasing local work function) support the idea that there is K accumulation in the collision area. Moreover, the driving force that caused the pulses to break into turbulent fragments could be the accumulation of potassium. From the discussion of the boundaries in 6.2.1 we can also see that the boundary from the oxygen covered state to the excitable state (wave fragments) shifts with increasing K coverage shifts to higher P_{H2}. All of this suggests that the K enrichment caused by mass transport of pulses might "shift" the reaction condition in the collision area from the center of excitable state in the bifurcation diagram to the border between the oxygen covered state and the excitable state. Even a complete shift into oxygen covered state is considerable (which means when K coverage is high enough, in the collision area the pattern becomes stationary).

2. The origin of "spider web".

As we can see from fig.6.15, the tip of the "cone" structure originated from the center of a target pattern and then slowly moved with the propagating pulses. Since a target pattern normally nucleates at a defect on the surface, one hypothesis could be: K was originally enriched near some surface defect and induced instabilities on the wave front. The wave front became distorted (but not broken like in the collision area) during propagation, as clearly shown in fig.6.23. K is transported with the pulses but since more K is transported by faster propagating part of the wave front, an instability results generating the lines perpendicular to the pulse fronts ("spider web").

6.3.6 Estimation of K coverage by PEEM

Very often it will be useful to make an estimate of the K coverage from PEEM intensity. Alternatively one might use LEED or AES, but this is time consuming and one risks contamination of the sample.

Since in each experiment, surface is always precovered with NO, so we tried to do it in

following procedure:

1. Deposit K onto clean Rh(110) surface with certain amount, determined by LEED pattern.

2. Introduce NO with pressure of 1.54×10^{-6} mbar.

3. Turn the sample to PEEM, measure the PEEM intensity under different screen voltages and temperatures (depending on the requirement of subsequent experiment)

4. Clean the sample

Repeating 1 to 4, for a certain PEEM screen voltage and temperature, we finally get the relationship of K coverage and its corresponding PEEM intensity.

a). According to Fowler's theory, for a fixed screen voltage, the PEEM intensity is a function of surface work function only: $I(\Delta\phi) \propto (h\nu - \phi - \Delta\phi)^2$ [17, 18], in which I is the PEEM intensity that has subtracted the CCD camera offset, hν is the photon energy of the light source, Φ is the work function of clean Rh(110) surface. When $h\nu - \phi \le \Delta\phi$, the PEEM intensity reaches a minimum, so I and $\Delta\Phi$ are bijective mapping.

In our experiment the offset of CCD camera is measured to be very small compared to the total intensity, so there is nearly linear dependence of $\sqrt{I(\Delta\phi)}$ on the work function change $\Delta\Phi$.

b) In the work function measurement of K+O coadsorption in chapter V, during the oxygen coadsorption, the work function when the surface is finally saturated behaves as a function of the initial K coverage only. When we coadsorb NO with K to the Rh surface, NO adsorb to the surface dissociatively, but the N desorbs very fast and leaves K+O phase only, according to our experiment in the LEEM/XPEEM Trieste. So we can expect similar relationship of the saturation work function and the K coverage.

In the experiments for K+O coadsorption, for an O_2 exposure of ~120L ($P_{O2}=1 \times 10^{-7}$ mbar) the surface is saturated. In our experiments in the NO+H_2/K/Rh(110) system, the exposure is >200L ($P_{NO} = 1.54 \times 10^{-6}$ mbar), so one can expect the surface is also saturated (can also be seen from the final PEEM intensity, which remains unchanged) before the step 3 in the measurement.
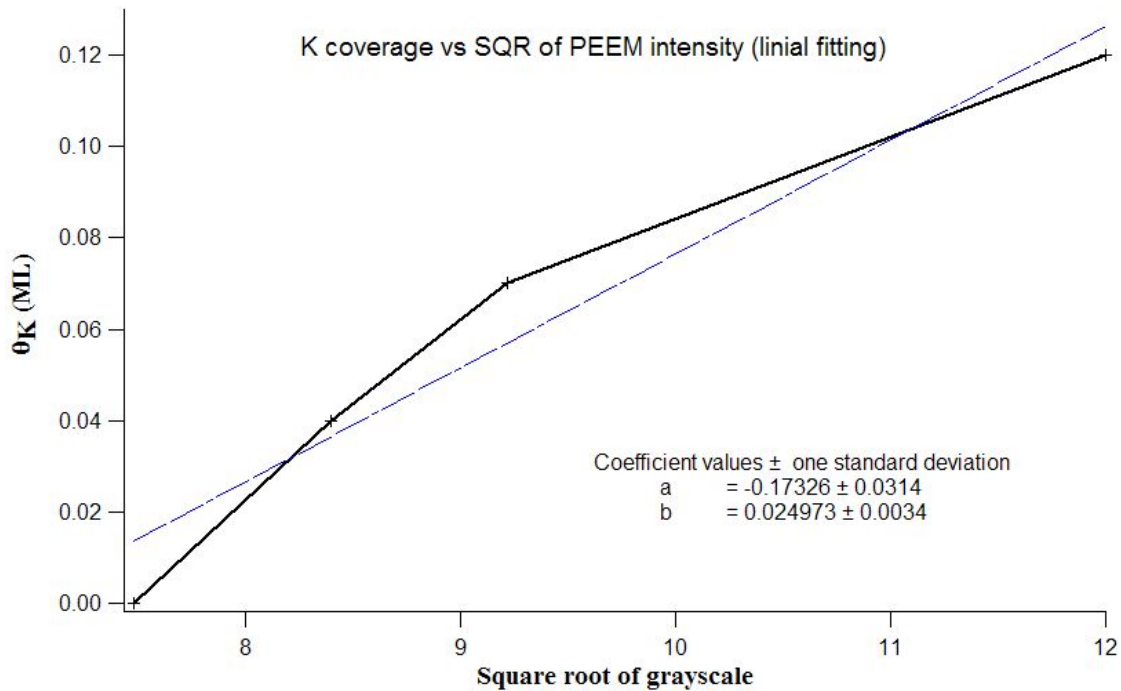
Fig.6.51 Estimated K coverage versus square root of PEEM intensity,
V_{screen} =5.3kV, P_{NO}=1.54x10^{-6} mbar, NO exposure is 240L

The dependence of the work function change on the K coverage is linear only at low K coverages.   As a reference, for clean Rh(110) surface, as we measured in chapter V, the dependence is approximately linear only at θ_K <0.16ML.   For the K+O coadsorption, the work function change (when O is saturated) and θ_K is approximately linear only at θ_K < 0.12ML (shown in fig.5.4).

So for a rough estimation, for our system we can make an approximation of a linear dependence of the saturation work function change on K coverage. Hence, then θ_K and the square root of PEEM intensity also can be approximately regarded as an approximate linear relationship.

Fig.6.51 shows an example of the measurement result.   As one can see from the graph, the curve is quite close to a line.   We tried to do a linear fitting with the form y = a + bx, (y is the K coverage and x is the square root of the PEEM intensity), and the error is significant, but for a rough estimate, this is sufficient (at least the uncertainty is not bigger than to estimate the K coverage from LEED)

6.4 Summary

The systematic investigation of pattern formation in the NO+H$_2$/K/Rh(110) system at

different coverage of K provided interesting results.   The conclusions are:

6.4.1 The influence of K existence on ignition of the pattern.

From the discussion of boundaries in 6.3.1, we saw that we have a dramatic increase of P_{H2} necessary for ignition with increasing θ_K.   This means for K coverage which can be identified by LEED ($\theta_K > 0.025ML$), the K actually has a inhibition effect of the ignition of the reaction.

6.4.2 The influence of K on wave propagation.

From the discussion of 6.3.4, we can see that generally, K coadsorption on the Rh(110) surface has significant "inhibition" effect on the wave propagation.   Particularly, from the discussion of 6.3.2, it can be seen that the influence of K on the propagation in two crystallographic directions ($[1\bar{1}0]$ and $[001]$) is different.   As θ_K increases, the propagation in the $[001]$-direction is more inhibited than that in the $[1\bar{1}0]$-direction.   This effect is so strong that at $\theta_K>0.067ML$, the wave fragments traveling in the $[001]$-direction totally disappeared and instead, wave fragments moving along the $[1\bar{1}0]$-direction appear.

6.4.3 Mass transport of K with wave propagation

The previous results provided indirect evidences to a mass transport of K.   First it is the increasing PEEM intensity in the collision area; the bright area expands as more pulses collide.   Secondly, inside the collision area, turbulent wave fragments exist, which look similar to the wave fragments obtained under the same temperature and H_2 pressure but at higher K coverage.

For a real proof, a chemical analysis is needed, which will be provided in chapter VII.

6.4.4 Influence of K existence on new patterns

Generally, with coadsorbed K, new patterns are found:

a. Turing-like stationary pattern.

This kind of stationary pattern seen here is different from those in the H_2+O_2/K/Rh(110) system (in which a more regular and homogeneous pattern was obtained only from reducing condition).   Started from an oxygen covered surface, the patterns are not formed by reduction fronts, but appeared simultaneously everywhere.   The appearance of such stationary patterns only depends on the K coverage, the temperature and H_2 partial pressure (when P_{NO} is fixed).

b. "Spider webs"

The "spider webs" discussed in 5.1.3 and 5.1.4 have similarity to the pattern discovered in a biochemistry system formed by cAMP guided amoeba cells called "Dictyostelium discoideum"[6].   However, the origin might be different.   As discussed before, the tips of the cones nucleated near the center of the target patterns.   They then slowly move along the $[1\bar{1}0]$-direction during wave propagation.   One can speculate that the origin of the pattern might come from local enrichment of K near the defects and K mass transport. Alternatively, a local modification of the surface, for example, by oxide formation, can be considered as possible cause.

c. Zebra-like pattern

Similar zebra-like patterns have been reported on a $NO+H_2$/K/Rh(110) system but with a Pt pad in the middle of the single crystal area.   The zebra like pattern discovered here just depends only on the K coverage, the temperature and the H_2 partial pressure (P_{NO} is fixed). The possible explanation for the zebra-like pattern might be the anisotropy of diffusion for different species (K, N, O, H) depending on the conditions.

d. "Fingering" pattern.

The origin of this pattern might come from the different mobilities of the reacting species on the reduced area (the fingers) and on the oxygen covered area, i.e., a high mobility on the reduced part and low mobility on the oxygen covered area outside of the "fingers".   It is

also suspected that the area between the "fingers" have a higher K coverage due to K mass transport.   We know that K actually has "inhibition effect" on wave propagation, which might also play a role in the "fingering".

VII. K Mass transport in the NO+H$_2$/K/Rh(110) system

7.1 Evidence for a Mass transport in NO+H$_2$/K/Rh(110) system

In pattern formation in the NO+H$_2$/K/Rh(110) system at different θ_K, one significant phenomenon is the enhanced brightness in the collision area of pulses and reduction fronts. In most situations, the PEEM intensity didn't go to zero in the collision area, instead, there was a continuous increase of local intensity and an expansion of size of the area which has such an increasing intensity.   After turning off H$_2$, the higher intensity in this area remained.

   All of these observations suggest a redistribution of K on the surface, i.e., a mass transport by wave propagation.   In order to prove this, a chemical analysis was conducted in a LEEM/XPEEM setup in the synchrotron facility in Trieste.
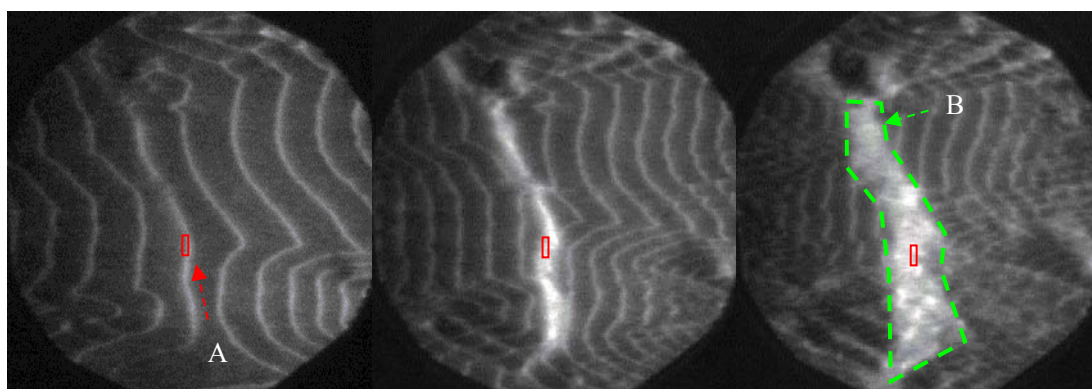
(a) $\Delta t = 0s$ (b) $\Delta t = 240s$ (c) $\Delta t = 680s$
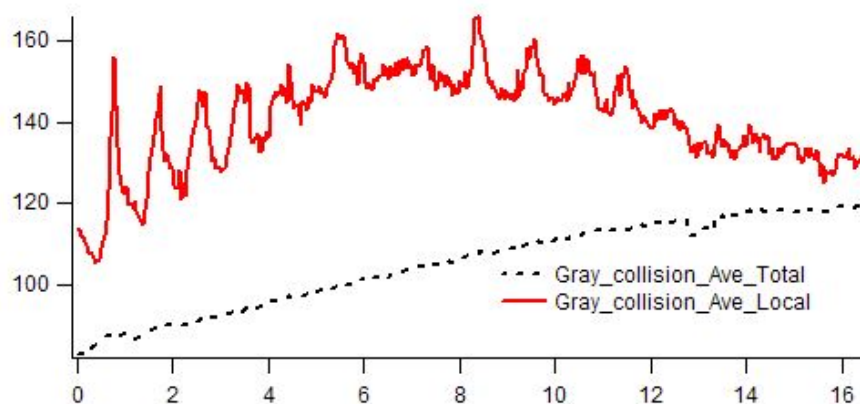
(d)Average PEEM intensity of area A (red solid line) and B (black dashed line)
Fig.7.1 PEEM intensity of collision area, (a)(b)(c) target pattern in NO+H$_2$ /K/Rh(110) system, θ_K =0.067ML, P$_{NO}$ =1.54x10^{-6} mbar, P$_{H2}$ = 1.8x10^{-5} mbar, T=510K, (d) PEEM intensity

change in time, measured in two areas in (a) (b) (c), A (red) and B (green)

Fig.7.1 shows one experiment where such phenomena were discovered. The average PEEM intensity was measured at two areas, A and B, as shown in fig.7.1. Compared to the integral intensity of area B, the PEEM intensity in the smaller area A reflects the local change of the work function. In the $NO+H_2/K/Rh(110)$ system (See Chapter VI), at the collision area, is the intensity became brighter and the bright area expanded as more and more pulses collide. When the collision area became quite broad (with a width of about 50μm) reacted of about 12min, inside the collision zone there are still some turbulent pattern inside. The average PEEM intensity of both areas shows a general increase over time, as more and more pulses collided. As shown by the red line in fig.7.1 (d) this results in a quite irregular intensity signal after ~12min.

After turning of H_2, the PEEM intensity of the collision area remained brighter than the surrounding area. This suggests a redistribution of K due to a mass transport of K by pulse propagation. The decrease of the PEEM intensity in the small area maybe can be explained by a redistribution of K in that area (or possibly some kind of restructuring).

Following Fowler's theory (see Chapter VI), one can estimate that the intensity increase corresponds approximately to a maximum K coverage of about ~0.12ML. The original coverage of the homogeneous K distribution was ~0.067ML.

7. 2 Chemical and structural analysis of pulses

In order to quantitatively investigate the mass transport process, a chemical analysis was conducted using the synchrotron source in Trieste. Different experiments were carried out and XPS spectra of different species (K, N, O, Rh) were taken during the reaction.

7.2.1 K and N distribution

(1) Target patterns

In this experiment, about 0.08ML of K was deposited onto the surface. A target pattern was initiated, as shown in the MEM image in fig. 7.2. The pulses have lower work function, so in MEM they appear as dark area. The pulse speed was measured to be about 0.1μm /s.
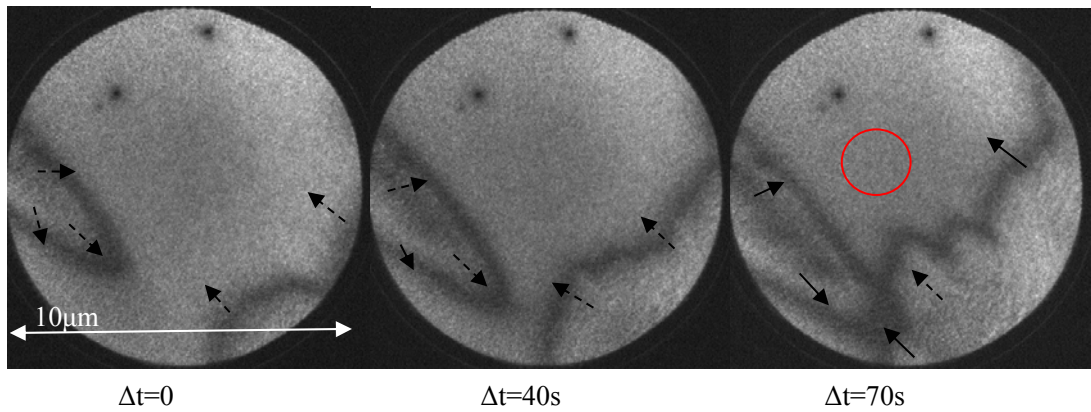
Fig.7.2 MEM at 0eV, target patterns, red circle is the position of X-ray light beam where spot XPS analysis was made, P_{NO} =2.5x10^{-7} mbar, P_{tot} = 8.4 x10^{-7} mbar T= 194 ° C (3.05mV), θ_K~0.08ML

The XPS beam (marked by red circle in fig.7.2) was focused at a spot where pulses were going to pass by.

(a)K2p

(b) N1s

(c) Coverage profile of K and N
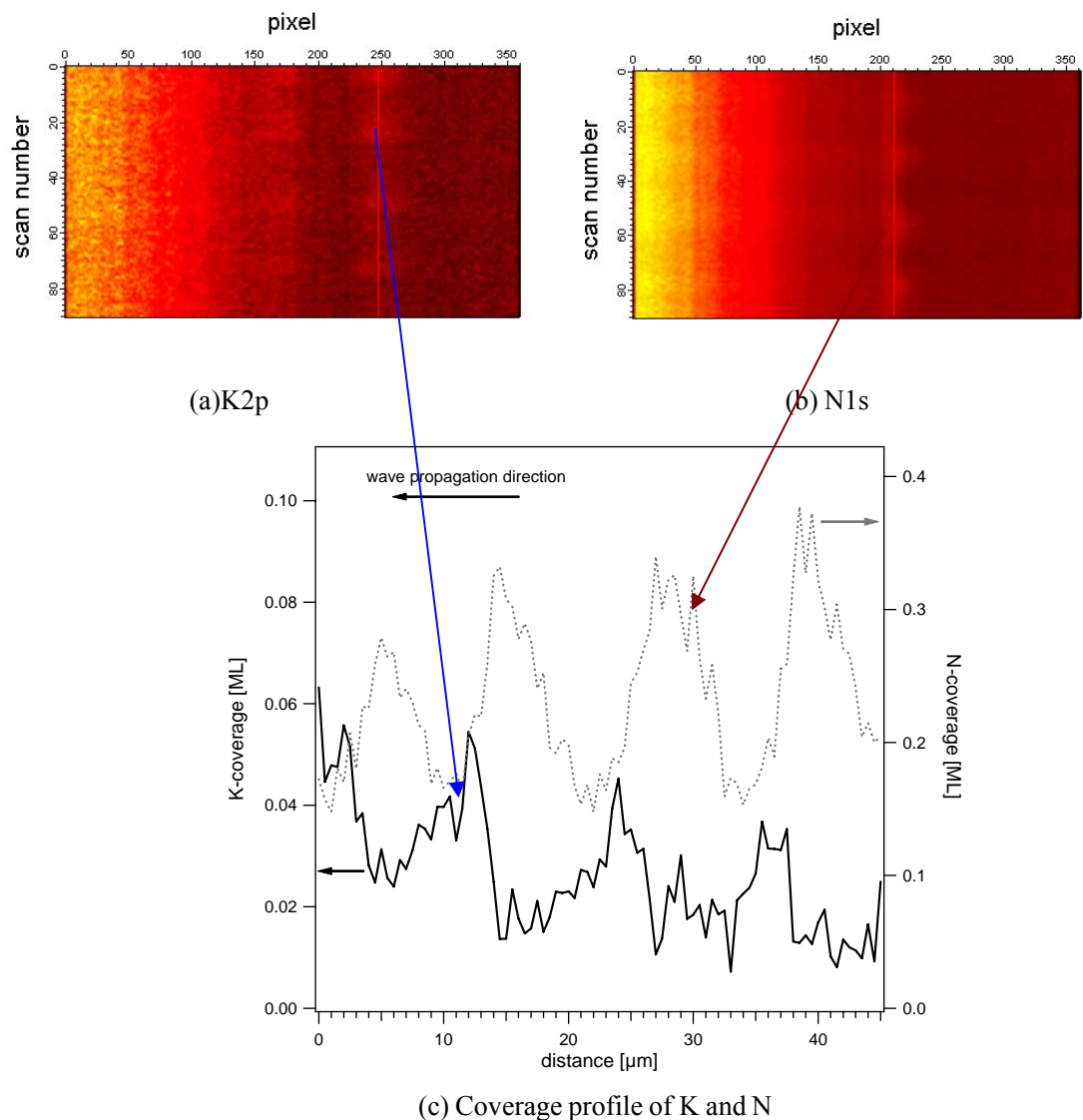
Fig.7.3. K and N distribution on pulses of target pattern shown in fig. 6.3, (a)(b) XPS signal of the pulse, the beam position was shown in fig.7.2 by red circle, and the period of each frame in (b) and (c)

is 5s; (c) Profile transferred from scanning in (a)(b), with a constant wave velocity of ~0.10μm/s

During the measurement, N1s and K2p signals were taken alternatively (with a time delay of 2s between each other), and they both oscillate with a period of about 120s.　Considering the wave velocity of about 0.10μm/s ,　and assuming the shape of pulse doesn't change during the short experimental period, we can transfer the signal from a dependence of time to a profile, as shown in fig.7.3 (c).　It can be easily seen that each K pulse is in front of a nitrogen pulse.　The movement of K caused by the N pulses corresponds to the mass transport of K in the pulse trains which was reported before.　Moreover, there is a decrease of the K signal from one pulse to the next.　The less in the K concentration shows that the K is transported by pulses.　In fig.7.3 the maximal coverage of K decreased about 0.015ML after 3 pulses passing by, so the change in the K coverage is about 0.005ML per pulse.
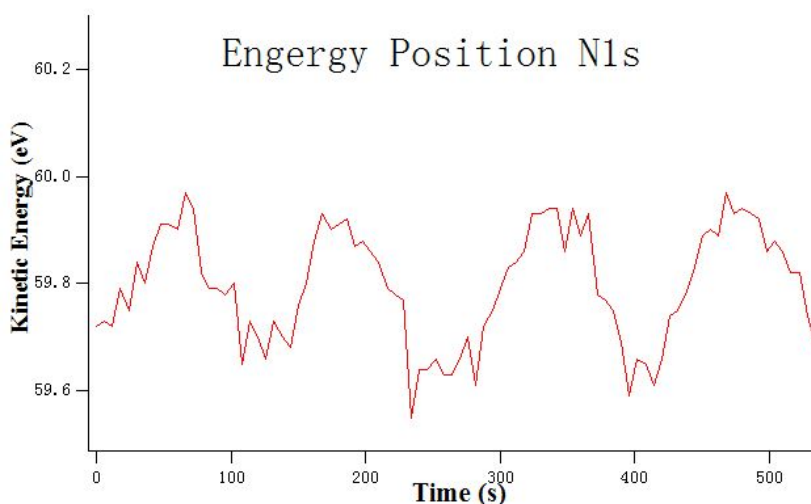
Fig.7.4 Oscillation of energy position (kinetic energy) of N1s signal from the same experiment as shown in fig.7.2 (peak positions were determined by peak fitting with one component)

As shown in fig.7.4, there is also a periodical change of N peak position (fitting N1s by 1 peak only) of the same period like shown fig.7.3.　The peak position has a shift of about 0.3eV.　This shift is consistent with a change from c(2x4)-2O,N structure to (2x1)-N structure according to the literature [42].

(2) Spiral waves

After the reaction had been initiated, spiral waves were obtained.　Then K deposition was started for 30s at 6.00A.　Afterwards the spirals and target patterns still existed (as shown in fig.7.5), where the spiral waves exhibit a period of about 120 seconds

(a) $\Delta t = 180s$ (b) $\Delta t = 300s$ (c) $\Delta t = 400s$
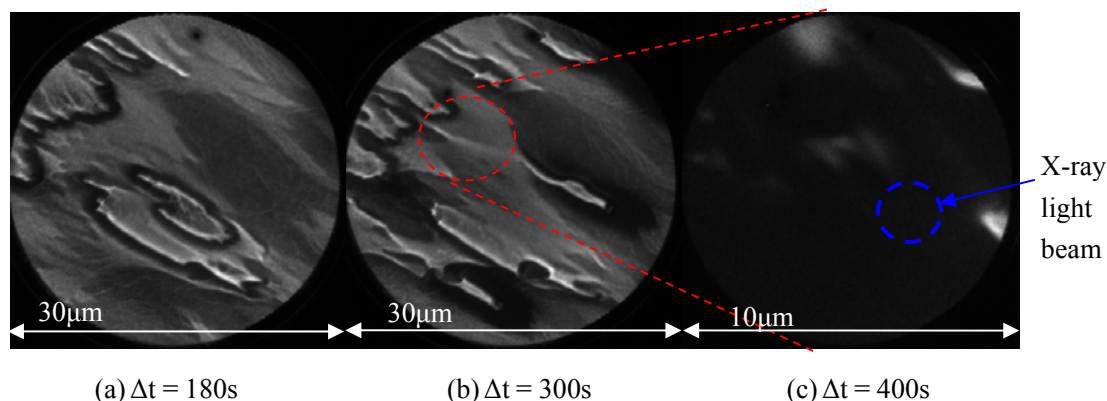
Fig.7.5. Spiral waves, (MEM at -0.90eV), a micro-spot XPS analysis was conducted at the position indicated in (c), marked by blue dashed circle. Δt means the time after the ending of K deposition. $P_{NO} = 2.5 \times 10^{-7}$ mbar, $P_{tot} = 9.23 \times 10^{-7}$ mbar, T= 469K, $\theta_K \sim 0.08$ML
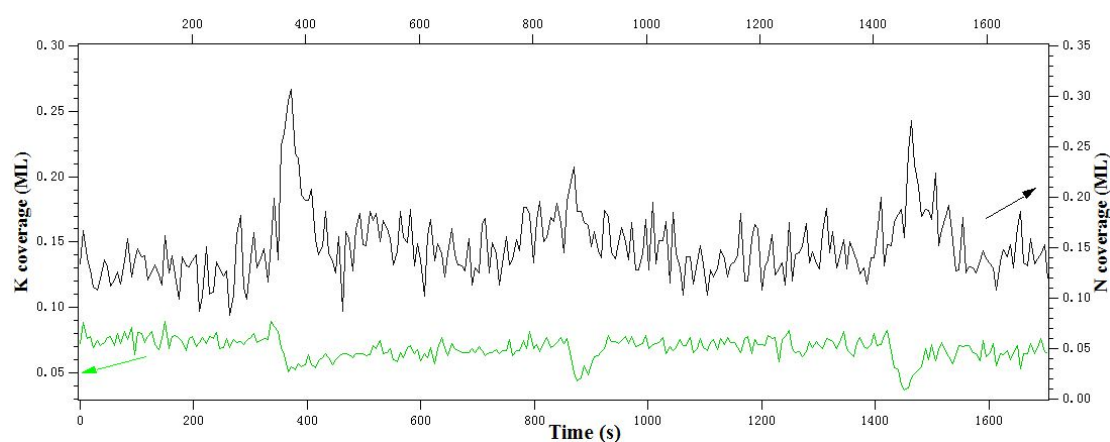
Fig.7.6 Local K and N coverage on an area where spiral waves passed by, in NO+H$_2$ /K/Rh(110) system, the pattern and experimental condition is shown in fig.7.5

As shown in fig.7.6, again we obtain a periodical change of N1s and K2p signals (measured alternatively, with a time delay of 2s between each other), with a period of about 510 seconds (later 560 seconds).   After three N1s peaks the K coverage decreased by about 0.016ML, so for each N1s peak about 0.005ML K was depleted by each pulse.

One notes that the period during measurements of XPS (~500 second) is much larger than the one seen from MEM measurements.   Apparently, pulse propagation is continuously slowing down after the K deposition.

7.2.2 O distribution in the pulses
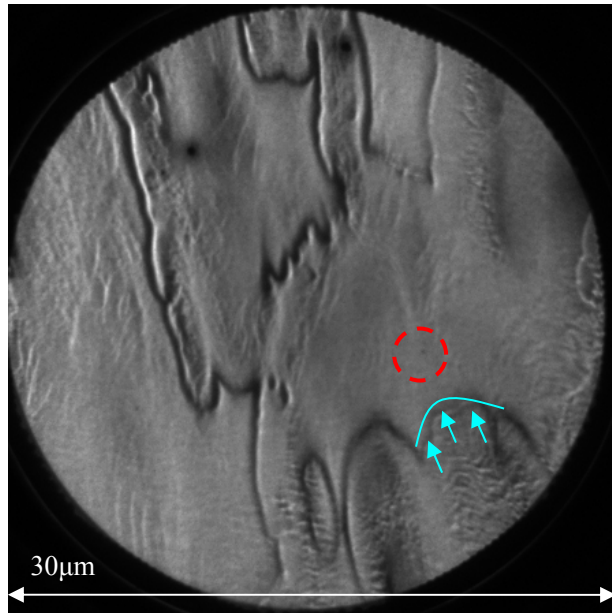
Fig.7.7 Spiral waves and target waves, (MEM at 0eV)

The oxygen 1s signal was measured, in the same area as in experiment in fig.7.3, as shown in fig.7.7 (greater scale), using a photon energy of 635eV.   The area probed by the μXPS measurement is marked by red dashed circle, and the wave front is marked by a blue line. The wave velocity is about 0.1μm/s.
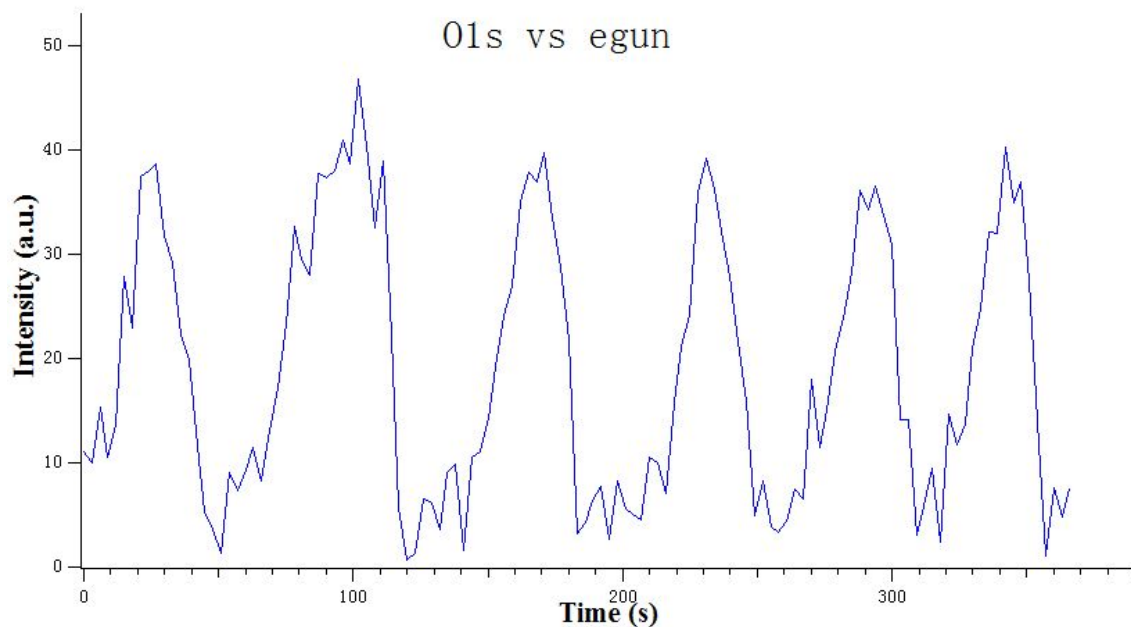
Fig.7.8 O1s signal versus time

As in the previous calibration calculation, for the wave velocity of ~0.1μm/s, we can transfer fig.7.8 to a spatial profile as shown in fig.7.9.
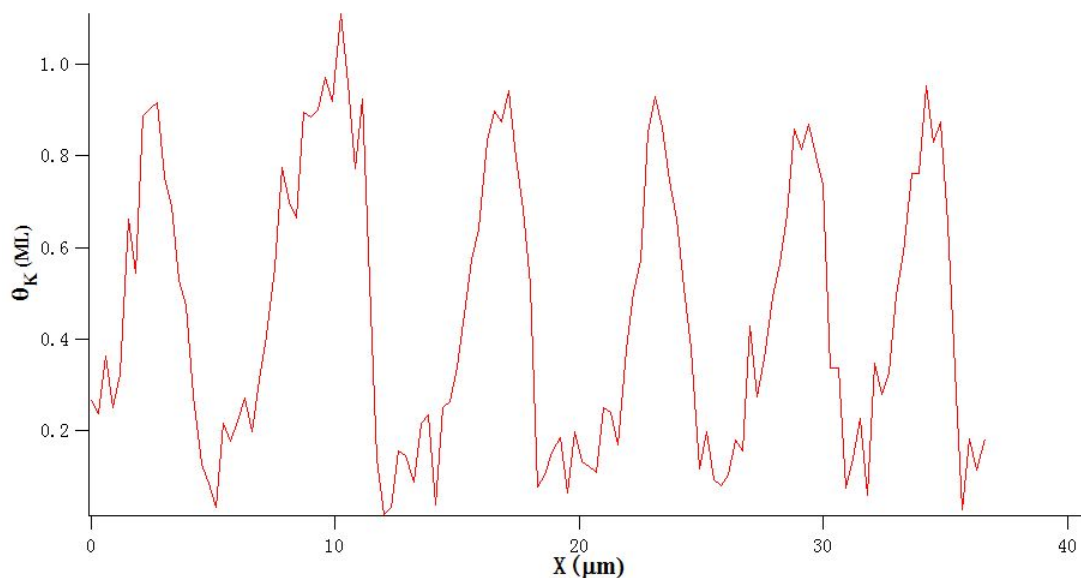
Fig. 6.9 O concentration profile in a pulse train

As shown in fig.7.9, the O1s signal exhibits regular oscillations.   At about 10μm the level rises above 1ML, presumably due to noise.

7.2.3 Synchronization of O1s and N1s signal

(1) Direct measurement of O1s and N1s (plus K2p) was failed

Using XPS to analyze the waves, we need to know the complete element distribution, which means we need to correlate N1s, O1s and K2p (and of course, Rh3d for coverage calibration) signals.   However, as indicated above, N1s, K2p, Rh3d signals were measured with a different photon energy that the O1s signal.   So we first tried to get N1s and O1s at the same photon energy of 635eV.

t = 0s   t =20s   t = 40s
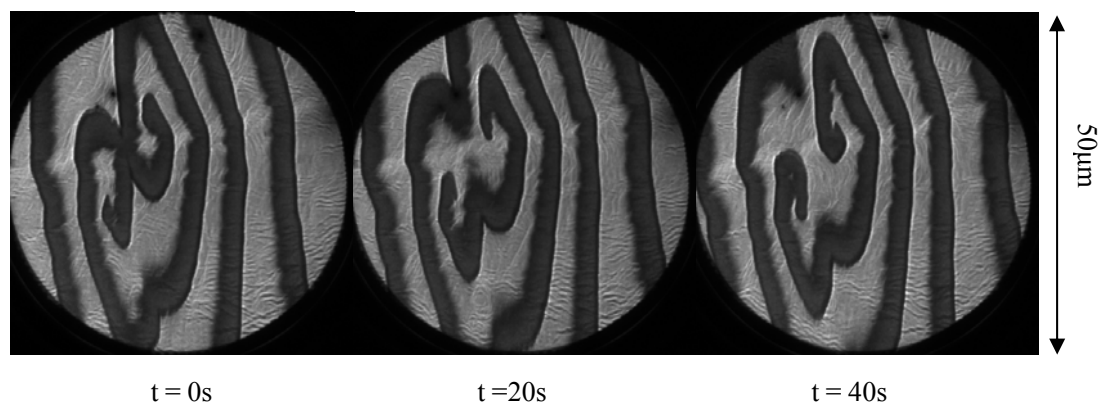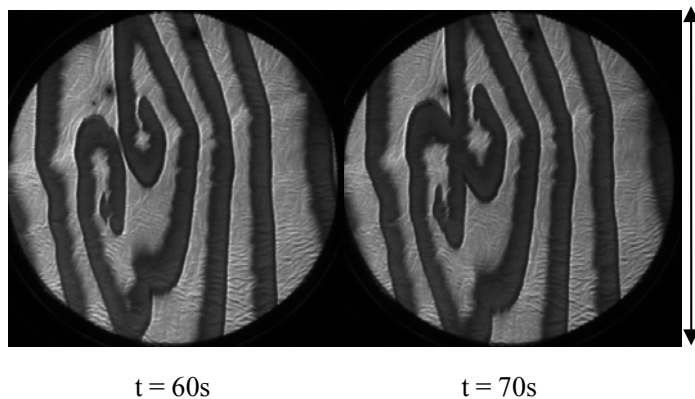
Fig.7.10 MEM at 1.35eV, during reaction on the unpromoted Rh(110) surface.
P_{NO}=2.5x10^{-7} mbar,
P_{tot}=8.4x10^{-7} mbar,
T= 467 K

50μm

t = 60s   t = 70s

The patterns to be measured with XPS are shown in fig.7.10. Two spiral waves with a period of about 70s were present when we start the XPS measurement.
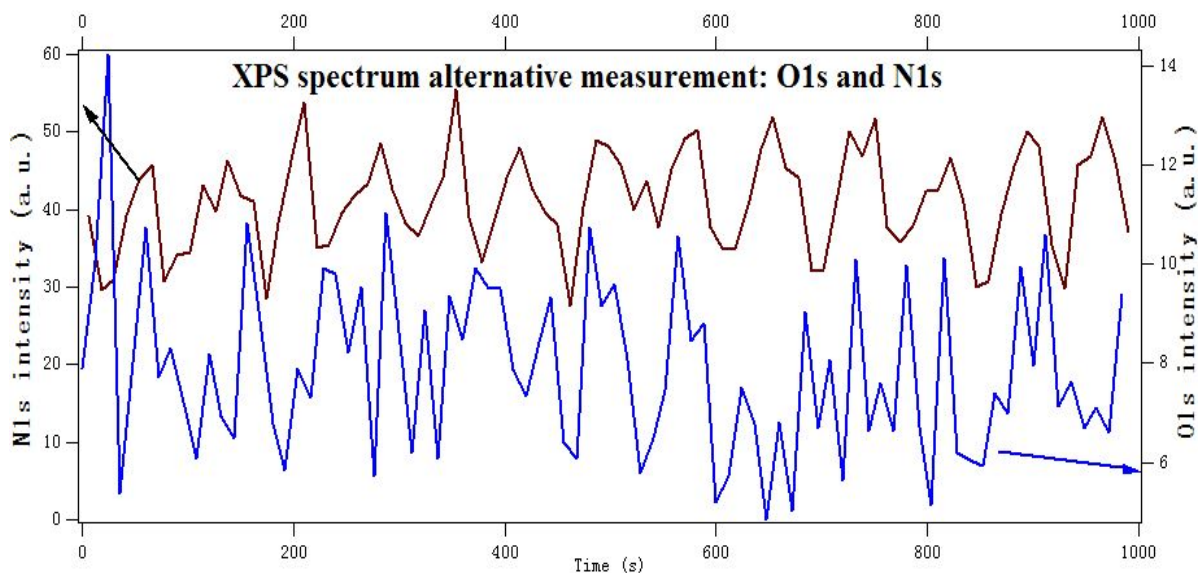
Fig.7.11. XPS of N1s and O1s measured alternatively (with a time delay of 2s between each other), during experiment displayed in fig.7.10. hv = 635eV, P_{NO} =2.5x10^{-7} mbar, P_{tot} = 8.4 x10^{-7} mbar, T = 467K

The results are displayed in fig.7.11. N1s and O1s signals are shown together, (starting voltages: O1s 105eV, N1s 235eV).

The N1s signal has a period of about 84 second (very stable), the O1s spectra which had been obtained were very weak, so the phase correlation is difficult to see due to the irregular behavior.

(2) Synchronization using diffracted electron beams

110

From the direct measurement of O1s and N1s signals with the same photon energy, no useful results were obtained. The phase difference can not be extracted. So we tried to use an auxiliary electron gun to synchronize the O1s and N1s signal.

(a)LEEM at 2.2eV on (0,0) point, on a target pattern   (b) μLEED scanning (1 frame = 2 seconds)
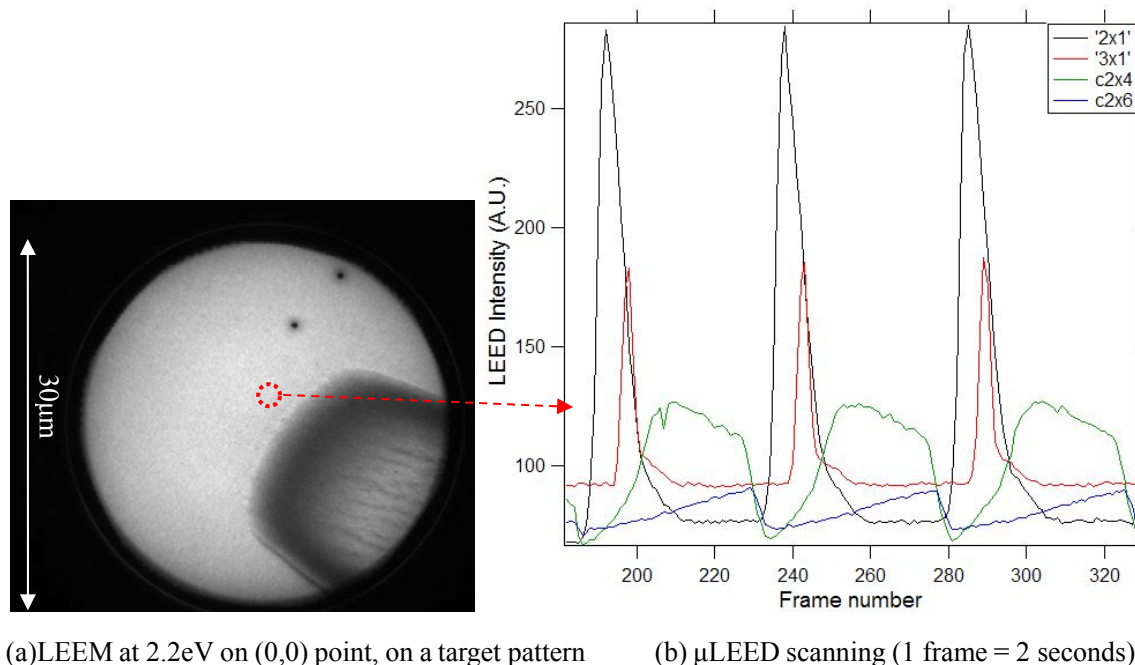
Fig.7.12 Periodical change of LEED intensity on a target pulse train. (the pressures are not calibrated); The area to make μLEED scanning is marked by red dashed circle in (a). In (b) the '2x1' and '3x1' phases are related to N, c(2x4) phase is related to O,N coadsorption, and c(2x6) phase is related to O adsorption. θ_K~0.12ML , $P_{NO} = 5.4\times10^{-7}$ mbar, $P_{H2} = 4.63\times10^{-6}$ mbar

The principle is as following: As shown in fig.7.12(b), in the pulse train, there is a periodic change between the N induced (2x1) structure, which corresponds to a reduced surface, and the c(2x4) and c(2x6) structure, respectively, corresponds to N+O coadsorption state and the pure O covered state. Consequently, there is also a periodic change in the intensity of the diffracted electron beam (1/2,0). So measuring the XPS signal of N1s simultaneously with the diffracted electrons of (1/2,0), the phase difference of N1s and diffracted (1/2,0) beam should be 0, as shown in fig.7.13. If the O1s is measured also together with the diffracted (1/2,0) beam, from the phase difference of signal of O1s and the electron gun, the phase difference of O1s signal and N1s signal can possibly be determined.

To realize this method, the X-ray beam was exposed to the same area hit by an electron beam. An aperture (marked by red dashed circle in fig.7.13(a)(b)) was put into the

diffraction plane of LEED so that only diffracted electrons from the (0,0) beam and (1/2,0) beam were collected by the detector. Whenever the intensity from the diffracted beams reaches a maximum, we should also obtain maximum intensity the of N1s signal (called in-phase).

(a) LEED at 43eV, (2x1) structure   (b) LEED at 43eV, c(2x4) structure

(c) N1s signal versus time on a pulse train
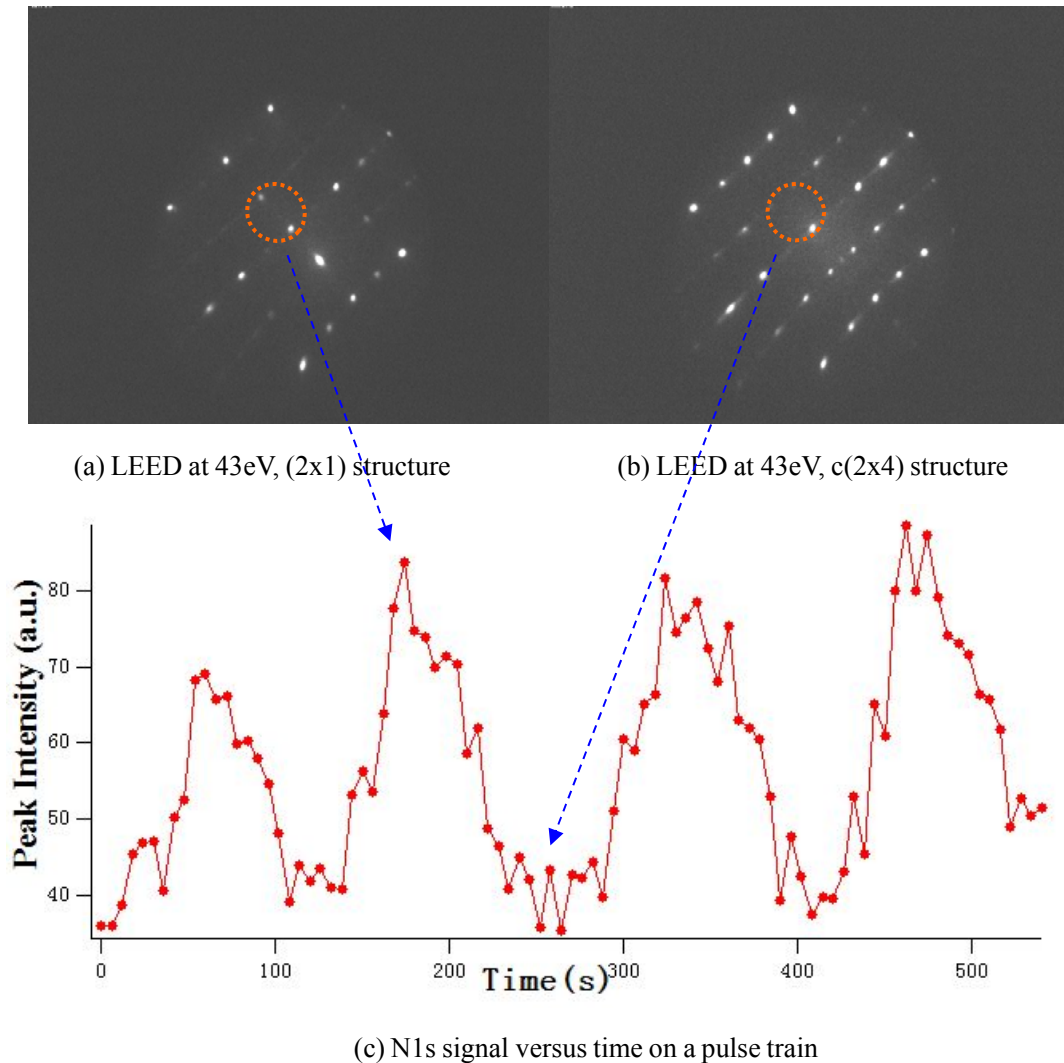
Fig.7.13. Relationship of intensity of diffracted electrons of (0,0) and (1/2,0) point from LEED and intensity of XPS N1s signal. (a) is taken where the intensity of LEED (2x1) structure reaches maximum, and (b) is taken where the intensity of LEED (2x1) structure reaches minimum

Experiment
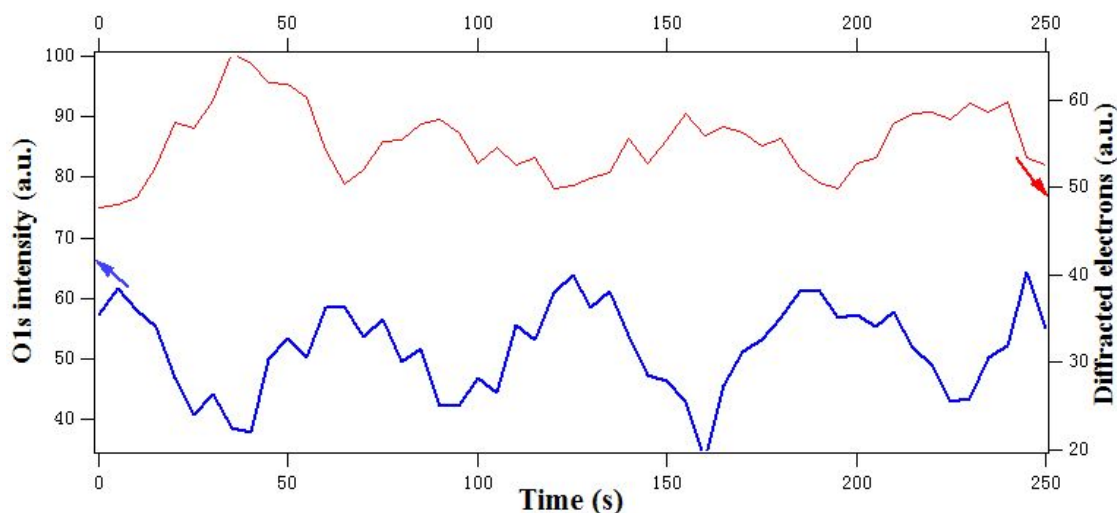
Fig.7.14 XPS signal of O1s and diffracted electrons from (0,0) beam and (1/2,0) beam. The signals of N1s and diffracted electrons were taken alternatively (with a time delay of 2s), in the NO+H_2/K/Rh(110) system, in the same experiment displayed in fig.7.11

The experiment is the same like as displayed in fig.7.11. First the XPS signal of O1s and diffracted electrons from (0,0) and (1/2,0) beams were taken alternatively at photon energy of 635eV, as shown in fig.7.14. The O1s signal has a period of about 60 seconds. The intensity of the diffracted electrons has also similar period of 60 seconds.
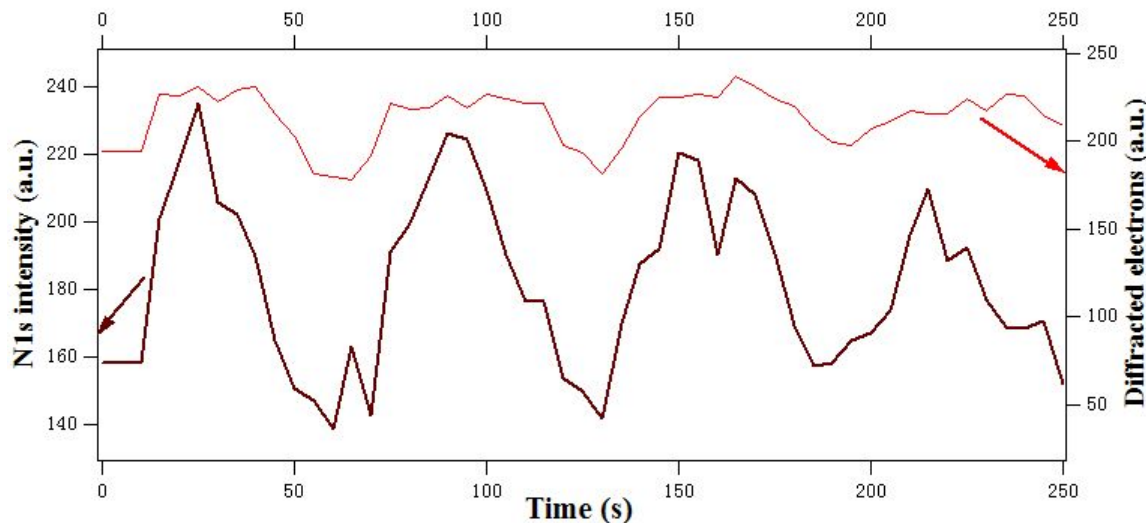
Fig.7.15 XPS of N1s signal and signal of diffracted electrons from (0,0) beam and (1/2,0) beam. The signal of N1s and diffracted electrons were taken alternatively (with a time delay of 2s)

Afterwards XPS signal of N1s and diffracted electrons from (0,0) and (1,2,0) beams were also measured alternatively at a different photon energy of 459eV, as shown in fig.7.15. The N1s signal has a period of about 60 seconds. The intensity of diffracted electrons has also similar period of 60 seconds. Comparing the two time series of signals of diffracted electrons of the two experiments, we can put them together with the same phase, so the

phase difference of O1s and N1s is also obtained.
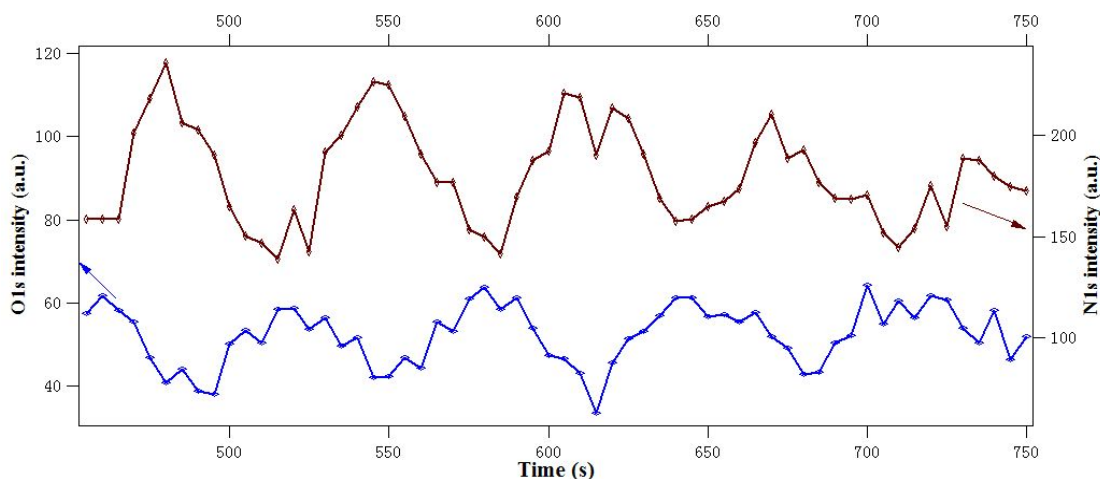
Fig.7.16 final synchronized O1s and N1s XPS signal, which shows the true phase difference of N1s and O1s on a pulse train is out-of-phase

As shown in fig.7.16. It is clear that the O1s and N1s signal are almost entirely out-of-phase. This is consistent with the LEED pattern in fig.7.12(b).

So finally, it was proven that O1s and N1s intensity (or coverage) are totally anticorrelated (which means a phase difference of π) by synchronizing them by the diffracted electrons from (0,0) beam and (1/2,0) beam.

7.2.4. Complete profile of pulses (K+N+O)

Finally, we tried to get K, N, O signal in one profile.   The experiment conditions were:

P_{NO} =2.5x10^{-7} mbar, P_{tot} = 9.23 x10^{-7} mbar, T= 469K.   K was deposited at 6.00A, 70 second.   With stable pulse train, first, using a photon energy of 459eV, the K2p and N1s signal were measured alternatively.   Then change the photon to 635eV, the O1s signal was also measured.   By the synchronization method described in the previous section, we can put the K2p, N1s and O1s signal in one complete profile.
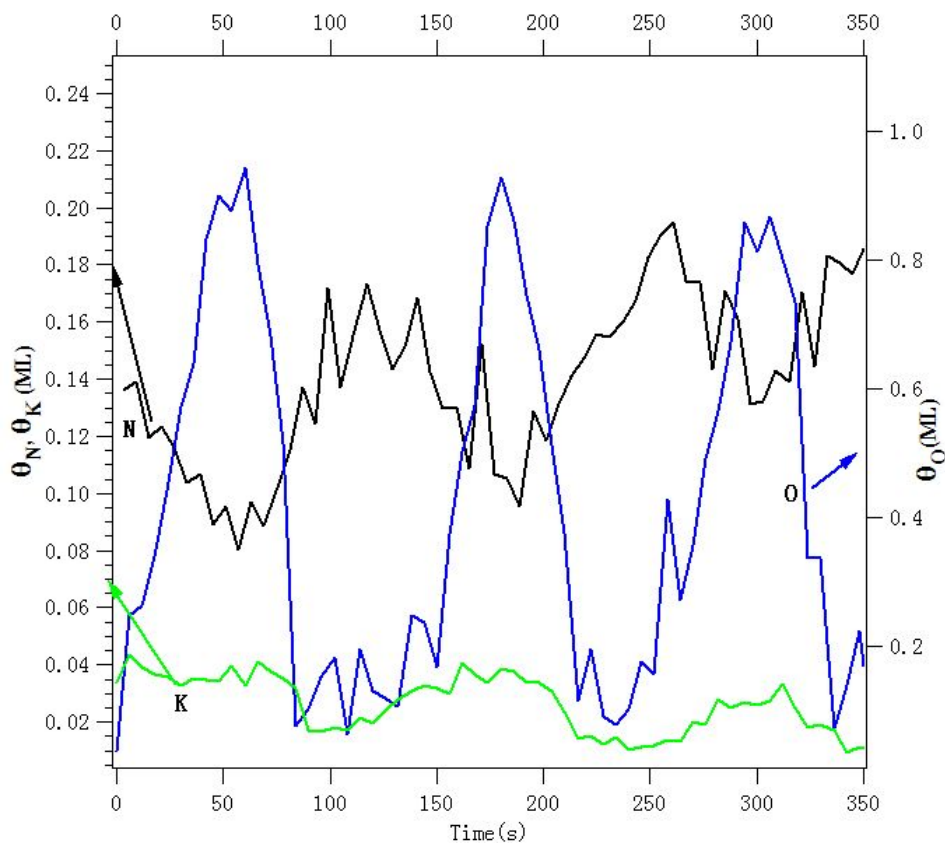
Fig.7.17 Time dependence of O1s, K2p and N1s XPS signals (synchronized) measured in a small area in a pulse train, P_{NO} =2.5x10^{-7} mbar, P_{tot} = 9.23 x10^{-7} mbar, T = 469K. θ_K ~ 0.08ML

From fig.7.17 we can see that the O1s and N1s signal are almost anticorrelated, the K signal reaches maximum together with the O1s signal, and before the N1s pulse reaches its maximum. In a pulse train, the K coverage is decreasing over time, about 0.005ML on average per pulse. This value is consistent with previous measurements. One can also see from fig.7.18 this decrease is not constant, but became smaller as time went on.

Considering the wave velocity of about 0.1μm/s, and assuming that the shape of the pulses is stable, the coverage change on the probed area measured vs. time can be transferred into a spatial profile as shown in fig.7.18. This figure more clearly shows the elemental distribution in a pulse train.
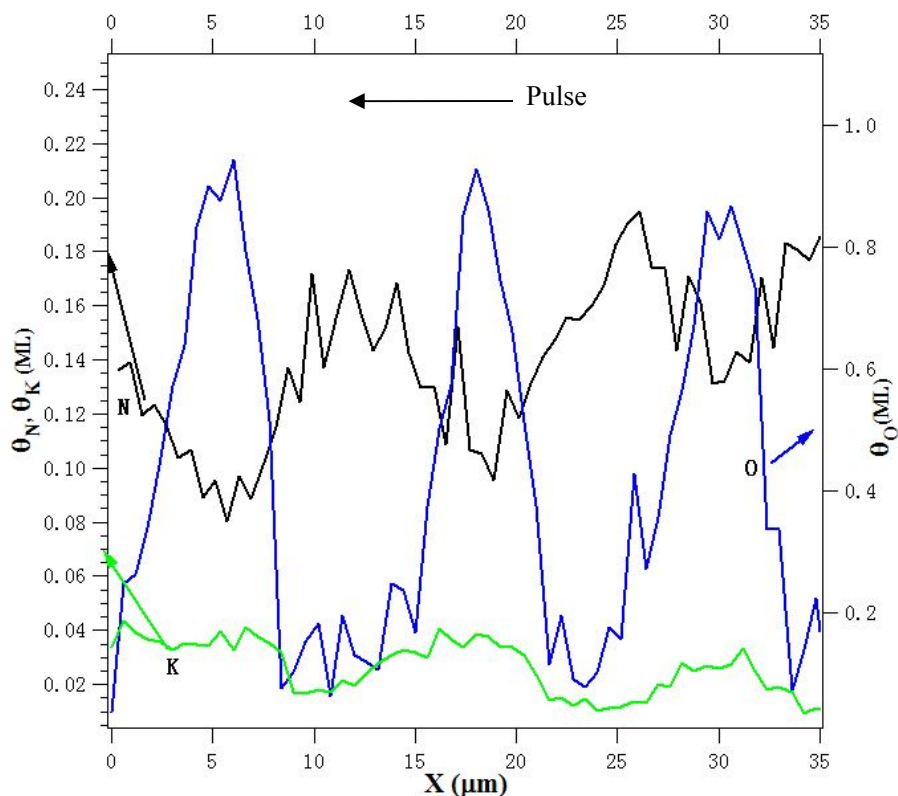
Fig.7.18 Spatial correlation profile of a pulse train, P_{NO} =2.5x10^{-7} mbar, P_{tot} = 9.23 x10^{-7} mbar, T = 469K. θ_K ~ 0.08ML

7.2.5 Structural analysis on pulses.

To get more information on the adsorbate distribution in a pulse train, a structural analysis by LEED was conducted. First, spiral waves were initiated after K was deposited onto the Rh(110) surface.
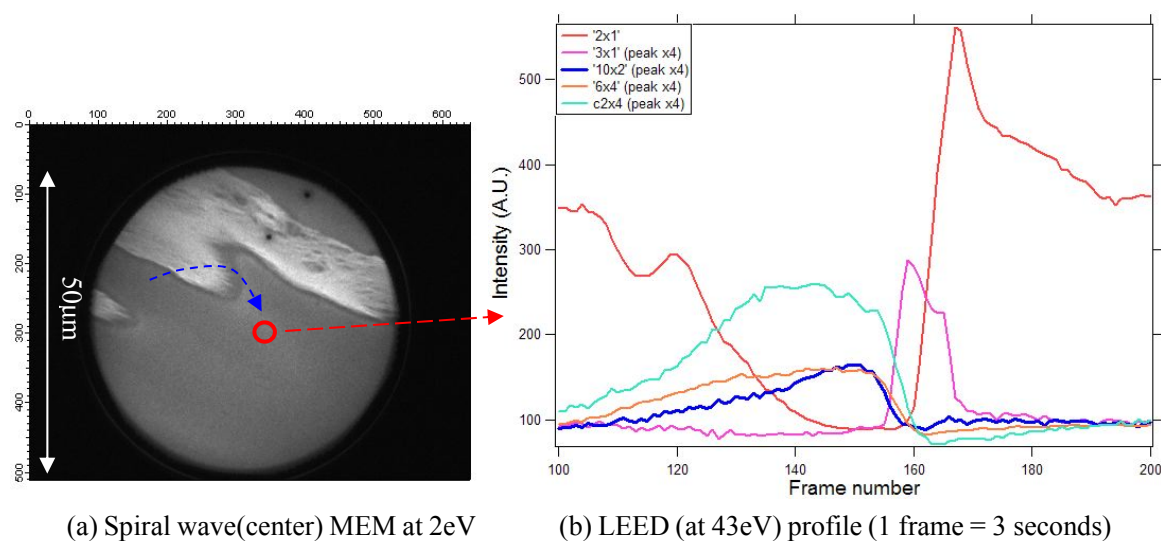
(a) Spiral wave(center) MEM at 2eV   (b) LEED (at 43eV) profile (1 frame = 3 seconds)

Fig.7.19 LEED profile of a spiral wave in NO+H$_2$ reaction on Rhodium (110) surface. (The area probed

by the LEED beam is marked by red dashed circle in (a), with a diameter of 1~2µm). θ_K ~0.067ML, P_{NO} =2.7x10^{-7} mbar (uncalibrated), P_{H2} =2.0x10^{-7} mbar (uncalibrated), T = 527K,

As shown in Fig.7.19 are the various intensities of the LEED patterns in small area passed by a spiral wave (shown in fig.7.19(a)).   The direction of movement is indicated by blue dashed curved arrow.   The intensities are shown in fig.7.19(b).   The area probed by µLEED is marked by red circle in fig.7.19(a).   As shown in fig.7.19(b), between the c(2x4) structure, which is related to a O covered phase, and the (2x1) and (3x1) structures, which are related to a N covered surface, there is a weak 10x2 structure, resulted from K+O coadsorption, as described in Chapter IV.   The existence of the K+O coadsorbate phase supports the idea of K transport by wave propagation.   The 6x4 structure which is also weak still needs to be assigned.

7. 3. Chemical and structural analysis of the Collision Area

7.3.1 Chemical analysis
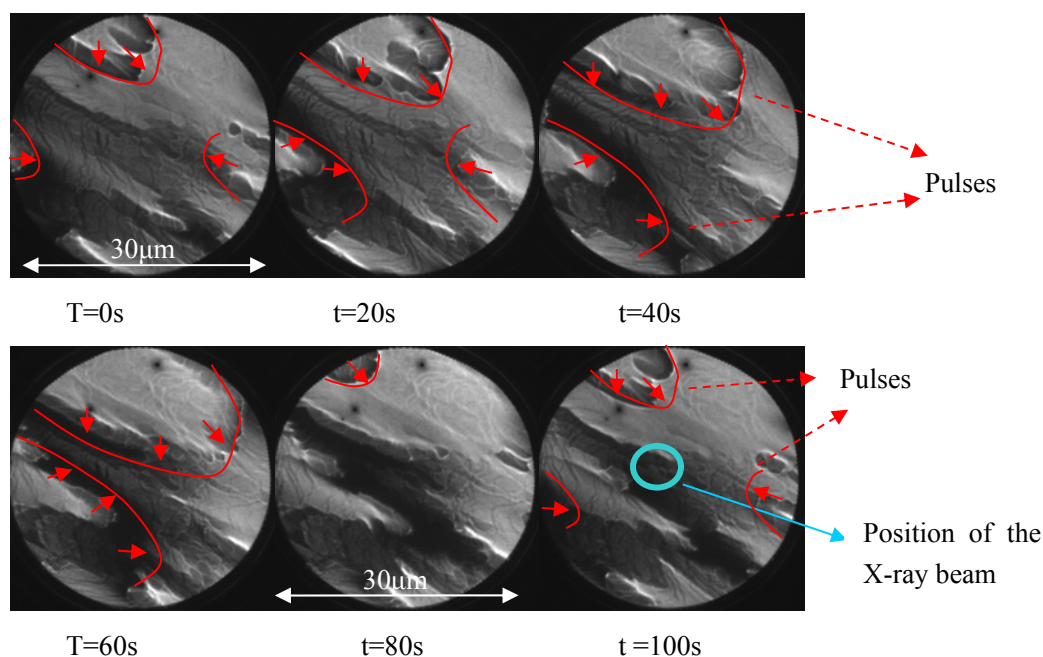
Fig.7.20. MEM on spiral waves in NO+H$_2$/K/Rh(110) system, on area where pulses collide (pulses marked by red curves, arrows indicated there movement), P_{NO} = 2.5x10^{-7} mbar (uncalibrated value), P_{tot} = 7.05x10^{-7} mbar (uncalibrated value), T = 468K,

Next we focus on the area where the pulses collide.   Spiral waves were initiated, as shown in fig.7.20.   Afterwards, the X-ray beam was moved to the collision area of several pulses

(marked by the blue circle in fig.7.20).   The K deposition time was 70s, at current of 6.00A
(corresponding θ_K ~0.04ML).   Approximately after each 100s, the pulses collided in this
area.
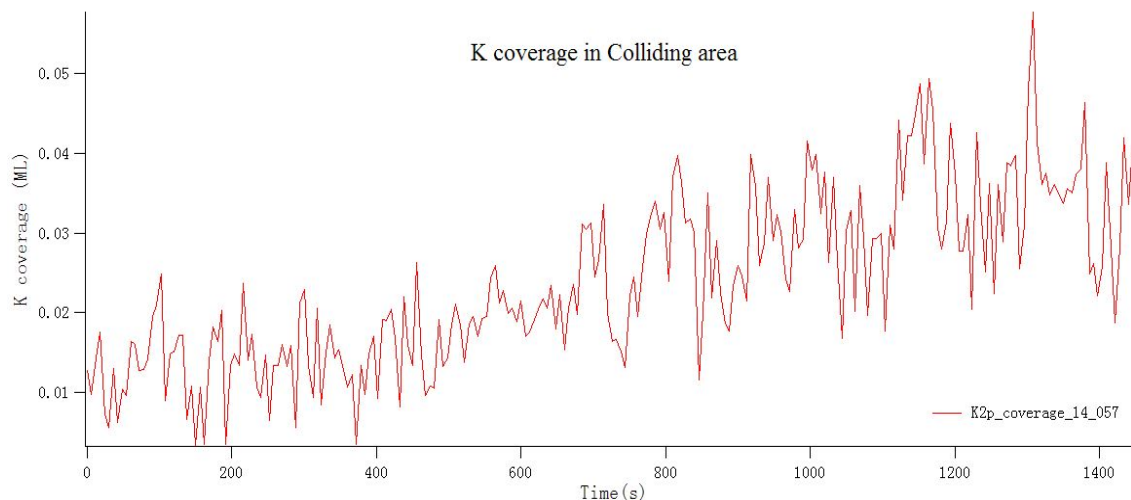
Fig.7.21. K coverage change of collision area of pulses, measure by XPS, in NO+H$_2$/K/Rh(110) system,
     in the same experiment displayed in fig.7.20

The K2p signal was measured in the marked area and the results are shown in fig.7.21.

One can see K coverage increases by a factor of 4, from about 0.01ML to 0.04ML.   During

the time from 400s till about 1400s, pulses have collided in that area for 10 times. So each

collision causes an average local K coverage increase of about 0.003ML.

The low initial K coverage in fig.7.21 might be questioned, which accounts only to around

0.01ML, compared to the original K coverage of the surface which was ~0.04ML.   The

value was calculated according to characteristic curve of the K dispenser.   One can suspect

that a decreasing deposition rate of K dispenser over time might be one reason for this.

Another possibility is that before the area probed by X-ray became a collision area, this area

was passed by pulses, which could have depletion effect on the K coverage by the mass

transport effect described above.   So when this area became finally the collision area, the K

coverage was already quite low, like 0.01ML

The signal to noise ratio is about 16.7%, but the background intensity is just similar to the

previous measurements, which means the measurement of K2p signal can be trusted.

7.3.2 Comparison to the H$_2$+O$_2$/K/Rh(110) system

For a comparison, in the $H_2+O_2/K/Rh(110)$ system, also an enrichment of potassium of the reaction was found. The enrichment of potassium was, however, driven just by the chemical affinity between oxygen and potassium. This affinity led to condensation of K+O into large coadsorption islands, finally a stationary pattern.

In the $NO+H_2/K/Rh(110)$ system, K mass transport occurs in pulses. The K accumulation in the collision area will not result in a stationary pattern, but phenomenon remains dynamic as indicated by turbulent waves inside the collision area.

7.4 Modeling of the NO+H₂/Rh(110) system promoted by potassium

From the experimental results in our experimental results, a theoretical model of the $NO + H_2/K/ Rh(110)$ reaction was developed, by combination of two successful models for $NO+H_2 /Rh(110)$ and $H_2 +O_2/K/Rh(110)$. Combining them with site-blocking effect of K by coadsorbed N atoms, following set of partial differential equations (PDE) is built up:

$$\frac{\partial \theta_H}{\partial t} = \tilde{k}_1 p_{H_2} (\max(\theta_{*,1},\theta))^2 - k_3 (\theta_H)^2 - 2k_5\theta_H\theta_O + D_H \frac{\partial^2 \theta_H}{\partial x^2}, \qquad (7.1)$$

$$\frac{\partial \theta_N}{\partial t} = k_2 p_{NO} \max(\theta_{*,2},\theta) - k_4 (\theta_N)^2 + D_N \frac{\partial^2 \theta_N}{\partial x^2}, \qquad (7.2)$$

$$\frac{\partial \theta_O}{\partial t} = k_2 p_{NO} \max(\theta_{*,2},\theta) - k_5 (\theta_H)^2 + D_O \frac{\partial^2 \theta_O}{\partial x^2}, \qquad (7.3)$$

$$\frac{\partial \theta_K}{\partial t} = D_K \frac{\partial}{\partial x}\{g(\theta_N)\frac{\partial \theta_K}{\partial x}\} - \frac{D_K E_b}{RT} \frac{\partial}{\partial x}\{g(\theta_N)D_K\tilde{\theta}_K(1-\theta_K)\frac{\partial \theta_O}{\partial x}\}, \qquad (7.4)$$

$$\theta_{*,1} = \begin{cases} 1-\theta_H - \alpha_1\theta_N - \beta_1\theta_O & \text{For } \theta_N < 0.5 \\ 1-\theta_H - (2-\alpha_1)\theta_N - \frac{2}{3} - \beta_1\theta_O & \text{For } \theta_N \geq 0.5 \end{cases}$$

$$\theta_{*,2} = 1-\theta_H - \alpha_2\theta_N - \beta_2\theta_O,$$

$$\tilde{\theta}_K = \frac{\theta_K}{\theta_K^{max}}, \quad \theta_K^{max} = 0.22, \quad g(\theta_N) = \max(1-\varepsilon\theta_N,0)$$

$$\tilde{k}_1 = k_1 \exp(-\delta\theta_K), \qquad k_4 = v_4 \exp(\frac{-(E_4^0 - \theta_O E_{Re\,p})}{RT})$$

119

$$D_K = D_K^0 \exp(\frac{-(E_K' + \theta_O(E_K'' - E_K'))}{RT})$$

Coverage of all the adsorbates are denoted by θ_H, θ_N, θ_O, and θ_K, and the vacancies involved were denoted by $\theta_{*,1}$ and $\theta_{*,2}$. The chemisorption of hydrogen and NO is described by $\tilde{k}_1$ and k_2, the desorption of hydrogen and nitrogen are described by k_3 and k_4, and the formation of water is described by k_5.

Equations (7.1)-(7.4) described the reaction-diffusion system of H, O and N with diffusion being represented by the last term. The K coverage is shown to drastically reduce the reactivity of oxygen with hydrogen encoded by an exponential decrease of the hydrogen sticking coefficient ($\tilde{k}_1$) with K coverage.

Equation (7.4) represents the mass transport effect of K in the reaction. The first term stands for normal Fickian diffusion and the second term (drift term) represents the transport of K in the gradient of the chemical potential given by the O coverage. In the second term, E_b is the gain of adsorption energy as K migrates from clean surface to O coverage surface. As shown in the formula of D_K. K has much lower mobility in the oxygen covered area than in the reduced or N covered area. As the O coverage increases, the activation energy of K diffusion is described to linearly increase. This suggests the possible existence of stationary pattern when K and O aggregate. The pattern was found in subsequent investigations of pattern formation of NO+H_2 /K/Rh(110) in a wide temperature range and explored by chemical analysis. With a different experimental procedure, the stationary patterns can be very regular and develop very fast.

7.5 Comparison between theoretical and experimental results

7.5.1 The result of pulses
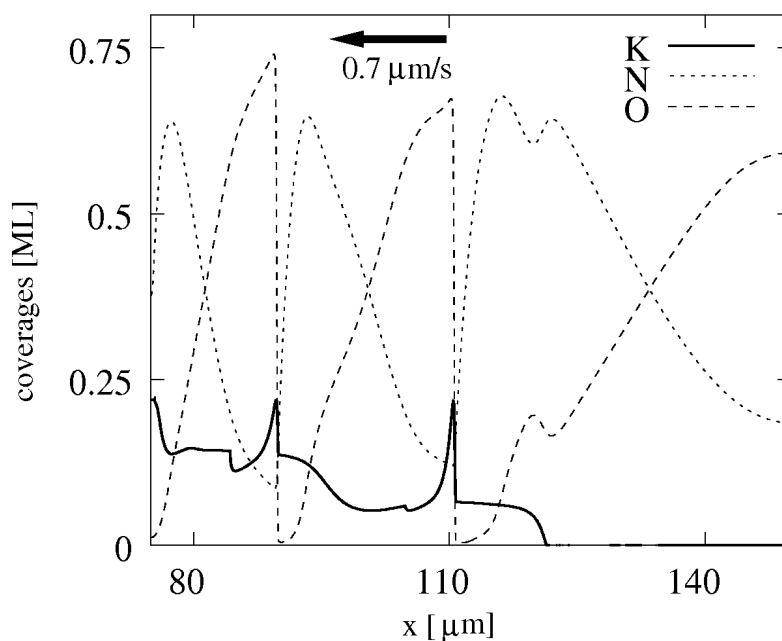
Fig.7.22 Simulated profile of pulses. (Initial conditions: $\theta_K^{init}=0.08$, $\theta_H^{init}=2\times10\text{-}8$, $\theta_N^{init}=0.01$, $\theta_O^{init}=0.89$). Reaction parameters: T=550 K. p (NO)=1.09×10^{-6} mbar, p(H$_2$)=8×10^{-6} mbar. [43]

By applying our simplified model described in Chapter II, a simulation was made which provides the N, K, O distribution in a pulse train, as shown in fig.7.22. One can already see a significant K peak in front of each N pulse, and after the O maxima. This picture is consistent with the experimental results shown in fig.7.18 and fig.7.19. Secondly, although the height of the K peak intensity doesn't significantly decrease like in fig.7.3, the general decrease of the K coverage can still be seen on the profile in fig.7.22 along the direction of the propagation.

There are also some differences to the experiment: 1. in the simulation, the K distribution in front of each pulse appears as a much sharper profile, compared to the experiments; 2. the amount of K coverage decrease shown in fig.7.23 is at least 0.08ML per pulse, which is about one order of magnitude higher than the experimental results shown in figs.7.3, 7.6 and 7.18.

7.5.2 The result of collision area
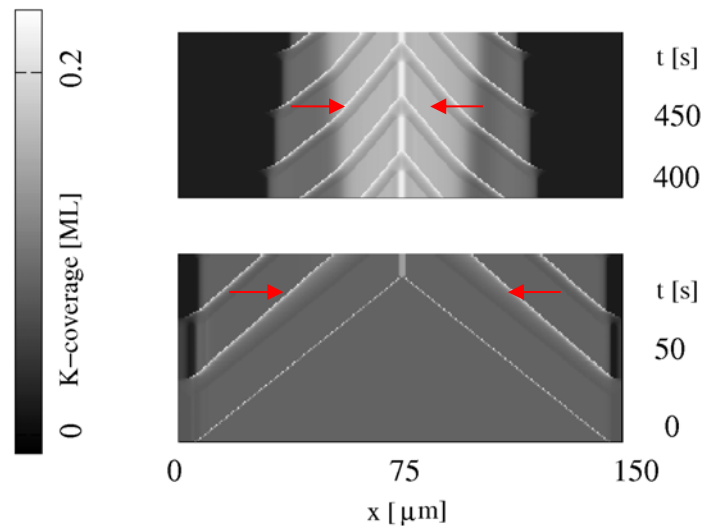
Fig.7.23 Simulated profile of collision area of two series of pulses, the conditions are the same with

fig.7.22 [43]

The simulations shown in fig.7.23 demonstrate that in the collision area, the K coverage increases, within 400s, rising from 0.08ML to ~0.2ML.   One also see that the width of the K enriched area expands over time.   This is qualitatively quite consistent with the experimental data.   In the simulation, the increase of K coverage at collision area is due to K mass transport with pulses.   The simulations thus support the interpretation of the experimental data given above

From fig.7.23 one can estimate that the local K coverage increase by each collision of pulses is ~0.01ML -0.02ML.   Compared to experimental results in 7.3.1, the numerical difference that might be caused by initial conditions, for example, the initial K coverage, in simulation it was set to 0.08ML, while in experiment, it was less than 0.04ML.

The theoretical simulation results shown in fig.7.23 still exhibits some difference to the experiment.   For example, fig.7.1 shows that in the experiment, when the K accumulation area expanded, inside this area turbulent waves became visible.   This effect was not reproduced in the simulation yet.

7.6 Discussion:

1. For the pulse trains, the distribution of K, N and O as shown by XPS measurement clearly demonstrates a mass transport of K by the propagating pulse.   The K peak appears between the N pulse and the O enriched area.

2. As a consequence for the K mass transport, the surface area passed by the pulses experiences a decrease in K coverage.

Under our experimental conditions (P_{NO} = 2.5x 10^{-7} mbar, P_{tot} ~10^{-6} mbar), the decrease of K coverage by each pulse was measured to be about 0.003-0.006ML per pulse on average (depending on K amount pre deposited).   Since the K coverage of the surface is usually ~0.05ML-0.10ML, this transport effect is very significant.

3. The depletion rate of K by mass transport is not constant, but decreases with local K coverage. Otherwise, if the decreasing rate of 0.003-0.006ML were constant, after 20- 30 pulses passing by, we should have already reached 0 coverage of K, which did not happen.

4.   In the collision area of pulses, the K coverage increases as pulses collide.   The average K coverage increases about 0.003ML after each collision of pulses.

5. The theoretical simulations shows agreement with the experimental data.   Details still need further improvement.

VIII. Analysis of Stationary Patterns in the NO+H2/K/Rh(110) System

"Turing-like" stationary pattern in NO+H2/K/Rh(110) reaction

Stationary pattern were not be obtained in the H_2+O_2 and $NO+H_2$ reaction on the unpromoted Rh(110) surface. In $H_2 +O_2$ reaction on a K promoted Rh(110) surface, irregular stationary patterns can develop via reaction fronts when an oxygen covered surface was chosen as the initial state and regular Turing-like structures were obtained when reducing conditions were chosen as the initial state [13].

In the $NO+H_2$ reaction on a K promoted Rh(110) surface, irregular stationary pattern developed via reduction fronts or regular Turing-like pattern can be both obtained when an oxygen covered surface was chosen as the initial state. That regular Turing-like pattern will be the focus in this Chapter.

8.1 General
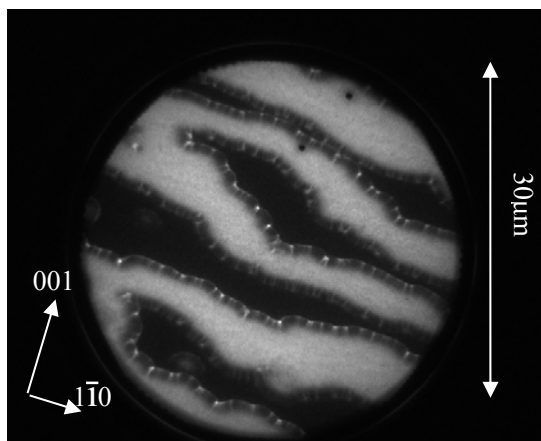
Fig.8.1 MEM at 0.3eV . Stationary pattern in $NO+H_2$ reaction on K-promoted Rhodium (110) surface, $\theta_K \sim 0.12ML$, $P_{NO} = 6.7x10^{-7}$ mbar, $P_{H2} = 10.8x10^{-7}$ mbar, T=548K, the pressure is not calibrated but values direct from the ion gauge.

At the synchrotron source in Trieste a chemical and structural analysis of the stationary patterns was conducted. First, certain amount of K was deposited (~0.12ML, corresponding to a LEED pattern). Then under constant NO pressure H_2 was slowly increased until wave fragments traveling in the [1$\bar{1}$0]-direction appeared. Afterwards, H_2

was continuously increased where the fragments disappeared and stripes like structures appeared.   These stripes represented a stable struture.   Compared to the stationary pattern described in Chapter VI, similar stripe-like structure exists.

The bright area (named as area I) in MEM in fig.8.1 has a higher work function, and the dark area (named as area II) has a lower work function.   The dark area in are of similar width ($\sim 10^0 \mu$m) in the [$1\bar{1}0$]-direction like those bright islands in PEEM (as shown in fig.6.18 and fig.6.27 in Chapter VI) which also have low work function.   Their length in the [$1\bar{1}0$]-direction are also comparable ($\sim 10^1 \mu$m) (cannot be directly seen in fig.8.1 due to the limit of field of view).

8.1.1. Chemical analysis

(a) MEM 0.3eV
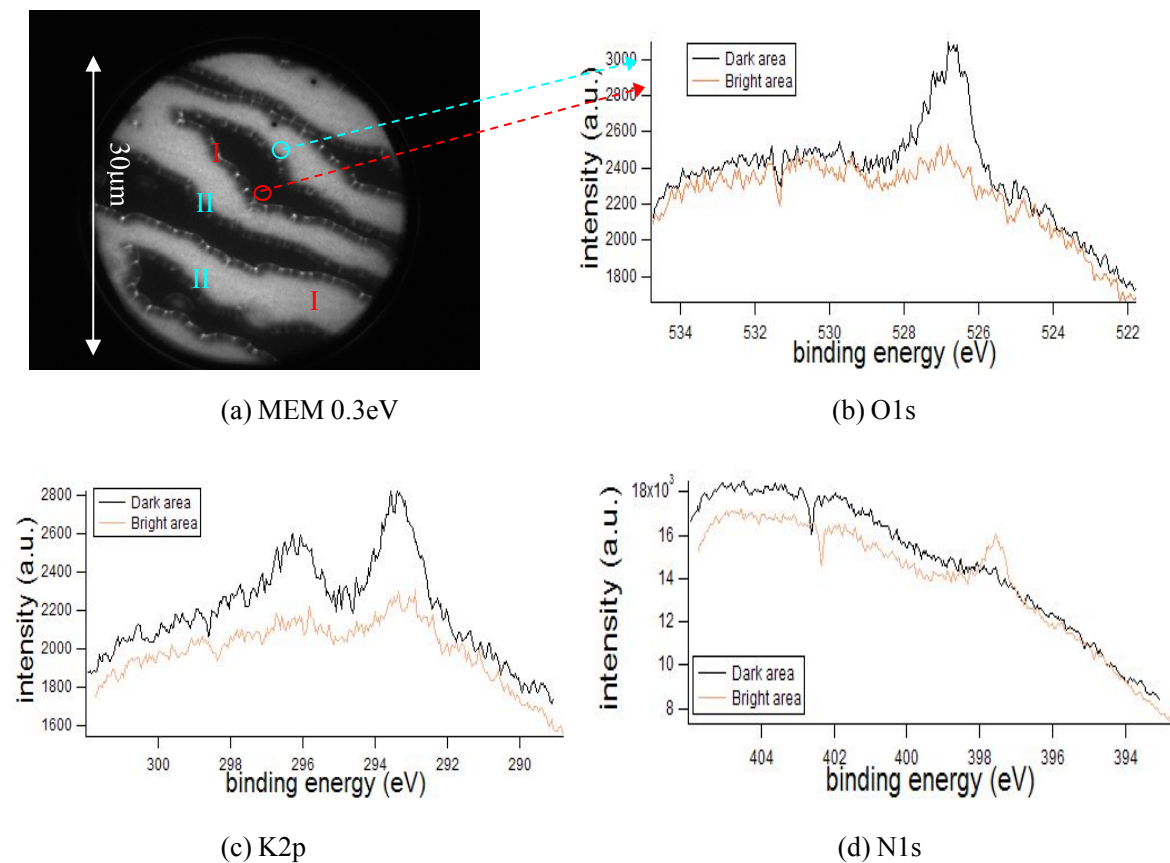
(b) O1s

(c) K2p

(d) N1s

Fig.8.2. MEM and μXPS analysis of the stationary pattern, experimental conditions are the same like in fig.8.1, (a) MEM; (b) O1s; (c) K2p; (d) N1s.

From fig.8.2, we can see that O and N are enriched in different areas.   In all XPS spectra in fig.8.2, red curves refer to area I (bright area in MEM in fig.8.2a, with higher work function),

and the black curves refer to area II (dark area in MEM, with lower work function).   The result shows that in this stationary pattern, O enriched area has actually a lower work function than the N enriched area, and that K tends to reside in the O covered area.

Taking a closer look, it can be seen that the area I with higher work function (N enriched area) actually consists of two different regions, as shown in fig.8.3.(b), and the area II with low work function seems to have no significant sub-domains: small islands and area surrounding them.   This will be finally discussed in 8.2.

(a) PEEM   (b) MEM 2.5eV
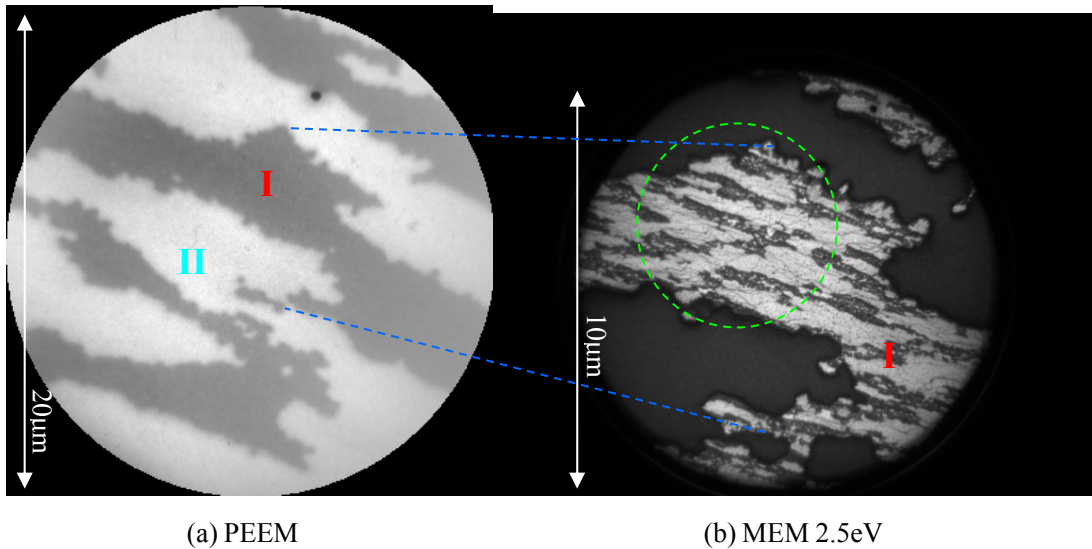
Fig.8.3. Stationary pattern, which shows in the area I (N enriched area) there are two sub domains.   The PEEM and MEM images were taken at another spot of the sample from same experiment as in fig.8.1. (a) PEEM; (b) Zoom in by MEM on the part indicated in fig.8.3 (a)

8.1.2 Structural analysis

(a) LEED 2x1+1x2+c(2x2)   (b) LEED 10x2
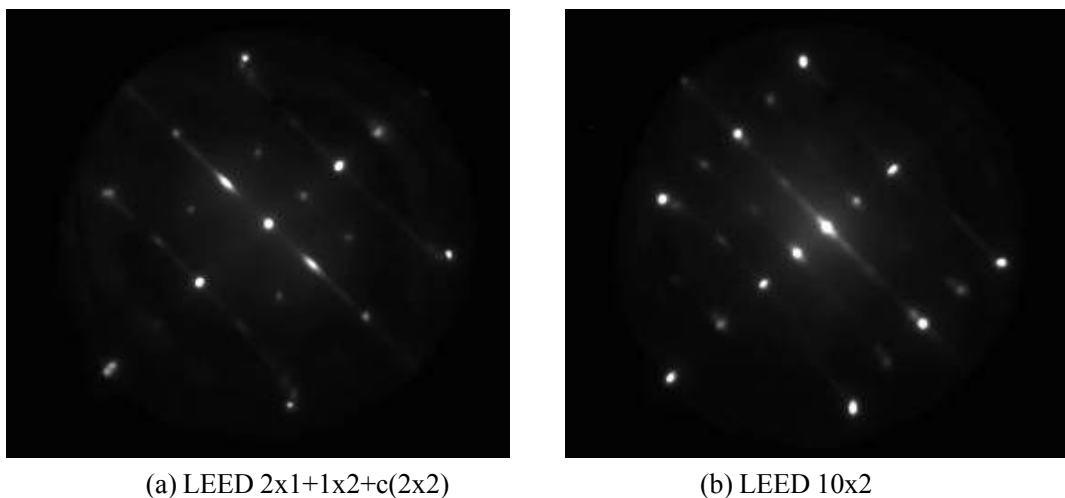
Fig.8.4 µLEED at 43eV: (a) From area I (dark part) in fig.8.3a; (b) From area II (bright part) in fig.8.3a

LEED analysis was made for different areas of the stationary patterns, as shown in Fig.8.4,

fig.8.4(a) was taken from the dark area in the PEEM image in fig.8.3(a) (high work function).   The extra-beams correspond to seems like a p(2x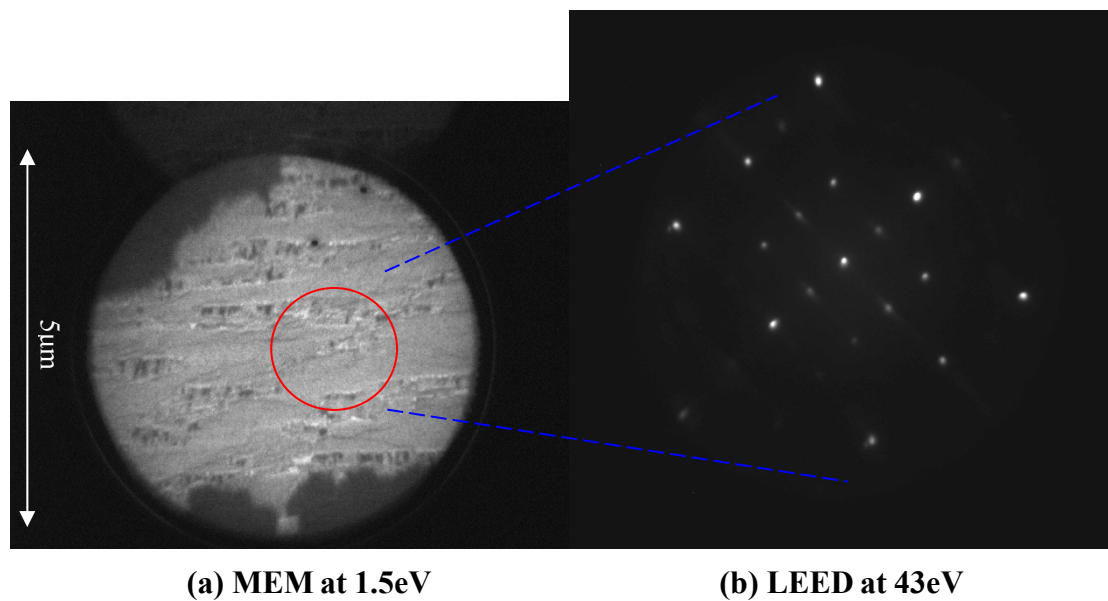2) structure, which might also be superposition of 1x2 +2x1+ c(2x2) structures from different sub domains shown in fig.8.3(b).   Fig.8.4.(b) was taken from the bright area in fig.8.3(a), i.e., low work function area.   This area exhibits a 10x2 structure.

8.2 Inhomogenety in area I (bright area in MEM)

8.2.1. Structural Analysis

(a) MEM at 1.5eV   (b) LEED at 43eV

Fig.8.5. Area I of fig.8.3 (position marked by green dashed circle in fig.8.3b) , in an enlarged scale, with corresponding LEED pattern.

As mentioned in 8.1.1, there were two different sub domains in the area I, shown by MEM in fig.8.3(b).   In order to have a closer look at the area I in fig.8.1-fig.8.3, fig.8.5 (a) displays a MEM image with a smaller scale on the same area in fig.8.3 (b).   This image was taken without contrast aperture, and therefore the islands inside the area I appear not so clear as in fig.8.3(b).   To analyze these two domains, we use LEED and XPS.   Because the minimum size of the electron beam (as indicated by the red circle in fig.8.5.(a)) is about 2~3μm, we cannot get separate signals for each domain.   However, with dark field imaging we obtained some information, as shown in fig.8.6 and fig.8.7, in which the border of area I and area II is marked by blue dashed line, the area I is in the center of view.

(a)LEED at 43eV	**(b) LEEM (dark field) at 43eV**
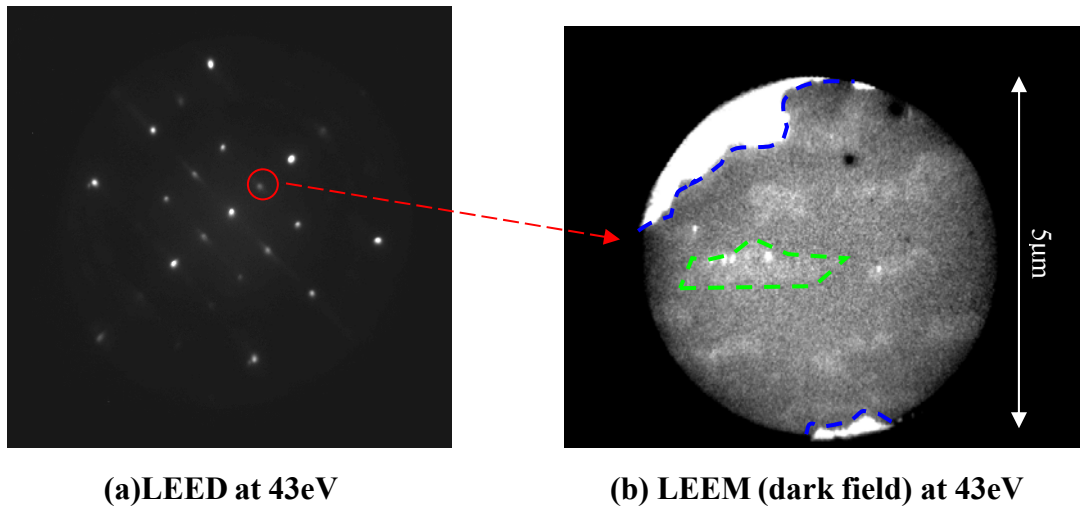
Fig.8.6. Dark field imaging with (0,1/2) beam in LEED, E_k = 43eV

(a)LEED at 43eV	**(b) LEEM (dark field) at 43eV**
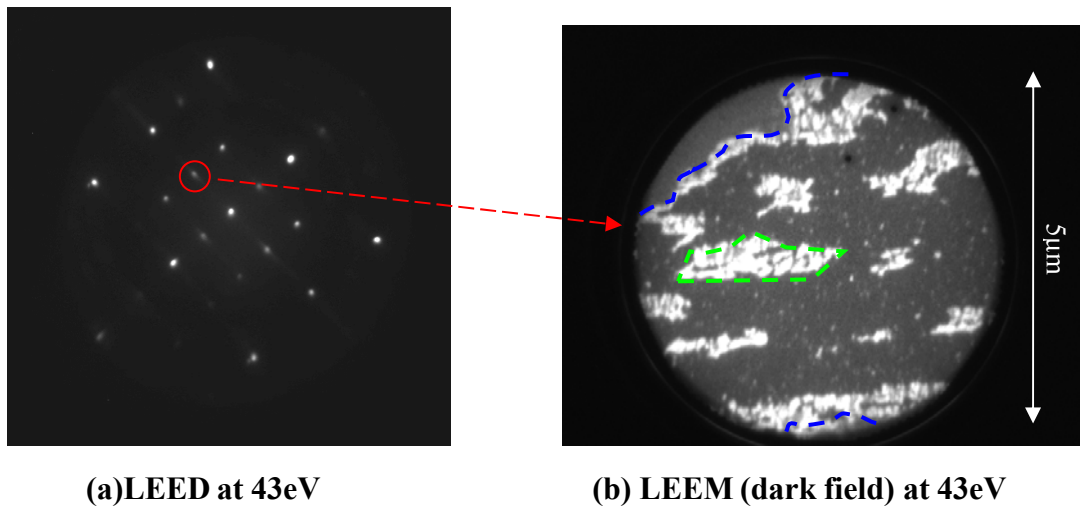
Fig.8.7. Dark field imaging with (1/2,0) beam in LEED, E_k = 43eV

From fig.8.6 and fig.8.7 one can see the dark field images have similar intensity distribution. There are bright islands in both fig.8.6(b) and fig.8.7(b) (indicated by green dashed lines), and the islands in fig.8.7(b) are brighter than those in fig.8.6(b).   Also, in fig.8.6, the oxygen enriched area (upper left part, distinguished by blue dashed line) is brighter than the islands, in fig.8.7 it is vice versa.

The (1/2, 0) beam contributes from the (2x1)-N structure formed by the N adsorption, and the (0, 1/2) beam is due to the (1x2) structure formed by potassium or oxygen adsorption, or the 2nx2 (n = 4, 5, 6) structures formed by the oxygen potassium coadsorption [26].

All of the above suggest that those islands shown in fig.8.6 (b) and fig.8.7 (b) might have more N and K than the surrounding area, and the oxygen enriched area shown in fig.8.6(b)

and fig.8.7(b) seems to have oxygen and K coadsorption which formed 2nx2 (n=4, 5, 6) structures..

(a)LEED at 43eV   (b) LEEM (dark field) at 43eV

Fig.8.8 Dark field imaging on (1/2, 1/2) point in LEED, $E_k = 43eV$
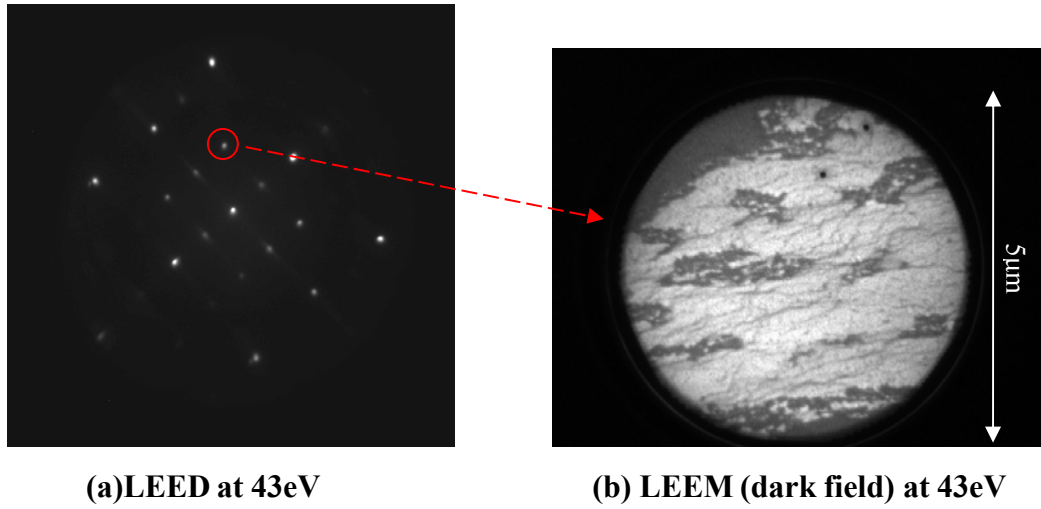
(a)LEED at 43eV   (b) LEEM (dark field) at 43eV
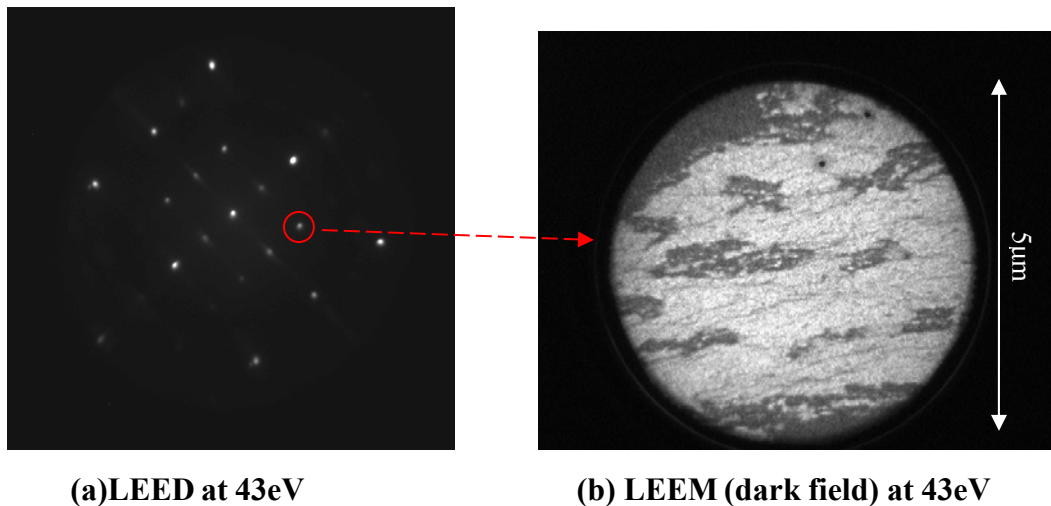
Fig.8.9 Dark field imaging on (-1/2, 1/2) point in LEED, $E_k = 43eV$

Fig.8.8 and fig.8.9 should come from the same structure, and they both show inverted contrast to fig.8.6 and fig.8.7, and the area around those islands has higher intensity.

To summarize the facts:

1. In area I in the stationary pattern, there is a phase separation into a c(2x2) structure and a 1x2 +2x1 structure. The islands (marked by green dashed line) in fig.-fig have 2x1 structure and a weaker 1x2 structure. The area surround the islands has c(2x2) structure. From fig.8.3b it can be seen, inside area I, the islands have lower work function than the area surround the islands, and they both have higher work function than area II. This indicates

130

the bright islands in fig.8.6(b) and fig.8.7(b) might be corresponding to the gray area (element I) we saw between the islands and the dark area in fig.6.27 in chapter VI.

2. According to previous research, the 1x2 reconstruction might be related to O or K adsorption and 2x1 reconstruction might be related to N adsorption. And from the XPS in fig.8.2, it also shows that in "area I" in fig.8.1-fig.8.3 there was still some small O intensity. This indicates there might also be some oxygen in the "area I". The origin of the c(2x2) area still needs to answer, if it is related to simply from O, N, K adsorption, or other contamination, for example, carbon from CO adsorption?

8.2.2. Origin of c(2x2) structure

Since the previous experiment took a very long time (>2 hours), there is a risk of carbon contamination from the residual gas or even from the bulk. The question is whether the c(2x2) is related to a carbon contamination. XPS was again applied to check this point.

(a)

(b)

(c)

(d)
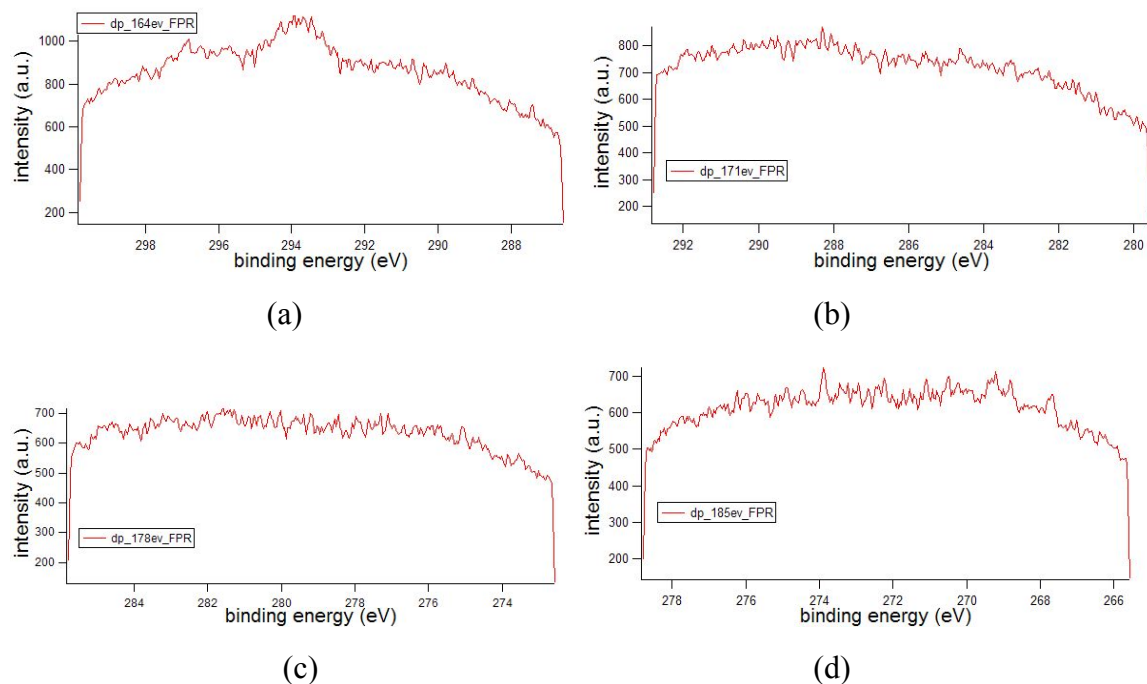
Fig.8.10 XPS for checking carbon contamination, starting energy (a) 164eV; (b); 171eV;

(c)178eV;(d)185eV. The two peaks at 297eV and 294 eV belong to K2p

According to literature, C1s has binding energy of 284.2eV [44]. An XPS spectrum was taken from 266eV to 300eV. No other peak was found, so no significant C1s signal was detected.

The absence of C1s signal might also be because that C1s intensity is too low that it is below the sensitivity of XPS.   We can make a little estimation of the upper limit of C1s intensity. The cross sections of C1s and K2p at photon energy of 459eV are 0.35mb and 1.5mb [44] $(1mb = 1x10^{-31}m^2)$.   So for the same photon flux and the same peak intensity, the amount of carbon is about 4 times as much as potassium.   In fig.8.10(a) and fig.8.10(b), since no C1s signal was found, C1s intensity should be smaller than the background noise, which is about ~0.48% against background.   In the same condition, the ratio of K2p signal to noise is ~0.899.   So the amount of carbon is less than 2% of the K coverage (~0.12 ML).   This means the amount of carbon is less than $2.6x10^{-3}$ ML, therefore the c(2x2) seems not be due to CO adsorption.

From the above discussion we can see the existence of carbon in the c(2x2) area is not supported by XPS.   If we suppose the amount of oxygen is not enough to cause 1x2 reconstruction of Rh(110) surface, the possibility might exists that the c(2x2) structure comes from coadsorption of oxygen and nitrogen on 1x1 Rh(110) surface with potassium existence [45, 46].   But till now it is still not clarified yet.   A further proof might be provided by STM investigation.

8.2.3 Origin of the stationary pattern, experimental explanation.

Simulation of this Turing-like stationary pattern still does not exist, but an possible explanation would be:

1. As described in the discussion of wave propagation in Chapter VI and of coadsorbed K in Chapter VII, the potassium existence may have an inhibition effect on wave propagation

2. From the dispersion relationship in $NO+H_2$/Rh(110) system discussed in Chapter VI, we can see that under our experimental conditions (T~520K, θ_K ~ 0.067ML), there is a minimum wavelength for pulses that can propagate, which is about ~20μm

3. From the average size of the stripes and islands structure found in experiment in this Chapter and in Chapter VI, we can see that the average width of the reduced area (area I in fig.8.1-fig.8.3) between those K enriched oxygen covered area can be compared to or

is smaller than the 20μm.

4. This means, under normal experimental conditions where such patterns were obtained ($T<600K$, $\theta_K <0.12ML$), pulses were inhibited to propagate among those islands. This could be the reason why the surface with the islands became stable.

The K enrichment in the oxygen covered area (area II in fig.8.1-fig.8.3) can be explained by the strong affinity of K+O and by the high mobility of K on reduced area (area I in fig.8.1-fig.8.3) and low mobility on oxygen covered area[12]. Further investigation with a refined model is required to clarify the origin of the stationary patterns.

8.3 Comparison with the $H_2 +O_2$ /K/ system and NO+H_2/Rh(110) system

In the unpromoted H_2+O_2/Rh(110) and NO+H_2/Rh(110) system, stationary patterns were not theoretically predicted nor experimentally obtained.

In the H_2+O_2/K/Rh(110) system, a stationary pattern was experimentally obtained and theoretically explained[13, 32]. In the NO+H_2/K/Rh(110) system, stationary patterns can were obtained. Their appearance only depends on the partial pressure, K coverage and the temperature (so called state-dependent).

Chemical and structural analysis shows that the Turing like stationary patterns also have a phase separation into different regions ordered as discussed in 8.2.

As discussed in 8.2.3, the origin of such stationary pattern might be due to effect of K on wave propagation.

8.4 Discussion & Summary:

For the Turing-like stationary pattern in NO+H_2/K/Rh(110) system, we can give a short summary:

8.4.1 Phase separation

In the Turing like stationary pattern in the NO+H_2/K/Rh(110) system, phase separation leads to two regions: K enriched oxygen covered area and N enriched reduced area ("area I" in

fig.8.1-fig.8.3). Both areas exhibit ordered adsorbate phases. In the K enriched area a (2nx2) (n = 4, 5, 6,) structure is detected and in the reduced Area I a 1x2+2x1+c(2x2) separation of patterns is found. The K enriched oxygen covered area has a lower work function than the N enriched reduced.

8.4.2 Sub domains of the N enriched reduced area

The N enriched reduced area ("area I" in fig.8.1-fig.8.3) was consists of two sub domains; small islands with 1x2 and 2x1 structure and area with c(2x2) structure, which is located between the (1x2) and (2x1) phases. The area with c(2x2) structure has a higher work function than the area with 1x2+2x1 structures. Both areas indicate might have a small amount of O adsorbed. The small islands with (1x2) and (2x1) originate from O, K and N coadsorption. The origin of the c(2x2) structure of the area surrounding the islands is not clarified; one can speculate that it results from O+N coadsorption.

8.4.3 Theoretical explanation

Till now no theoretical explanation is clarified for the "Turing-like" stationary pattern, although the shape of the islands (element III in Chapter VI) looks similar like the theoretically predicted "spike" in and "broad strata" stationary pattern in an active media with long-range inhibition [47]. As speculated in 8.2.3, "inhibition effect" of K on wave propagation might be considered as an influencing component.

IX. Oxide formation

Previous experiments on K+O coadsorption have shown that [26], at high K coverage (>0.12ML) and high oxygen dose (>10^{1}L), oxides will form on the Rh(110) surface. For understanding the patterns in NO+H$_2$/K/Rh(110), it is important to determine where oxide how it is formed and influences pattern formation. For example, the "inhibition effect" of K on wave propagation could be due to oxide formation since both became significant at high K coverage (>0.67ML). However, during the reaction of NO+H$_2$/K/Rh(110), no oxide was found in the collision area of pulses. The failure to detect oxides might be due to the fact that the initial θ_K was not high enough (>0.08ML) to ensure that θ_K can be accumulated up to >0.12ML in the collision area. In order to first investigate the properties of the oxide, we have to start from K+O coadsorption.
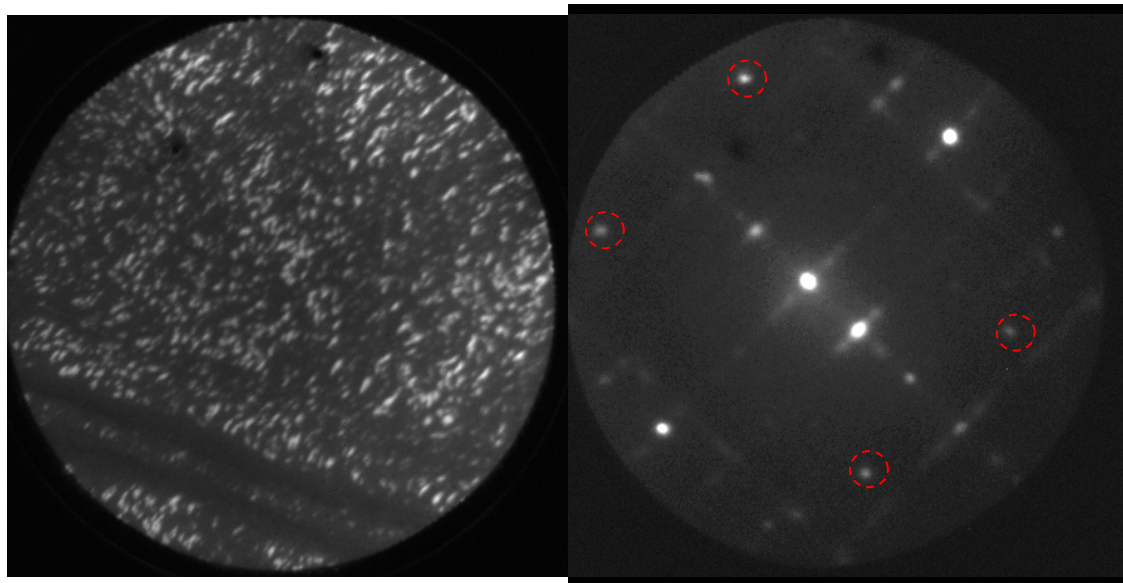
(a).LEEM at 37eV on (0,0) point　　　　　　　(b) LEED at 37eV

Fig.9.1 Oxide formed by O$_2$ and K coadsorption on Rh (110) surface,

P$_{O2}$ = 1x10^{-7} mbar, θ_K ~ 0.2ML, T~520K, (a) LEEM; (b) LEED

First a large amount of K was deposited onto the sample at T~520K with a coverage of K near ~0.2ML. This value is near saturation value, according to the calibration of dispenser in fig.5.8. Afterwards we introduce oxygen. After some time, in LEEM many bright dots appeared on the originally homogeneous sample surface, as shown in 9.1(a). LEED pattern shows a c(2x4) structure with missing spots in the (±1/2, ±1/4), (±1/2,- ±3/4)

positions, as shown in fig.9.1(b).   The c(2x4) structure with these missing points is assigned to oxide formation ([26]).
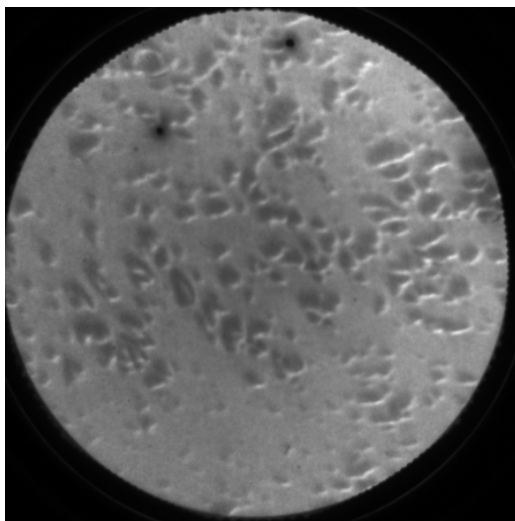

Fig.9.2 MEM image at -2.0 eV on the area with suspected oxide islands shown in fig.9.1, this means the islands have actually lower work function

As shown in fig.9.2, a MEM image of the same area in fig.9.1(b) shows that the bright islands in the LEEM image in fig.9.1 appear as dark islands.   This demonstrates that they have lower work function than the area surrounding them.

9.1. Chemical analysis of suspected oxide islands

After the oxide islands were obtained, under the same experimental conditions, an µXPS analysis was conducted.

In order to investigate whether a lower limit of K coverage for oxide formation exists, another experiment was done, with less K (~0.14ML).   The K was deposited onto the surface at T~520K.   Then the sample was exposed to ~2.7L of O_2.   Islands were seen growning on the surface, as shown in fig.9.3.
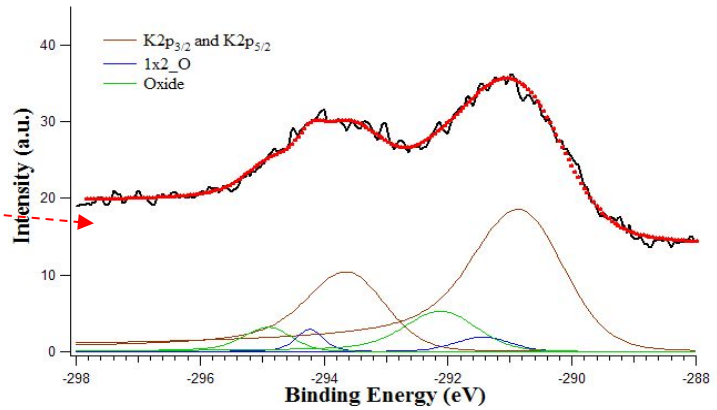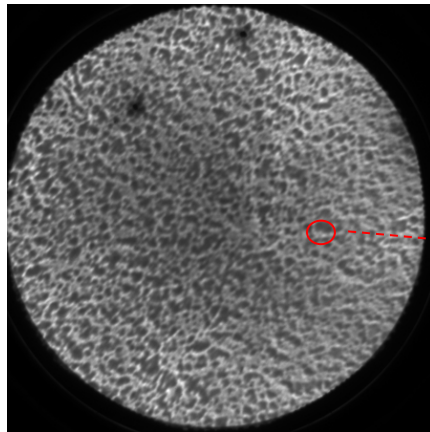
(a) MEM at -1.5eV, on suspected oxide islands (b) XPS, K2p

(c)XPS, O1s
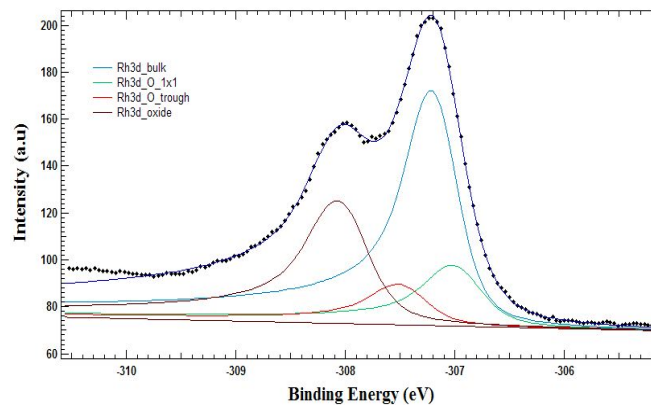
(d) XPS, Rh3d$_{5/2}$

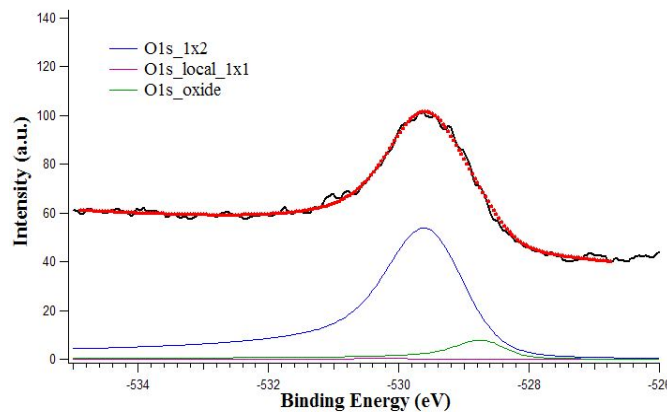**Fig.9.3.** μXPS spectrum of the area with oxide islands in fig.9.1, θ_K ~0.14ML, after ~2.7L O$_2$ was introduced, P$_{O2}$ = 4x10^{-8} mbar. (a) MEM image of the probed area (The position of the X-ray light beam is marked by red circle) (b) K2p; (c) O1s; (d) Rh3d

As shown in fig.9.3, the XPS spectra show that a significant amount of oxide exists already on the probed area.   However, the size of the light beam was too large to separately measure the spectrum in and outside the islands.   The μXPS spectrum shown in fig.9.3 actually contains signals from both areas: the oxide islands and the surrounding area.   In order to analyze the areas separately, we also tried to grow larger islands, but this resulted in

just a higher islands density.

9.2 Structural analysis: dark/bright field images of oxide.

In order to obtain more information, a bright/dark field imaging was conducted.   LEEM
images taken from different diffracted electron beams selected in the LEED diffraction plane
are shown in fig.9.4- fig.9.6.

(a) LEED at 60eV   (b) LEEM at 60eV with (1/2, 5/4) beam
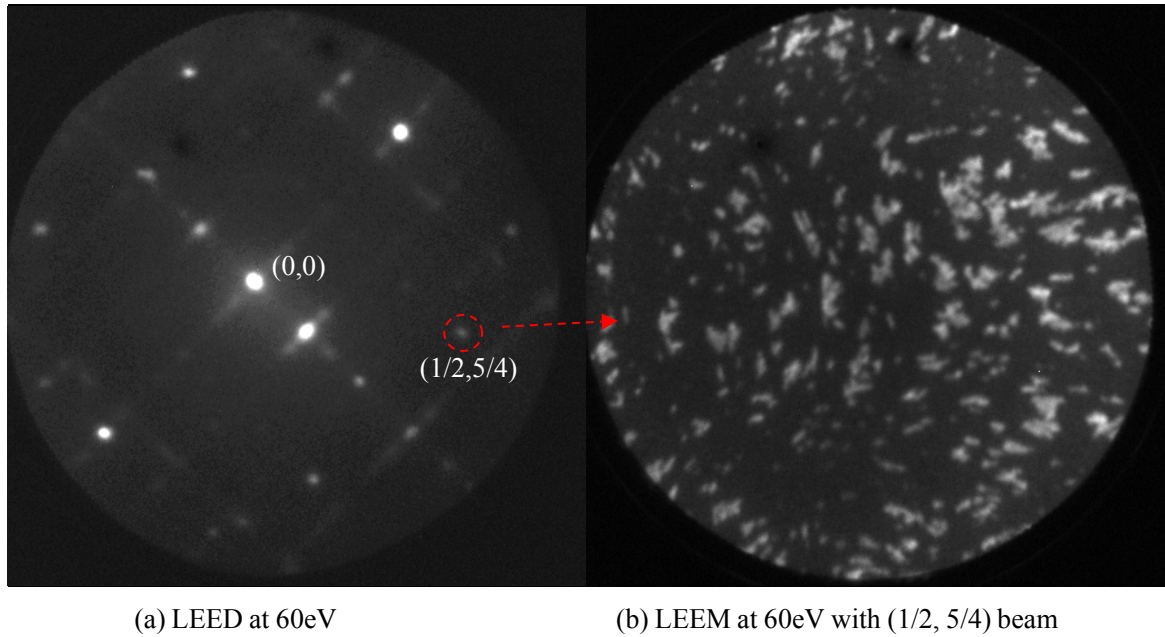
Fig.9.4 Dark field imaging of LEED beam (1/2,5/4) (marked by red dashed circle in (a)

(a) LEED at 60eV   (b) LEEM at 60eV with (-1/2, 5/4) beam
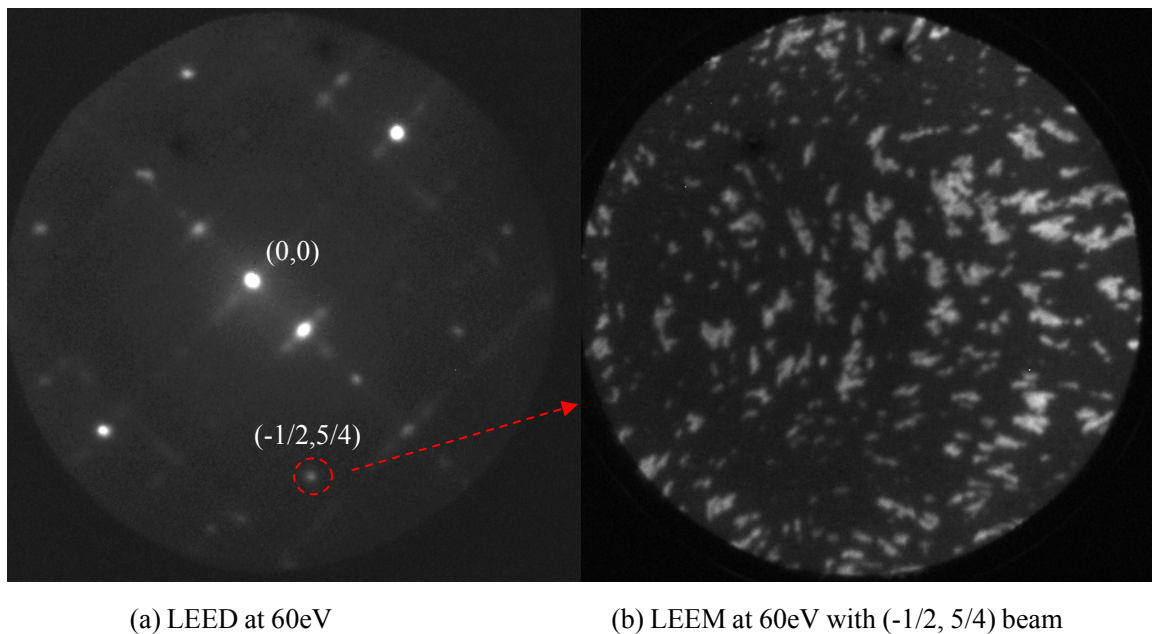
Fig.9.5 Dark field imaging with LEED beam (-1/2,5/4) (marked by red dashed circle in (a)

The dark field image in fig.9.4(b) and fig.9.5 (b) were taken from the (1/2,5/4) and (-1/2,5/4)

beams.   These beams are related to a c(2x4) structure with missing points which is assigned to oxide.   In the above images, we can see islands with a high intensity, and a similar contrast like the LEEM image in fig.9.1.   This indicates that the islands discovered in fig.9.1 and fig.9.2 are actually related to oxide formation.   The oxide signals in the μXPS spectrum in fig.9.3 are a contribution of the oxide islands.

(a) LEED at 60eV   (b) LEEM at 60eV with (0, 1/2) beam

Fig.9.6 Dark field imaging of LEED beam (0, 1/2) (marked by red dashed circle in (a))
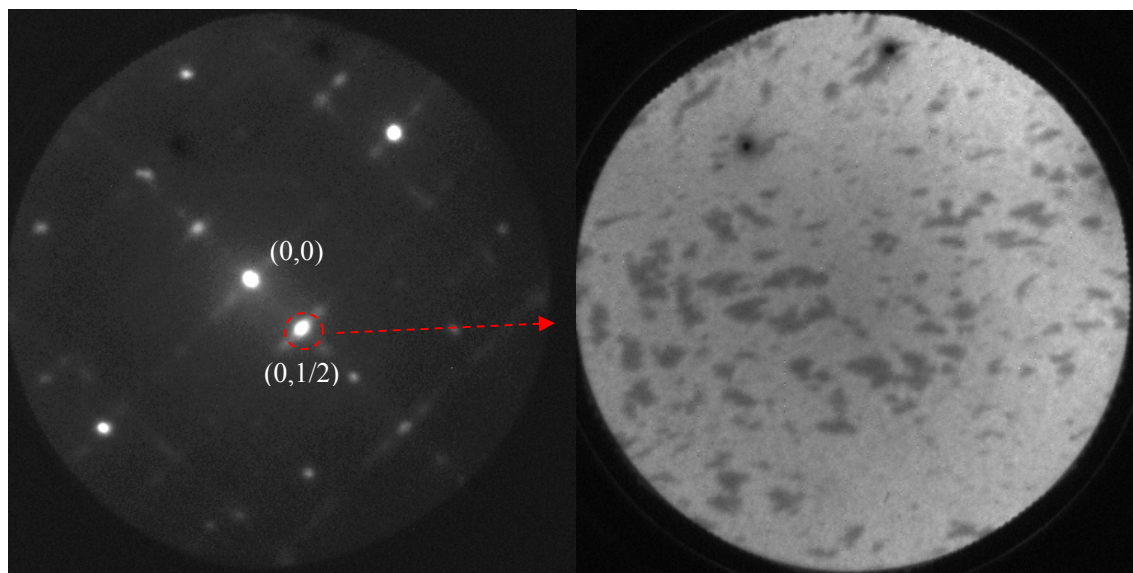
The dark field image with the LEED beam (0,1/2) shown in fig.9.6 has a inverted contrast from the dark field images with the LEED beams (1/2, 5/4) and (-1/2, 5/4) shown in fig.9.4 and fig9.5 which are correspond to oxide.   This contrast is also inverted from the bright field image of the LEED (0,0) beam shown in fig.9.1.   The strong (0,1/2) beam corresponds to a 1x2 substrate reconstruction, but the intensity of this beam is also related to 2nx2 (n = 4, 5, 6) or c(2x4) structures.

The inverse contrast in dark field images with the (1/2,5/4) and (0,1/2) beams indicates that the corresponding surface structures are localized in different areas.   The c(2x4) structure may belong to the oxide islands and the 2nx2 (n = 4, 5, 6) structure may belong to the area outside of the islands.

The oxide islands have a lower work function which might be due to K enrichment in the oxide islands or, more likely, be just a property of Rh oxides.

9.3 Stability of oxide

After the oxide was formed, we tried to remove it from the surface simply by reduction with H_2. For that purpose, first H_2 at pressure 6×10^{-8} mbar was introduced for 300s, then at 1×10^{-7} mbar for 900s.   A LEED pattern and a LEEM image of the surface are shown in fig.9.7.
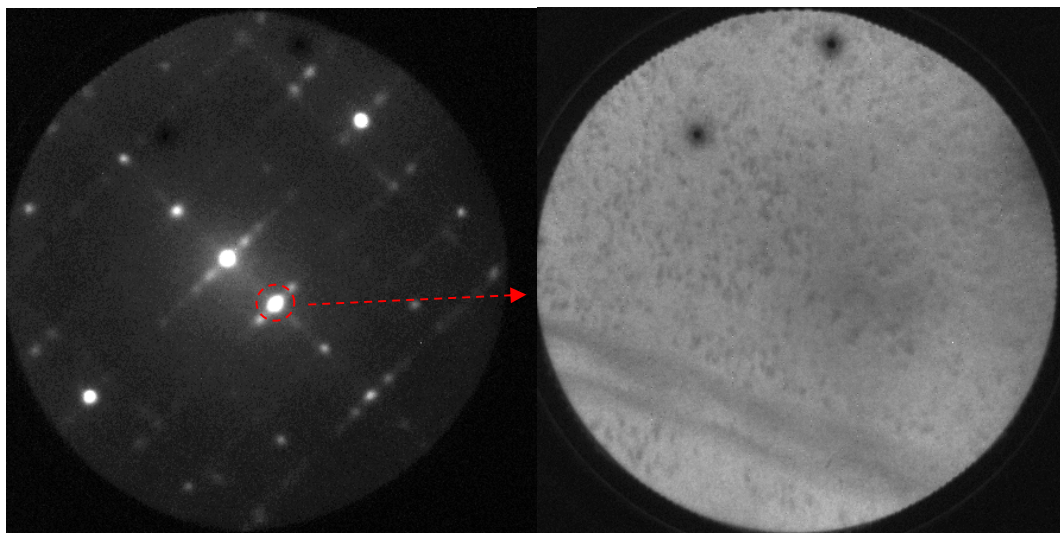
(a) LEED at 37eV (b) LEEM at 37eV on (0,1/2) point

Fig.9.7 Surface after treatment of H_2 ($P_{H2} = 6\times10^{-8}$ mbar for 300s, and $P_{H2} = 1\times10^{-7}$ mbar for 900s), T ~ 523K

In LEED we still see a c(2x4) structure with missing beams.   The LEEM image also shows that many small islands still exist on the surface.   The contrast is inverted because dark field image taken with the (0,1/2) beam was used.   This means that the oxides are very stable under H_2 of low pressure and low temperature.   Even raising the H_2 pressure to 7×10^{-7} mbar (which is close to the limit of the device) does not remove the oxides.
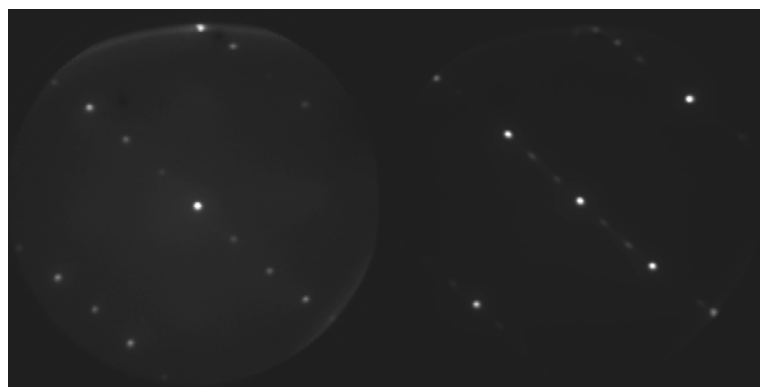

(a) (b) (c)

<div align="center">(d)   (e)</div>

Fig.9.8 LEED at 37eV, ,(a) T= 623K, P_{H2}= 7x10^{-7} mbar (b) T= 743K, P_{H2}= 3.5x10^{-7} mbar. (c) T= 763K, P_{H2}= 3.5x10^{-7} mbar. (d) (e)T= 803K, P_{H2}= 3.5x10^{-7} mbar

Then the sample was heated to 623K.　The oxide related beams were gone, as shown in fig.9.8(a). The LEED pattern then just shows a 8x2 structure, which is due to K+O coadsorption [26].

This means that at higher temperature (at least, around 623K) oxide can be removed by exposure to H_2.　The 8x2 structure still exists, which means that the stability of the oxide is lower than the stability of the 8x2 structure caused by K+O coadsorption.　Even after lowering the H_2 pressure to 3.5x10^{-7} mbar and raising temperature to 743K, LEED pattern remains 8x2, as shown in fig.9.8(b).

When T = 763K, the LEED pattern changes into c(8x2), as shown in fig.9.8(c).　This structure still belongs to K+O coadsorption, but a with lower oxygen coverage.　At T = 803K, the LEED pattern changes into 1x2, then into a streaky 1x3, as shown in fig.9.8(d) and fig.9.8(e). The 1x2 and streaky 1x3 are related to a K covered surface, and the change from a 1x2 to a streaky 1x3 may be initiated by desorption of K, according to the LEED phase diagram in fig.4.8.　Decreasing T to 523K and turning off the H_2, the streaky 1x3 still remains.　This proves that the surface was reduced.　On clean Rh(110) surface, in previous experiment, the surface can be reduced just by H_2 at 5x10^{-7}mbar at 500K
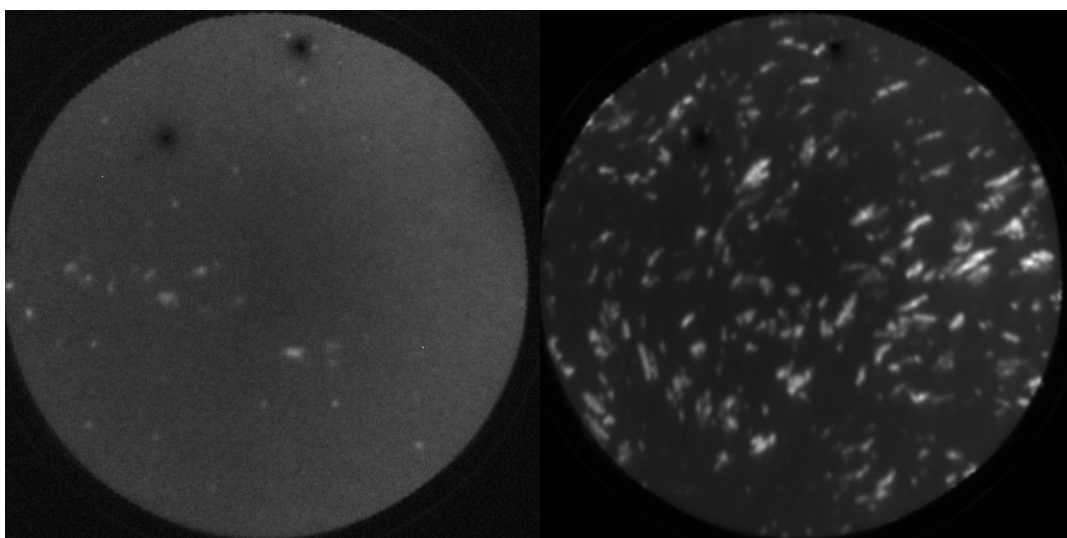
(a) LEEM at 60eV   (b) LEEM at 21eV

Fig.9.9 LEEM images of oxide, (a) after some time of LEED measurement, (b) at another spot not exposed to the electron gun.   Both images are dark field images with (1/2,5/4) beam.

One interesting point is that the oxide can also be reduced simply by the electron gun.   As shown in fig.9.9, after observing LEED for some time, we see that the number of the islands in LEEM became less than before exposure to the LEED electron beam.   Moving to another spot at the surface, the islands are again quite numerous.   After a similar time with LEED, again many islands disappeared in that area.

After all, we can see the oxide is not very stable with H_2 in the atmosphere.   For comparison, the 2nx2 K+O adsorbate related structure are more stable.

9.4 Summary

Oxides during pattern formation in the NO+H_2/K/Rh(110) system were not found.   The failure may be due to the fact that the formation of oxide requires a quite high K coverage (~0.14ML) under these experimental conditions (T~460-600K, P_{total}<1x10^{-6} mbar), and under such conditions, stable patterns can hardly be initiated.

The stability of oxide is significantly influenced by temperature: by P_{H2}~7x10^{-7}mbar, and for T<620K, the oxide was stable, but for T >620K, it was immediately removed.

Under the same H_2 pressure, the oxide required much lower temperature to be reduced, compared to structures of chemisorbed oxygen and K+O coadsorption structures.   At high K coverage, the oxygen covered surface requires quite high temperature for the oxygen to be

removed by H_2.

X. Summary

The NO+H$_2$/K/Rh(110) system exhibits very complicate but also interesting behavior, as shown from previous chapters. If we combine the discussion of the previous results, we formulate the following points:

0. With coadsorbed potassium the basic excitation cycle for pulses in the unpromoted system NO+H$_2$/K/Rh(110) remains intact: one observes pulses, target patterns and spiral waves.

1. In pattern formation of the NO+H$_2$/K/Rh(110) system, the potassium acts as some kind of "inhibitor" for wave propagation, including ignition of reaction. Oxide formation is not necessary for such kind of "inhibition" behavior, which is caused by the lowering of the H$_2$ sticking coefficient by coadsorbed potassium.

2. Mass transport of K due to wave propagation is phenomenon of general interest. It results here from the resulsive interaction between coadsorbed potassium and nitrogen. The nitrogen adlayer acts as a   for potassium. A substantial K concentration there fore piles up in front of each nitrogen pulse propagating across the surface.

3. Compared to the NO+H$_2$/Rh(110) system, the K existence in the system results in two kinds of stationary patterns, (i) one type of Turing-like patterns are in the bistable regime, formed by K redistribution from collision of reduction fronts, like in the H$_2$+O$_2$/K/Rh(110) system; (ii) Turing like pattern forming from the homogeneous state and leading to a separation into ordered phases.

4. Formation of an oxide in the NO+H$_2$/K/Rh(110) system requires a quite high K coverage, and the oxide is not stable under high temperature. Presumably oxide formation plays no role in most of the patterns discussed here. However, it cannot be completely excluded that

under some conditions oxide formation might be involved.

5. The theoretical simulation shown in chapter VII gives good agreement with the experiment.   The turbulent structures in the collision area and the Turing-like stationary patterns have so far not been simulated.

6. With spectromicroscopic techniques available at synchrotron sources the concentration profile of pulses, the existence of ordered adsorbate layers and the chemical states of the adsorbed species were investigated.

A   List of Abbreviations

AES	Auger electron spectroscopy
AM	Alkali metal
BZ	Belousov-Zhabotinsky
cAMP	Cyclic adenosine monophosphate
FHN	Fitzhugh-Nagumo
L	Langmuir, $1L = 10^{-6}$ Torr·s
LEED	Low energy electron diffraction
LEEM	Low energy electron microscopy
mb	millibarn, 1 milibarn $= 10^{-31} m^2$
MEM	Mirror electron microscopy
ODE	Ordinary differential equantion
PDE	Partial differential equation
PEEM	Photoemission electron microscopy
QMS	Quadrapole mass spectroscopy
SPEM	Scanning photoelectron microscopy
STM	Scanning tunneling microscopy
RD	Reaction-diffusion
UHV	Ultrahigh vacuum
WF	Work function
XPS	X-Ray Photoelectron Spectroscopy

B   Acknowledgment

Literature

[1] H.Haken, *Information and Self-organization: A Macroscopic Approach to Complex Systems*, Springer-Verlag, 1988

[2] H. Bénard, *Les tourbillons cellulaires dans une nappe liquide*, Rev. G_en. Sci. Pures Appl. **11**, 1261-1271 ,1900

[3] E.L.Koschmieder, *Bénard Cells and Taylor Vortices*, Cambridge Univ. Press, 1993

[4] B. P. Belousov, Периодически действующая реакция и ее механизм *(A Periodic Reaction and its Mechanism)*, Сборник рефератов по радиационной медицине (Compilation of Abstracts on Radiation Medicine), 147:145, 1959

[5] A. M. Zhabotinsky, Периодический процесс окисления малоновой кислоты растворе (исследование кинетики реакции Белоусова), *(Periodic Processes of Malonic Acid Oxidation in a Liquid Phase)*, Биофизика [Biofizika], 9:306–311, 1964.

[6] John J. Tyson, and J. D. Murray, *Cyclic AMP Waves during Aggregation of Dictyostelium Amoebae*, Development, **106**, 421-426, 1989

[7] G. Ertl and J. Küppers, *Low Energy Electrons and Surface Chemistry*, 2nd ed. VCH, Weiheim, 1985.

[8] F. Fischer, *The Conversion of Coal into Oils*, Ernst Benn Ltd., 1925

[9] R. B. Anderson, *The Fischer-Tropsch Synthesis*, Academic Press, Inc., 1984

[10] R. Imbihl and G. Ertl, *Oscillatory Kinetics in Heterogeneous Catalysis*, Chem. Rev., **95**, 697-733, 1995

[11] F. Mertens and R. Imbihl, *Square Chemical Waves in the Catalytic Reaction $NO+H_2$ on a Rhodium(110) Surface*, Nature, **370**, 124-126

[12] H. Marbach, G. Lilienkamp, Han Wei, S. Guenther, Y. Suchorski and R. Imbihl, *Ordered Phases in Alkali Redistribution during a Catalytic Surface Reaction*, Phys. Chem. Chem. Phys. , **5**, 2730-2735, (2003)

[13] M. Hinz, S. Guenther, H. Marbach, and R. Imbihl, *Mathematical Modeling of Reactive Phase Separation in the System $Rh(110)/K/O_2+H_2$,* J. Phys. Chem. B, 108, 14620-14626, 2004

[14] F. Mertens, R. Imbihl, *Pulse Propagation and Oscillatory Behavior in the $NO+H_2$*

Reaction on a Rh (110) Surface, J. Chem. Phys., **105**, 4317-4322, 1996

[15] R.Imbihl, *Handbook of Surface Science* **vol.3***, dynamics*

[16] W.Engel, M.E.Kordesch, H.H.Rotermund, S.Kubala, and A. von Oertzen, *A UHV-Compatible Photoelectron Emission Microscope for Applications in Surface Science*, Ultramicroscopy, **36**, 148-153, 1991

[18] A. Schaak, *Dissertation*, University of Hannover, (1999)

[17] K. Christmann, *Introduction to Surface Physical Chemistry*, Steinkopf/Springer, 1991

[19] S. Guenther, B. Kaulich, L. Gregoratti and M. Kiskinova, *Photoelectron Microscopy and Applications in Surface Science*, Progress Surf. Sci., **70**, 187-260, 2002

[20] K. Oura, V. G. Lifshits, A. A. Saranin, A. V. Zotov, M. Katayama, *Surface Science, an Introduction, Springer*, 2003

[21] R. M. Tromp, *Low Energy Electron Microscopy*, IBM J. Res. Dev., **44**, 503-516, 2000

[22] R. M. Tromp: http://www.research.ibm.com/leem/

[23] M. Babout, M. Guivarch, R. Pantel, M. Bujor, and C. Guittard, *Mirror Electron Microscopy Applied to the Continuous local Measurement of Work-function variations*, J. Phys. D: Apply. Phys., **13**, 1161-1167, 1980

[24] R. P. W. Scott, *Chrom-Ed Series*, http://www.chromatography-online.org/GC-Tandem/ Quadrapole-Mass-Spectrometer/rs37.html

[25] A. Locatelli, http://www.elettra.trieste.it/nanospectroscopy/microscope/ SPELEEM.html

[26] S. Guenther, R. Hoyer, H. Marbach, R. Imbihl, F. Esch, C. Africh, G. Comelli, M. Kiskinova, *K and mixed K+O adlayers on Rh(110)*, J. Chem. Phys., **124**, 014706 (2006)

[27] M. Kiskinova, *Surface Structure and Reactivity: Reactions on Face-Centered Cubic (110) Metal Surfaces Involving Adatom-Induced Reconstructions*, Chem. Rev., **96**, 1431-1448, 1996

[28] S. A. Lindgren and L. Wallden, *Electronic structure of clean and oxygen-exposed Na and Cs monolayers on Cu(111)*, Phys. Rev. B, **22**, 5967-5979, 1980

[29] M. P. Kiskinova, *Poisoning and Promotion in Catalysis Based on Surface Science Concepts and Experiments*, Elsevier, 1992

[30] F. Mertens, R. Imbihl, *Parameter-Dependent Anisotropy of Front Propagation in the $H_2 + O_2$ Reaction on Rh(110)*, Chem. Phys. Lett., **242**, 221-227, 1995

[31] A. G. Makeev, R. Imbihl, *Simulations of Anisotropic Front Propagation in the H_2+O_2 Reaction on a Rh(110) Surface*, J. Chem. Phys., **113**, 3854-3863, 2000

[32] H. Marbach, M. Hinz, S. Guenther, L. Gregoratti; M. Kiskinova, R. Imbihl, *Mass Transport of Alkali Metal in Reaction Fronts on a Catalytic Metal Surface,* Chem. Phys. Lett., **364**, 207-212, 2002

[33] A. Schaak, R. Imbihl, *Existence Diagram for Chemical Wave Patterns in the $NO+H_2$ Reaction on Rh(110)*, J. Chem. Phys., **107**, 4741-4743, 1997

[34] Th. Schmidt, A. Schaak, S. Guenther, B. Ressel, E. Bauer, R. Imbihl, *In situ Imaging of Structural Changes in a Chemical Wave with Low-Energy Electron Microscopy: the System Rh(110)/NO+H_2*, Chem. Phys. Lett., **318**, 549-554, 2000

[35] H. Marbach, S. Guenther, T. Neubrand, R. Imbihl, *Mass Transport of Alkali Metal with Pulses: catalytic NO reduction with hydrogen on Rh(110)/K*, Chem. Phys. Lett., **395**, 64-69, 2004

[36] Y. Xu, H. Marbach, R. Imbihl, I. G. Kevrekidis, M. Mavrikakis, The Effect of Coadsorbed Oxygen on the Adsorption and Diffusion of Potassium on Rh(110): a First-Principles Study, J. Phys. Chem. C, **111**, 7446-7455, 2007

[37] A. Schaak, S. Shaikhutdinov, R. Imbihl, *H/D-Isotope Effects in Chemical Wave Propagation on Surfaces: the O2+H2 and NO+H2 Reactions on Rh(110) and Rh(111)*, Surf. Sci. **421**, 191-203 (1999)

[38] F. Mertens, R. Imbihl, *Control of the Shape of Chemical Wave Patterns in the $NO+H_2$ Reaction on Rh(110) by Adsorbate-Induced Reconstructions*, Surf. Sci., **347**, 355-366, 1996

[39] I.M. Irurzun, R.Imbihl, J.L. Vicente, E.E.Mola, *An Analysis of Turbulent States in the NH_3 + NO Reaction on Pt{100}*, Chem. Phys. Lett., **389**, 212-217, 2004

[40] A. Linder, D.Bonn and J. Meunier, *Viscous Fingering in Complex Fluids*, J.Phys.: Condens. Matter, **12**, A477-A482, 2000

[41] F.Mertens, R.Imbihl, *Pulse Propagation and Oscillatory Behavior in the $NO+H_2$ Reaction on a Rh(110) Surface*, J. Chem. Phys., **105**,   4317-4322, 1996

[42] B. Baraldi, V. R. Dhanak, M. Kiskinova, R. Rosei, *Molecular and Mixed Coadsorbed Layers Produced by NO Adsorption on (1x1) and (1x2) Rh(110)*, Appl. Surf. Sci., **78**, 445-

456, 1994

[43] H. Liu, H. Uecker, M. Hinz, L. Qiao, I. G. Kevrekidis, S. Guenther, A. Locatelli, R. Imbihl, *Mass Transport of Alkali Metal with Pulses in a Surface Reaction*, Phys. Rev. Lett., submitted

[44] J. J. Yeh and I. Lindau, *Atomic Subshell Photoionization Cross Sections and Asymmetry Parameters: 1≤Z≤103*, Atomic data and nuclear data tables, **32**, 1, (1985)

[45] P. W. Murray, G. Thornton, M. Bowker, V. R. Dhanak, A. Baraldi, R. Rosei, M. Kiskinova, Mixed O+N Layers on a Rh(110) surface: *Competition between Nitrogen and Oxygen Reconstructive Interactions*, Phys. Rev. Lett. **71**, 4369-4372, 1993

[46] M.Gierer, F. Mertens, H. Over, G. Ertl, R. Imbihl, *Structural Analyses of the c(2x4)-N+2O and the (2x1)-N Phases on Rh(110) by Low-Energy Electron Diffraction*, Surf. Sci., **339**, L903-L908

[47] A. S. Mikhailov, *Foundations of Synergetics I: Distributed Active Systems*, Springer-Verlag, 1990

Curriculum Vitae

Personal:

Birthday: Oct.09,   1978

Place of birth: Wanxian, Sichuan, China

Status: Single

Education:

June 22, 1997   Graduate from Nankai Middleschool, Chongqing

1997-2001   Studied physics in Peking University and received degree "Bachelor of Science", with the thesis "Diagnostic measurement of femtosecond laser pulse" accomplished in Chinese Academy of Sciences, supervised by Prof. Dr. Jie Zhang.

2001-2004   Studied physics in the international program in the Institute of Solid State Physics in University of Hannover and graduated as Dipl. Phys. (Master of Science), with the topic "Electronic properties of thin alkali metal film on the semiconductor surface" supervised by Prof. Dr. H. Pfnuer.

Since 2004   Begin the doctorate on the topic of this thesis in the Institute of Physical Chemistry in the Leibniz Universty of Hannover.   The doctorate work is supervised by Prof. Dr. R.Imbihl